uOttawa

L'Université canadienne
Canada's university

FACULTÉ DES ÉTUDES SUPÉRIEURES ET POSTOCTORALES

uOttawa

L'Université canadienne
Canada's university

FACULTY OF GRADUATE AND POSDOCTORAL STUDIES

Fathalla Shalouf

AUTEUR DE LA THÈSE / AUTHOR OF THESIS

Ph.D. (Civil Engineering)

GRADE / DEGREE

Department of Civil Engineering

FACULTÉ, ÉCOLE, DÉPARTEMENT / FACULTY, SCHOOL, DEPARTMENT

Seismic Retrofit of Reinforced Concrete Frames with Diagonal Prestressing of FRP Strips

TITRE DE LA THÈSE / TITLE OF THESIS

Murat Saatcioglu

DIRECTEUR (DIRECTRICE) DE LA THÈSE / THESIS SUPERVISOR

CO-DIRECTEUR (CO-DIRECTRICE) DE LA THÈSE / THESIS CO-SUPERVISOR

EXAMINATEURS (EXAMINATRICES) DE LA THÈSE / THESIS EXAMINERS

Marie-Anne Erki

David Lau

Beatriz Martin-Perez

Dan Palermo

Gary W. Slater

LE DOYEN DE LA FACULTÉ DES ÉTUDES SUPÉRIEURES ET POSTDOCTORALES /
DEAN OF THE FACULTY OF GRADUATE AND POSTDOCORAL STUDIES

Seismic Retrofit of Reinforced Concrete Frames with Diagonal Prestressing or FRP Strips

By

Fathalla Shalouf

A thesis presented to the School of Graduate Studies and Research of the University of Ottawa in partial fulfillment of the requirements for the degree of Doctor of Philosophy in Engineering

Ottawa- Carleton Institute for Civil Engineering

Department of Civil Engineering

Faculty of Engineering

The University of Ottawa

Ottawa, Ontario, Canada

July 2005

Your file Votre référence
ISBN: 0-494-11021-X
Our file Notre référence
ISBN: 0-494-11021-X

ACKNOWLEDGEMENT

This thesis was conducted under the supervision of Dr. Murat Saatcioglu, to whom I would like to express my sincere gratitude for his guidance and support. My appreciations extend to Dr. Nove Naumoski and Alain Boisvenue for there assistance. I would like to thank my friend Sayed Ahmad for his assistance during the experimental phase of research.

My special thanks to my parents, my wife, my brothers and my sisters for their encouragement during my study.

Finally, I gratefully acknowledge the University of Ottawa for providing me the opportunity to conduct my studies.

Abstract

Performance of reinforced concrete structures during previous earthquakes has indicated that the majority of buildings designed prior to the enactment of modern seismic codes and those designed more recently in regions where code enforcement is difficult to achieve, have suffered seismic damage associated with non-ductile frame construction. Because it is not economically feasible to replace seismically deficient building infrastructure with new and improved buildings, seismic retrofit strategy remains to be the most viable approach to seismic risk mitigation.

Currently, there are retrofit techniques available to stiffen and strengthen non-ductile concrete frames with unreinforced masonry infill panels, while other techniques are used to improve deformability of elements. The available retrofit techniques may be viewed in three categories; i) those that involve the addition of structural elements, such as steel bracing systems or concrete shear walls to control deformations, ii) those that involve surface treatment of masonry walls by adding concrete overlays with steel mesh, bonding steel plates on both sides and using fiber reinforced polymer (FRP) composite materials, and iii) those that involve reinforcing masonry walls internally. The first category of retrofit methods, while stiffens and strengthens the frames, often results in a change of dynamic properties of structures by increasing mass and reducing period of the structure.

The main objective of the proposed research is to develop new and improved seismic retrofit techniques for non-ductile reinforced concrete frame structures with and without masonry infill walls. The techniques to be investigated involve the application of surface bonded and FRP anchored diagonal FRP sheets and externally applied diagonal prestressing.

The experimental and the analytical results indicate that the two techniques used in the research were able to control the structure deflection.

The initial prestressing in the cables has effect on the structure drift demand. If it is high, the strands yield and may even rupture during loading and result in high drift demand, as opposed to non-prestressed strands that may continue remaining elastic. However, the

situation reverses during small drift demands, where, increased prestressing results in reduced drift demands as long as the strands remain elastic. This implies that there exists an optimum level of prestressing.

Also the results indicate that CFRP strips can be used to effectively control lateral drift during strong earthquakes, protecting non-ductile frame buildings.

Table of Content **Page**

Acknowledgement i

Abstract ii

Table of content iv

List of Tables vii

List of figures viii

Notations xiv

Chapter 1 Introduction 1

1.1 General 1

1.2 Seismic Retrofit Techniques 2

1.3 Objectives 3

1.4 Scope 3

Chapter 2 Literature Review 5

2.1 Introduction 5

2.2 Experimental Research 5

2.3 Analytical Research 11

Chapter 3 Experimental Research 13

3.1 Introduction 13

3.2 Specimen Description 14

3.3 Design of Unretrofitted Frames with Masonry Infills 15

3.4 Design of Infilled Frames Retrofitted With Prestressed Strands 17

3.5 Design of Infilled Frame Retrofitted with FRP Strips 19

3.6 Preparation of Specimens 20

3.7 Material Properties 23

3.8 Instrumentation and Test Setup 24

3.9 Loading Program 25

Chapter 4	Test Results and Observed Behavior	26
4.1	General	26
4.2	Performance of Specimen BR-1 (Frame with unretrofitted brick wall)	26
4.3	Performance of Specimen BR-2 (Frame-brick wall assembly retrofitted with cables)	29
4.4	Performance of Specimen BR-3 (With FRP wrapped columns and retrofitted frame-brick wall assembly with Cables)	33
4.5	Performance of Specimen BL-3 (Frame-block wall assembly retrofitted with diagonal FRP sheet strips)	35
Chapter 5	Analytical Research	39
5.1	General	39
5.2	Program DRAIN-RC	39
5.3	Analysis of Test Specimens	41
5.3.1	Modeling of Test Specimens	41
5.3.2	Analysis Results and Comparisons with Experimental Data	43
5.4	Applications to Practice	45
5.4.1	Selection of the structure	45
5.4.2	Modelling of the structure	47
5.4.3	Selection of ground motion records	48
5. 4.4	Retrofitting by diagonal prestressing	49
5.4.4.1	Static inelastic pushover analysis	49
5.4.4.2	Dynamic inelastic time history analysis	56
5. 4.5	Retrofitting by diagonal FRP strips	58
5.4.5.1	Pushover Anlaysis	59
5.4.5.1	Dynamic Inelastic Analysis	60
Chapter 6	Summary and Conclusions	62
6.1	Summary	62

6.2 Design Strategy 63
6.3 Conclusion 65
References 69
Tables 75
Figures 79
Appendix A 170

List of Tables

Table 3.1	Characteristics of concrete mixture for unretrofitted and retrofitted infilled frame by FRP sheet (BR-1 and BL-3)	75
Table 3.2	Characteristics of concrete mixture for retrofitted infilled frame by cables (BR-2 and BR-3)	75
Table 3.3	Compressive strength of concrete block units and prism	76
Table 3.4	Compressive strength of masonry brick units and prism	76
Table 3.5	Mechanical properties of carbon fibers as described from manufacturer	77
Table 3.6	Specimen displacement per loading cycle	77
Table 5.1	Loads and materials properties	78
Table 5.2	Sections sizes and reinforcement arrangement	78

List of Figures

Fig.3.1	Details of reinforced concrete frames	79
Fig.3.2	Column and beam cross sections	80
Fig.3.3	Column splices above the foundation	80
Fig.3.4	Detail of beam - column connections	81
Fig.3.5	Knee frame model for sliding shear failure of masonry infill wall	81
Fig.3.6	Diagonal compression strut under lateral loading	82
Fig.3.7	Effect of displacement on strand behavior	82
Fig.3.8	Locations of strain gauges on frame reinforcement	83
Fig.3.9	Foundations ready to cast	84
Fig.3.10	Plastic tubes and steel hooks embedded in foundation	85
Fig.3.11	A Typical column cage	85
Fig.3.12	Complete frame formwork	86
Fig.3.13	Reinforcement for top beam	87
Fig.3.14	Two of the bare frames after casting	88
Fig.3.15	Masonry prisms	89
Fig.3.16	Externally post-tensioned cables applying gravity loads	90
Fig.3.17	Hollow steel sections welded with steel angle	90
Fig.3.18	Steel plates supporting strands on the foundation	91
Fig.3.19	Specimen retrofitted with diagonal FRP sheets	91
Fig.3.20	Holes for FRP anchors	92
Fig.3.21	Specimen BR-3, retrofitted with diagonal prestressing and FRP Wrapping	93
Fig.3.22	Steel stress-strain relationship for # 15 reinforcement	94
Fig.3.23	Stress-strain relationship for # 6.38 stirrups and ties	94
Fig.3.24	Stress-strain relationship for #15 prestressing strand	94
Fig.4.1	Hysteretic lateral load - lateral displacement relationship for BR-1 (Uuretrofitted specimen)	95
Fig.4.2	Flexural crack at beam critical section at 0.5 % drift (BR-1)	95
Fig.4.3	Diagonal cracks in masonry wall at 0.5 % Drift (BR-1)	96

Fig.4.4	Diagonal tension cracks in masonry wall and flexural cracks in beam at 0.75 % lateral drift (BR-1)	96
Fig.4.5	Widening of beam flexural cracks at 1.0 % lateral drift (BR-1)	97
Fig.4.6	Formation of diagonal tension cracks in columns at 1.0 % lateral drift (BR-1)	97
Fig.4.7	Crack pattern in specimen BR-1 at 1.0 % lateral drift	98
Fig.4.8	Crack pattern in specimen BR-1 at 1.25 % lateral drift	98
Fig.4.9	Concrete deterioration and widening of diagonal cracks in column at 1.5 % lateral drift (BR-1)	99
Fig.4.10	Crack pattern in specimen BR-1 at 1.5 % lateral drift	100
Fig.4.11	Crack pattern in specimen BR-1 at 1.75 % lateral drift	101
Fig.4.12	Damage to specimen BR-1 at 2.0 % lateral drift	102
Fig.4.13	Failure of masonry and buckling of column bars at 2.5 % lateral drift (BR-1)	103
Fig.4.14	Out of plane failure of the wall at 2.5 % lateral drift (BR-1)	104
Fig.4.15	Deterioration of specimen BR-1 at 3 % lateral drift (front view)	105
Fig.4.16	Deterioration of specimen BR-1 at 3 % lateral drift (back view)	106
Fig.4.17	Hysteretic lateral load - lateral displacement relationship for BR-2 (Retrofitted specimen)	107
Fig.4.18	Flexural crack at beam critical section at 0.5 % lateral drift (BR-2)	107
Fig.4.19	Crack at top of the close column at 0.75 % lateral drift (BR-2)	108
Fig.4.20	Separation in mortar joints at 0.75 % lateral drift (BR-2)	108
Fig.4.21	Diagonal tension cracks in masonry wall at 0.75 % lateral drift (BR-2)	109
Fig.4.22	Cracks at top of close column at 1.0 % lateral drift (BR-2)	109
Fig.4.23	Cracks at bottom of far column at 1.0 % lateral drift (BR-2).	110
Fig.4.24	Relaxation of diagonal prestressed cable at 1.0% drift, Front view (BR-2)	110
Fig.4.24	Relaxation of diagonal prestressed cable at 1.0% drift, Side view (BR-2)	111
Fig.4.25	Deterioration of specimen BR-2 at 1.25 % lateral drift	111

Fig.4.26	Concrete deterioration and widening of diagonal cracks in bottom of left column and wall at 1.5 % lateral drift (BR-2)	112
Fig.4.27	Cracks at bottom of right column, at 1.5 % lateral drift (BR-2)	113
Fig.4.28	Concrete deterioration and widening of cracks at the bottom of left column and wall at 1.75 % lateral drift (BR-2)	114
Fig.4.29	Hysteretic lateral load - lateral displacement relationship for BR-3 (Retrofitted specimen)	115
Fig.4.30	Separation in mortar between wall and column at 0.3 % lateral drift (BR-3)	115
Fig.4.31	Formation of diagonal crack at 0.5 % lateral drift (BR-3)	116
Fig.4.32	Deterioration of specimen BR-3 at 0.5 % lateral drift (BR-3)	116
Fig.4.33	Flexural crack at beam critical section at 0.75 % lateral drift (BR-3)	117
Fig.4.34	Widening of gap between wall and column at 1.0 % lateral drift (BR-3)	117
Fig.4.35	Increased separation in mortar joints at 1.0 % lateral drift (BR-3)	118
Fig.4.36	Concrete deterioration and buckling of column bars at 1.25 % lateral drift (BR-3)	119
Fig.4.37	Hysteretic lateral load vs. lateral displacement relationship for retrofitted frame (BL-3)	120
Fig.4.38	Horizontal cracks appear in column at 0.4 % Lateral drift (BL-3)	120
Fig.4.39	Crack at head joints start to appear at 0.4 % lateral drift (BL-3)	121
Fig.4.40	Separation of fibers along wall diagonal at 0.4 % lateral drift (BL-3)	121
Fig.4.41	Local delamination of FRP in compression a strut at 0.4 % lateral drift (BL-3)	122
Fig.4.42	Increased local delamination of FRP in a compression strut at 0.5 % lateral drift (BL-3)	122
Fig.4.43	Formation of horizontal cracks in the mortar joint at 0.5 % lateral drift (BL-3)	123
Fig.4.44	Separation between wall and column at 0.75 % lateral drift (BL-3)	124
Fig.4.45	Rupturing of fibers across the joint between the wall and frame, at 0.75 % lateral drift (BL-3)	125

Fig.4.46	Separation of fibers along wall diagonal at 0.75 % lateral drift (BL-3)	126
Fig.4.47	Formation of shear cracks in a column near the top, at 1.0 % lateral drift (BL-3)	126
Fig.4.48	Additional horizontal cracks in column at 1.0 % lateral drift (BL-3)	127
Fig.4.49	More separation between the wall and column at 1.0 % lateral drift (BL-3)	128
Fig.4.50	Shear cracks in a column near the top, at 1.0 % lateral drift (BL-3)	129
Fig.4.51	More separation between wall and column at 1.25 % lateral drift (BL-3)	130
Fig.4.52	Visible bending of longitudinal reinforcement and ties in upper part of the right column at 1.75% lateral drift (BL-3)	131
Fig.4.53	Significant concrete cover spalling in column at 1.75% lateral drift (BL-3)	132
Fig.4.54	Rupturing of fiber anchors at 1.75% lateral drift (BL-3)	133
Fig.5.1	Hysteretic models used in DRAIN-RC	135
Fig.5.2	Analytical models used for push-over analysis of test specimens	135
Fig.5.3	Hysteretic force-displacement relationship for BR-1(Unretrofitted specimen)	136
Fig.5.4	Hysteretic force-displacement relationship for BR-2 (Retrofitted with a diagonal prestressing force of 75 kN/cable)	136
Fig.5.5	Hysteretic force-displacement relationship for BR-3 (Retrofitted with a diagonal prestressing force of 125kN/cable)	137
Fig.5.6	Hysteretic force-displacement relationship for BL-3 (Retrofitted with diagonal FRP strips)	137
Fig.5.7	Five-storey moment resistant frame building	138
Fig.5.8	Two dimensional lumped frames used in analysis	139
Fig. 5.9	Acceleration time histories of artificial records used for Vancouver	145
Fig.5.10	Lateral drift demand envelopes under artificial records used for Vancouver	145
Fig.5.11	Arrangement of prestressing cables in two dimensional lumped frames	146

Fig.5.12	The effect of prestressing on drift demands (4 cables/diagonal in the model)	147
Fig.5.13	The effect of prestressing on interstorey drift demands (4 cables/diagonal in the model)	148
Fig.5.14	The results of pushover analysis for the 5-storey building (Retrofitted buildings have 8 cables/diagonal in lumped frame model)	149
Fig.5.15	The results of pushover analysis for the 5-storey building, with potential strength decay indicated beyond 1% drift ratio (Retrofitted buildings have 8 cables/diagonal in lumped frame model)	149
Fig.5.16	The effect of prestressing on drift ratios and interstorey drift ratios (Retrofitted buildings have 8 cables/diagonal in lumped frame model)	150
Fig.5.17	The effect of prestressing on total and interstorey drift ratios (8 cables/diagonal in lumped frame model)	151
Fig.5.18	Effect of amount of prestressing cables on total and interstorey drift ratios (Retrofitted No P/S)	152
Fig.5.19	Effect of the amount of prestressing cables on total and interstorey drift ratios (Retrofitted P/S = 25 kN)	153
Fig.5.20	Effect of the amount of prestressing cables on total and interstorey drift ratios (Retrofitted P/S = 50 kN)	154
Fig.5.21	Effect of the amount of prestressing cables on total and interstorey drift ratios (Retrofitted P/S = 75 kN)	155
Fig.5.22	Effect of the amount of prestressing cables on total and interstorey drift ratios (Retrofitted P/S = 100 kN)	156
Fig.5.23	Effect of the amount of prestressing cables on total and interstorey drift ratios (Retrofitted P/S = 125 kN)	157
Fig.5.24	Effect of amount of prestressing cables on total and interstorey drift ratios (Retrofitted P/S = 150 kN)	158
Fig.5.25	Effect of different arrangements of prestressing cables on total and interstorey drift ratios (Retrofitted buildings have 8 cables/diagonal in lumped frame model with P/S =100 kN))	159

Fig.5.26 The effect of prestressing on interstorey drift ratios (Retrofitted No P/S) 160
Fig.5.27 The effect of prestressing on interstorey drift ratios (Retrofitted P/S = 50 kN) 160
Fig.5.28 The effect of prestressing on interstorey drift ratios (Retrofitted P/S = 100 kN) 161
Fig.5.29 The effect of prestressing on interstorey drift ratios (Retrofitted P/S = 150 kN) 161
Fig.5.30 Maximum ductility response for beams at each storey 162
Fig.5.31 Maximum ductility response for columns at each storey 162
Fig.5.32 Moment versus flexural hinge rotation of columns for unretrofitted and retrofitted buildings 163
Fig.5.33 Moment versus shear hinge rotation of columns for unretrofitted and retrofitted buildings 164
Fig.5.34 Moment versus flexural hinge rotation of columns for unretrofitted and retrofitted buildings 165
Fig.5.35 Effect of different arrangement of prestressing cables on interstorey drift (Retrofitted buildings have 8 cables/diagonal in lumped frame model with P/S =100 kN)) 166
Fig.5.36 Structure retrofitted with diagonally placed CFRP strips 166
Fig.5.37 Effect of the amount of CFRP layers on total and interstorey drift ratios 167
Fig.5.38 Effect of the amount of CFRP layers on total drift ratio obtained from dynamic time history analysis 168
Fig.5.39 Maximum ductility response for beams at each storey, obtained from dynamic time history analysis (Building retrofitted by FRP sheets) 168
Fig.5.40 Maximum ductility response for columns at each storey obtained from dynamic time history analysis (Building retrofitted by FRP sheets) 169

Notations

A_p - Cross sectional area of prestressed strand.

d_b - Longitudinal bar diameter.

D_i - Diagonal length of infill wall.

D_f - Compressive force in diagonal strut required to generate sliding shear failure of unreinforced masonry wall.

EI - Flexural rigidity of reinforced concrete member.

E_p - Modouls of elasticity of prestressed strand.

E_m - Modulus of elasticity of masonry unit.

F_y - Yield stress of prestressed strand.

F_p - Force in prestressed strand.

f_p - Stress in prestressed strand.

F_{pi} - Initial force in prestressed strand.

f_{pi} - Initial stress in prestressed strand.

f_{max} - Maximum stress in prestressed strand.

f_{lu} - Ultimate tensile strength of FRP sheet in MPa.

F_{lu} - Ultimate tensile strength of FRP sheet in kN.

f'_m - Compression strength of masonry unit.

G - Shear modulus.

h - Total high of reinforced concrete structure.

I - Importance factor.

k - The ratio of masonry elastic modulus to masonry compressive strength. k = 750 for concrete block, and 500 for clay brick.

L_p - Length of diagonal presstress strand.

M_v - Higher mode effect factor.

t_f - Average thickness of carbon fiber reinforced polymer.

μ - Poisson's ratio.

R_d - Ductility related force modification factor.

R_0 - Over strength related force modification factor.

$S(T_a)$ - Design spectral response acceleration, as a ratio to gravitational acceleration, corresponding to fundamental period T_a.

T_a - Fundamental period.

t_o - Shear stress between mortar and masonry.

t - Average width of masonry.

W - Dead load of structure.

Ws - Effective width of diagonal compression strut.

W_f - Width of carbon fiber reinforced polymer.

V_b - Horizontal force required to generate ultimate bending moment in the frame.

V_s - Horizontal force resistance.

V_i - Base shear force required to generate sliding shear failure in unreinforced. wall.

V_{total} - Base shear force required to generate sliding shear failure in infilled frame.

Chapter 1

Introduction

1.1 General

Performance of reinforced concrete structures during previous earthquakes has indicated that the majority of buildings designed prior to the enactment of modern seismic codes and those designed more recently in regions where code enforcement is difficult to achieve, have suffered seismic damage associated with non-ductile frame construction. These frames often contain unreinforced masonry walls, increasing their vulnerability against seismic damage. More recent earthquakes, including the 1989 Loma Prieta Earthquake in San Francisco, the 1994 Northridge Earthquake in Los Angeles, the 1995 Kobe Earthquake in Japan and the 1999 Kocaeli Earthquake in Turkey have underlined once again seismic risk associated with non-ductile construction in major metropolitan centers. In some cases seismic resistance of these buildings was not sufficient even under moderate levels of earthquake excitation. While the widespread use of masonry walls, often in the form of infill walls classified as non-structural elements, have increased seismic risk in older buildings, some researchers argued that they could contribute significantly to seismic resistance of buildings (Klingner and Bertero 1978, Mehrab et al 1996, Bertero and Brokken 1983).

Because it is not economically feasible to replace seismically deficient building infrastructure with new and improved buildings, seismic retrofit strategy remains to be the most viable approach to seismic risk mitigation. Developing new and improved seismic retrofit methodologies for non-ductile concrete frame structures constitutes the scope of the current research project.

1.2 Seismic Retrofit Techniques

Currently, there are retrofit techniques available to stiffen and strengthen non-ductile concrete frames with unreinforced masonry infill panels, while other techniques are used to improve deformability of elements. The available retrofit techniques may be viewed in three categories; i) those that involve the addition of structural elements, such as steel bracing systems or concrete shear walls to control deformations, ii) those that involve surface treatment of masonry walls by adding concrete overlays with steel mesh, bonding steel plates on both sides and using fiber reinforced polymer (FRP) composite materials, and iii) those that involve reinforcing masonry walls internally. The first category of retrofit methods, while stiffens and strengthens the frames, often results in a change of dynamic properties of structures by increasing mass and reducing period of the structure. Siegel, et al. (1994) reported that one such application in San Francisco to strength a five-story unreinforced masonry building resulted in damage during the Loma Prieta Earthquake. The secondary category of techniques is susceptible to surface dilapidation and anchorage problems, while they may enhance lateral resistance of unreinforced masonry significantly. Abrams, et al. (1993) experimentally studied the effect of single sheet of steel mesh fixed in wall by using ferro cement plaster. He concluded that the technique enhanced the ultimate flexural capacity of the wall as much as 2.5 times. Bhende et al. (1994) used steel plates anchored to an unreinforced masonry wall with steel anchors. They found that the out of plane capacity of the wall was increased as mush as ten times with respect to the reference wall. Taghdi, M. (1998) used externally applied steel strips on reinforced concrete, unreinforced masonry and reinforced masonry walls and reported significant increases in strength and ductility of the resulting systems. The third category of retrofitting was tested by Kehoe (1996), who drilled holes in masonry walls and placed steel reinforcement bonded with epoxy-cement paste inside the walls. Dawe et al. (1994) strengthened masonry walls with prestressing steel, achieving increased flexural cracking capacity and enhanced crack control. While the above techniques can be used for seismic retrofitting existing non-ductile reinforced concrete frames with and without masonry walls, new and improved techniques are needed for economically viable, structurally sound and less intrusive solutions to seismic risk mitigation.

1.3 Objectives

The main objective of the current research is to develop new and improved seismic retrofit techniques for non-ductile reinforced concrete frame structures with and without masonry infill walls. The techniques to be investigated involve the application of surface bonded and FRP anchored diagonal FRP sheets and externally applied diagonal prestressing.

1.4 Scope

The scope of the current research consists of experimental and analytical components, with the following specific tasks:

- Review of previous research on seismic retrofitting concrete frame structures.
- Design and construction of three half-scale reinforced concrete frames with unreinforced brick masonry infill walls.
- Design and construction of a half-scale reinforced concrete frame with unreinforced concrete block masonry infill wall, companion to similar specimens tested in the earlier phase of the same overall investigation.
- Retrofitting two of the frames with brick infill walls by different levels of external prestressing, using seven-wire strands.
- Retrofitting the frame with concrete block masonry wall with carbon FRP strips along the wall diagonals while anchoring the strips to the frame by means of specially devised FRP anchors.
- Preparation of specimens, test set-up and instrumentation for testing under constant gravity load and incrementally increasing lateral deformation reversals.
- Testing all four specimens under in-plane load reversals and data acquisition.
- Evaluation of test data.
- Static inelastic (push-over) analysis of test specimens to verify analysis techniques against experimental results.
- Static inelastic (push-over) analysis of selected reinforced concrete frame structures with different levels of seismic resistance, retrofitted with different amounts of prestressing strands and levels of prestressing.

- Dynamic inelastic response time history analysis of selected reinforced concrete frame structures retrofitted with diagonal prestressing.
- Static inelastic (push-over) analysis of selected reinforced concrete frame structures with diagonal FRP strips.
- Dynamic inelastic response time history analysis of selected reinforced concrete frame structures retrofitted with diagonal FRP strips.
- Development of a design strategy for seismic retrofitting with diagonal prestressing or FRP strips.

Chapter 2

Literature review

2.1. Introduction

Seismic performance and retrofitting of reinforced concrete frames and masonry walls have been investigated in the past. These investigations can be grouped as; i) experimental research and testing, and ii) analytical research and analysis of structures. The majority of previous research was on the experimental investigation of in-plane and out-of plane seismic performance of existing buildings, with and without retrofitting. The following sections provide an overview of previous research in the area.

2.2 Experimental Research

An experimental study was conducted by Klingner, R. E and Bertero, V. V. in 1978 to investigate the behavior of infilled frames under severe earthquake ground motions. An eleven-story building, with 18.3 m by 61 m floor plan and a 2.74 m storey height was selected as the prototype structure. A three bay frame was selected for the investigation. Four tests were conducted on specimens having 1-1/2 bays and 3-1/2 stories, representing actual boundary conditions. The first specimen was a bare frame. It was tested and infilled with clay brick masonry wall subsequently for re-testing. The third test was conducted on a companion virgin frame infilled with clay bricks, while the fourth test was identical to the third, except conducted on another virgin frame infilled with concrete blocks. The researchers concluded that significant improvements were introduced by infilling a bare frame. In all tests it was possible to achieve distributed infill cracking and high-energy dissipation. Brittle shear failure was minimized. Bertero, V. and Brokken, S. (1983) continued with a similar experimental study, in which they investigated the effect of different infill panels on seismic resistance. Four different types of infill were

considered. These included, i) hollow-unit clay masonry, ii) concrete block masonry, iii) split bricks with exterior WWF (welded wire fabric) reinforcement where the wires were spliced with dowels anchored in the surrounding frame members and iv) lightweight concrete panels. The test frames were modeled to represent actual boundary conditions with 1-1/2 bays and 3-1/2 stories, as in the case of the previous research. The researchers concluded that, in the elastic range the fundamental period of the structure was decreased by more than 54% by adding infill panels, while the mass was increased less than 10%. They further concluded that, damaged and undamaged frames could be retrofitted for seismic resistance by adding reinforced infill panels, properly anchored to the surrounding frame members. They achieved this with infill panels consisting of solid brick, reinforced externally with welded wire fabric reinforcement anchored to the frame and covered with cement mortar. The resulting system had high energy dissipation capacity.

Khan, L. F. and Hanson R. D. (1979) conducted experimental research to provide a qualitative understanding of how infill reinforced concrete walls interacted with existing reinforced concrete frames. Five specimens were tested. The specimens consisted of; i) a bare frame, ii) a frame with monolithically cast wall, iii) a frame with cast-in-place wall, iv) a single precast panel wall, and v) a frame with multiple precast panel walls. The researchers concluded that the use of infills greatly strengthened and stiffened reinforced concrete frames. They also found for each infilled structure that the failure of infill resulted in severe shear column failure. At drift ratios of 1% for the cast-in-place wall and of about 2% for the multiple panel precast wall, the column failed in shear. They concluded that the load capacity degraded quickly because of inadequate confinement of the column core. To minimize column shear failure, they recommended column strengthening suggested by Higashi, Y and Kokusho, S. (1975).

Altin, Ersoy and Tankut (1992) studied experimentally the effect of different types of infill walls on seismic resistance. Four different types of infill walls were used. One frame was filled by a cast-in-place panel with diagonal bars, where the bars were welded to the frame reinforcement. The second frame was filled by a cast-in-place panel with

vertical bars, lapped with dowels epoxy glued into the holes drilled in the beams while the horizontal bars were welded to column reinforcement. The third frame was filled by cast-in-place panel with bars concentrated at wall boundaries, and welded to the frame reinforcement. The fourth frame was cast together with the panel, and all the bars were well anchored into the frame. The researchers observed in all specimens that the yielding of longitudinal reinforcement in columns close to the foundation level coincided with the formation of a horizontal crack in the infill along the foundation beam. Sliding shear failure occurred along this crack at higher loads. The infills became ineffective under reversed cyclic loading if they were not well connected to the surrounding members of frame. It was observed that, infilled frames behaved elastically up to the ultimate load, beyond which they were able to dissipate significant energy under reduced loads. The researchers also concluded that the introduction of infill panels into the frame lead to significant changes in the dynamic characteristic of structures.

Mehrabi et al. (1996) experimentally studied the contribution of infill panels to two reinforced concrete frames designed to have two different levels of strength. The first frame was weaker and designed for lateral wind loading. The second frame was stronger and designed for earthquake loading. Both types of frames were designed according to the ACI 319-89 Building Code (1989). In the design of either frame, the contribution of infill panels was ignored. The weak frame was infilled with hollow brick masonry and the strong frame was inflled with solid masonry units. The researchers found that the stiffness of the weak frame infilled with hollow masonry was 15 times greater than the companion bare frame. The stiffness of the strong frame infilled with solid masonry was 50 times greater than the companion bare frame. They concluded that, the total resistance of the infilled frame was equal to the flexural resistance of bare frames plus the sliding shear strength of the infills. The researchers further concluded that the infill panels can significantly improve the performance of reinforced concrete frames. The specimen with strong frame and solid masonry dissipated more energy than that of weak frame with hollow masonry. They also argued that the resistance of the infill was not influenced by the connection between the frame and the panel.

Weeks et al (1994) repaired concrete masonry walls with carbon fiber sheets in a five-story building. It was concluded that the carbon fiber improved the behavior and increased the stiffness of the walls. Laursen et al. (1995) conducted another experimental study on the use of FRP on masonry walls. The researchers retrofitted a masonry wall with Carbon FRP overlays. It was tested twice; i) first without the FRP, to create a scenario representing damage caused by earthquake motion, and ii) secondly, after retrofitting with FRP overlays. They concluded that the behavior of the wall was improved and strength was increased by retrofitting with FRP sheets.

Schwegler (1995) experimentally investigated three masonry walls that were retrofitted with carbon FRP sheets. Two of the walls were retrofitted with diagonal FRP sheets and the third wall was retrofitted with conventional woven fabric that was bonded to the entire surface of the wall without any anchorage. He observed that the ductility of the wall was improved and the shear capacity was increased by a factor of 1.4 in the latter case, while the increase was by a factor of 4.3 in the walls with FRP diagonals.

El-Attar et al. (1997) conducted small scale shake table tests to study the behavior of gravity load designed reinforced concrete structures subjected to earthquakes. During the experiments they observed that gravity load designed reinforced concrete structures experienced significant reductions in lateral stiffness after the first few cycles of moderate ground shakings. This reduction was caused by lack of confinement and associated ductility, as well as pulling out of discontinuous positive beam reinforcement. The researchers also found that gravity load designed reinforced concrete buildings without infill walls experienced large lateral deformations with increased P-Δ effects, and illustrated the drift control achieved with the use of infill walls.

Taghdi, M. (1998) tested four concrete block masonry walls and two reinforced concrete walls under simulated seismic loading. Two masonry walls were unreinforced and two were partially reinforced. The concrete wall had minimum reinforcement. One specimen in each set was retrofitted with diagonal (and vertical in the case of concrete wall) steel

strips. The researchers concluded that the diagonal steel strips significantly increased the strength and ductility, and lead to more energy dissipation.

Ehsani et al. (1999) tested three unreinforced brick walls retrofitted with vertical glass fiber reinforced polymer (GFRP) sheets. The specimens were subjected to cyclic out-of-plane loading. They concluded that the ultimate flexural strength was significantly increased. Also they found that the deflection was 2.5 % of the wall height. This wall deflection was almost 14 times the maximum allowable deflection. Paquette et al. (2001) tested two unreinforced masonry walls, also retrofitted with vertical GFRP. The specimens were subjected to cyclic out-of-plane loading by using a shaking table. They concluded that the ultimate flexural strength was significantly increased by the GFRP retrofitting.

Michael et al. (2001) used ten unreinforced masonry walls, retrofitted with FRP to conduct thirteen tests. Some of the specimens were tested without the FRP and then tested again as a partially cracked wall reinforced with FRP. The following parameters were investigated: i) Type of the fiber reinforcement; ii) amount of fiber reinforcement; iii) layout of fiber reinforcement; iv) effect of moderate compressive axial load; and v) cyclic behavior. The specimens were subjected to monotonically increasing lateral out-of- plane loads and only one wall was loaded cyclically. They concluded that the strength and ductility of the specimens were increased significantly by FRP retrofitting.

Ersoy et al (2003) tested seven identical one-bay, two-story infilled reinforced concrete frames under reversed cyclic loading. All frames were infilled with hollow clay masonry. Six of the walls were retrofitted by carbon FRP sheets. The frames were built to simulate old existing buildings in Turkey, which did not satisfy the existing Turkish Code. The first specimen served as reference. The second specimen was completely covered by two diagonal layers of FRP on each face of the infill wall. The FRP layers were bonded on the wall by Epoxy only. The FRP layers were not extended or anchored to frame members. The FRP delaminated from the wall during the early stages of testing, which did not result in any significant increase in specimen strength. But it did result in improvement

of specimen behavior. The third specimen was completely covered by two diagonal layers of CFRP on one face only. The layers were extended to the frame members and were anchored by specially developed FRP anchors by Serrato, F. (2002). However, there was no anchorage to the wall, except for surface bonding. The anchorage to frame was not sufficient and the FRP delaminated from the frame at the early stage of loading. There was no significant increase in the strength of specimen. To avoid delamination, the researchers used more FRP anchors in the next specimen. They also wrapped the ends of the columns at the top with two layers of FRP, where they had observed reinforcement splice failures, due to inadequate reinforcement splicing. The strength of this specimen was 2.36 times the reference specimen, and also exhibited increased ductility. Because of the cost associated with the use of FRP, the next specimen had strips of FRP along wall diagonals, which resulted in 75% reduction in the amount of FRP used. A single layer of 200 mm wide FRP strip was applied along each diagonal. The ends of FRP strips were extend and anchored into the frame members. The resulting strength in this specimen was 2.13 times that of the reference specimen, while ductility was also improved. The failure was initiated by debonding of CFRP strip near the foundation, followed by the yielding of longitudinal column reinforcement and crushing of concrete at the base of the first storey columns. To avoid this failure, the first-storey columns of the next specimen (Specimen #6) were warped by two layers of FRP. The height of the wrapped confinement area was extended up to the expected plastic hinge length of 150 mm. The failure was initiated in this specimen by the failure of the anchors used in tension FRP strips, resulting in sudden unloading. The failure in this specimen changed from a ductile flexure failure to a brittle shear fail of the first story beam-column joint. Moreover, the strength in this specimen was less than that of the previous specimen, developing 1.8 times the strength of the reference specimen. The next specimen was retrofitted in the joint area by FRP wrapping. However, this extra effort did not lead to any improvement in specimen behavior, which developed approximately the same strength as the previous specimen, reaching 1.89 times the strength of the reference specimen.

Erdem et al. (2003) tested two-storey, three-bay 1/3 scale undamaged reinforced concrete frames. Only the middle bay of RC frame was infilled by hollow clay tile. The first

specimen was strengthened with reinforced concrete infill walls and the second one was strengthened with carbon FRP in the existing infilled wall in the middle bay. The columns of the middle bay were wrapped with short carbon FRP sheets to prevent premature failure at region of lap splice. The researchers concluded that the increase in the lateral load resistance in both frames were almost the same, and was approximately equal to 5.0 times that of the bare frame. They also found that lateral deformability provided by the reinforced concrete infill wall was very high, while that of the frame strengthened with FRP was low.

2.3 Analytical Research

Holmes (1961) studied the effects of infill walls on frame stiffness. He analytically modeled the contribution of infill walls by means of equivalent compression diagonal struts. He introduced an expression, defining the width of diagonal struts to be modeled in analysis. Similar approaches have been taken by smith (1966), he examined the behavior of infilled frames and adopted a simplified equivalent strut model to replace the wall, and many other researchers as infill walls primarily provide compression resistance along their diagonals when subjected to lateral loads, with negligible resistance in diagonal tension.

The effective width of diagonal struts to be taken in analytical models has been a source of controversy among researchers. Researchers have proposed different approaches for this purpose. Stafford-Smith and Carter (1969) modified the equation introduced by Holmes (1961) making the width of the compression diagonal struts inversely proportional to the frame/infill relative stiffness. Paulay and Priestley (1992) recommended that the width of the diagonal compression strut could be taken as 25 % of the infill wall diagonal length. Saneinejad and Hobbs (1995) used the effect of the infill wall as diagonal strut in their analytical work for the elastic and plastic behavior of steel frames infilled with masonry walls.

Yaw-Jeng et al (1999) modeled three specimens, one of them was bare frame and the other two were partially and completely filled with masonry wall. They simulated the

bricks by subblocks and these sublocks are assumed to be connected by springs. The stiffness of these springs is related to the strength of the mortar. And they also simulated the concrete frame as the infilled wall, the concrete frame are cut in subblocks. The steel reinforcement assumed to be perfectly bonded with concrete.

Researches concluded that, the finite element method is a powerful method to study the behavior of structure under loads. Dhanasekar and Page (1986) and Liauw and Lo (1988) have modeled the steel frame by using linear and nonlinear element beam and interface elements to model the interaction between the infilled wall and the bounding frame. Dhanasekar and Page have used nonlinear orthotropic model to simulate the behavior of the infilled wall, while Liauw and Lo have used smeared crack model to simulate the infilled wall. Schmidit (1989) has used smeared crack elements to model the behavior of the reinforced concrete frame and the infilled wall.

Asteris (2003) proposed a new finite element technique to model the behavior of infilled frames under horizontal loads. The analysis included a step-by-step approach, on the basis of contact length between the frame and the infill wall, as well as its stress during its distortion by the horizontal load.

Chapter 3

Experimental research

3.1. Introduction

Experimental research was conducted to investigate the strength and deformability of non-ductile reinforced concrete frames with masonry infill walls. The experimental program consists of tests of four identical reinforced concrete frames, three of which were infilled with unreinforced brick masonry and the fourth one was infilled with unreinforced concrete block masonry. The frames were designed according to an old ACI code (ACI 318-1963) without the consideration of earthquake effects to reflect conditions in an existing building constructed prior to the enactment of seismic provisions of modern building codes.

The specimens were tested to investigate the effectiveness of two seismic retrofit methodologies that constituted the main objectives of the current research program. The experimental program was the continuation of a similar project that had been conducted at the Structures Laboratory of the University of Ottawa, involving the same reinforced concrete frame and concrete block masonry infill walls. One of the specimens tested in the earlier phase was retrofitted using FRP sheets and the other was tested without any retrofit, to serve as a control specimen. Therefore, the control (unretrofitted) specimen with block masonry was not repeated in the current investigation, and the test data obtained in the earlier phase was adopted. The only block masonry specimen that was prepared for testing was used to investigate the effectiveness of FRP strips as diagonal tension elements, as opposed to covering the entire wall surface with FRP, as was done in the earlier phase. The other three specimens, with clay brick masonry walls, constituted a new series, with one frame-wall assembly tested as the control specimen without any

retrofit. The primary objective of this series of tests was to explore the possibility of developing a new seismic retrofit strategy that involved diagonal prestressing of concrete frames, with and without masonry infills. Therefore, the remaining two specimens were prestressed diagonally.

The specimens were first subjected to uniformly distributed gravity loads, simulating dead load on the structure, followed by the application of incrementally increasing inelastic lateral drift reversals, simulating seismic loading.

3.2. Specimen Description

The specimens consisted of a single storey one bay frame with 250 mm square columns and a 250 mm wide and 350 mm deep beam at the top. The bottom beam served as the foundation, and was fixed on the laboratory strong floor to have full fixity. The details of reinforcement cage, designed based on ACI 318-1963, are shown in Figure 3.1. The longitudinal reinforcement in columns consisted of 8-15 M bars which resulted in 2.56 % reinforcement ratio. The beam longitudinal reinforcement at the mid-span consisted of 2-15 M top bars and 2-15 M bottom bars. The beam reinforcement at the supports consisted of 3-15 M top bars and 2-15 M bottom bars (continuous). The reinforcement details are as shown in Figure 3.2. This translated into tension reinforcement ratio of 0.53% at mid-span. Top and bottom reinforcement ratios were 0.8% and 0.53%, respectively. The transverse beam reinforcement was designed to be 6.35 mm diameter closed stirrups with 90-degree bends and 6 d_b (38.8 mm) extensions. The stirrups were placed at a spacing of one half the minimum cross-sectional dimension of beam, which was equal to 125 mm. Column ties consisted of the same size reinforcement, and were placed as perimeter ties with 90-degree bends at a spacing of 125 mm. The longitudinal column reinforcement was lap spliced as per ACI 318-1963, which required the lap length to be 24 times the bar diameter. This resulted in a lap length of 390 mm above the foundation beam, as shown in Figure 3.3.

The ultimate positive bending moment capacity of the beam at mid-span and at supports was computed as 46 kN·m. The negative beam moment capacity near the supports was

computed to be 70 kN·m. The ultimate bending moment capacity of the columns at 20% P_o was determined to be 70 kN·m. The ACI 318-1963 Building Code did not require any beam-column joint reinforcement. Therefore, there were no ties in the joints. This is illustrated in Figure 3.4.

3.3 Design of Unretrofitted Frames with Masonry Infills

It is important to review the fundamental behaviour of a frame infill wall assembly before the specimens can be designed. The frame and the infill wall are expected to respond to lateral forces together at low levels of horizontal loads. As the lateral load increases, the behavior changes and a complex interaction of the flexure-dominant frame and shear-dominant wall takes place. This results in the separation of the wall from the frame near diagonal tension corners, while developing a diagonal compression strut between the opposite compression corners. The separation may occur at 50% to 70% of the horizontal shear capacity of infill walls (Paulay and Priestley (1992).

There are several failure modes for masonry infilled frames. These include:

- Horizontal shear sliding of the infill wall, generally at or close to the mid-height of the wall, as illustrated in Fig. 3.5.
- Compression failure of diagonal struts, as illustrated in Fig. 3.6.
- Shear or flexural failure of a column or a beam.
- Tension failure of column, in frames with high aspect ratios
- Failure of frame members due to lack of transverse confinement reinforcement
- Failures of columns in reinforcement splice regions.

The strength of an infilled wall-frame assembly can be considered as the summation of the strengths of the bare frame and the infill wall. It was reported by Paulay and Priestley (1992) that the strength of an infill wall is usually governed by horizontal sliding, while diagonal crushing capacity of struts remains higher. Although the strut capacity degrades with cyclic loading, the sliding shear failure occurs earlier. Therefore, the lateral force resistance associated with horizontal sliding was taken as the infill capacity. Computer

program SAP 2000 was used to determine the lateral load capacity of the bare frame without the infill wall. The results indicated that the lateral load capacity of the bare frame was 130 kN and occurred when the negative moment capacity of the top beam reached 70 kN.m. At this stage of loading the beam positive moment was 46 kN.m.

The infill wall capacity against sliding shear failure was computed based on the recommendation by Paulay and Priestley (1992). Accordingly;

$$D_f = \frac{t_0 D_i t}{1 - \mu \frac{h}{L}} = \frac{0.03 f'_m D_i t}{1 - 0.3 \frac{h}{L}} \qquad 3.1$$

Where; D_f is the compressive force in a diagonal strut required to generate sliding shear failure of unreinforced masonry wall, f'_m is the compression strength of masonry unit, t_o is shear stress between the mortar and masonry, and t is the average width of masonry. Di is the diagonal length and computed as shown below;

$$D_i = \sqrt{(1825)^2 + (1825)^2} = 2581\text{mm}$$

For masonry block walls:

D_f = (0.03 x 15 x 2581 x 103)/ (1- 0.3(1825/1825)) = 172137 N

$V_i = D_f \text{ Cos } 45$

V_i = 172 Cos 45 =122 kN

$V_{total\ (unretrofitted)} = V_i + V_b$

$V_{total\ (unretrofitted)}$ = 122 + 130 = 252 kN

For masonry brick walls:

D_f = (0.03 x 21.4 x 2581 x 75.71x 2)/ (1- 0.3(1825/1825)) = 358419 N

$V_i = D_f \text{ Cos } 45$

V_i = 358 Cos 45 =253 KN

$V_{total\ (unretrofitted)} = V_i + V_b$

$V_{total\ (unretrofitted)}$ = 253 + 130 = 383 KN

In addition to the capacity calculations presented above, the effective width of wall strut was calculated as recommended by Paulay and Priestley (1992). This value was also used as a guide in establishing the strip width for FRP retrofitting.

$$W_s = 0.25\ D_i \qquad 3.2$$

$W_s = 0.25 \times 2581 = 645$ mm

Where, D_i is the diagonal length of the infill wall

3.4 Design of Infilled Frames Retrofitted With Prestressed Strands

Two of the specimens with brick masonry infill walls were retrofitted against lateral seismic forces by diagonal prestressing. This was expected to improve strength and ductility. Horizontal displacements imposed on infilled frames lead to the separation of the wall from the frame near diagonal tension corners, while developing diagonal compression struts near compression corners. Although further diagonal compression by prestressing cannot be justified along the struts, the initial prestress is counteracted by diagonal strut forces during response, reducing the level of prestressing and completely unloading the strands under increasing lateral drift. However, on the tension side, prestressing would control diagonal tension, thereby improving strength and potentially wall deformability. Placing the strands on both sides of the frame avoids out-of plane deformations, and should be done as a good design practice. This was done for the specimens tested in the current experimental program.

The total lateral force capacity of retrofitted specimen was calculated to be the summation of contributions from unretroffited frame-wall assembly and the horizontal component of the strands. Because the strands elongate during lateral loading, the initial prestress has to be decided with due considerations given to the subsequent tensioning caused by the lengthening of cables. The horizontal displacement of the infilled frame needs to be estimated, as illustrated in Fig. 3.7. Recorded test data obtained in the earlier phase of the investigation by Serrato, F. (2002) were used for this purpose.

The following properties were used in designing diagonal prestressing strands.

E_p= 196000 MPa

A_p =2x140 = 280 mm^2

F_y = 1860 MPa

$L_p = ((252.5)^2 + (223.5)^2)^{0.5}$ =337.2 cm

$$K_p = (E_p \times A_p)/L_p \qquad 3.3$$

K_p = (196000 x 280)/3372 = 16275 N/mm = 16.3 kN/mm

$(F_p)_{diagonal\ at\ yield} = F_y \times A_p$ =1860 x 280 = 520800 N = 521 KN

Where; L_p is the length of diagonal strand, F_p is the force in prestressing strand and F_{pi} is the initial force in prestressing strand. The expected column failure is to be at 1% lateral drift ratio, which translates into 20 mm horizontal displacement. The initial prestressing force in cables then becomes;

521- F_{pi} = 16.3 x 20 Cos 39

F_{pi} = 268 kN

Lateral force capacities of retrofitted specimens are computed below for two different levels of prestressing:

1) At F_{pi} = 150 kN;

$(F_p)_{diagonal} - F_{pi}$ = 16.3 x 20 Cos 39

$(F_p)_{diagonal}$ - 150 = 16.3 x 20 Cos 39

$(F_p)_{diagonal}$ = 403 kN

V_s = 403 Cos 39 = 313 kN

$V_{total\ (retrofitted)} = V_i + V_b + V_s$

$V_{total\ (retrofitted)}$ = 383 + 313 = 696 kN

2) At F_{pi} = 250 kN

The maximum resistance of the retrofitted infilled frame can be calculated as:

$(F_p)_{diagonal}$ - 250 = 16.3 x 20 Cos 39

$(F_p)_{diagonal} = 503$ KN

$V_s = 503 \text{ Cos } 39 = 391$ KN

$V_{total\ (retrofitted)} = V_i + V_b + V_s$

$V_{total\ (retrofitted)} = 383 + 391 = 774$ KN

Both F_{pi} = 150 kN and F_{pi} = 250 kN were used to retrofit two separate frame-wall assemblies, with 313 kN and 391 kN increases in lateral load capacity, respectively, while also improving ductility upon yielding of the steel strands.

3.5 Design of Infilled Frame Retrofitted with FRP Strips

The frame infilled with concrete block masonry was retrofitted with diagonal FRP strips to compare with the performance of a companion specimen retrofitted with FRP sheets covering the entire wall surface in the earlier phase of the investigation. The retrofit design was intended to increase lateral load resistance without expecting improvements in lateral deformability. The design was based on providing additional diagonal tension capacity by using carbon FRP sheets along wall diagonals. To maintain symmetry, the strips were placed on both sides of the wall. This resulted in two layers of FRP strips in each direction, resisting tension.

The total lateral load capacity of retrofitted specimen was calculated as the summation of contributions from unretroffited specimen and the horizontal component of diagonal tension force in CFRP strips. The material properties of composite FRP strips were adopted from an earlier experimental program, in which the same material was used in retrofitting concrete columns at the University of Ottawa (Enabelsy, G., 2001). Accordingly, the ultimate tensile strength of each FRP composite strip (f_{lu}) was approximately 700 MPa, with an average thickness of 0.9 mm.

$V_{total\ (retrofitted)} = V_{total\ (unretrofitted)} + F_{lu} \text{ Cos } 45$

$F_{lu} = f_{lu}\, w_f\, t_f$

Where; f_{lu} is the ultimate tensile strength of FRP composite in MPa, F_{lu} is the ultimate tensile force in FRP composite strip in kN, t_f is the average thickness of a single layer of CFRP composite strip and w_f is the width of CFRP strip.

F_{lu} = (700 MPa) (2 Layers) (0.9 mm) (615 mm) = 774900 N = 775 KN

$V_{total\ (retrofitted)}$ = 122 +130 + 775 Cos 45

$V_{total\ (retrofitted)}$ = 800 kN

The above lateral load capacities indicate that the retrofitted system was designed to increase the load capacity from 252 kN to 800 kN

3.6 Preparation of Specimens

The specimens were prepared in the Structures Laboratory of the University of Ottawa. The steel reinforcement was ordered from a local steel supplier, pre-bent to design specifications, except for the small size transverse reinforcement (d_b = 6.35 mm) used for frame elements, which were bent in the Structures Laboratory. Twenty eight strain gauges were placed on steel bars as illustrated in Figure 3.8. The formwork was manufactured from 20 mm thick plywood.

Each frame was built on an I-shaped foundation which was secured on the laboratory strong floor to provide fixity. They were heavily reinforced as shown in Figure 3.1. Figure 3.9 illustrates the construction of two foundations side by side. Four plastic tubes were embedded in each foundation to allow for holes, through which the specimens were secured on the laboratory strong floor by steel bolts. Four steel hooks were provided to be cast in concrete so that the specimen could be lifted and positioned for testing, as shown in Figure 3.10.

First the foundations were cast, with column starter bars protruding, to be spliced with column longitudinal reinforcement. The column reinforcement was assembled as illustrated in Figure 3.11. Complete formwork for the columns and the top beam was built for simultaneous casting of the frame elements, as shown in Figure 3.12. The beam cage was placed in the formwork prior to assembling the upper part of column cages and the remaining part of the formwork. This is illustrated in Figure 3.13. The specimens were cured for two weeks after casting concrete, and the formwork was then removed. Figure 3.14 illustrates bare frames after the removal of formwork. A mason was hired to

build masonry walls to simulate the actual construction practice. The brick wall consisted of two layers; these layers were separated from each other. The width of each layer was the same as the width of single brick, which was 90 mm. Each layer was built on the surface of columns. The space between the two layers was 70 mm. One specimen was infilled by block and three specimens were infilled by brick. Masonry prisms were prepared on the same day, as show in Figure 3.15.

Gravity loading on the columns and the beam was applied by external post-tensioning cables (#13 seven-wire strands). The cables were stressed by a hand-held hydraulic jack between steel hollow sections (3" x 3"x 3/8") placed on the frame and underneath the foundation beam, as illustrated in Figure 3.16. Each column was subjected to 400 kN of gravity load by means of 4 cables, where each cable was stressed to 100 kN. These 4 strands were tensioned between two sets of steel supports, each consisting of three hollow steel sections welded together with a steel plate to distribute the load uniformly. The gravity loading for the beam was applied as a three point load. This was done by stressing two cables at each location, one on either side of the specimen, between three sets of hollow steel sections. Each beam cable was stressed to 20 kN, resulting in a total of 40 kN gravity load at each location.

The first specimen, labeled as BR-1, was infilled with a brick wall and was tested without a retrofit (reference specimen). The second specimen, labeled as BR-2, was identical to the first one, also infilled with a brick wall. This wall was retrofitted through diagonal post-tensioning with a pair of # 15 seven-wire strands along each diagonal, resulting in one strand on each side. The strands were stressed between two supports, one at each diagonal corner of the frame. The top corner supports consisted of a hollow steel section (4" x 4"x 1/2") welded on a steel angle with a 45-degree orientation such that the angle was placed bearing against the beam-column connection. The bottom supports were similar, but bolted on the foundation as they could not take advantage of full support of the corners. This is illustrated in Fig. 3.17. During the test, the bolts of the bottom supports became loose and the bottom supports were changed with thick steel plates bolted with the foundation to the strong floor as shown in Fig.3.18. Two cables were used

to apply a total of 150 kN of diagonal force in each direction (each cable was prestressed to 75 kN). The behavior of the strands was monitored by placing two strain gauges on each cable.

The third specimen, labeled as BL-3 was infilled by concrete blocks and was companion to two similar walls tested earlier in the previous phase of the same investigation by Serrato (2002), one without (BL-1) and the other with retrofit (BL-2). The retrofitted wall had both sides of the infill wall covered with two layers of CFRP sheets on each side, where the fiber directions were aligned with wall diagonals (one layer per diagonal on each side, resulting in a total of two layers per diagonal). The third concrete block wall specimen, tested as part of the current investigation and labeled as BL-3, was retrofitted with CFRP diagonal strips as shown in Figure 3.19. One strip of CFRP was applied on each side per diagonal, resulting in a total of two layers per diagonal. They were glued on the wall by epoxy resin and the ends were fixed to the reinforced concrete frame corners, by means of specially developed CFRP anchors. The following steps were followed to place the strips:

- Five holes were drilled at each corner on both sides of the frame as shown in Figure 3.20 (diameter = ½" and depth = 4").
- Loose concrete was removed.
- Epoxy putty filler was applied on the wall surface, to fill the mortar joints and to smoothen the blocks.
- A hand-held sanding machine was used to smoothen the putty.
- The surface was cleaned by blowing air and washing with water, and then left for drying.
- Epoxy resin coat was applied on the puttied surface.
- Each fiber sheet was saturated first with epoxy resin and placed on the surface. A final coat of epoxy was applied to finish the surface.
- A ribbed steel roller was used to remove the air pockets, while providing compaction and bleeding excess epoxy.
- During the FRP placement operation the holes that had been drilled for the anchors were protected by inserting circular wooden pieces, so that the holes

would not be filled up with epoxy. These wooden pieces were then removed after the FRP strips had dried.

- The FRP anchors were manufactured from a single layer of carbon fibers, 20 mm in width and 500 mm in length.
- The holes were saturated with epoxy resin.
- The anchors were saturated in epoxy resin and folded into and forced into the holes by a steel rod.
- The ends of the anchors were opened and glued on diagonal CFRP strips that had been placed on the wall by means of epoxy.

The fourth specimen with clay brick infills, labeled as BR-3, was intended to investigate the effect of the level of diagonal prestressing. It was retrofitted after testing BR-1 and BR-2 to assess the required level of diagonal prestressing for BR-3. Because the failure of BR-2 was triggered by column failure in the reinforced concrete frame, rather than the infill wall, the columns of BR-3 was first retrofitted with two layers of CFRP wrapping at column ends, covering 500 mm end regions. This is shown in Figure 3.21. The specimen was then retrofitted with diagonal prestressing, using the same size strands used in BR-2 (# 15 seven-wire strands). However, this time the external post-tension was increased to 125 kN per cable, resulting in a total prestressing force of 250 kN for each diagonal direction.

3.7 Material Properties

Ready mix concrete with 10 mm maximum aggregate size and 100 mm slump was used to cast the specimens. Two batches of concrete were used to cast the frames of four specimens. Batch # 1, with the mix design shown in Table 3.1, was used to cast the frames of Specimens BL-3 and BR-1. Batch # 2, with the mix design shown in Table 3.2, was used to cast the frames of Specimens BR-2 and BR-3. Standard cylinder tests were performed 14 days and 28 days after casting, as well as on the day of testing of frame–wall assemblies. The compressive strength values are also included in Tables 3.1 and 3.2, for Batches #1 and #2.

Compressive strength tests of masonry units and prisms were also conducted to establish the characteristics of walls. A total of 4 concrete block units were selected randomly for compression testing. Also, four concrete block prisms were prepared, each consisting of two blocks with "N" type mortar in the joint. Figure 3.15 illustrates the prisms. Similar compression tests were conducted for the masonry units and prisms. The compression test results are tabulated in Table 3.3 and 3.4.

The properties of reinforcing steel and strand were established by standard coupon tests. Coupons were prepared from deformed #15 bars that were used as longitudinal beam and column bars, smooth 6.35 mm diameter reinforcement used for column ties and beam stirrups and #15 strand used to retrofit the specimen. Tension tests were performed to establish the stress-strain characteristics of reinforcement. Figures 3.22, 3.23 and 3.24 illustrate the stress-strain relationships obtained from coupon tests.

The properties of FRP sheets were obtained from the manufacturer's specifications. Carbon fibers had 4275 MPa tensile strength and 380000 MPa elastic modulus, with linear stress-strain behaviour up to tensile rupturing. Table 3.5 provides the properties of the carbon fibers used in FRP sheets, from which strips were made to retrofit Specimen BL-3. The sheets contained uni-directional fibres.

3.8 Instrumentation and Test Setup

The specimens were secured on the laboratory strong floor by means of four high-strength bolts to ensure full fixity at the foundation level, prior to testing. Gravity loading was applied by means of external vertical prestressing as described in the previous section. A 1000 kN capacity MST hydraulic actuator was used to apply horizontal loading. The stroke capacity of the actuator was 500 mm, which allowed maximum horizontal displacements of 250 mm in the pushing and pulling directions. The hydraulic actuator was connected at one end to the steel plate and at the other end to a steel reaction frame. Two 1000 MPa strength Dywidag Prestressing bars were placed on each side of the top beam, running alongside, connecting two loading steel plates, one at each end.

These bars were used during the pulling load stage, while pushing was done against the steel end at the near side.

A light steel frame was fixed to the concrete foundation to mount the instrumentation. It was important to take the measurements relative to the foundation, rather than the laboratory strong floor to eliminate potential errors that might result from the slippage of the specimen as a whole. An MTS temposonic LVDT was used to measure lateral displacements at the centerline of the lateral load. A backup reading was taken through another LVDT, which was attached to the top beam. Electric resistance strain gauges were placed on reinforcement, as indicated in Fig. 3.8 to measure internal strains.

All the instrumentation, including the load cell and stroke LVDT's of the MTS actuator, was connected to a data acquisition system and MTS controller for data collection. The electrical-resistance strain gauges were also connected to the same data acquisition system.

3.9. Loading Program

Each specimen was loaded by gravity loads, as explained earlier, by means of external prestressing. This was done prior to the application of lateral deformation reversals to simulate dead and live loads on the frame. Lateral loading was applied in displacement control mode with three complete cycles at each deformation level. Lateral drift ratio was used as a measure of deformation level. Initial elastic loading was applied at 0.1 % lateral drift ratio, increasing by 0.1 % increments until 0.5 % drift ratio. After the drift ratio reached 0.5 %, the specimen was loaded in increments of 0.25 % drift ratio. The loading continued until failure occurred, which was indicated by a strength drop of 50% or more. The loading history is tabulated in Table 3.6.

Chapter 4

Test results and observed behavior

4.1 General

Test results and observed behavior of four infilled wall frames are presented in this chapter. The observations include the progression of damage in terms of changes in crack patterns and material failure. Recorded data are plotted in the form of lateral load-lateral displacement hysteretic relationships. The strain gauge data are also used to explain the observed behavior, including those measured on diagonal retrofitting cables and diagonal FRP strips. The following sections describe the details of specimen behavior.

4.2 Performance of Specimen BR-1 (Frame with unretrofitted brick wall)

BR-1 was the reference specimen that reflected a typical frame design in 1960's. The specimen was tested following the loading program described in Chapter 3. The hysteretic force-displacement relationship recorded during testing is plotted in Fig. 4.1 and the hysteretic strain-displacement relationships recorded during testing of all strain gauges are plotted in Fig. A1

No visible cracks were observed during the initial cycles between 0.1% and 0.4% drift ratios. The first flexural crack formed at the end of the top beam, near the loading end, during initial pushing to 0.5 % lateral drift ratio (10 mm). This is shown in Fig. 4.2. The longitudinal bottom beam reinforcement started yielding at the same load stage, near the loading end, developing strains of 0.00235 in Gauge # 21 and 0.0023 in Gauge # 23. Diagonal tension cracks appeared in the brick wall during the same load stage, as illustrated in Fig. 4.3. Similar cracks occurred at the other end of the beam, when the specimen was pulled to the same drift level in the opposite direction. Bottom beam

reinforcement developed yielding in the same region, attaining 0.00358 and 0.0033 strains in Gauges # 17 and # 19, respectively. This level of drift was attained at 301 kN and 247 kN of lateral loading in the push and pull modes, respectively. The specimen remained essentially intact without any serious damage, and continued resisting additional loads.

Additional flexural cracks were observed at the ends of the top beam during the 0.75 % lateral drift ratio (15 mm). The top steel at the end of the beam started to yield during the first pull towards 0.75 % drift ratio, giving strain readings of 0.00217 and 0.00207 in Gauges #22 and #24, respectively. The column longitudinal reinforcement started to yield near the top beam on the loading side, during initial pushing to 0.75 % drift ratio, reaching a strain of 0.0022 in Gauge # 27. The formation of diagonal tension cracks in the wall proceeded through the mortar joints, forming a zig zag crack pattern. This is shown in Fig. 4.4. The 0.75 % drift ratio was attained at 389 kN and 298 kN of lateral load during pushing and pulling, respectively. The frame and the wall remained intact with no serious sign of structural damage. The specimen continued carrying additional loads.

During the next deformation stage, the frame-wall assembly was forced to deform to 1.0 % lateral drift ratio (20 mm). The masonry wall started separating from the frame, near the top far end corner. The previous cracks became wider. This is shown in Fig. 4.5. Very thin diagonal tension cracks formed in the joint at the same corner and at the top of the column, as illustrated in Fig. 4.6. The frame and wall continued remaining intact, with no serious sign of structural damage, developing 406 kN and 327 kN load resistance during pushing and pulling, respectively. Fig. 4.7 shows the specimen at the end of 1.0% drift cycles. The column longitudinal reinforcement started yielding near the base, during pushing at 1% drift ratio, developing a strain of 0.00216 in Gauge # 7.

The specimen sustained relatively stable loops until 1.25 % drift ratio at 25 mm lateral displacement during pushing, and 1.75% during pulling, prior to developing significant strength decay. The maximum lateral load resistance was recorded at 1.25 % drift ratio

during pushing, and was equal to 412 kN. This value was 107 % of the calculated maximum lateral load resistance of 383 kN. The damage observed at this drift level is illustrated in Fig. 4.8. The main column reinforcement of the near end column started yielding at this stage of loading near the base, developing strains of 0.00234 and 0.00232 in Gauges #3 and #4, respectively. The yielding of main reinforcement was observed at additional locations, including top of the same column, with a strain value of 0.00224 in Gauge # 25. Steel yielding was also observed in top beam reinforcement at the far end, Strain Gauge # 18 showing a value of 0.0022. The bottom beam reinforcement also yielded at the same location when the specimen was pulled to 1.25 % drift ratio, showing load resistance of 345 kN. This was evident from Gauges #5 and # 6 with strain readings of 0.00216 and 0.00237, respectively. During the second cycle of 1.25 % drift ratio, new inclined cracks were formed in both columns near the bottom portions.

The load resistance showed a marginal drop when the specimen was first forced to 1.5 % drift ratio. The recorded load was 400 kN. The resistance remained approximately constant at 349 kN when it was pulled in the opposite direction. The previously formed crack near the top of far end column became wider as cover started spalling and exposing the longitudinal reinforcement. This is shown in Fig. 4.9. The damage observed at this stage of loading is illustrated in Fig. 4.10.

The load resistance reached near maximum values (about 400 kN) starting at 0.75 % drift cycles and remained approximately constant until the end of 1.5 % drift cycles during pushing. The specimen maintained approximately the same resistance between 1% and 1.75% drift cycles during pulling. Gradual stiffness decay was observed due to reversed cyclic loading, as evidenced by the reduced slopes of unloading and reloading branches. This was attributed to gradually increasing cracking, which resulted in the softening of the specimen. A rapid deterioration of strength was recorded beyond 1.5% drift in pushing and 1.75% drift in pulling, marking the deformation capacity of the wall.

When the lateral drift ratio reached 1.75 %, at 35 mm horizontal displacement, the inclined crack in the top damaged region of the far end column became wider and the

horizontal resistance dropped to 281 kN during pushing. However, the specimen maintained its capacity in the opposite direction, which was 333 kN (pulling). The specimen showed a significant reduction in lateral stiffness, at this stage of loading. The damage observed is illustrated in Fig. 4.11.

As the lateral drift ratio reached 2 % at 40 mm horizontal displacement, the column longitudinal reinforcement showed signs of buckling in compression and started bending. Some bricks started crushing under diagonal compression. The horizontal resistance dropped to 205 kN during pushing and to 303 kN during pulling. The specimen showed a significant reduction in its lateral stiffness. The damage observed at 2 % drift ratio is illustrated in Fig. 4.12.

The specimen was continued to be loaded beyond 2% drift ratio. As the lateral drift ratio reached 2.5 % at 50 mm horizontal displacement, some of the bricks on one side of the wall were damaged, and fell down, exposing the layer of bricks behind, which showed signs of out of plane failure. This is illustrated in Figs. 4.13 and 4.14. During this stage of loading, the longitudinal column reinforcement was bent significantly under compression. The strength of the specimen during pushing was reduced to 188 kN, which indicated more than 50 % drop in capacity. The specimen was considered to have failed at this stage. Another three cycles were applied at 3 % lateral drift ratio that corresponded to 60 mm horizontal displacement. The bricks in both layers almost completely fell down during this stage. The longitudinal column reinforcement buckled and the column ties opened up. A substantial drop in load resistance was observed. The horizontal load resistance dropped to 92.5 kN during pushing and 158 kN during pulling. The test was decided to be stopped. The damage observed at this stage of loading (end of testing) is illustrated in Figs. 4.15 and Fig. 4.16.

4.3 Performance of Specimen BR-2 (Frame-brick wall assembly retrofitted with cables)

BR-2 was a frame-wall assembly retrofitted by diagonal prestressing cables. The specimen was tested following the same loading program used in testing BR-1, as

described in Chapter 3. The hysteretic force-displacement relationship recorded during testing is plotted in Fig. 4.17 and shows a significant improvement in strength and inelastic deformability over BR-1. The hysteretic strain-displacement relationships recorded during testing of all strain gauges are plotted in Fig. A2

No visible cracks were observed during initial cycles between 0.1% and 0.3% drift ratio. A slight separation between the frame and the wall was observed at the far top corner of frame during initial pushing to 0.4 % lateral drift ratio (8 mm). The first flexural crack was observed during initial pushing to 0.5 % lateral drift ratio (10 mm) in the top beam, near the loading end. This is shown in Fig. 4.18. A similar flexural crack formed at the other end of the beam when the specimen was pulled to the same drift level in the opposite direction. This level of drift was attained under 431 kN and 326 kN lateral loads in the push and pull modes, respectively. The specimen remained essentially intact without any serious damage, and continued resisting additional loads.

During the next deformation level, the frame-wall assembly was forced to deform to 0.75% lateral drift ratio (15 mm). The first flexural crack in a column was observed during this load stage at the top of the column near the loading end. This is depicted in Fig. 4.19. The column longitudinal reinforcement started yielding at the same location, reaching a strain of 0.00201 in Gauge # 27. When the load was reversed to 0.75 % drift ratio in the opposite direction, the bottom beam reinforcement developed yielding at the far end, attaining 0.00208 and 0.00213 strains in Gauges # 17 and # 19, respectively. The diagonal tension crack was observed in the wall following the mortar joints. A close-up view of diagonal crack in the mortar joint is illustrated in Fig. 4.20. The bricks also developed some cracking near the vicinity of the diagonal cracks in mortar joints, as shown in Fig. 4.21. This level of drift ratio was attained at 530 kN and 442 kN lateral loads during pushing and pulling, respectively. The specimen maintained its complete integrity with no serious sign of structural damage. It continued carrying additional loads.

During 1.0 % lateral drift cycles at 20 mm horizontal displacement, more cracks formed within the top portion of the near-end column, while the existing cracks became wider. This is shown in Fig. 4.22. The column longitudinal reinforcement started yielding in the far end column, immediately below the top beam, reaching a strain of 0.00316 in Gauge # 26. Other cracks also appeared near the bottom of the same column, during the same drift level, as illustrated in Fig. 4.23. The column longitudinal reinforcement started yielding near the base during pushing to 1.0 % drift ratio, developing a strain of 0.00227 in Gauge # 4. The bottom beam reinforcement started yielding at the far end, giving a strain reading of 0.00209 in Gauge # 23. When the load was reversed to 1.0 % lateral drift in the opposite direction, the column longitudinal reinforcement started yielding near column base at the loading side, developing a strain 0.00205 in Gauge # 5. The diagonal prestressing cable became loose at this level of drift, as shown in Fig. 4.24. Both the frame and the wall remained intact, with no serious sign of structural damage. This level of drift was attained at 678 kN and 560 kN lateral loads in the push and pull modes, respectively.

Increased deterioration occurred in the columns as cycles of 1.25% drift ratio were applied. More cracks appeared at the bottom of the far end column, accompanied by additional steel yielding. The strain values recorded in this column reached -0.0021 and 0.0055 in Gauges # 1 and # 3, respectively. Reversal of the load at 1.25 % lateral drift ratio resulted in additional steel yielding in the opposite columns, the strain values reaching 0.00294, 0.00232 and - 0.00248 in Gauges #2 , # 6 and #7, respectively. This loading also resulted in the yielding of additional column reinforcement immediately underneath the top beam, developing a strain of 0.00224 in Gauge # 25. Also yielding at this stage was the top beam reinforcement at the far end, developing a strain of 0.0022 in Gauge # 18.

The specimen developed its peak load resistance of 746 kN at 1.25 % drift ratio, corresponding to 25 mm lateral displacement during pushing. This value was equal to approximately 107.2 % of the calculated maximum lateral load resistance of 696 kN. The force resistance of retrofitted specimen improved over the unretrofitted control specimen,

sustaining 1.81 times the lateral load resistance of BR-1 (746/412). The average strain value on diagonal prestressed cable was measured to be 7270 micro strain, which occurred at a lateral drift ratio 1.25 % while pushing. The specimen sustained somewhat lower resistance when pulled, developing 644 kN of resistance at 1.25 % drift ratio. It maintained its integrity without a sign of major structural distress, as shown in Fig. 4.25.

The amount of cracks significantly increased during 1.5 % drift cycles at 30 mm horizontal displacement. The cracks in the bottom far side column became wider and the cover started spalling and exposing column ties. Also, the diagonal cracks in the bricks became wider. This is shown in Fig. 4.26. Similarly increased cracking was observed in the column on the loading side as shown in Fig. 4.27. Some strength drop was observed at this stage of loading, reducing to 586 kN. This was attributed to the onset of the failure of the frame-wall assembly, as observed in the companion control specimen. However, the effect of the prestressing cable became clear at this stage of loading and the load resistance stabilized, with continued dissipation of energy up to 2.0% drift ratio. The specimen experienced little strength decay when pulled to the opposite direction with a load resistance of 622 kN. Column spalling increased at 1.75 % drift ratio at 35 mm horizontal displacement, exposing longitudinal column reinforcement. Also, some pieces of brick started to crush and fell down. This is shown in Fig. 4.28. The column steel yielded at this stage of loading near the loading side of the top beam, developing a strain of 0.0045 in Gauge # 28. A further marginal strength decay was observed to 535 kN and 414 kN in the push and pull modes, respectively.

As the lateral drift ratio reached 2 % at 40 mm horizontal displacement, the column longitudinal reinforcement showed signs of buckling in compression and started to bend. Some bricks started falling down, and the horizontal resistance dropped to 473 kN during pushing and 550 kN during pulling. The specimen was continued to be loaded beyond 2 % drift ratio. As the lateral drift ratio reached 3.0 % at 60 mm horizontal displacement, the resistance of the specimen started to increase, reaching 527 kN during pushing. This increase was attributed to the contribution of diagonal prestressing cables, which developed higher tension as the specimen drifted horizontally, extending the cable. In the

opposite direction, however, the load continued dropping, though very slowly, reaching 484 kN. The test was stopped having reached 3% lateral drift, as the prestressing strands were stressed to 9580 and 9568 microstrains in pushing and pulling respectively.

4.4 Performance of Specimen BR-3 (With FRP wrapped columns and retrofitted frame-brick wall assembly with Cables)

Specimen BR-3 consisted of a seismically deficient reinforced concrete frame and a brick masonry infill wall, retrofitted with diagonal prestressing cables. The columns were retrofitted by wrapping two layers of carbon FRP sheets at top and bottom ends. This was found necessary in view of the observed performance of BR-2. The prestressing cables were positioned diagonally and prestressed to 125 kN, each. The specimen was tested following the loading program described in Chapter 3. The hysteretic force-displacement relationship recorded during testing is plotted in Fig. 4.29. The hysteretic strain-displacement relationships recorded during testing of all strain gauges are plotted in Fig. A3

Test observations indicated no visible cracks during the initial cycles at 0.1% and 0.2% lateral drift ratios. A very thin separation crack formed between the column and the wall at the top far-end corner during the first cycle (pushing) of 0.3 % lateral drift ratio at 6 mm displacement. This is shown in Fig. 4.30. This level of drift was attained at 404 kN and 406 kN of lateral loading in the push and pull modes, respectively. The specimen remained essentially intact, without any serious damage, and continued resisting additional loads.

No further damage was observed at 0.4 % lateral drift cycles at 8 mm displacement. During the cycles of 0.5 % lateral drift ratio (10 mm), diagonal tension cracks in the wall were formed and proceeded through the mortar joints, forming a zig zag crack pattern. This is shown in Fig. 4.31. Separation between the other column and the wall occurred during the first pull cycle at 0.5 % drift ratio. This level of drift was attained at 488 kN and 415 kN of lateral loading in the push and pull modes, respectively. The specimen

remained essentially intact, without any serious damage as shown in Fig, 4.32. The specimen continued resisting additional loads.

During the next deformation stage, the frame-wall assembly was forced to deform to 0.75 % lateral drift ratio (15 mm). More cracks appeared during this stage. Vertical flexural cracks formed at the loading end of the beam, during initial pushing, as previously formed cracks have become wider. This is illustrated in Fig. 4.33. The column on the loading side indicated the yielding of longitudinal reinforcement near the top beam, developing a strain of 0.00275 in Gauge # 27. The bottom beam reinforcement also started yielding during the first pull towards 0.75 % drift ratio, giving strain readings of 0.00208 and 0.00202 in Gauge # 17 and # 19, respectively. This was accompanied with yielding of reinforcement in the far end column, near the top beam, developing a strain of 0.00211 in Gauge # 26. The specimen remained intact during this stage of loading, without any significant damage. This level of drift was attained at 641 kN and 613 kN of lateral loading in the push and pull modes, respectively.

When all specimens were loaded to 1.0 % lateral drift (10mm), the previous cracks all become wider. This is shown in Figs. 4.34 and 4.35. The column longitudinal reinforcement started yielding also near the base in both columns, developing strains of 0.00218 and 0.0022 in Gauges # 7 and # 3, respectively during the initial push to 1.0% drift. Similar yielding was initiated in other column re-bars as the load was reversed, developing strains of 0.00207 and 0.00207 in Gauges #5 and #1, respectively. The specimen sustained relatively stable loops during 1.0 % drift cycles prior to developing a sudden failure when forced to deform towards 1.25% lateral drift. The maximum load resistance at 1.0 % drift ratio was 715 kN. This is equal to 92.4 % of the calculated maximum lateral load resistance of 774 kN. The load resistance improved due to retrofitting, and reached to 1.74 times the resistance attained in unretrofitted BR-1 (715/412). The average maximum strain in diagonal prestressing cable was attained at this stage of loading, and was measured to be 8095 micro strains. The specimen sustained somewhat lower resistance when pulled to 1% drift, developing 675 kN of resistance. Unlike the unretrofitted specimen, the stiffness remained unchanged during these cycles,

as evidenced by the slopes of unloading and reloading branches of hysteresis loops. This was attributed to effect of relatively high prestressing imposed on the specimen which resulted in the closing of cracks, maintaining approximately the uncracked stiffness.

During the first push cycle at 1.25 % drift ratio (25 mm), a diagonal crack was formed at mid-height of the column near the loading side. This was a sudden shear crack and resulted in a drastic drop in load resistance, marking the failure of the specimen. This is illustrated in Fig. 4.36. It was clear that, retrofitting improved lateral load capacity, with little stiffness degradation, which imposed higher shear forces on the columns. The column end regions were well protected against shear failure by FRP jackets, which shifted the column critical region to the mid-height region. The specimen was left for further repair, retrofit and re-testing.

4.5 Performance of Specimen BL-3 (Frame-block wall assembly retrofitted with diagonal FRP sheet strips)

BL-3 was companion to a control specimen that was tested in an earlier phase of the same investigation by Serrato (2002), except retrofitted by diagonal FRP Sheets. The specimen was tested following the loading program described in Chapter 3. The hysteretic force-displacement relationship recorded during testing is plotted in Fig. 4.37. The figure also shows the envelope curve of the unretrofitted control specimen with otherwise identical properties, tested by Serrato (2002). The hysteretic strain-displacement relationships recorded during testing of all strain gauges are plotted in Fig. A4

Test observations indicated no visible cracking during the initial cycles at 0.1% and 0.3% drift ratios. Some noise was heard during these initial load applications, indicating signs of local stretching and possible debonding from the blocks. However there was no sign of damage. The lateral drift of 0.3% was attained at 558 kN and 278 kN of loading in the push and pull modes, respectively. The specimen remained essentially intact, without any serious damage, and continued resisting additional loads.

The first horizontal flexural crack formed in the column on loading side when the specimen was loaded to 0.4% lateral drift (8 mm) on the push side. This is shown in Fig. 4.38. The column longitudinal reinforcement started yielding near the top beam, on the loading side, during pushing to 0.4 % drift ratio, developing a strain of 0.002236 in Gauge # 27. The formation of diagonal tension cracks in the wall was observed, proceeding through the mortar joints, forming a zig zag crack pattern. This is shown in Fig.4.39. Some local separation of fibers from each other was observed along the longitudinal direction, as the strips were stretched and tried aligning themselves. This occurred in the central region of the wall, as shown in Fig. 4.40. The FRP strips in compression showed signs of buckling, as the sheets displayed clear bulging and out-of-plane bending, as shown in Fig.4.41. This level of drift was attained at 632 kN and 272 kN of load resistance in the push and pull modes, respectively. The specimen remained essentially intact, without any serious damage, and continued resisting additional loads.

When the lateral drift ratio reached 0.5 %, at 10 mm horizontal displacement, additional buckling and bending of the compression strips were observed. This is illustrated in Fig. 4.42. A horizontal crack appeared in the wall central region, along the mortar joint, which continued through the FRP strips, as evidenced by the distortion displayed in the FRP, as shown in Fig. 4.43. A crack was formed between the wall and the far-end column near the top corner, separating the wall from the frame. This crack propagated towards the FRP strip, causing it to tear on one side, resulting in fiber rupturing due to shear. This was, however a localized FRP rupture, and the strip continued developing tension. The FRP anchors were in tack, maintaining anchorage of the FRP strip to the concrete frame. The top beam reinforcement developed compression yielding, as indicated by a strain reading of -0.00205 in Gauge # 24. The frame and wall remained intact, with no serious sign of structural damage. This level of drift was attained at 623 kN and 312 kN of lateral load resistance in the push and pull modes, respectively.

When the lateral drift ratio reached 0.75 % at 15 mm horizontal displacement, the columns and the block wall clearly separated. This is illustrated in Fig. 4.44. The cracks ruptured fibers at the frame corners and the longitudinal separation of fibers from each

other became clear as shown in Figs. 4.45 and 4.46. The longitudinal reinforcement started yielding near the base in both columns, developing strains of 0.00204 and 0.00207 in Gauges #7 and #3, respectively. During the push phase, the bottom beam reinforcement at the loading end started yielding, developing strains of 0.00259 and 0.00218 in Gauges # 21 and # 23, respectively. The specimen experienced strength degradation starting with the second cycle of 0.75% drift during pushing and 1.0% drift during pulling. The maximum lateral load resistance occurred at 0.75 % lateral drift ratio during pushing, and was equal to 659 kN. This value was equal to 97 % of the calculated maximum lateral load resistance of 682 kN. The improvement in load resistance due to retrofitting resulted in 2.41 times the lateral load resistance recorded in unretrofitted specimen (659/273). The maximum strain on FRP occurred when the maximum load resistance of the specimen was attained and was measured to be 5302 micro strains, at the centre of the bottom corner of the FRP strip. The specimen sustained somewhat lower resistance when pulled, developing 424 kN of resistance at 1.0 % drift ratio. This was attributed to the fact that the first load exertion at each deformation level was always by pushing, and the specimen was already damaged when it was pulled.

When the specimen was forced to deform to 1.0 % lateral drift ratio (20 mm), the amount of cracking increased significantly. Increased shear and flexural cracks were observed in the column closer to the applied load. This is shown in Figs. 4.47 and 4.48. During the first reversal of load at 1.0 % drift, the reinforcement in far-end column started yielding near the base, developing a strain of 0.00212 in Gauges # 4. The longitudinal reinforcement of the same column also showed yielding at the top, near the top beam, reaching a strain of 0.00231 in Gauge # 25. The separation between the column and the infill wall became more pronounced as shown in Fig. 4.49. The horizontal resistance of the structure decayed beyond 1% drift, at a faster rate during pushing than pulling. This level of drift was attained at 559 kN and 424 kN in the push and pull modes, respectively.

During the cycles of stable load resistance, gradual stiffness decay was observed under reversed cyclic loading, as evidenced by the reduced slopes of unloading and reloading slopes. This was attributed to gradually increasing cracking which resulted in the

softening of the specimen. A rapid deterioration of strength was recorded beyond 1.0% drift in pushing and 1.25% drift in pulling, making the deformation capacity of the wall.

When the lateral drift ratio reached 1.25 % at 25 mm horizontal displacement, the shear cracks and the separation between the column and the infill wall became wide. These are shown in Fig. 4.50 and Fig. 4.51. The horizontal resistance of the structure dropped down to 469 kN and 384 kN during pushing and pulling, respectively.

The specimen was continued to be loaded beyond 1.25 % drift ratio. As the lateral drift ratio reached 1.75 % at 35 mm horizontal displacement, the longitudinal column bars started to bend, showing signs of buckling. The column ties opened and the cover concrete spalled off. These are illustrated in Figs. 4.52 and 4.53. The fiber anchors ruptured at this stage of loading and the separation between the column and the infill wall became wider. This is shown in Fig.4.54. When the resistance of the structure dropped below 50 % of the maximum load resistance, the test was stopped at 275 kN and 305 kN in the push and modes, respectively.

Chapter 5

Analytical research

5.1 General

This Chapter presents the details of analytical research on masonry infilled reinforced concrete frame structures, under seismic loading. It consists of two main tasks:

- Modeling and static inelastic (Push-over) analysis of all four test specimens, and comparisons with experimental data.
- Modeling and inelastic analysis of a 5-storey frame building, designed on the basis of NBCC-2005, under incrementally increasing static lateral loading.
- Modeling and dynamic inelastic analysis of the same 5-storey frame building under a selected earthquake record.

All analyses were conducted using computer software "DRAIN-RC." (Saatcioglu et al. 1997)

5.2 Program DRAIN-RC

Computer program DRAIN R/C is a modified version of the well established program DRAIN-2D developed at the University of California, Berkeley by Kanaan and Powell (1973). DRAIN-2D is a general purpose computer program for dynamic inelastic analysis of two dimensional structures under earthquake motions. It performs step-by-step- linear acceleration numerical integration for dynamic analysis. The stiffness matrix is assembled by following the stiffness method of analysis. The program includes five different types of elements, consisting of; i) beam-column element, ii) beam element with perfectly elasto-plastic hysteretic model, iii) truss element, iv) semi-rigid connection element and v) shear panel element, representing infill panels. Later, the

program was modified by Powell (1975) to introduce a reinforced concrete beam element with degrading stiffness characteristics. Inelasticity was introduced by hinges placed at member ends. The moment-rotation relationship for each hinge is based on the extended version of Takeda's model. In 1993 the computer program was modified by Alsiwat at the University of Ottawa. The reinforced concrete element was modeled as an elastic line element having three inelastic springs at each end to account for inelasticity due to flexural, anchorage slip and shear, as outlined below:

1. **Flexural Modeling**: Each beam element was modeled as an elastic line element with an inelastic flexural spring at each end to simulate plastic hinging. The Takeda model was assigned to each spring to account for flexural hysteretic behavior of reinforced concrete elements, as illustrated in Fig. 5.1(a).
2. **Anchorage Slip Modeling**: Inelastic behavior of extension and/or slippage of anchored reinforcement in adjoining members were modeled by adding an additional spring at each end of a member, and assigning a hysteretic model. The hysteretic model was created by Saatcioglu, Alsiwat and Ozcebe (1992). The primary force- anchorage slip relationship was modeled by integrating steel strains within the embedment length of reinforcement (Alsiwat and Saatcioglu, 1992). This model is shown in Fig. 5.1(b).
3. **Shear Modeling**: Each beam element was modeled to have an elastic line element and two inelastic shear springs, one at each end of the beam. The hysteretic shear model consists of a tri-linear primary curve with break points at cracking and yielding. The model was developed by Ozcebe and Saatcioglu (1989), and is shown in Fig. 5.1(c).

Further modifications were introduced to the program by Shooshtari (1998). He removed those elements that are not relevant to reinforced concrete structures and named the modified program DRAIN-RC. The modifications introduced include the following additional features:

1. **Pushover Analysis**: Incremental static inelastic analysis capability was introduced to the program.
2. **Secondary Moment Effect**: Secondary moments due to P-Δ effects were introduced to the program.

3. **Axial Force-Moment Interaction Model**: The effect of P-M interaction on strength and stiffness of reinforced concrete members was introduced by incorporating the hysteretic model developed by Saatcioglu et al. (1983).
4. **Infill Walls Elements**: The effect of infill walls was introduced by incorporating the hysteretic model that was developed by Klingner and Berero (1978).

Further details of computer software DRAIN-RC can be found elsewhere (Saatcioglu et al. 1997).

5.3 Analysis of Test Specimens

Static inelastic (pushover) analyses were conducted using computer software DRAIN-RC to verify the analysis techniques against test data. The analyses included all four walls tested, with and without retrofitting. The following are the basic features of the test specimens analyzed.

- Unretrofitted frame-brick infill wall specimen (BR-1)
- Frame-brick infill wall specimen (BR-2) retrofitted by diagonal prestressing with an initial prestressing force of f_{pi} =75 kN.
- Frame-brick infill wall specimen (BR-3) retrofitted by diagonal prestressing with an initial prestressing force of f_{pi} =125 kN.
- Frame-concrete block wall specimen (BL-3), retrofitted by diagonal strips of CFRP sheets.

5.3.1 Modeling of Test Specimens

The specimens consist of a single bay reinforced concrete frame and an infill wall. The frame elements were modeled as line elements with appropriate geometric and stiffness properties. The infill wall element was modeled with two diagonal elements, each representing struts and ties that develop under reversed cyclic loading. The retrofitted specimens had an additional diagonal element, either in the form of a cable tie or an FRP

strip tie. Figure 5.2 illustrates the analytical models used for push-over analysis of test specimens.

The frame elements had flexural rigidities (EI) specified for columns and the beam, reduced 50% to allow for softening due to cracking. Shear modulus G was computed through the relationship between G, E and the Poisson's ratio μ. Flexural yield moments were computed based on sectional and material properties, as well as the accompanying levels of axial load. Flexural yielding and post-elastic behavior was incorporated through Takeda's hysteretic model, already built into the software DRAIN-RC.

The masonry walls were modeled using diagonal struts. Diagonal tension resistance of infill walls was neglected. The struts were modeled with truss elements, with elastic modulus E, and the effective area of masonry strut A. The modulus of elasticity of masonry E_m was calculated as suggested by Hamid et al (1987) and Grimm et al (1984), as indicated below.

$$E_m = k f'_m \qquad 5.1$$

Where f'_m is the compressive strength of masonry, and k is a coefficient equal to 750 for concrete block, and 500 for clay brick.

The effective strut width was taken as 25% of the diagonal wall length, as suggested by Priestley and Paulay (1992). The researchers also reported that the capacity of diagonal infill masonry struts is governed by the sliding shear resistance of wall, which occurs prior to the crushing of struts. The equation suggested for wall capacity, associated with sliding shear, is described in Chapter 3. This equation was used to compute the diagonal force capacity as governed by sliding shear. This level of compressive strut force was used to define the wall capacity and assigned to the bi-linear strut (truss) element as yield resistance. The post-yield behavior of the truss element (representing the infill wall) was specified to have a zero slope, without any strain hardening.

The behavior of prestressing cables was modeled with diagonal truss elements that could resist tension only. One truss element along each diagonal was used to specify the initial tension due to prestressing. This allowed further tensioning of the element in the direction of diagonal tension tie, under increasing lateral deflection, and reduction in initial prestressing in the opposite diagonal, parallel to the wall strut. The cable strength and post-yield slope of the axial tension-axial deformation relationship was established by a coupon test and bilinear idealization of this relationship. Accordingly, 5.7 % of the cable's elastic modulus was specified as strain hardening beyond yielding.

The FRP strips, produced from FRP sheets, were modeled as diagonal truss elements that could resist tension only. Any potential contribution of FRP strip to the enhancement of wall struts was neglected. The FRP strip width was taken equal to the actual width used in the test. The strain gauges placed across the width showed some variation of strains, with a maximum value taking place in the central portion of the strip, and reductions towards the edges. An average stress value of $0.85f_{FRP}$ was deemed appropriate in specifying the tensile capacity of FRP strips. The tensile strength of FRP (f_{FRP}) was established by a coupon test and was equal to 700 MPa. Linear elastic stress-strain relationship was used for the FRP strips. During loading, however, the FRP tensile capacity was not reached prior to the failure of frame and infill wall. This was consistent with experimental observations.

5.3.2 Analysis Results and Comparisons with Experimental Data

The result of static inelastic (push over) analyses for the four frame-infilled wall assemblies are show in Figs. 5.3 through 5.6 in the form of primary force-displacement relationships. These curves are superimposed on experimentally recorded hysteretic relationships for easy comparison.

The results shown in Fig.5.3 indicate that the analytical force-displacement relationship agrees very well with that recorded during testing for the unretrofitted specimen with brick masonry wall. The experimental strength value of 412 kN and corresponding lateral drift ratio of 1.25 % were both in close agreement with analysis results. Both the strength

and stiffness values exhibited good agreement, verifying the validity of the analytical approach taken.

Figure 5.4 shows the comparison of analytical and experimental force-displacement relationships for specimen BR-2. This frame-wall assembly was retrofitted with prestressing cables, each having an initial prestressing force of F_i = 75 kN. Similarly good agreement was obtained between the analytical and experimental results, as before. The experimental strength value of 746 kN and the corresponding lateral drift ratio of 1.25 % were both in close agreement with those computed analytically. Both the strength and stiffness values obtained were in good agreement, verifying the validity of the approach taken for a case that involves initial prestressing.

Figure 5.5 shows the comparison of analytical and experimental results for specimen BR-3, which was companion to BR-2 except for the level of initial prestressing. The initial prestressing in this specimen was increased to F_i = 125 kN (from 75kN used earlier). This specimen developed its capacity at 1.0 % lateral drift ratio, at a lateral force of 715 kN, when it failed suddenly due to shear in one of the columns. The specimen had FRP jackets at the ends of the columns to prevent the column failure observed in BR-2. Specimen BR-2 had suffered from the hinging of columns at their ends and the failure was gradual. However, the failure in BR-3 was abrupt and caused by diagonal tension in one of the columns between the retrofitted end regions. The test was terminated when the column failed due to shear. The analysis did not consider shear failure in columns, and hence showed continued deformability. However, the maximum load resistance and the initial stiffness agreed well with those recorded experimentally.

Figure 5.6 shows the comparison of analysis results with experimental hysteretic curve for specimen BL-3, which was retrofitted with CFRP strips. This specimen had concrete block masonry as the infill wall. The experimental strength value was 659 kN, occurring at 0.75% lateral drift ratio. These values agreed fairly well with analysis results. However, the initial stiffness was underestimated analytically perhaps because the effect of FRP sheets along the compression strut was neglected. Furthermore, the FRP sheets resulted in

crack control, which was neglected in the analysis. However, the overall strength in the first loading direction showed good agreement.

5.4 Applications to Practice

The seismic retrofit technologies developed in the experimental phase of research was extended to investigate their applicability in practice. Having verified the analysis tool, DRAIN-RC, and element modeling by reproducing experimentally recorded force-deformation relationships analytically as described earlier in this Chapter, the next task involved the application of diagonal prestressing and diagonal FRP strips to a selected reinforced concrete frame building. This task consisted of the selection of a 5-storey reinforced concrete frame building designed for Vancouver, Canada, and the analysis of the building under different retrofit schemes to conduct an analytical parametric investigation. The analyses consisted of i) static inelastic pushover analysis of the frame with different levels of diagonal prestressing and different amounts of strands, ii) dynamic inelastic analysis of the frame with different diagonal prestressing parameters, iii) static inelastic pushover analysis of the frame retrofitted with diagonal FRP strips, and iv) dynamic inelastic analysis of the frame retrofitted with diagonal FRP strips. This Chapter provides the description of the building selected, and the analyses conducted, with analytical conclusions drawn for practical applications.

5.4.1 Selection of the structure

A 5-storey reinforced concrete frame building, designed on the basis of the National Building Code of Canada (NBCC 2005) for Vancouver, was selected for analysis. A typical floor plan and the elevation of the building are illustrated in Fig. 5.7. The floor plan was selected to be symmetrical to eliminate the effects of torsion. The building was designed, following the base shear expression given below.

$$V = \{S(T_a)\, M_v\, I\, W\}/\{R_d R_0\} \qquad 5.2$$

Where;

T_a : Fundamental period

S (T_a) : The design spectral response acceleration, as a ratio to gravitational acceleration, for the fundamental lateral period of building T_a

M_v : Higher mode effect factor

I : important factor

W : Dead load of structure

R_d : Ductility related force modification factor

R_0 : Over strength related force modification factor

The product $S(T_a)$ M_v I W represents the elastic base shear in NBCC 2005. The fundamental period T_a, for calculating the base shear was computed using the code recommended empirical expression. This expression is shown below for a concrete frame building:

$$T = 0.075\ (h)^{0.75} \qquad 5.3$$

Where; h: total high of reinforced concrete structure

The base shear, computed as described above, was distributed along the height of the structure, following the inverted triangular force distribution recommended by NBCC-2005. The soil type for the current study was selected as very dense soil and soft rock (Site Class C). The calculated base shear was 2070 kN and was rounded to 2000 kN

The structure was then modeled and analyzed under the design seismic forces to compute design shear forces, bending moments and axial forces to proportion the structural elements. The design data are and sectional characteristics of the frame elements are presented in Table 5.1 and Table 5.2.

The objective of the current research project is to develop seismic retrofit technologies for existing, and mostly older buildings that were designed in the past. Therefore, the

design was empirically modified to simulate an old building that was constructed in 1970s. A review of design base shear requirements in 1970 and 2005 editions of NBCC revealed that seismic force requirement has increased by factor of 3.0 between 1970 and 2005. Therefore, flexural capacities of frame elements were reduced by 3.0. The resulting building was clearly an old, seismically deficient and yet realistically designed frame building to be used in the parametric investigation.

5.4.2 Modelling of the structure

Consideration of the entire building for analysis involves 3-dimensional space frames. Some computer software has the capability of conducting three dimensional analyses. However, often building frames are analyzed as 2-dimensional plane frames in two orthogonal directions, separately and independently. This requires the modelling of structures in two orthogonal directions. Computer program DRAIN-RC is intended for planar analysis of structures, either under static inelastic pushover loading or dynamic inelastic earthquake excitations. Therefore, the three-dimensional structure should be modeled as series of two dimensional frames linked together to reflect the stiffness and strength of the entire structure in each direction. The selected building consists of four interior frames and two exterior frames with three bays in the short direction. Due to the rigidity of the slab diaphragm, each frame was assumed to have the same horizontal displacement. This was ensured by using rigid beam elements with infinite axial rigidity and very small flexural rigidity. These elements only allow the transfer of lateral forces from one frame to the other without any transfer of moment between the frames.

The structure to be modeled consists of four interior and two exterior frames. The frames with the same characteristics can be lumped together in order to simplify the analysis. This indicates that the frame under consideration can be modeled by two frames, one representing four interior frames (with four times the strength and stiffness of individual frames) and the other representing two exterior frames (with two times the strength and stiffness of individual frames), linked with rigid links. This is illustrated in Fig. 5.8. The stiffness properties of each elastic element can be found by using the principles of

mechanics. The strength of each member is specified by assigning cracking moment, yield moment and shear yield force assigned to appropriate inelastic springs. Modelling of loading, unloading and reloading stiffnesses for flexure, anchorage slip and shear during inelastic load reversals is done through hysteretic models. The hysteretic models assigned to member end springs consist of primary elastic force-deformation relationships, which describe the stiffness and strength boundaries and rules describing post-yield stiffness variations. Only the primary curves for force-deformation relationships for different components of member deformations need to be calculated. Element properties during the other phases of loading are computed by the rules of the hysteretic models assigned.

While inelastic static pushover analysis requires the input of forces incrementally, dynamic analysis requires the input of ground motion in terms of ground accelerations. This data is used along with structural mass to compute dynamic response, following the step-by-step linear acceleration method. Therefore, the structural mass needs to be specified. This is done by assigning the storey mass to one of the nodes at that floor level.

5.4.3 Selection of ground motion records

Dynamic analysis of the building was carried out using the most recent Canadian seismic data provided by the Geological Survey Canada . It was proposed to use earthquake records with 2% probability of exceedance in 50 years for design purposes (NBCC-2005). Artificial earthquake records generated by Adam et al.. compatible with the uniform hazard spectra of NBCC-2005, were used in the analysis. Eight artificial earthquake records were generated for long and short period ranges, as shown in Figs. 5.9(a) and 5.9(b). The records were based on M (magnitude) 7.2 and M 6.5 for long and short period hazards with hypocentral distances of 70 km and 30 km, respectively. These two scenario events represented only the hazard due to crustal and subcrustal earthquakes and did not include the hazard due to the great future earthquake along the Casacdia subduction zone. Therefore, additional four earthquake records on the Cascadia subduction zone were simulated with a magnitude M 8.5, as illustrated in Fig. 5.9(c). All of the twelve artificial

earthquake records were used to analyze the building in Vancouver. The lateral drift envelope for each case is illustrated in Fig. 5.10. It was then decided to continue further analysis with the most critical record, which was the Short Event No: 2. This was done for the analysis of retrofitted structures, even though it was recognized that the change in stiffness due to retrofitting could result in the shortening of the period, which could interact with the frequency characteristics of the ground motion.

5. 4.4 Retrofitting by diagonal prestressing

The effect of diagonal prestressing as a seismic retrofit strategy was invenstigated analytically by first conducting static inelastic pushover analyses, followed by dynamic inelastic analyses. The analyses were conducted for different levels of prestressing, different amounts of prestressing strands and different locations (bays) of prestressing. This resulted in an analytical parametric investigation, providing guidelines for practical applications.

5.4.4.1 Static inelastic pushover analysis

The 5-storey frame building was retrofitted diagonally within the interior bay of both exterior frames (one of the lumped frame representing the exterior frames in the model). Figure 5.11 illustrates the arrangement of prestressing cables schematically. Each diagonal cable shown in the figure is either stress free (non-prestressed) initially or prestressed to different levels, as per the parametric investigation. During resistance to lateral loading, the stress in one cable would increase due to diagonal tension, and the other in the opposite diagonal would decrease due to diagonal compression, and could become stress free (loose). This was modeled by considering a truss element. The truss element was capable of introducing tension yielding through a bilinear primary curve, with post-yield strain hardening. The characteristics of the force-deformation relationship was given such that the elastic rigidity was equal to the EA of steel cable, followed by a post yield rigidity equal to 5.7% of elastic EA to match the experimental stress-strain relationship for steel strand, which was tested in the Structures Laboratory of the

University of Ottawa. On the compression side, the truss element could model buckling of the cable, with zero load resistance in compression.

The static load was applied on the structure incrementally. The distribution of total base shear was consistent with the requirements of NBCC-2005, following an inverted triangular distribution consistent with the first mode response. The base shear computed corresponded to the current NBCC level for Vancouver. However, to simulate an existing seismically deficient building to be retrofitted, the resistance of each member was reduced by a factor of 3.0. This was found to be the approximate ratio between the current design force level and that required by NBCC in 1970s. The resulting frame building was therefore seismically deficient and did develop yielding and subsequent collapse, prior to reaching the current design force level. However, retrofitted structures were able to provide resistance to design base shear, with varying degree of deformation demands. The presence of masonry walls was neglected in this part of the analysis.

The model and the analysis, as described above, were used to conduct an analytical parametric investigation, as outlined below.

Effect of the Level of Prestressing

The effect of the level of prestressing was first investigated by considering two 15 mm (nominal) diameter 7-wire strands in each of the diagonal on either side, resulting in a total of 8 strands, four in each diagonal direction. The strands used were the same size as those used in the experimental program with a total area of 4*140 mm^2 = 560 mm^2 in each diagonal. The cables were either left snug tight (without any prestressing) or prestressed to 100 kN tension each (approximately 40% of the ultimate strand capacity). The structure was loaded up to the level of base shear required by NBCC-2005. The load-drift and load-inter storey drift relationships are shown in Figs. 5.12 and 5.13. The results indicate that the unretrofitted building developed a total base shear resistance of approximately 1200 kN at 5% drift ratio, which is about 40 % below the NBCC-2005 force level. Retrofitting with diagonal strands improved load resistance substantially and the building was able to resist the total base shear of 2000 kN by developing 2% to 2.5%

drift ratios at the first to fifth floors, respectively. The effect of prestressing the cables improved initial stiffness, with reduced lateral drift, though the load resistance was approximately the same at peak drift ratio. A similar observation is made on force-inter storey drift relationships. The first storey drift ratio was about 2.5% for the retrofitted structures, which was reduced gradually for upper stories, developing about 1% drift at the roof level.

Further investigation of the effect of prestressing was conducted by considering four 7-wire strands on each side of the building in each direction, resulting in a total of 16 strands per floor. The same size strands as those used in the experimental program (15 mm nominal diameter 7-wire strands) were used with a total area of 8*140 mm^2 = 1120 mm^2 in each diagonal direction resisting tension. The increased amount of strands was used for increased load resistance. This amount of steel (1120 mm^2 of steel area in each direction) could be provided with fewer larger size strands. Seven different levels of prestressing were considered, starting with zero (non-prestressed) and increasing to 25, 50, 75, 100, 125 and 150 kN per strand, corresponding to approximately 0% 10%, 20%, 30%, 40%, 50% and 60% of the ultimate strand strength of 1860 MPa, respectively. The ultimate strength value given by the manufacturer matched very closely to that observed during coupon tests, as depicted in Chapter 3.

Figure 5.14 shows the force-lateral drift ratio relationship for selected analyses at the roof level. The unretrofitted frame developed approximately 1400 kN of resistance at 5% lateral drift, with a clear yield point at about 1% drift ratio. At the same drift level, retrofitted structures showed approximately 3700 kN to 4000 kN resistance, indicating about 2.5 to 3.0 times improvement in load resistance. This level of improvement was sufficient to bring the load resistance up to twice the current design force level, as per NBCC-2005.

It is important to have a closer look at the results, in view of the hysteretic models used and the reinforcement detailing that one would expect in a seismically deficient building. The hysteretic model used in the analysis, though simulated basic stiffness degrading

characteristics of reinforced concrete, did not incorporate strength degradation. Typically, non-seismic reinforced concrete frames can only develop about 1% drift if longitudinal splicing is done in the column critical region at the end, as was the case in the test specimens, and 2% drift when there was no splice deficiency but lack of concrete confinement. Hence, 5% drift at which the load comparison is made is not likely to be achieved in actual response. Therefore, the force deformation relationships are re-plotted in Fig 5.15 with an increased scale, magnifying the behaviour within the first 5% of lateral drift ratio. Possible strength decay scenarios are added to the Figure qualitatively with dashed lines, to show possible behaviour, had the strength decay was considered in analyses. The results indicate that the effect of prestressing is to stiffen the building, especially during initial loading. Depending on the level of prestressing and how quickly the yielding of steel is reached, the behaviour is different, though the strength envelops remains more or less constant when strength decay is neglected.

The variation of lateral drift ratio and inter-storey drift are plotted along the height of the building in Fig. 5.16, at NBCC-95 base shear level, except for the unretrofitted structure, which could only develop about 65% of the NBCC-95 force level. The force deformation relationships are re-plotted in Fig. 5.17, with an increased scale; the figures indicate the reduction in lateral drift demands with increasing level of prestressing. However, as the initial prestressing increased beyond 75 kN/strand (30% of ultimate), the improvement in drift control achieved was not as significant as those attained with lower levels of prestressing. This is explained with additional prestressing induced during response to lateral loading, which bring the strands to yielding, beyond which the improvement is limited. This implies that there exists an optimum level of prestressing.

Effect of the Amount of Prestressing Steel

The amount of lateral bracing (hence drift control) achieved by the retrofit technique investigated in this part of the research program can be attained either by providing the required level of initial prestressing or by the required steel area. However, as indicated earlier, there is a limit to how much the amount of initial prestressing can be applied, as beyond a certain level of initial prestress the steel strands yield during response due to the

additional diagonal tension caused by seismic forces. This reduces the effectiveness of lateral bracing. Therefore, while it may be economical to limit the area of steel strands, sometimes it may be necessary to use sufficient amount of steel, while limiting the prestress level to avoid premature yielding. The effect of the amount of strand area (number of strands) was investigated by analyzing the same 5-storey frame building with different number of 15mm nominal area 7-wire strands, while keeping the level of prestressing constant. This was done by considering 2, 4, 6, 8, 10, and 12 strands in each diagonal direction. As the level of prestressing was increased, the number of strands was reduced to attain approximately 1% drift. This level of drift ratio was targeted to protect nonductile frames of older buildings that usually control failure.

Figure 5.18 shows storey and inter-storey drift ratios for retrofitted and unretrofitted buildings, where retrofitting was done by providing different number of strands without prestressing. The results indicate that the unretrofitted building could only sustain 65% of NBCC-2005 design base shear. The drift demands plotted in Fig. 5.18 correspond to this level of loading. The drift demands for retrofitted buildings correspond to NBCC-2005 design base shear. Figure 5.18 also shows maximum tensile stresses observed in strands at maximum applied lateral loads. The results indicate that the maximum interstorey drift demand was unrealistically high for the unretrofitted building, reaching as high as 13% under 65% of NBCC-2005 base shear, at which level it suffered stability failure. The use of two 15 mm diameter strands improved lateral load resistance, developing full NBCC-2005 base shear, but at a maximum drift demand of about 12% at a strand tensile stress of 2260 MPa. Because of the small strand area used, the strands were not able to provide sufficient lateral bracing and they yielded and developed tensile stresses exceeding the ultimate stand capacity of 1860 MPa, indicating strand failure. The use of 4 strands in each diagonal direction (an increase of 100 % in steel area) resulted in a substantial improvement in drift demand, showing a maximum of 3 % storey drift at full NBCC-2005 base shear, while developing a post-yield stress of 1717 MPa in the strands. The use of additional 2 strands (total of 6 in each diagonal) improved drift control, while also reducing the maximum tensile stress in stands. Accordingly, the drift demand was reduced to approximately 1.5 %, at a level that that may be associated with the onset of

strength decay in nonductile frame columns. Further increase in the number of strands to 8 and 10 reduced drift demands to 1.25 % and to 1.0 %, respectively, with corresponding maximum strand stresses of 1140 MPa and 937 MPa, respectively.

Further investigation of the effect of the number of strands was conducted on the structure retrofitted with prestressed strands. The 5-storey frame building was retrofitted with strands that were prestressed to 25 kN, 50 kN, 75 kN, 100 kN, 125 kN, and 150 kN (corresponding to 10 %, 20%, 30%, 40%, 50% and 60% of the ultimate rupturing strength of strands). Figure 5.19 shows overall drift and interstorey drift ratios along the height of the structure, corresponding to 100 % of the design base shear computed on the basis of NBCC-2005, when the level of initial prestressing was 25 kN/tendon. The same figure also has the drift demands for unretrofitted building at its maximum load resistance, which was equal to 65% of the NBCC-2005 design base shear. As can be seen, the drift demands decrease with number of strands. As the number of strands increases, the maximum tensile stress in strands decreases. While the structure retrofitted with 2 strands exhibit a maximum computed stress in excess of the ultimate strength of strand, indicating failure, the structure retrofitted with 8 strands show that the strands remain elastic at maximum load resistance. Similar trends are observed in Figs. 5.20 through 5. 24, which show drift demands for structures retrofitted with different number of strands, while prestressed to different level. These figures also shows maximum tensile stresses observed in strands at maximum applied lateral loads. The comparison of drift demands among these figures shows the delicate balance between the amount of prestressing steel and the level of initial prestressing. If the initial prestressing is high, the strands yield and may even rupture during loading. The resulting drift demand may be high because of yielding, as opposed to non-prestressed strands that may continue remaining elastic. However, the situation reverses during small drift demands, where, increased prestressing results in reduced drift demands so long as the strands remain elastic.

Effects of the Cable Arrangement

The retrofit scheme used in all of the above analyses involved the use of strands within the middle bay of exterior frames (one bay in each of the two exterior frames),

throughout the height of the structure. This arrangement of cables is labeled as Arrangement # 1. Other retrofit schemes were also investigated to assess the need for retrofitting the entire building throughout its height. The 8-cable (in each direction) arrangement was selected in this part of the investigation, where all the cables were initially prestressed to 100 kN. This number of strands and the level of prestressing were selected because of superior performance achieved in contolling lateral drift, without developing inelasticity in the cables. Two additional arrangements were also considered, using 8 cables per bay in each direction, where each cable was prestressed to 100 kN, consisting of cables placed in; i) the first two stories and ii) the first three stories. These cable arrangements were labeled as Arrangements #2 and #3. An additional arrangement was also tried, where the cables were removed in stories where drift demands were not very height. Different number of cables was placed in different floors until a cable arrangement was reached such that the interstorey drift ratio was approximately 1%, beyond which it was expected that the non-ductile columns could develop early strength decay. This resulted in the use of 8 cables in each direction in the first two stories, which was reduced to 6 cables in the third storey, and 2 cables in the fourth storey. No retrofitting was done in the fifth storey (no cables). This arrangement was labeled as Arrangement # 4. Figure 5-11 Illustrates all the arrangements considered in the part of the investigation.

Figure 5-25 shows the deformation behavior of structures, retrofitted using the four arrangements described above, when subjected to incrementally increasing static lateral loads up to 100% of design base shear computed on the basis of NBCC-2005. Also included are the deformation characteristics of the unretrofitted building at 65% of NBCC-2005 base shear value, which was the maximum load the building could sustain. The results indicate that retrofitting the first two stories alone(Arrangement #2) had limited success, reducing the interstorey drift at the third-storey level to approximately 5%, while effectively controlling the first storey drift with a maximum drift ratio demand of 1%. In the same structure, the interstorey drift ratio at the roof floor level was reduced to about 3%. When the first three stories were retrofitted (Arrangement#3), the situation improved, with interstorey drift demand remaining 1% up to and including the third floor.

The top two stories showed interstorey drift ratios that varied between 1.5% and 1.7%. Retrofitting the entire building (Arrangement #1) resulted in unnecessarily high drift control, reducing interstorey drift demand to approximately 0.3% to 0.5% in upper two floors. Therefore, the possibility of reducing the number of cables, where they are not needed, was tied, which resulted in Arrangement #4. This arrangement consisted of gradually reduced number of cables, from 8 cables in the first two stories to 2 cables in the fourth level. The interstorey drift demands remained close to 1% throughout the height of the building.

5.4.4.2 Dynamic inelastic time history analysis

Dynamic inelastic time history analysis of the 5-storey building was conducted to assess the improvements attained through retrofitting. The structural properties used in the analysis remained the same as those used for static inelastic (pushover) analysis. Computer program DRAIN-RC was used, as explained earlier in this Chapter. All 12 artificial earthquake records, discussed in Section 5.4.3, were used to select the most critical record in terms of displacement response. The results indicated that, though the majority of records produced similar response, Short Event No. 2 gave the highest drift demands, and was selected for use in subsequent analyses.

Dynamic analyses were conducted to carry out a parametric investigation where the parameters were the number of strands and the amount of initial prestressing in each strand. Strand arrangement # 1 was used, as illustrated in Fig. 5.11, with 7-wire strands having a nominal diameter of 15 mm and an area of 140 mm^2/strand. The cables were placed in the middle bay of both exterior frames of the structure, with the number of cables in each diagonal direction varying between 2 and 18 for the lumped model frame (implying 1 to 9 cables per exterior frame). The cables were initially prestressed to different levels, ranging between zero to 150 kN per cable, corresponding to 0% to 60% of ultimate cable strength.

The results are presented in Figs. 5.26 to 5.29, in terms of interstorey drift ratios. They indicate that the maximum drift demand of about 2.4% for the unretrofitted frame could

be reduced to approximately 0.8% through retrofitting. However, the required number of strands to achieve a desired level of reduction varied depending on the level of initial prestressing. When the strands were provided snug tight (without prestressing), excessively high number of strands was needed (up to 7 strands in each diagonal, per bay per exterior frame) to attain maximum interstorey drift ratio of 1.3%. However, the same level of reduction in drift demands was achieved with 5 strands in each diagonal direction, (per exterior frame, per bay) when the strands were initially prestressed to 50 kN per strand. Further reduction in drift rations were obtained by increased initial prestressing. However, the results indicated that there is a trade off between the amount of strands and the level of prestressing. As the level of prestressing increased yielding of strands was recorded during response, diminishing the effectiveness of diagonal tension forces. The maximum levels of tensile stress in cables are indicated in the same figures.

Dynamic inelastic analysis also provided ductility demands for beams and columns. Maximum rotational ductility ratios, computed as the ratio of maximum chord rotation to chord rotation at initial yield, are shown along the heights of the building for beams and columns separately in Figs. 5.30 and 5.31. The ductility demands appear to be very high for the beams and the columns when the building was not retrofitted, implying failure. It should be noted that the hysteretic models used in the analysis did not have strength decay capabilities, hence resulting in unrealistically high ductility demands, whereas in actual structural response, these elements would have failed at much lower ductility ratios, especially if they represent older non-ductile buildings. Retrofitting the building with diagonally prestressed strands resulted in significant reductions in ductility demands, showing the effectiveness of the seismic retrofit technique. The ductility demands attained should be viewed relative to the flexural yield levels of members used in the analysis. The yield values assigned were reduced as much as 3 times, relative to the current NBCC-2005 requirements to simulate older buildings. For buildings with stronger elements, the ductility demands are expected to be significantly lower. Sample hysteretic relationships for a first storey column are plotted in Figs. 5.32 to 5.34 for flexural, shear and anchorage slip springs. The flexural hysteretic relationship shows moment versus inelastic hinge rotations, and does not include the rotation of elastic beam element. The

same is true for inelastic shear deformations. However, the rotations due to anchorage slip include combined elastic and inelastic deformations, as the springs representing these deformations model total anchorage rotations due to the extension and/or slippage of reinforcement outside the element. These rotations concentrate at member ends, without any deformation of the elastic beam element due to anchorage slip.

The dynamic analysis was extended to investigate the behaviour of buildings retrofitted with different arrangements of strands. The strand arrangements shown in Fig. 5.11 were also used for dynamic analysis, except for the number of cables used in Arrangement #4. Different number of cables was placed in different floors until a cable arrangement was reached such that the interstorey drift ratio was approximately 1%, beyond which it was expected that the non-ductile columns could develop early strength decay. This resulted in the use of 10 cables in each direction in the first two stories, which was reduced to 6 cables in the third storey, and 4 cables in the fourth storey. No retrofitting was done in the fifth storey (no cables). This arrangement was labeled as Arrangement # 4 for dynamic analysis. The results are shown in Fig. 5.35 in terms of interstorey drift demands. While discontinuous bracing along the height of the building resulted in the shifting of increased drift demands to upper stories, Arrangement # 1 produced a significant reduction in maximum drift demands, from 2.4% for the unretrofitted building to 1.2% for the retrofitted building (with 5 strands in each exterior frame, initially prestressed to 100 kN/cable). Arrangement # 4, with a gradually reducing number of strands from the first storey to the fifth, produced a more uniform drift demands along the height, indicating that the number of strands should be adjusted within a building for improved efficiency.

5.4.5 Retrofitting by diagonal FRP strips

The 5-storey frame building that was selected earlier and analyzed with diagonal prestressing strands was retrofitted diagonally within the interior bay of both exterior frames (one of the lumped frame representing the exterior frames in the model) with carbon fiber polymer (CFRP) sheets. This is shown in the elevation view given in Fig. 5. 36. Each diagonal strip shown in the figure is modeled with a truss element, capable of taking tension only. The truss element was modeled to behave elastically until the

rupturing strength of the fiber strip was reached. Arrangement #1 shown in Figure 5.11, illustrates the analytical model used for frame analysis, where each diagonal CFRP strip is modeled with a tension tie. The properties of tension ties were given such that the elastic rigidity was equal to the EA of the strip. The modulus of elasticity was 60,000 MPa as established by coupon tests in the laboratory and the strip width used was 625 mm. Different number of plies of CFRP was used, with different ply thickness. Each thickness of composite layer (saturated in epoxy) was 0.9 mm. The strength of each tie was computed from the measured material strength of CFRP coupons, which was 700 MPa. A parabolic variation of stress was assumed across the width of the strip, with an average uniform tensile stress of 0.85 * 700 = 595 MPa.

The masonry wall was modeled by means of diagonal struts, capable of resisting axial compression with a bilinear primary force-deformation relationship. Elasto-plastic hysteretic model was assigned for dynamic inelastic analysis. The characteristics of the force-deformation relationship were specified in the form of axial rigidity (AE) and post yield stiffness. The post yield stiffness (strain hardening portion) was specified to be zero. The effective wall width was computed as suggested by Paulay, T. and Priestley, and was taken as ¼ of the diagonal wall length, which was equal to 1.8 m.

5.4.5.1 Pushover Anlaysis

The analytical model described above was first used to conduct static inelastic lateral load analysis (pushover). Computer program DRAIN-RC was used as before. The static load was applied incrementally. The distribution of total base shear was computed on the basis of NBCC (2005), and was consistent with the requirements of the Code, following an inverted triangular distribution, simulating first mode response. The base shear computed corresponded to the current NBCC level for Vancouver. However, to simulate an existing seismically deficient building to be retrofitted, the resistance of each frame member was reduced by a factor of 3.0. This was found to be the approximate ratio between the current design force level and that required by NBCC in 1970s. The resulting frame building was therefore seismically deficient and did develop yielding.

The analytical model was first subjected to lateral loading without the retrofit. Force-roof displacement relationship obtained is shown in Fig. 5.37. The drift demand at each floor, as well as inter-storey drift demands along the height of the structure are also shown in the same figure. The results indicate a maximum inter-storey drift demand of about 12% for the unretrofitted building, which is a clear sign of failure. The analysis did continue well into the unrealistic range of deformations because the analytical models employed did not consider strength decay. When retrofitted with a single strip in each of the two exterior frames (2 layers in lumped frame model, representing two exterior frames), the drift demand was controlled somewhat, but did not show a substantial improvement, with the maximum drift ratio showing a value of about 11% at the second storey level. The stress recorded in the CFRP strip was slightly in excess of the rupturing strength, indicating the rupturing of the strips shortly before reaching the maximum applied load. Therefore, the number of CFRP layers was increased in subsequent analyses to 4 and 6 (2 and 3 per exterior frame). This resulted in a substantial improvement in response, drift demand reducing to approximately 1%, as illustrated in Fig. 5.37. It should be noted that, when 2 layers of CFRP strips were used in each of the two exterior frames the drift ratio was slightly in excess of 1% when the CFRP strips developed their rupturing strength. When the number of layers was increased to 3 per exterior frame, the reduction in drift demands was very small (slightly below 1%), while the maximum stress recorded in the strips was reduced to 459 MPa (while the rupturing strength was 595 MPa). The results indicate that CFRP strips can be used to effectively control lateral drift during strong earthquakes, protecting non-ductile frame buildings. Further investigation of CFRP strengthened frames with masonry infill walls was conducted by carrying out dynamic inelastic analyses.

5.4.5.1 Dynamic Inelastic Analysis

Dynamic inelastic analysis of the 5-storey building shown in Figure 5.38 was conducted using computer software DRAIN-RC to investigate the effectiveness of CFRP strips as a seismic retrofit technique. The structure was first subjected to 12 artificial earthquake records developed by Adam et al (2003) to match the uniform hazard spectra specified in NBCC-2005. These are the same records discussed earlier, with their characteristics

shown in Fig. 5.9. Although the response did not vary too much with the earthquake record employed, the Short Event No.2 was the most critical in terms of drift demands, and was used in subsequent analysis with the structure retrofitted with FRP strips. The frames were modeled as described in Sect 5.3.1, with inelastic hysteretic models assigned to the frame members, and elastic truss elements assigned to diagonal elements, representing the infill wall and the strips. The walls were modeled with diagonal struts and the strips were modeled with diagonal ties. The yield levels (strengths) of the frame elements were specified as 1/3 the amount required by NBCC-2005 to represent a seismically deficient older building designed in 1970s, as before.

Figure 5.38 shows interstorey drift demands along the height of the building. The unretrofitted structure showed a maximum drift demand of about 2.8% at the second storey level. The drift demand was reduced to approximately 1.4% by retrofitting the exterior frames such that a single FRP strip was placed in each diagonal direction on **one side** of each of the two exterior infill walls within the middle bay (two strips in each diagonal direction in the lumped frame model which represents two exterior frames). At the maximum drift level, the maximum tensile stress computed in the FRP strips was equal to the average rupturing strength of the strip (i.e., 595 MPa). The drift demand was further reduced to about 1% when a single layer of FRP strip is placed on **both** sides each of the infill walls in the middle bays of exterior frames. In this case the maximum tensile stress was reduced to 549 MPa.

Figures 5.39 and 5.40 illustrate the ductility demand in frame members during response. The results indicate that the unretrofitted building showed maximum beam and column ductility ratios of 17.5 and 13, respectively. This level was reduced to 6 and 4.

Dynamic analyses indicate that the FRP strips can be used effectively to control lateral drift demands in non-ductile reinforced concrete frame buildings while also reducing inelastic deformations (or eliminating inelastic deformations and promoting elastic response) in the frame elements significantly.

Chapter 6

Summary and Conclusions

6.1 Summary

A large number of building inventory in Canada and elsewhere in the world consists of moment resisting concrete frames, with or without masonry walls. Those frame buildings that were designed and built prior to the enactment of modern seismic design and detailing practices (especially prior to 1970s) may be seismically deficient. Two retrofit techniques were researched in this thesis for non-ductile reinforced concrete frame buildings; i) the use of diagonal FRP strips on masonry infill walls, and ii) diagonal prestressing. The research program consisted of experimental and analytical components. Four half-scale R/C frames were designed, constructed and tested under in-plane reversed cyclic loading. All the frames had an aspect ratio of 1.0 and a height of 2.0 m. The first specimen (BR-1) was infilled with a brick masonry wall without any retrofit. This wall was used as the reference specimen for brick wall-frame assemblies. The second specimen (BR-2) was infilled with brick masonry and retrofitted with diagonal prestressing cables, having an initial prestressing force of 75 kN/cable. The third specimen (BR-3) was also infilled with brick masonry and was retrofitted with diagonal prestressing cables, except with an increased initial pressing force of 125 kN/cable. The fourth and final specimen (BL-3) had a concrete block masonry infill wall, and was retrofitted with diagonal FRP strips. The latter wall was compared with unretrofitted companion wall that was tested earlier by Serrato (2002). The tests were conducted under constant gravity loading.

The results showed significant improvements in overall lateral force resistance. Because the frame elements were not retrofitted, the emphasis was placed on lateral bracing and

keeping the deformations within the elastic range of frame elements. This was achieved in both methods with substantial increases in seismic force resistance, while keeping lateral deformations within the elastic range of lateral drift.

The analytical studies involved the computation of force displacement envelop curves for the specimens tested, as well as extending the application of both retrofit techniques to a simple 5-storey reinforced concrete frame building to demonstrate their effectiveness in practice. A large number of analyses were conducted under different amounts of prestressing strands, prestressed to different levels. Furthermore, the use FRP strips to strengthen existing masonry infill walls was demonstrated using the same 5-storey building. Both static inelastic (pushover) load analyses under incrementally increasing lateral loads, and dynamic inelastic response time history analysis were conducted.

The results indicate that the strength and lateral bracing of concrete frame structures can be improved substantially by both methods of seismic retrofitting. The required amount of lateral bracing, both in terms of required diagonal prestressing and FRP strips can be established through structural analysis such that the drift demands remain within the elastic range of deformations.

6.2 Design Strategy

Non-ductile reinforced concrete frame buildings consist of structural components that are not designed and detailed following the modern seismic design provisions of current building codes. Therefore, two retrofit design strategies may be in order; i) retrofitting individual elements to improve their inelastic deformability, and ii) providing sufficient lateral bracing to control deformations so that the building remains essentially elastic with reduced deformation demands. In the former strategy, each and every critical element must be seismically retrofitted, which may not be feasible and economically attractive. Furthermore, this retrofit strategy does not protect brittle non-structural elements in the building against damage. It is believed that a significant proportion of casualties after every earthquake are caused by the collapse of non-structural elements, even if the lateral load resisting system remains functional. The second strategy, i.e.,

lateral bracing controls overall response by reducing deformations at the expense of increasing lateral force demands. The two retrofit methods researched in the current investigation fall under this category. Therefore, the design strategy to follow must protect non-ductile elements through drift control, while providing sufficiently high lateral force capacity.

It was demonstrated both experimentally and analytically that diagonal prestressing only the exterior frames of a multi frame, multi-bay building may be sufficient to achieve the objectives of drift control and increased strength. There is a clear tradeoff between the amount of initial prestressing and the amount of strands to be used. It may be more practical to employ fewer strands with increased prestressing to achieve the required strength within the elastic range of deformations. However, the initial prestressing should be kept below a certain level in order not to cause significant yielding in strands. This can be attained through push-over analysis of the building that is retrofitted. The design procedure for this technique involves a trial process, where different levels of initial prestressing and the number of strands should be employed until the target strength and drift ratio are achieved. The target strength may be taken as the elastic strength under the current code recommended elastic force level. The drift may be limited to a level beyond which the proper performance of non-ductile frame elements is jeopardized. It has been established experimentally that most non-ductile reinforced concrete columns have some inherent deformation capacity even if they are not designed following seismic design practices. Flexure dominant columns often maintain their strengths up to 2% drift ratio, while shear dominant columns fail beyond 1% lateral drift. Similarly, columns with longitudinal splice deficiencies of old practice, i.e., splice length of $20b_d$ to 24 b_d, fail after 1% drift cycles. The beams tend to be more ductile than columns, as they are not subjected to axial compression. Therefore, it may be advisable to limit the interstorey drift demand to 1% to ensure the integrity of non-ductile concrete elements.

A similar design approach may be employed for frames with masonry infill walls, to be retrofitted by FRP strips. Push-over analyses of the structure, with different plies of FRP sheets may be tried until the code elastic strength limits are attained. The FRP retrofitting

usually results in significant lateral rigidity. Hence, attaining the target drift limit of 1% does not often pose a challenge.

6.3 Conclusion

The following conclusions can be drawn from the research work reported in this thesis:

- Non-ductile reinforced concrete frames infilled with masonry walls have limited strength and ductility. The maximum strength of the specimen tested in the current investigation was attained at 1.25% lateral drift ratio, with failure followed rapidly thereafter, during 1.5% drift cycles. The maximum lateral load resistance of a 5-storey non-ductile frame masonry infill wall structure, established analytically, was about 65% of the resistance required by the current National Building Code of Canada (2005).
- Gravity load concrete frames, designed without appropriate seismic design and detailing practices, are likely to fail in the splice regions of columns. Lack of sufficient splice length and/or properly detailed hoops with 135 degree bends, leads to the opening of column ties and accompanying anchorage failure of spliced reinforcement. This type of failure occurred in the specimen tested (BR-1) at approximately 1.5% drift ratio.
- The deformability of non-ductile reinforced concrete frames appears to be compatible with that of unreinforced masonry infill walls. The unretrofitted frame-wall assembly tested in the current investigation showed simultaneous failures of the frame and the infill wall at about 1.5% drift ratio, until which the wall developed gradual cracking and stiffness degradation while maintaining its integrity.
- Diagonal prestressing non-ductile concrete frames is an effective seismic retrofit strategy. Diagonal prestressing controls diagonal cracking in infill walls (if present), braces the frame, and increases lateral force resistance. The specimen tested in the current investigation showed an increase of 334 kN of lateral force resistance (total resistance of 746 kN) due to prestressing by two 15 mm diameter 7-wire strands in each diagonal, where the initial prestressing force was 75 kN/strand. The increase in strength was approximately a factor of 1.8. The

strength increase attained in a 5-storey non-ductile frame building by prestressing only a single bay in exterior frames throughout the building height was found analytically to be in the order of 100%. Higher strength enhancement was obtained by increasing the number of strands or the number of retrofitted frames.

- The increase in initial level of prestressing in diagonal strands improves crack control in infill frames and enhances lateral bracing. As an example, the specimen prestressed with 125 kN/strand showed 715 kN of lateral resistance at 1% lateral drift, as compared with 677 kN attained in the companion specimen with 75 kN/strand initial prestressing. Similarly, the 5-storey frame building investigated analytically indicated increased strength initially with increased prestressing. However, this improvement was limited to lateral drift demands of up to approximately 1%. Although the increased prestressing improved building response in terms of stiffness (bracing) and strength during the early stages of lateral deformations, the yielding of prestressed strands at later stages of response resulted in approximately the same lateral load resistance, irrespective of initial level of prestressing. Hence, the initial level of prestressing should be established carefully for target drift demands in design. Often the drift capacity of a non-ductile frame is limited to 1% to 1.5% drift ratio, which is the range within which increased prestressing can be effective.
- The design of diagonal prestressing should be based on elastic response of non-ductile frames. This is because the retrofit technique is based on improved lateral resistance rather than enhanced ductility. Both the amount of strands and the level of prestressing should be determined such that the non-ductile frame remains elastic (or with limited inelasticity).
- Dynamic response of non-ductile reinforced concrete structures, under the governing design earthquake associated with uniform hazard spectra of NBCC-2005, indicate drift demands that can not be sustained by the structure. They also indicate unrealistically high ductility demands. Retrofitting the buildings with diagonal prestressing reduces both drift and ductility demands significantly. The amount of reduction in deformation demands depends on the amount steel strands used and the level of initial prestressing applied.

- The analytical research indicated that the most efficient cable arrangement included variable numbers of cables used along the height of the structure, with higher number of strands used in lower stories where higher lateral drift was recorded in the unretrofitted structure.
- Force-deformation relationships computed through push-over analysis provide reasonably good agreements with envelops of experimentally recorded force-deformation hysteresis loops.
- The use of surface bonded carbon FRP strips along masonry infill wall diagonals is an effective seismic retrofit methodology for bracing non-ductile reinforced concrete frames. The degree of bracing is dependent on the amount of FRP used in diagonal strips.
- The use of diagonal FRP strips as a seismic retrofit strategy results in a significant increase in lateral load resistance, without any improvement in ductility. A single layer of CFRP strip, surface bonded on either side of a masonry wall along both diagonals resulted in a strength increase equal to approximately 2. 0 to 2.4 times the strength recorded in non-retrofitted specimen, in the directions of initial load excursion, and the opposite direction, respectively. The increase in lateral force resistance was approximately equal to 386 kN.
- Retrofitting masonry walls with FRP sheets increases strength and stiffness, but not ductility. After 2 % lateral drift ratio, most of the strength gain due to FRP had been lost.
- FRP anchors used to fix the FRP strips to the enclosing frame members proved to be effective. These anchors were produced by bending 60 mm wide, 500 mm long strips of carbon FRP into two, and inserting them into the pre-drilled holes by about 50 to 80 mm. There was no failure of FRP anchors during the test.
- Static inelastic analysis of a 5-storey reinforced concrete building indicates that drift demands can be reduced from an unrealistically high value of 11 to 12% to approximately 1% by retrofitting masonry infill walls by means of surface bonded FRP strips. Similar reductions were observed when the structure was subjected to NBCC-2005 compatible design earthquake motions.

- The level of lateral bracing introduced through the use of diagonal CFRP strips is proportional to the number of plies used to retrofit the walls.
- Design of the retrofit methodologies developed in the current investigation can be performed through push-over analyses of buildings. The diagonal elements for such analyses can be modeled by means of diagonal ties.

6.4 Recommendations for Future Research

The following experimental and analytical research is recommended for future research:

- Tests of non-ductile reinforced concrete frames without infill walls, with and without retrofitting with diagonal prestressing, having different levels of initial prestressing and different amounts of prestressing steel to establish the effectiveness of the retrofit methodology for bare frames.
- Tests of reinforced concrete frame masonry infill wall assemblies, with and without retrofitting with diagonal prestressing, having different levels of initial prestressing and different amounts of prestressing steel to conduct an experimental parametric investigation to establish the significance of prestressing parameters.
- Dynamic inelastic analyses of frame structures having different periods, subjected to different ground motions, with and without diagonal prestressing to investigate the effectiveness of the retrofit strategy for structures having different dynamic characteristics.
- Tests of frame-masonry assemblies with two plies of CFRP strips on each face of masonry walls in each of the two orthogonal diagonals to investigate the significance of the amount of fibres.
- Dynamic inelastic analysis of different structural systems, including frame-shear wall interactive systems, as well as shear wall and coupled wall systems with and without retrofitting by diagonal CFRP sheets to investigate the effectiveness of the retrofit scheme in these systems.

Abrams, D.P., Angel, R. and Uzanski J. (1993). "Transverse Strength of Damaged URM Infills." Proceedings of ASCE Structures Congress, Irvinr, CA.

ACI Committee 318 " Code Requirements for Reinforced Concrete and Commentary (ACI 318-63)." American Concrete Institute, Detroit, 1963.

ACI Committee 318 " Code Requirements for Reinforced Concrete and Commentary (ACI 318-83)." American Concrete Institute, Detroit, 1983.

Adam, J., and Atkinson, G. "Development of seismic hazard maps for the proposed 2005 edition of National Building Code of Cabada" Canadian Journal of Civil Engineering, 30 2003, No.30, Pp 255-271.

Alsiwat, J. M.. " Effect of Anchorage Slip and Inelastic Shear on Seismic Response of Reinforced Concrete Frame." Ph. D Thesis, Department of Civil Engineering, University of Ottawa Canada, 1993.

Alsiwat, J. M., and Saatcioglu M. " Reinforcecement Anchorage Slip Under Monotonic Loading." Journal of Structural Engineering, Vol.118, 1992, Pp 2421-2438

Altin, S., Erosy, U., and Tankut, T., " Hysteretic Response of Reinforced-Concrete Infilled Frame" Journal of Structural Engineering, Vol.118, No.8, August, 1992, Pp 2133-2150.

Asteris, P. G. "Lateral Stiffness of Brick Masonry Infilled Plane Frame." J. Strut. Eng., 129(8), 1071-1079.

Bertero, V., and Brokken, S., " Infills in Seismic Resistant Buildings", Journal of the structural Engineering, ASCE, Vol. 109, No 6, June, 1983, pp 1337-1361.

Bhende, D. and Ovadia, D. (1994). "Out-of-Plane Strengthening Scheme for Reinforced Masonry Walls."Concrete International ACI, April, Pp30-34.

Dawe, J. L. and Aridru, G.G (1994). "Prestressed Concrete Masonry Walls Subjected to Uniform Out-of-Plane Loading," Canadian Journal of Civil Engineering. Vol. 20: pp 969-979.

Dencer, E., "Seismic Drift Demands of Reinforced Concrete Buildings" M.A.Sc Thesis, Department of Civil Engineering, University of Ottawa Canada, 2003.

Dhanasekar, M., and Page, A. W. (1986) "The Effect of Masonry Infill properties on the Behavior of Infilled Frames" Proc., Inst. Of Civ. Engrs., U.K., Part 2, 81 (Dec.), 593-605

Ehsani, M.R., Saadatmanesh, H., Velazques-Dimas, J. I., "Behavior of Retrofitted URM Walls Under Simulated Earthquake Loading", Journal of Composites for Construction, Vol. 3, No. 3, August 1999, pp. 134-150.

El-Attar, A. G., White, R. N., and Gergely, P., "Behavior of Gravity Load Designed Reinforced Concrete Buildings Subjected to Earthquakes," ACI Structural Journal, 94 (2), 1997, pp 133-145.

Elnabelsy, G., Ph.D. Candidate, Departement of Civil Engineering, University of Ottawa. Ottawa, Canada, 2001.

Erdem, I. , Akyuz, U., Ersoy, U. and Ozcebe, U. " A Comparative Study on the Strengthening of Frames, Seismic Assessment and Rehabilitation of Existing Building, 2003, Pp 407-432.

Ersoy U., Ozcebe G., Tankut T., Ugurhan Akyuz, Emrah Erduran and Ibrahim Erdem " Strengthening of Infilled Walls with CFRP Sheets" seismic Assessment and Rehabilitation of Existing Buildings, 2003, pp 305-334

Grimm, C., T., "Elastic Modulus of Clay Brick Masonry", Reinforced and Prestressed Masonry Symposium, University of Edinburgh, Scotland, 1984.

Hamid, A. A., Ziab, G., and El Nawany, O., "Modulus of Elasticity of Concrete Block Masonry", Proceeding of the 4th North American Masonry Conference, Los Angeles, Ca, 1987,pp. 7/1-7/13.

Higashi, Y., and Kokusho, S., " The strengthening Methods of Existing Reinforced Concrete Building," Proceeding of the U.S.-Japan Cooperative Research Program in Earthquake Engineering with Emphasis on the Safety of School Buildings, Honolulu Hawaii, Aug., 1975, pp.333-351.

Holmes, A. W., " Steel Frames with Brickwork and Concrete Infilling". Proc. Inst. Of Civ. Engrs., London, England, 19,1961, pp 473-478.

Jocelyn Paquette, Michel Bruneau and Andrf Filiatrault, "Out-of-Plane Seismic Evaluation and Retrofit of Turn-of-the-Century North Americian Masonry Walls", Journal of Structural Engineering, Vol. 127, 127, No. 5, May, 2001. Pp 561-569.

Kahn, L.F., and Hanson, R. D., "Infilled Walls for Earthquake Strengthening", Journal of Structural Engineering, ASCE, Vol. 105,No ST1 January 1979,pp 283-296.

Kanaan, A. E., Powell, G. H. (1973). DRAIN-2D:General Purpose Computer Program for Dynamic Analysis of Inelastic Plane Structures. University of California, Berkeley, California.

Kehoe, B.E. (1996). "Performance of retrofitted unreinforced masonry buildings." Paper No. 1417, Eleventh World Conference on Earthquake Engineering, Acapulco, Mexico.

Klingner, R. E., and Bertero,V.V., "Earthquake Resistance of Infilled Frames", Journal of the Structural Division, ASCE, Vol. 104,No ST6, June, 1978,pp. 973-989.

Laursen, P. T., Seible, F., Hegermier, G.A., and Innamorato, D. (1995). "Seismic retrofit and Repair of masonry walls with carbon overlays." Non-metallic (FRP) Reinforcement for Concrete Structures. Rilem.

Liauw, T. C., and Lo, C. Q. (1988) "Multibay Infilled Frames Without Ahear Connectors." ACI Struct. J., July-Aug., 423-428.

Mehrabi, A.B., Shing, P.B., Schuller,M.P., and Noland, J.N., "Experimental Evaluation Of Masonry-Infilled RC Frames", Journal of Structural Engineering, ASCE, Vol. 122, No.3, March 1996, pp228-237.

Michael L. Albert, Alla E. Elwi and J. J. Roger Cheng "Strengthening of Unreinforced Masonry Walls Using FRPs, Journal of Composites for Construction, Vol. 5, No. 2, May, 2001. Pp 76-84.

National Building Code of Canada (NBCC) Associated Committee on National Building Code, National Research Council Canada, Ottawa, Ontario, Canada, 1970.

National Building Code of Canada (NBCC) Associated Committee on National Building Code, National Research Council Canada, Ottawa, Ontario, Canada, 1995.

National Building Code of Canada (NBCC) Associated Committee on National Building Code, National Research Council Canada, Ottawa, Ontario, Canada, 2005.

Ozcebe, G., and Saatcioglu, M., " Hysteretic Shear Model for Reinforced Concrete Member." " Journal of Structural Engineering, Vol.115, 1989, Pp 132-148

Paulay, T. and Priestley, M.J.N., "Seismic Design of Reinforced Concrete and Masonry Building". John Wiley & Sons, Inc., Toronto, 1992.

Powell, G. H. Supplement to Computer Program DRAIN-2D. Supplement to Report, Drain-2D User's Guide, University of California, 36pp

Saatcioglu, M., Shooshtari, A. and Alsiwat, J. "Computer Program for Dynamic Inelastic Response History Analysis of Reinforced Concrete Structures (DRAIN-R/C), Reserarch Report No:OCEERC 97-18, Ottawa Carleton Earthquake Engineering Research Centre, Department of Civil Engineering, the University of Ottawa, Ottawa. Canada, 1997.

Saneinejad A. and Hobbs, B., "Inelastic design of Infilled frames", Journal of Structural Engineering, ASCE, Vol. 121, No. 4, April 1995, Pp 634-650.

"SAP 2000 Integrated Finite Elements Analysis and Design of Structures" Referenced and Tutorial Manual Ver 6.2 June 1998.

Schmidt, T. (1989). " An Approach of modeling Masonry Infilled Frames by the FE. Method and Modified Equavalent Strut Method." Darmstadt Concrete, Annu. J.on Concrete and Struct., 185-194.

Saatcioglu, M., Alsiwat, J. M., and Ozcebe, G. " Hysteretic Behavior of Anchorage Slip in R/C Members" Journal of Structural Engineering, Vol.118, 1992, Pp 2439-2458

Saatcioglu, M., Derecho, A. T., Corley, W. G. "Modelling Hysteretic Behavior of Coupled Walls for Dynamic Analysis." Eartquake Engineering and Structural Dynamic Vol.11, 1983, Pp 711-726

Saatcioglu, M., Shooshtari, A., and Alsiwat, J., "Computer Program for Dynamic Inelastic Response History Analysis of Reinforced Concrete Structures" OCEERC 97-18.

Serrato, F. "Seismic Retrofit of URM Infilled Panel in Reinforced Concrete Frames Using FRP Sheets", M.A.Sc Thesis, Department of Civil Engineering, University of Ottawa Canada, 2002.

Shooshtari, A., "Seismic Drift Demands of Reinforced Concrete Buildings." Ph. D Thesis, Department of Civil Engineering, University of Ottawa Canada, 1998.

Siegel, H. I. And Fowler, L. W. (1994). Jackson Brewery: upgrading an historic unreinforced brick building." Earthquake Spectra, Vol. 10, No. 1.

Smith, B. S. (1966). "Behavior of square infilled frames" J. Struct. Div., ASCE, 1992 (1), Pp 381-403

Stafford-Smith, B. and Carter, C., "A Method for the Analysis of Infilled Frames", Proc. Inst. of Civ. Engs., London, England, 44, 1969, Pp 31-48.

Schwegler, G. (1995). "Masonry construction strengthened with fiber composites in seismically endangered zones," 10th European Conference on Earth Engineering: Pp 2299-2303.

Tagdi, M., "Seismic Retrofit of Low-Rise Masonry and Concrete Walls by Steel Strip." Ph. D Thesis, Department of Civil Engineering, University of Ottawa Canada, 1998.

Weeks, J. Seible, F., Hegemier, G and Pristley, M.J.N (1994). "The U.S.-TccMar full-scale five-story masonry research building test." University of California, San Diego.

Yaw-Jeng Chiou, Jyh-Cherng Tzeng, and yuh-When Liou 'Experimental and Analytical Study of Masonry Infilled Frames" Journal of Structural Engineering, ASCE, Vol. 125, No.10, October 1999, Pp 1109-1117.

Table 3.1: Characteristics of concrete mixture for unretrofitted and retrofitted infilled frame by FRP sheet (BR-1 and BL-3)

Water-cement ratio	0.49
Water	130.9
Cement (Type 10)	267.1
Slag	61.1
10 mm aggregate	1960.4
Sand	867
Compressive strength at 7 Days	27.3
Compressive strength at 28 Days	31.1
Compressive strength at day of test	32.1

Table 3.2: Characteristics of concrete mixture for retrofitted infilled frame by cables (BR-2 and BR-3)

Water-cement Ratio	0.47
Water	129.0
Cement (Type 10)	274.47
Slag	61.4
10 mm aggregate	1961.0
Sand	866
Compressive strength at 7 days	27.9
Compressive strength at 28 days	31.7
Compressive strength at day of test	33.2

Table 3.3: Compressive strength of concrete block units and prism

	Retrofitted wall by FRP sheets			
Sample: 200 x 200 x400 mm standard unit	#1	#2	#3	#4
Compressive strength of concrete block masonry units (MPa)	14.9	15.7	15.9	15.3
Average compressive strength of concrete block masonry Units (MPa)	15.45			
Compressive strength of concrete block masonry prism (MPa)	9.0	7.9	8.8	8.7
Average compressive strength of concrete block masonry prism (MPa)	8.6			

Table 3.4: Compressive strength of masonry brick units and prism

	Unretrofitted and retrofitted wall by cables			
Sample: 245 x 90 x 79 mm standard unit	#1	#2	#3	#4
Compressive strength of brick masonry units (MPa)	20.0	18.8	19.1	19.5
Average compressive strength of brick masonry units (MPa)	19.35			
Compressive strength of brick masonry prism (MPa)	11.3	12.1	10.9	11.8
Average compressive strength of concrete brick prism (MPa)	11.525			

Table 3.5: Mechanical properties of carbon fibers as described from manufacturer

Mbrace fiber	Ultimate strength, MPa	Design strength, MPa	Design thickness, mm/ply	Tensile modulus of elasticity, MPa
CF 130 high tensile carbon	4275	3800	0.1651	228000

Table 3.6: Specimen displacement per loading cycle

Load cycle	Specimen lateral displacement (mm)	Lateral drift (%)
1	2	0.1
2	4	0.20
3	6	0.30
4	8	0.40
5	10	0.50
6	15	0.75
7	20	1.0
8	25	1.25
9	30	1.5
10	35	1.75
11	40	2.0
12	45	2.25
13	50	2.50
14	55	2.75
15	60	3.0

Table 5.1 Loads and materials properties

Title	Floor	Roof
Dead Loads (KN/m^2)	5	3.5
Live Loads (KN/m^2)	2.4	2.2
Compressive Strength of Concrete (MPa)	30	
Yield Strength of steel (MPa)	400	

Table 5.2 Sections sizes and reinforcement arrangement

Frame	Floor	Beam Section and Reinforcement	Coulmn Section and Reinforcement	
			Interior	Exterior
Interior	1-4	300x450 3#25 top, 2#20 bottom	450x450 8#25	400x400 8#20
	5	300x400 3#20 top, 2#15 bottom	450x450 8#25	400x400 8#20
Exterior	1-4	300x450 3#25 top, 2#20 bottom	400x400 8#20	300x300 8#20
	5	300x400 3#20 top, 2#15 bottom	400x400 8#20	300x300 8#20

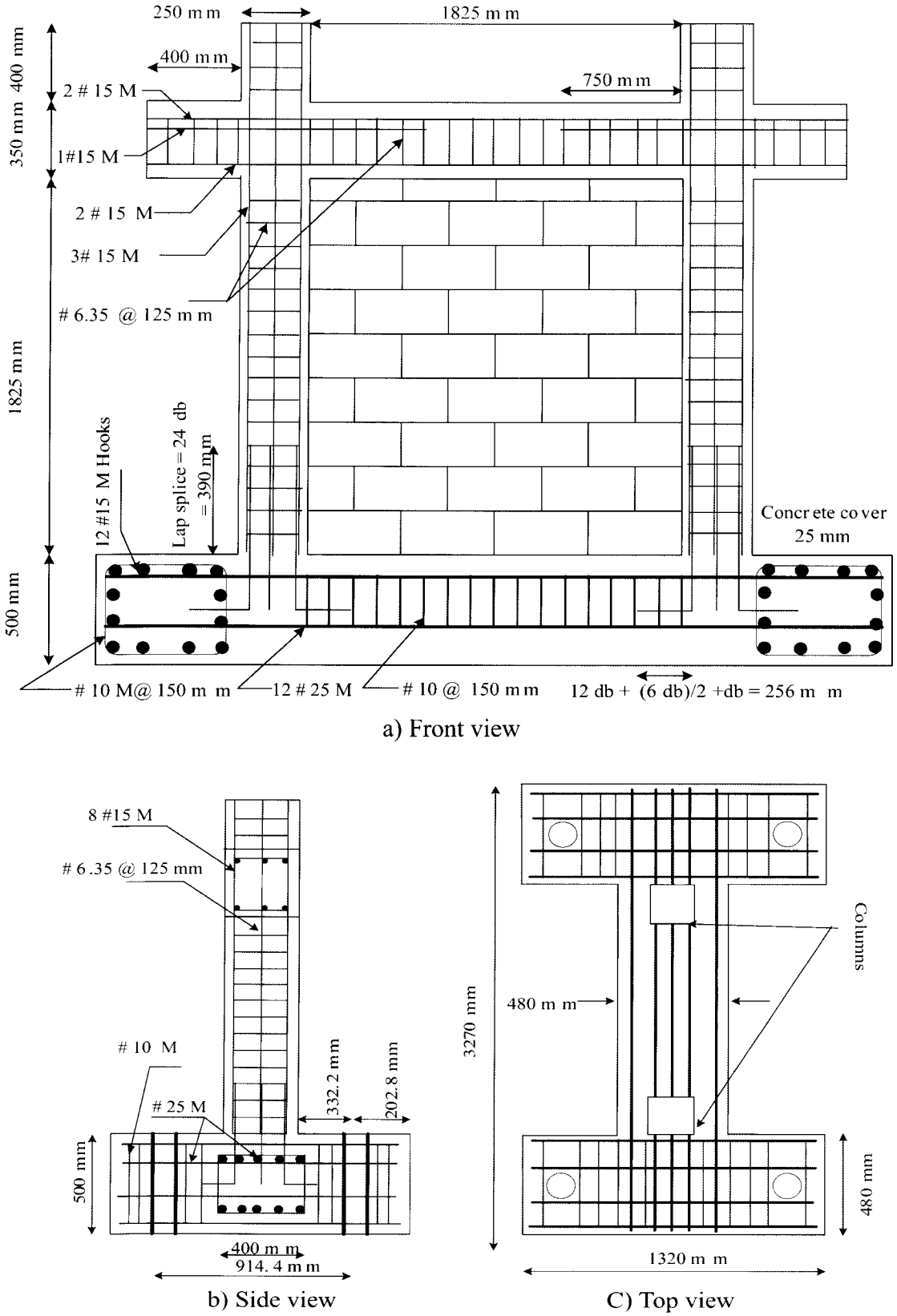

Figure3.1: Details of reinforced concrete frames

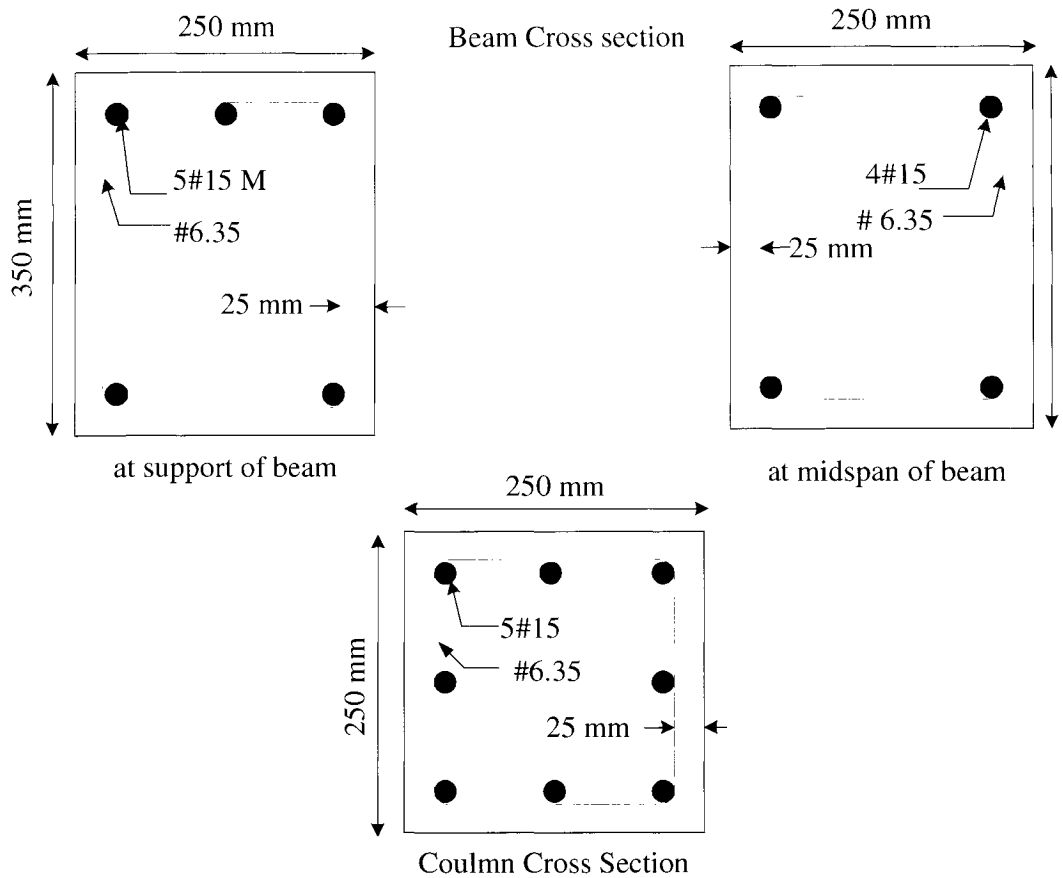

Figure 3.2: Column and beam cross sections

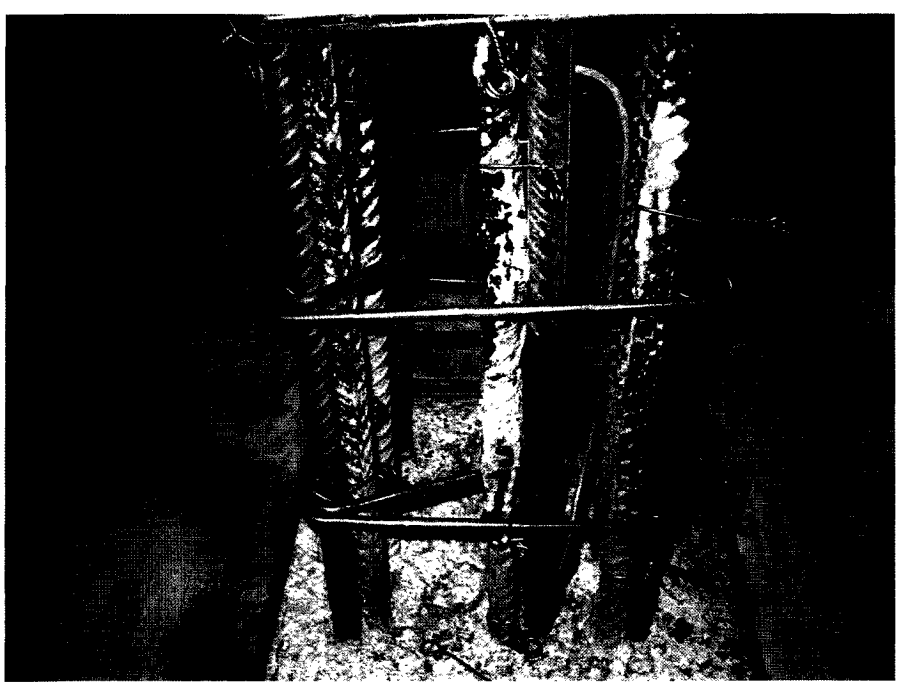

3.3: Column splices above the foundation

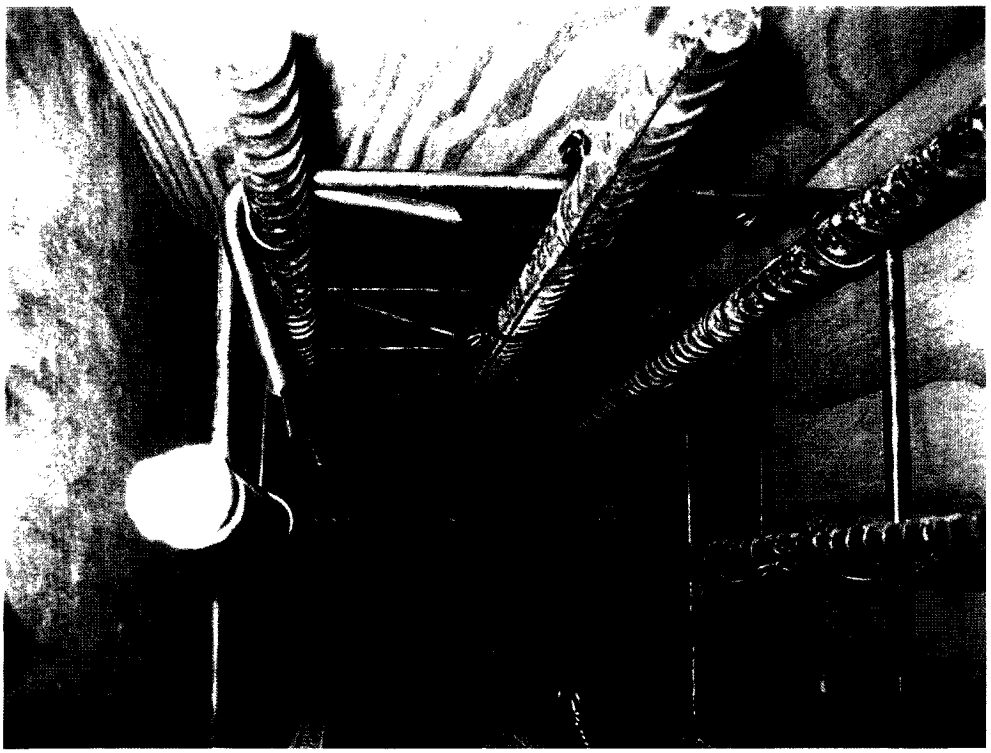

Figure 3.4: Detail of beam - column connections

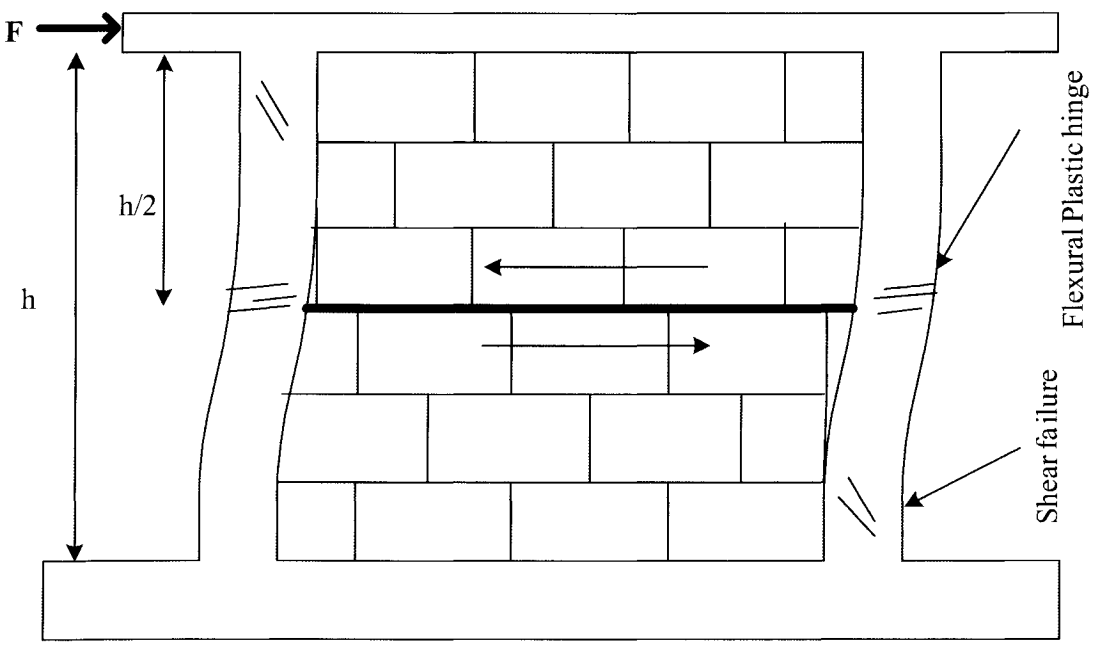

Figure 3.5: Knee frame model for sliding shear failure of masonry infill wall

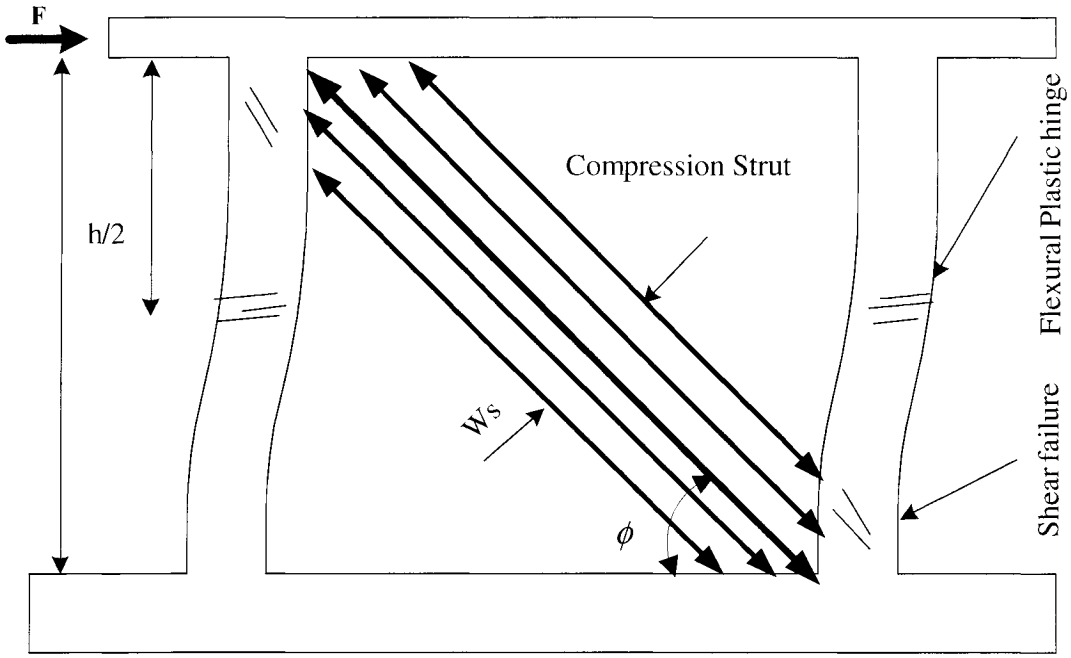

Figure 3.6: Diagonal compression strut under lateral loading

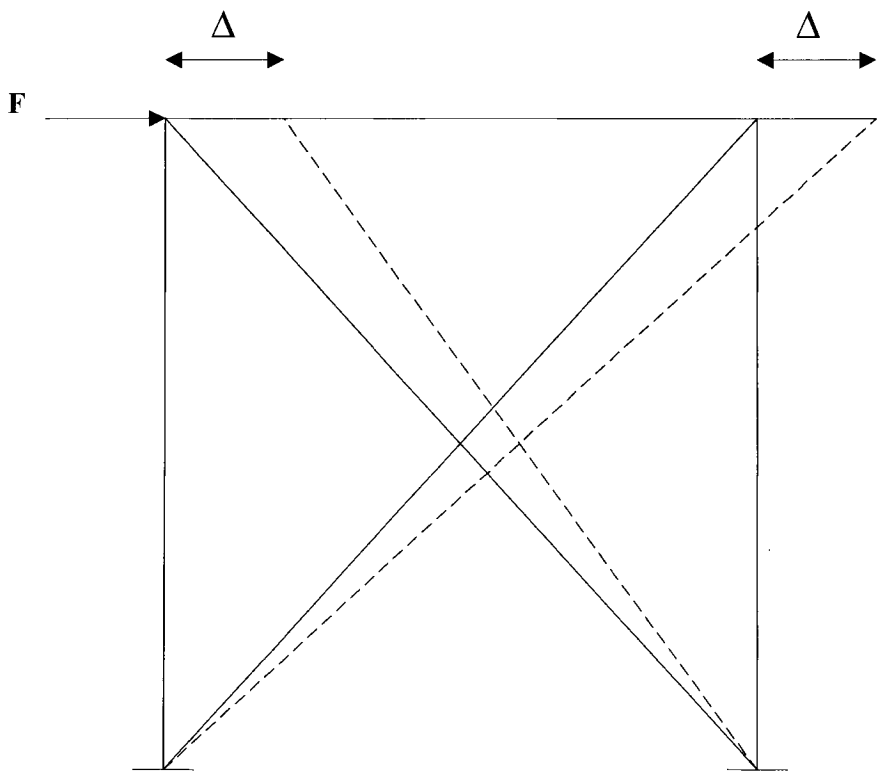

Figure3.7: Effect of displacement on strand behavior

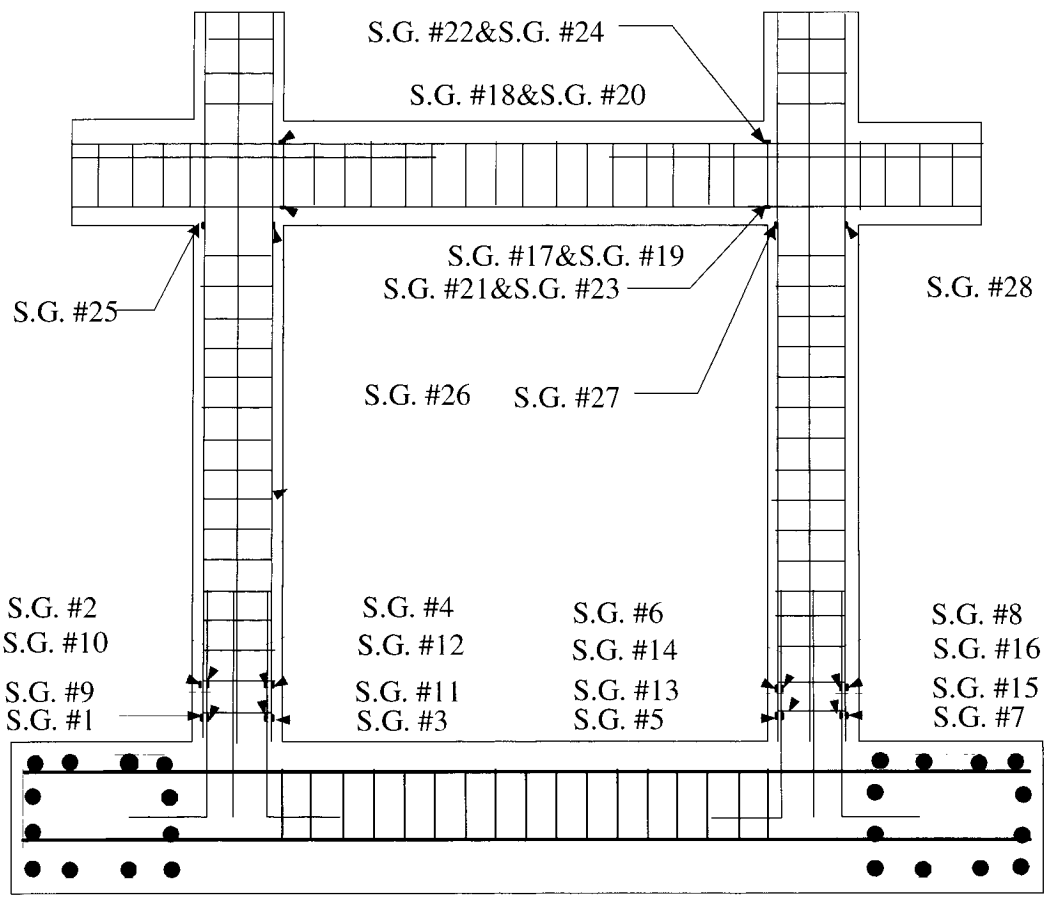

Figure 3.8: Locations of strain gauges on frame reinforcement

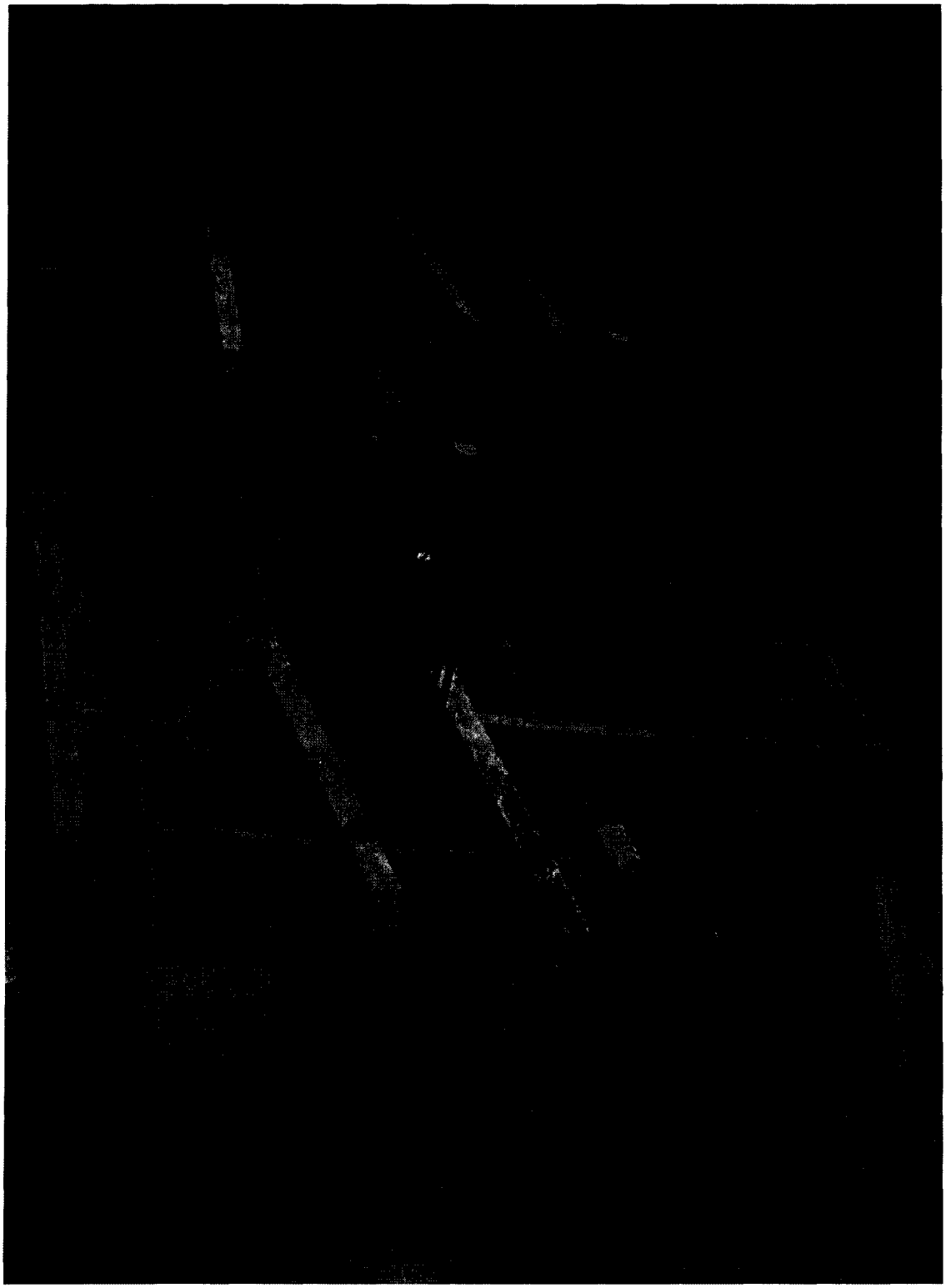

Figure 3.9: Foundations ready to cast

Figure 3.10: Plastic tubes and steel hooks embedded in foundation

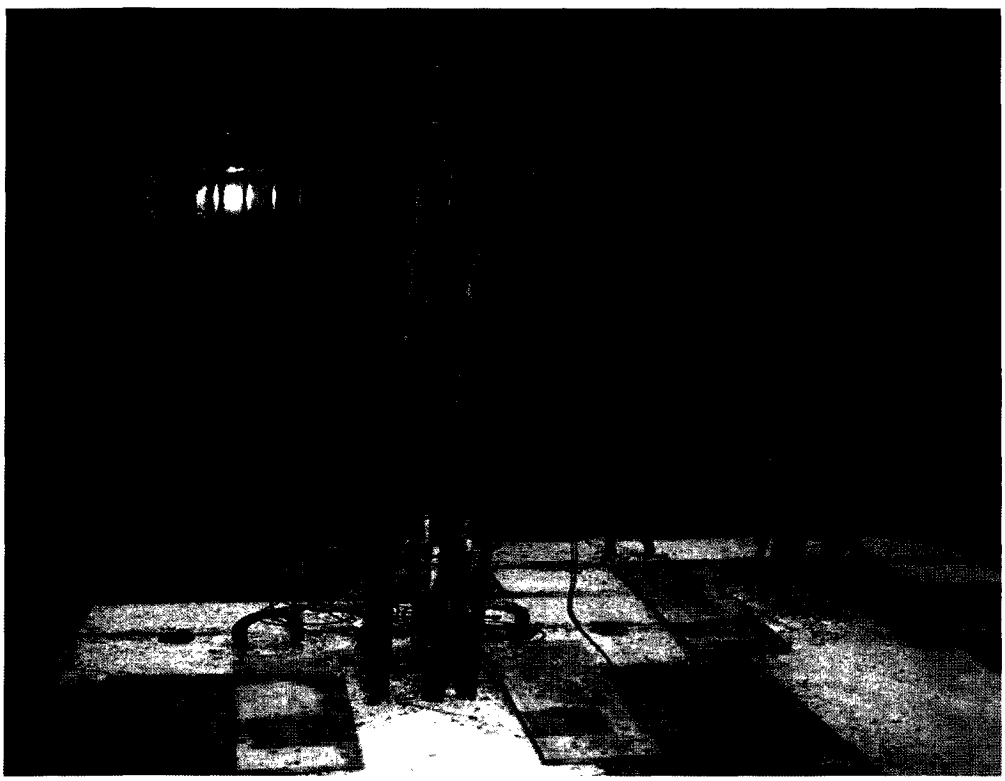

Figure 3.11: A Typical colum n cage

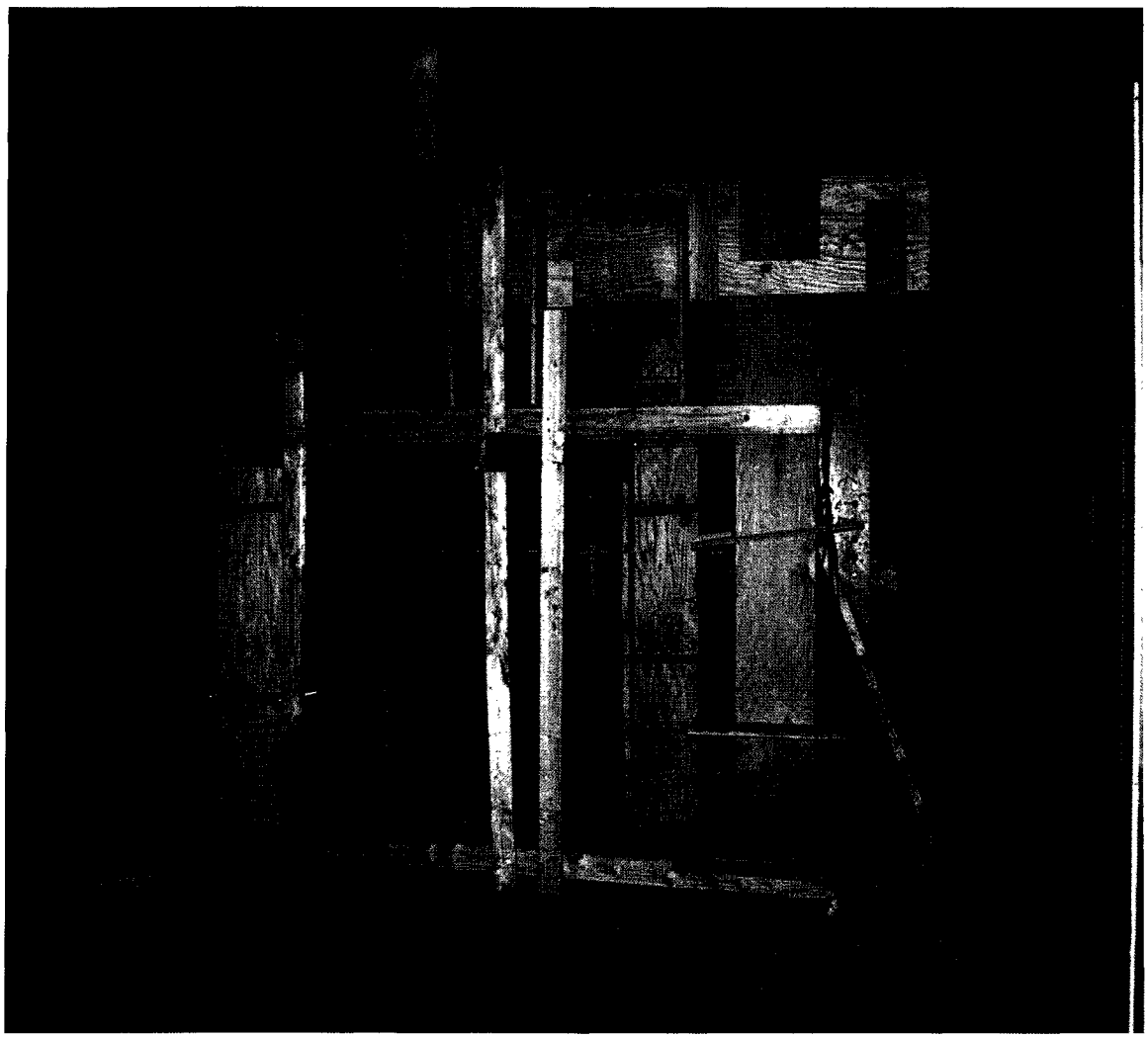

Figure 3.12: Complete frame formwork

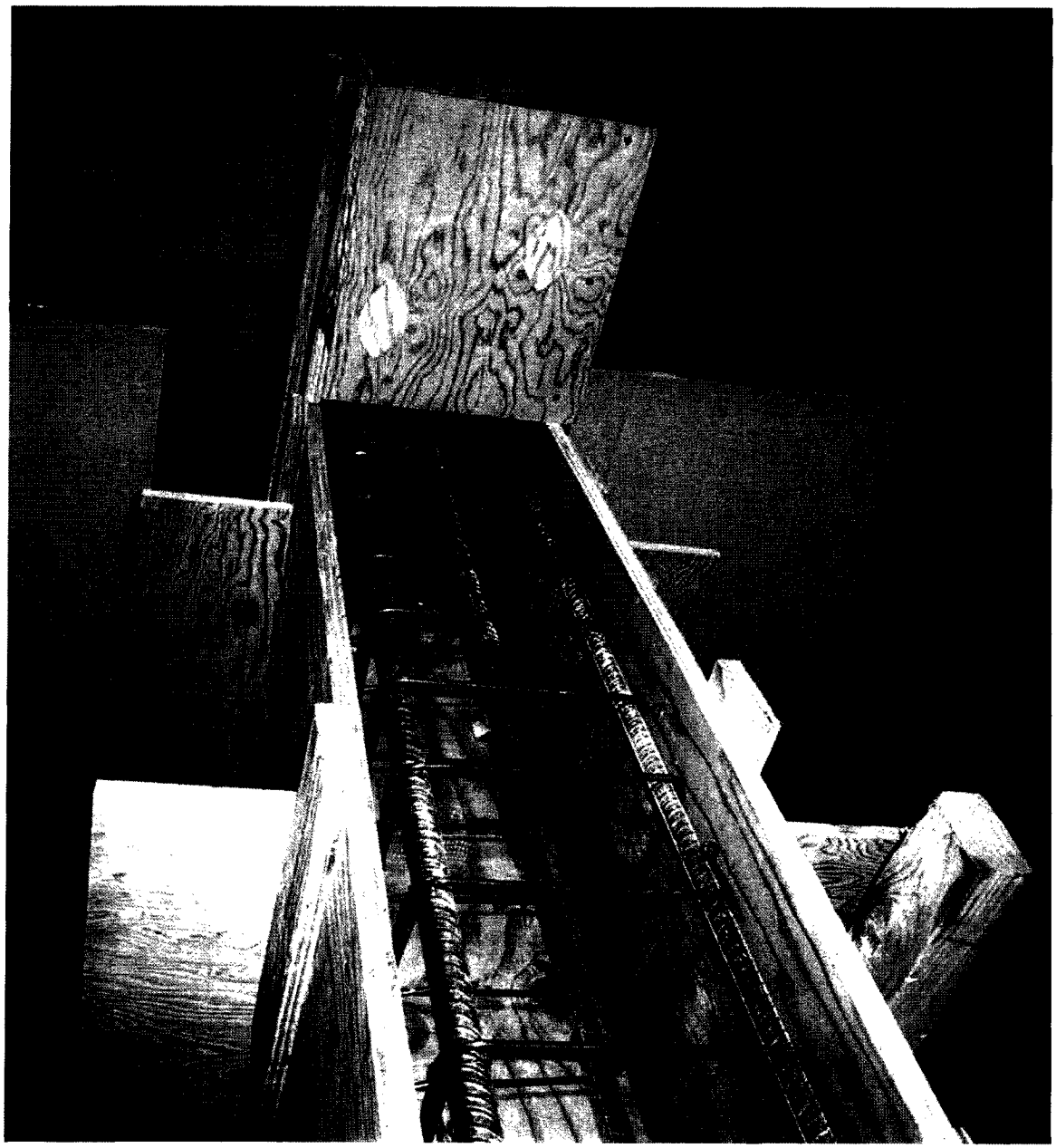

Figure 3.13: Reinforcement for top beam

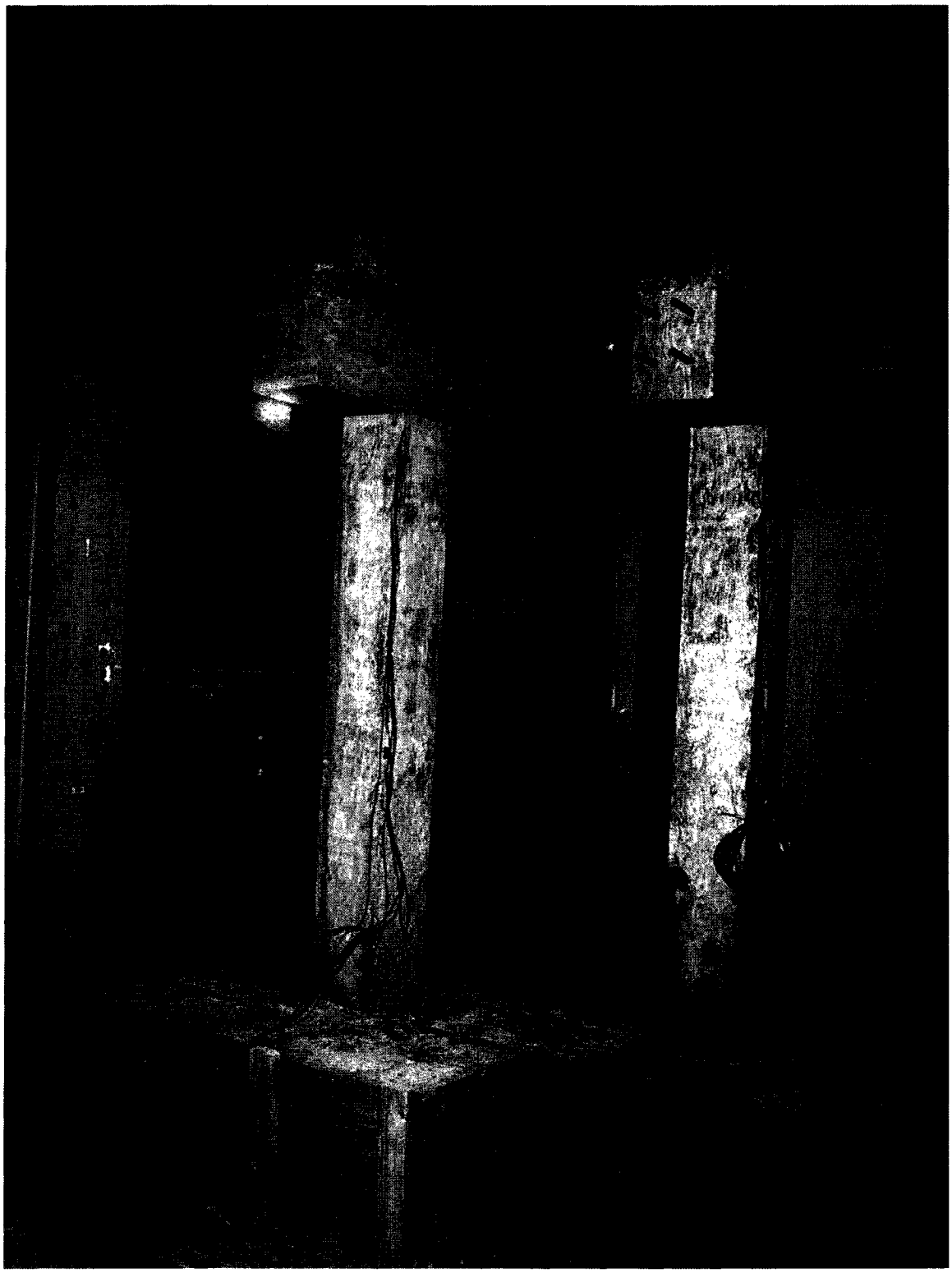

Figure 3.14: Two of the bare frames after casting

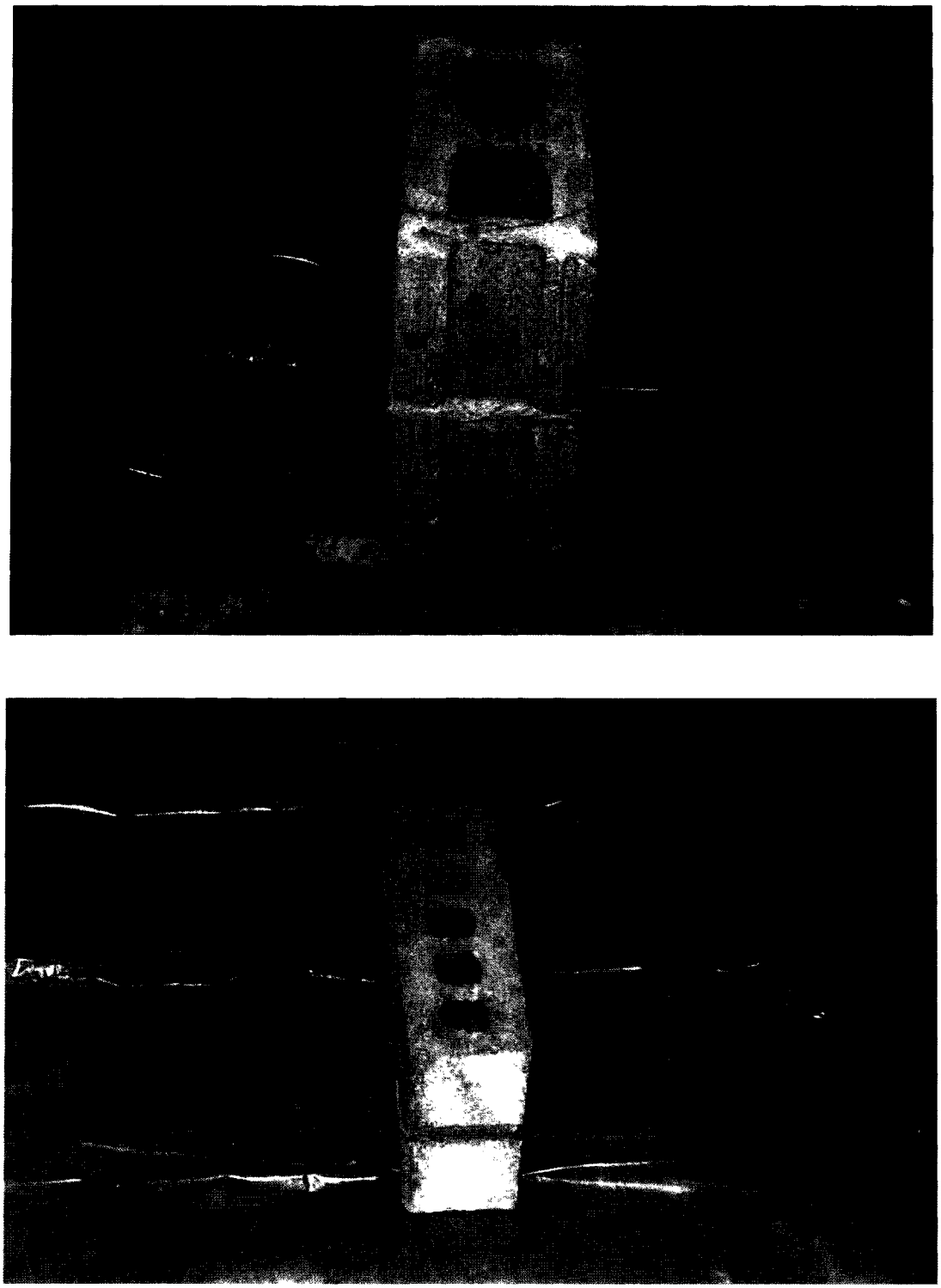

Figure 3.15: Masonry prisms

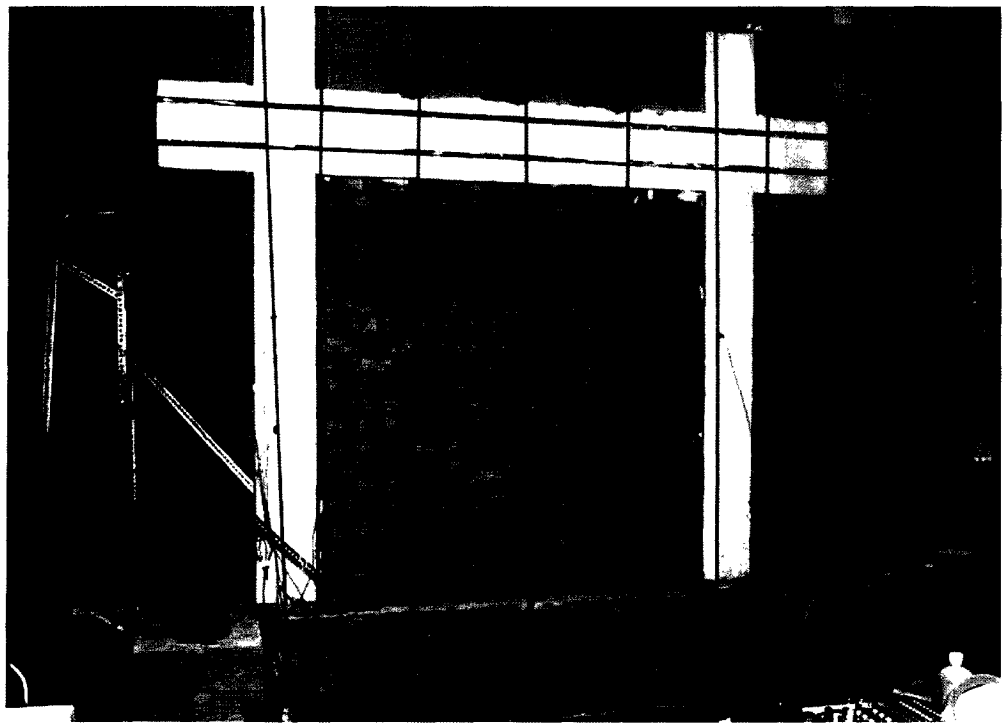

Figure 3.16: Externally post-tensioned cables applying gravity loads

Figure 3.17: Hollow steel sections welded with steel angle

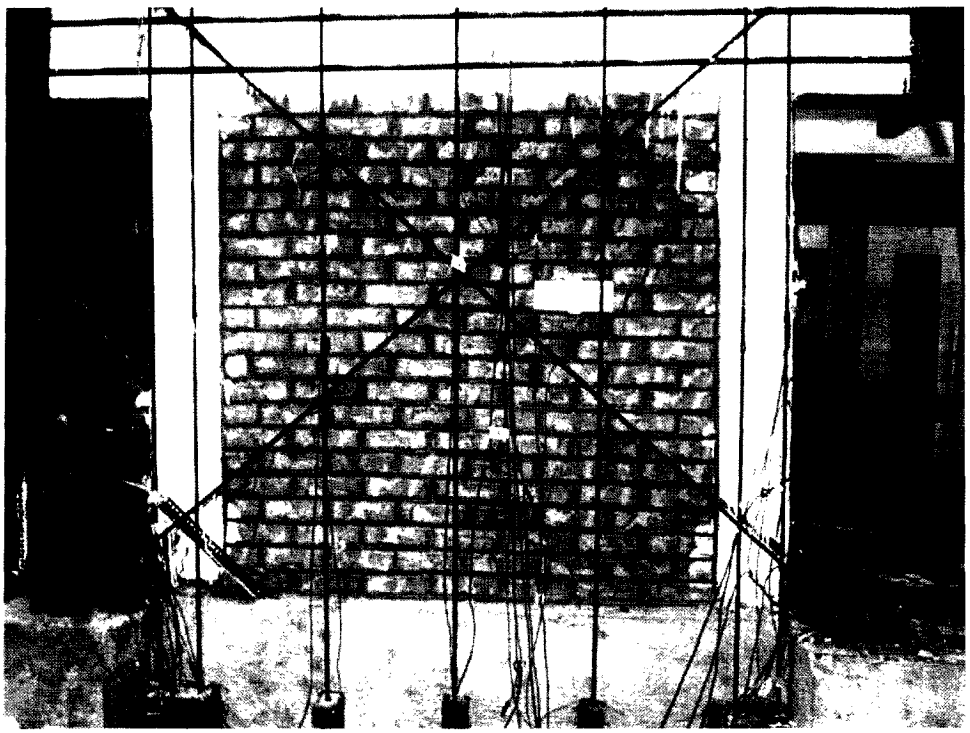

Figure 3.18: Steel plates supporting strands on the foundation

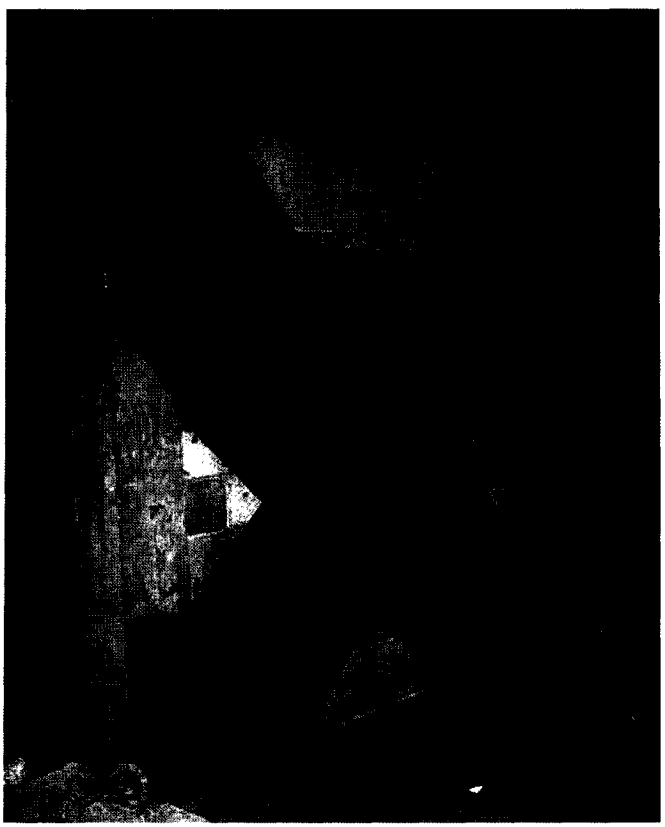

Figure 3.19: Specimen retrofitted with diagonal FRP sheets

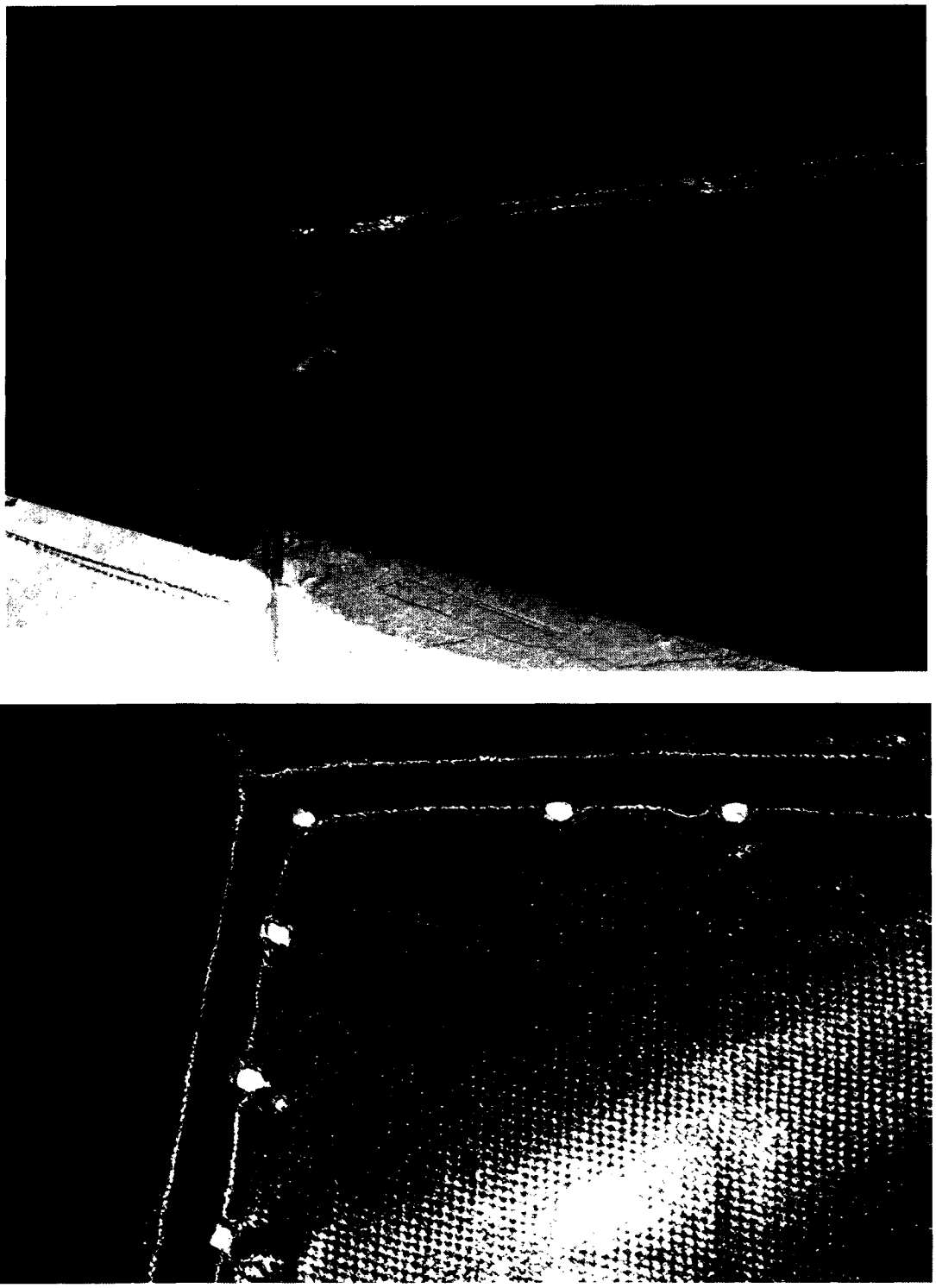

Figure 3.20: Holes for FRP anchors

Figure 3.21: Specimen BR-3, retrofitted with diagonal prestressing and FRP wrapping

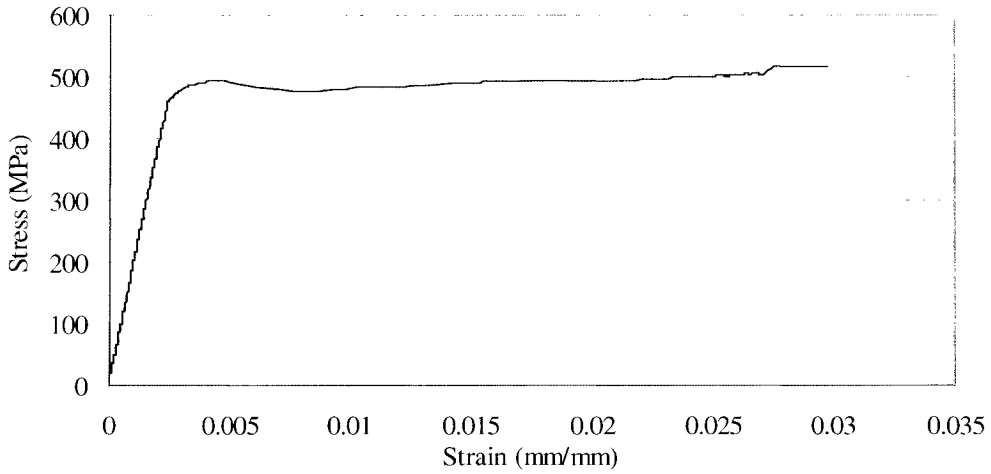

Figure 3.22: Steel stress-strain relationship for # 15 reinforcement

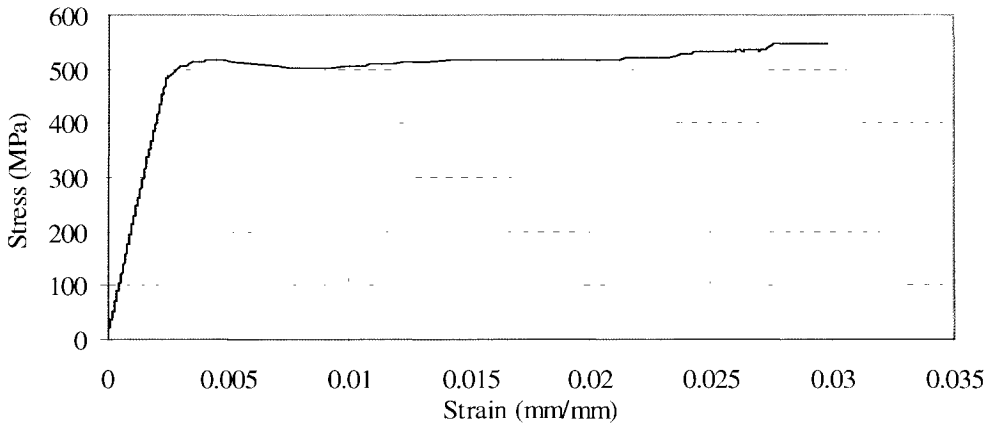

Figure 3.23: Stress-strain relationship for # 6.38 stirrups and ties

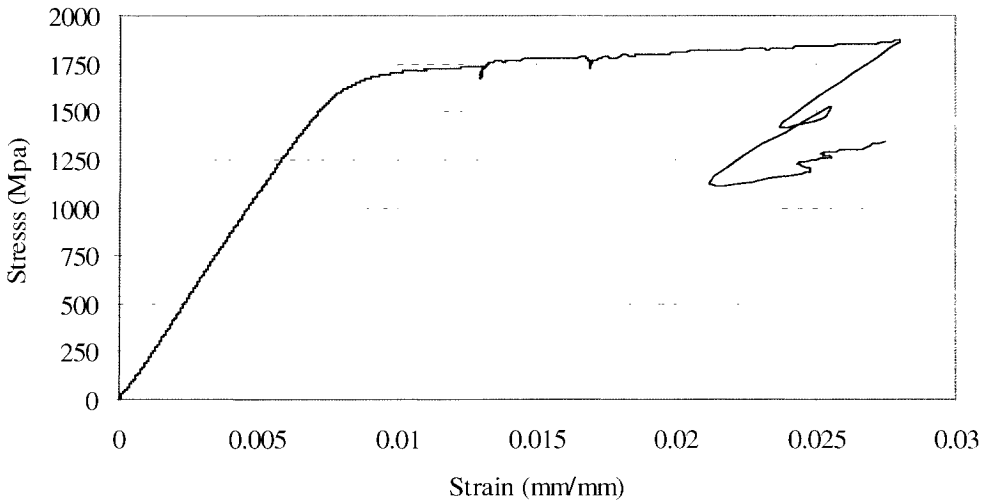

Figure 3.24: Stress-strain relationship for #15 prestressing strand

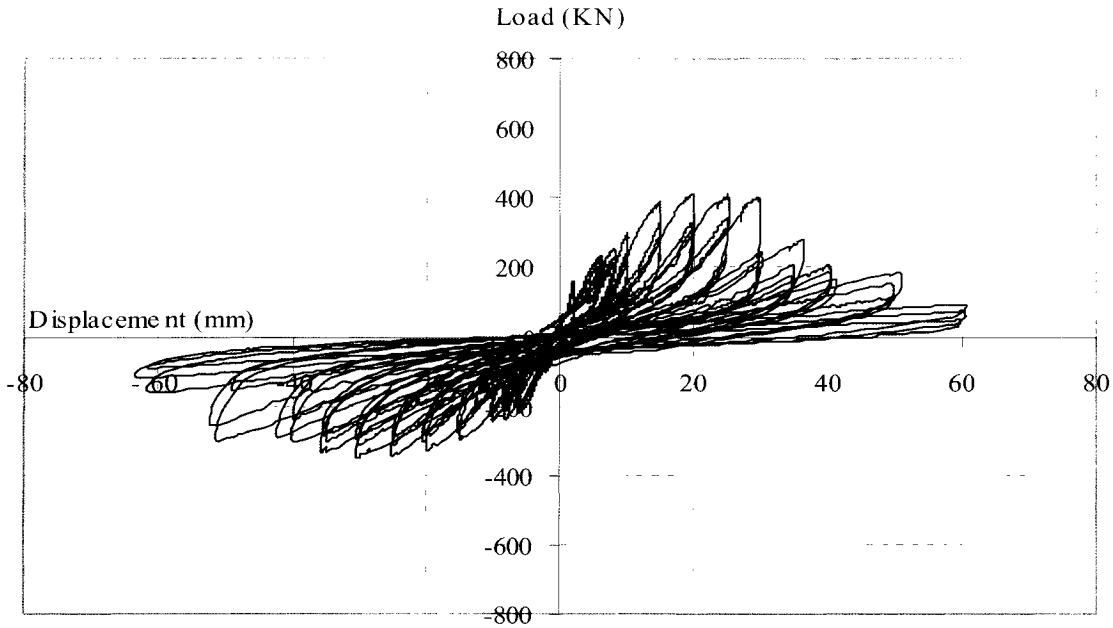

Figure 4.1: Hysteretic lateral load - lateral displacement relationship for BR-1 (Uuretrofitted specimen)

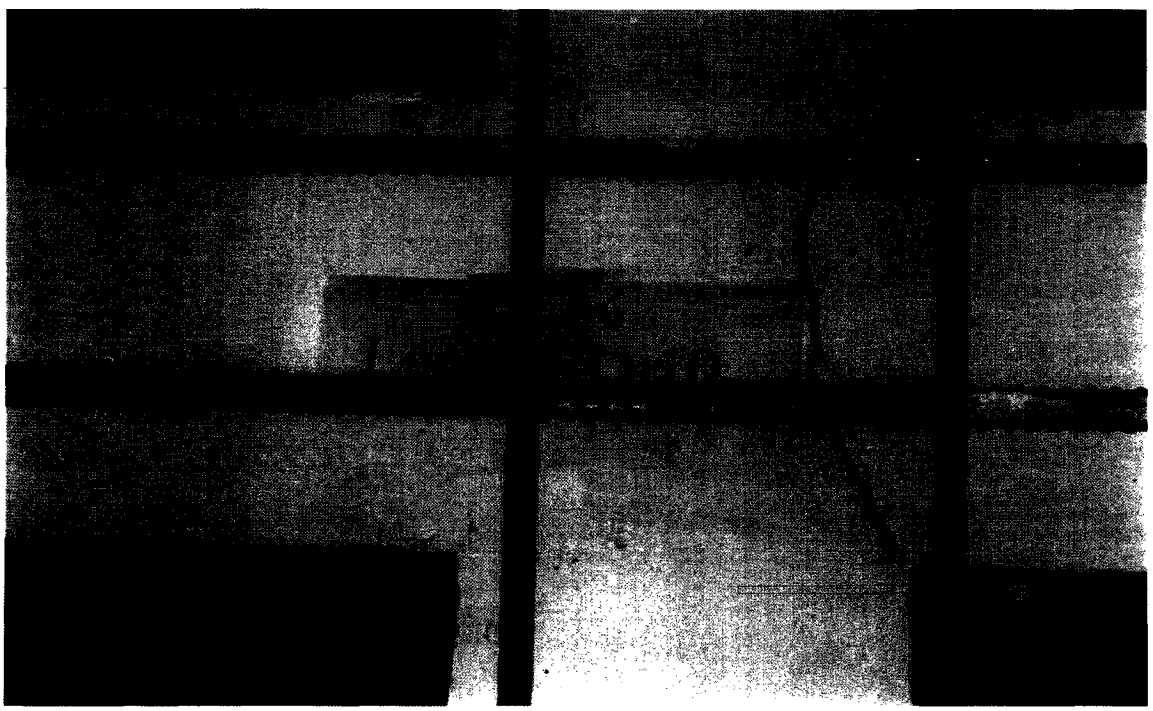

Figure 4.2: Flexural crack at beam critical section at 0.5 % drift (BR-1)

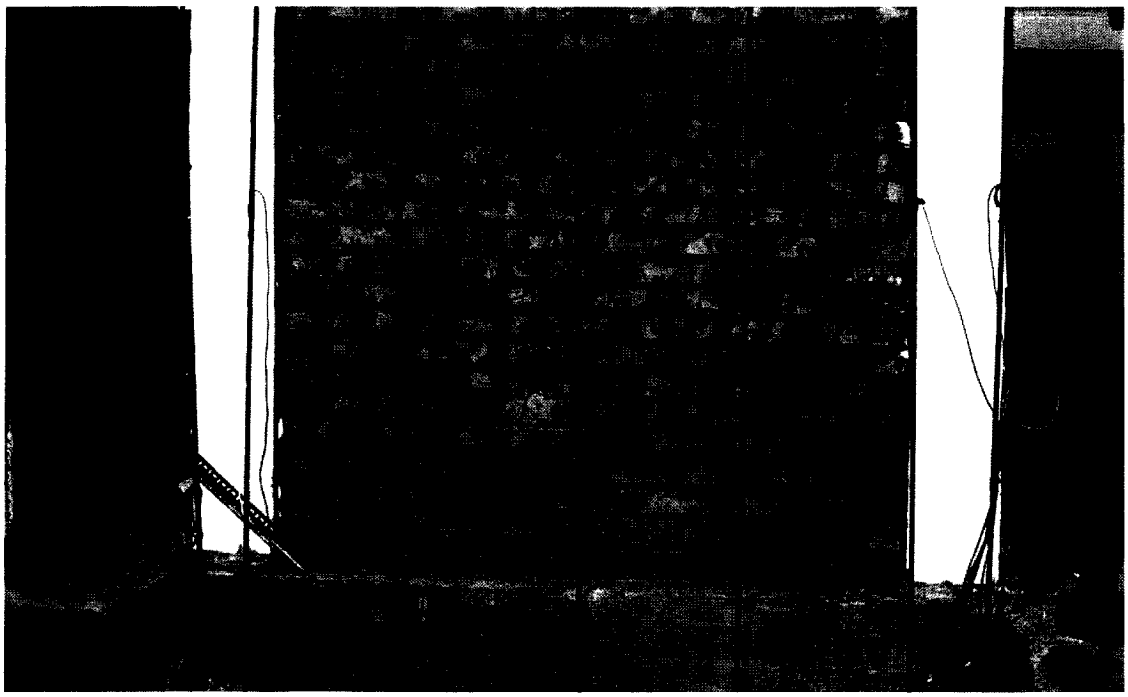

Figure 4.3: Diagonal cracks in masonry wall at 0.5 % Drift (BR-1)

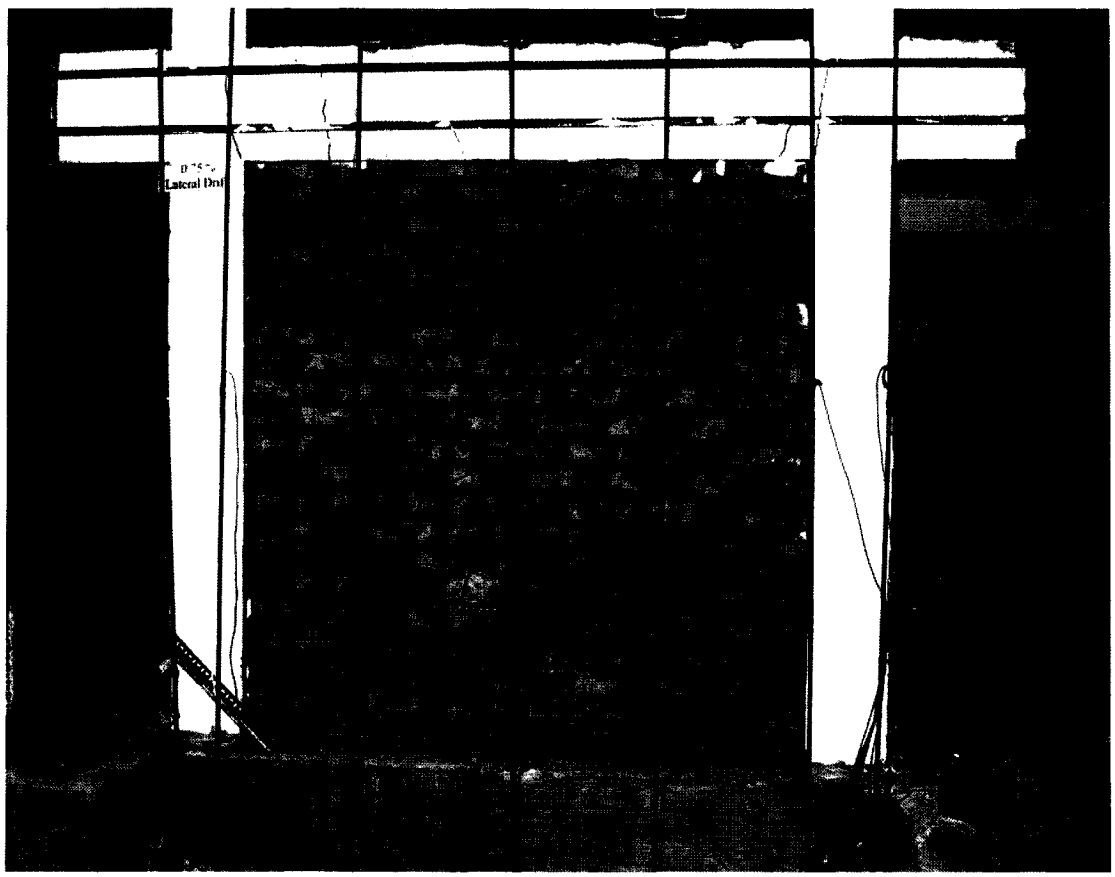

Figure 4.4: Diagonal tension cracks in masonry wall and flexural cracks in beam at 0.75 % lateral drift (BR-1)

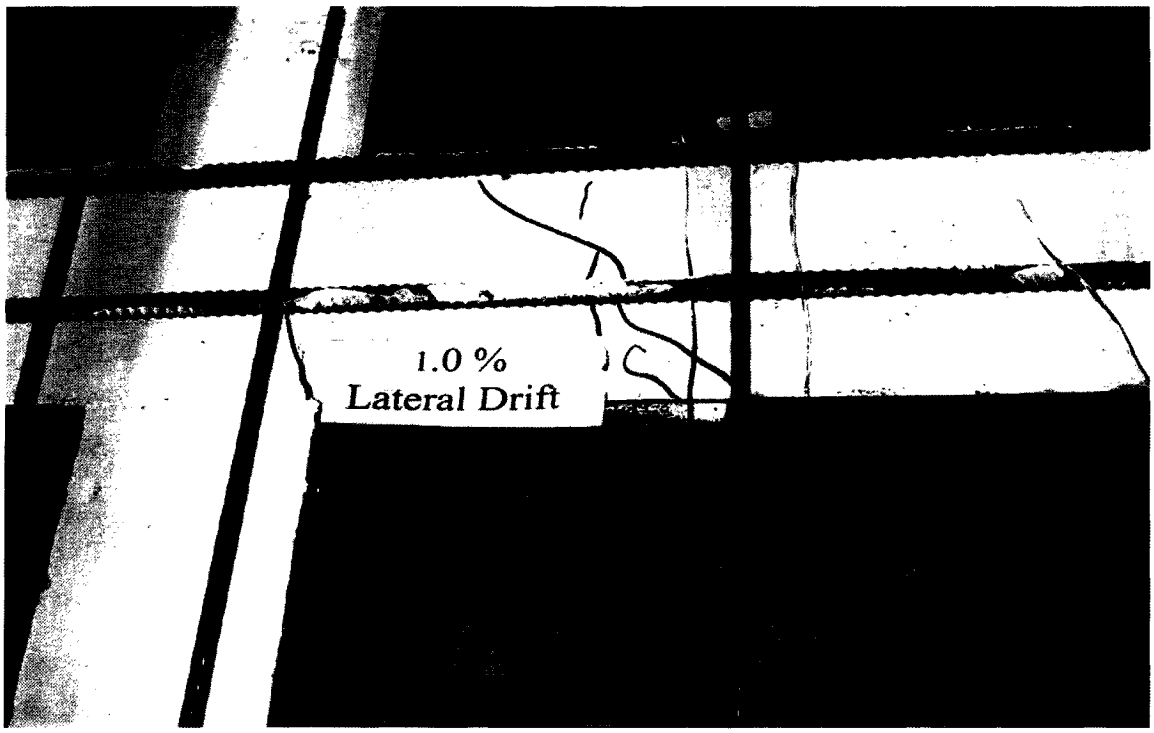

Figure 4.5: Widening of beam flexural cracks at 1.0 % lateral drift (BR-1)

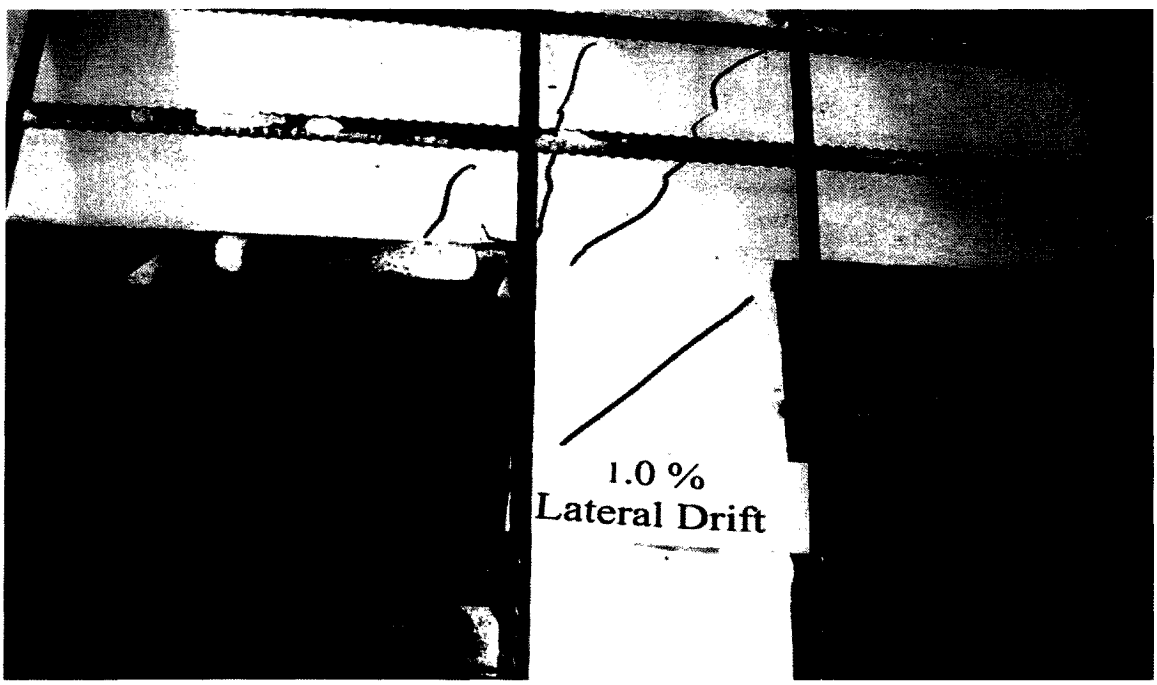

Figure 4.6: Formation of diagonal tension cracks in columns at 1.0 % lateral drift (BR-1)

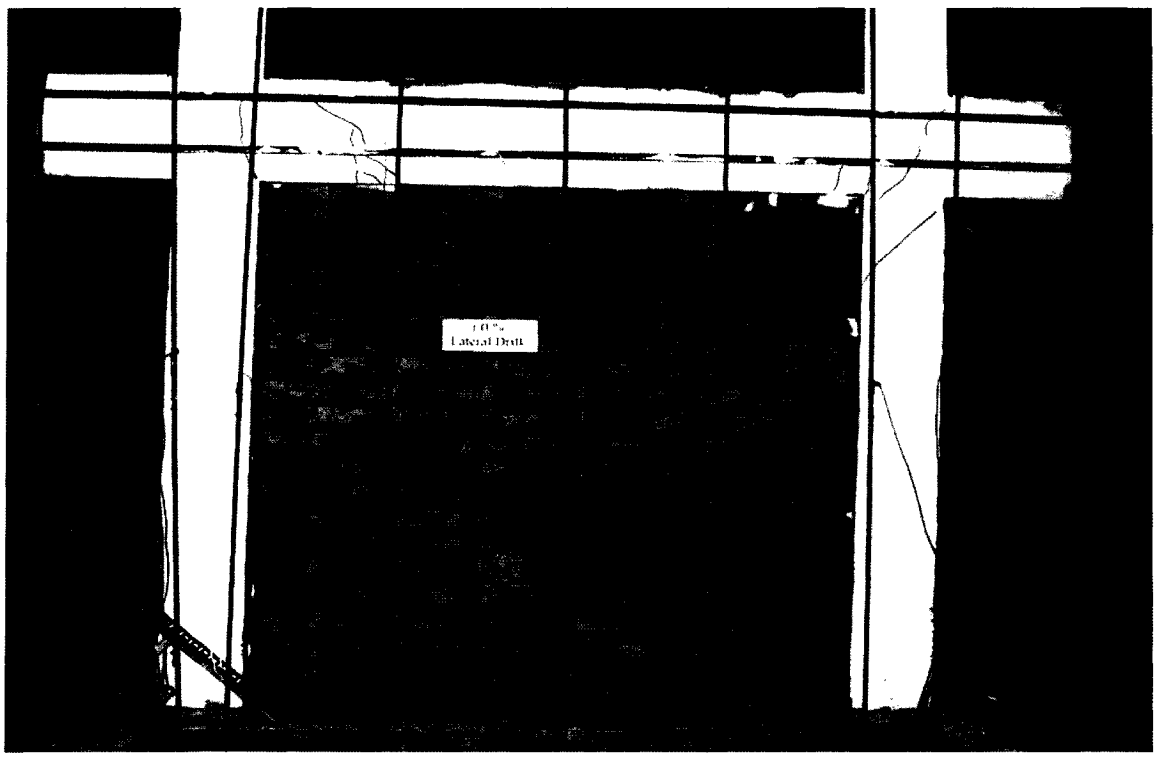

Figure 4.7: Crack pattern in specimen BR-1 at 1.0 % lateral drift

Figure 4.8: Crack pattern in specimen BR-1 at 1.25 % lateral drift

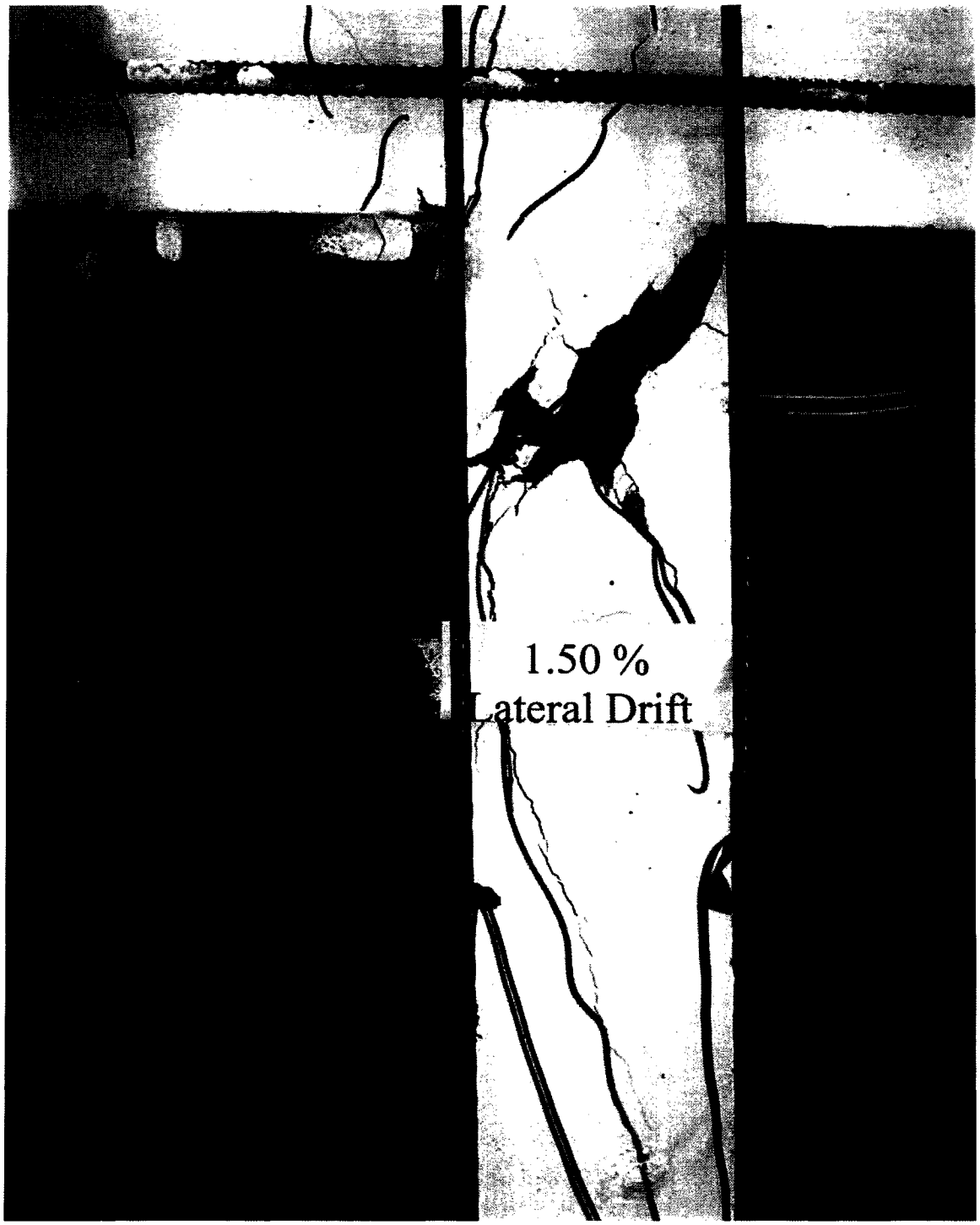

Figure 4.9: Concrete deterioration and widening of diagonal cracks in column at 1.5 % lateral drift (BR-1)

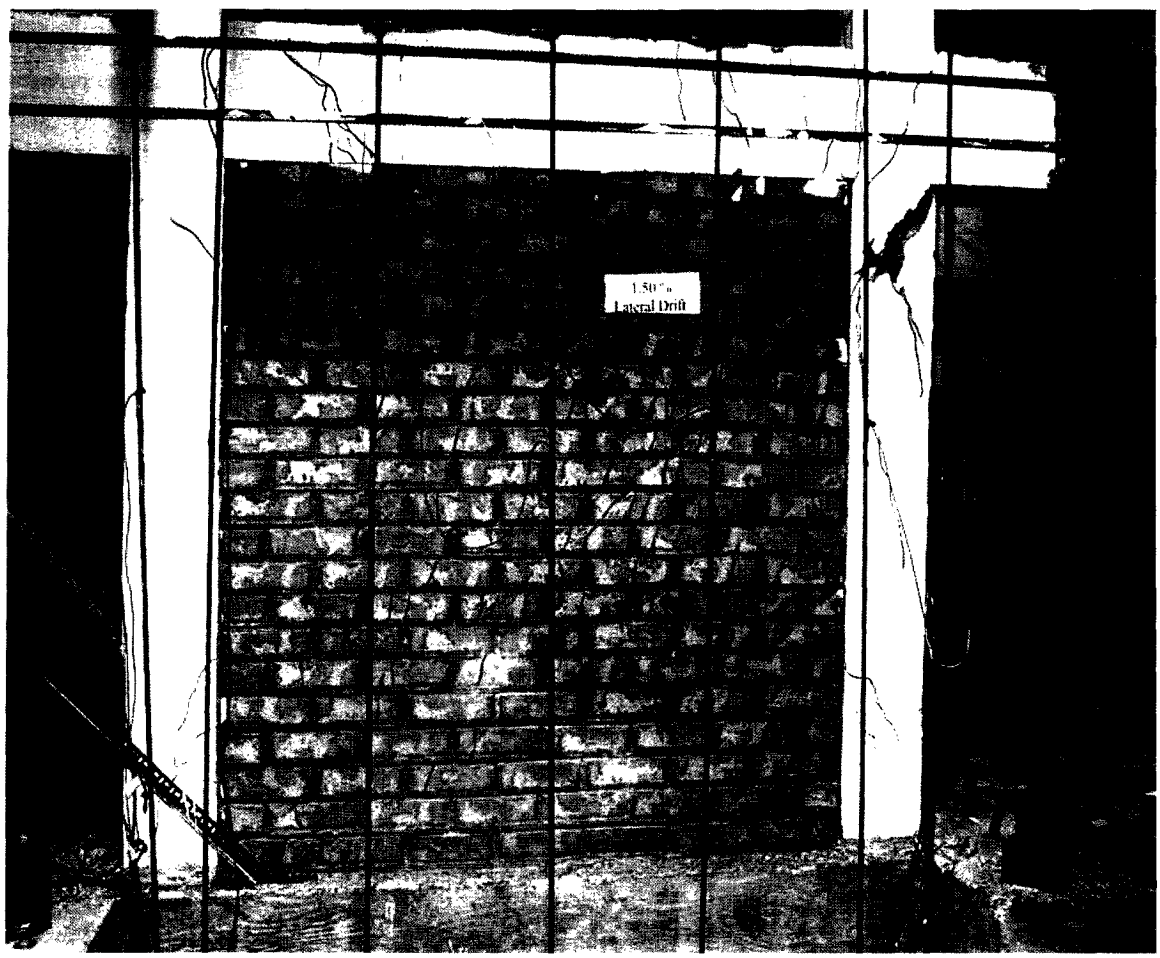

Figure 4.10: Crack pattern in specimen BR-1 at 1.5 % lateral drift

Figure 4.11: Crack pattern in specimen BR-1 at 1.75 % lateral drift

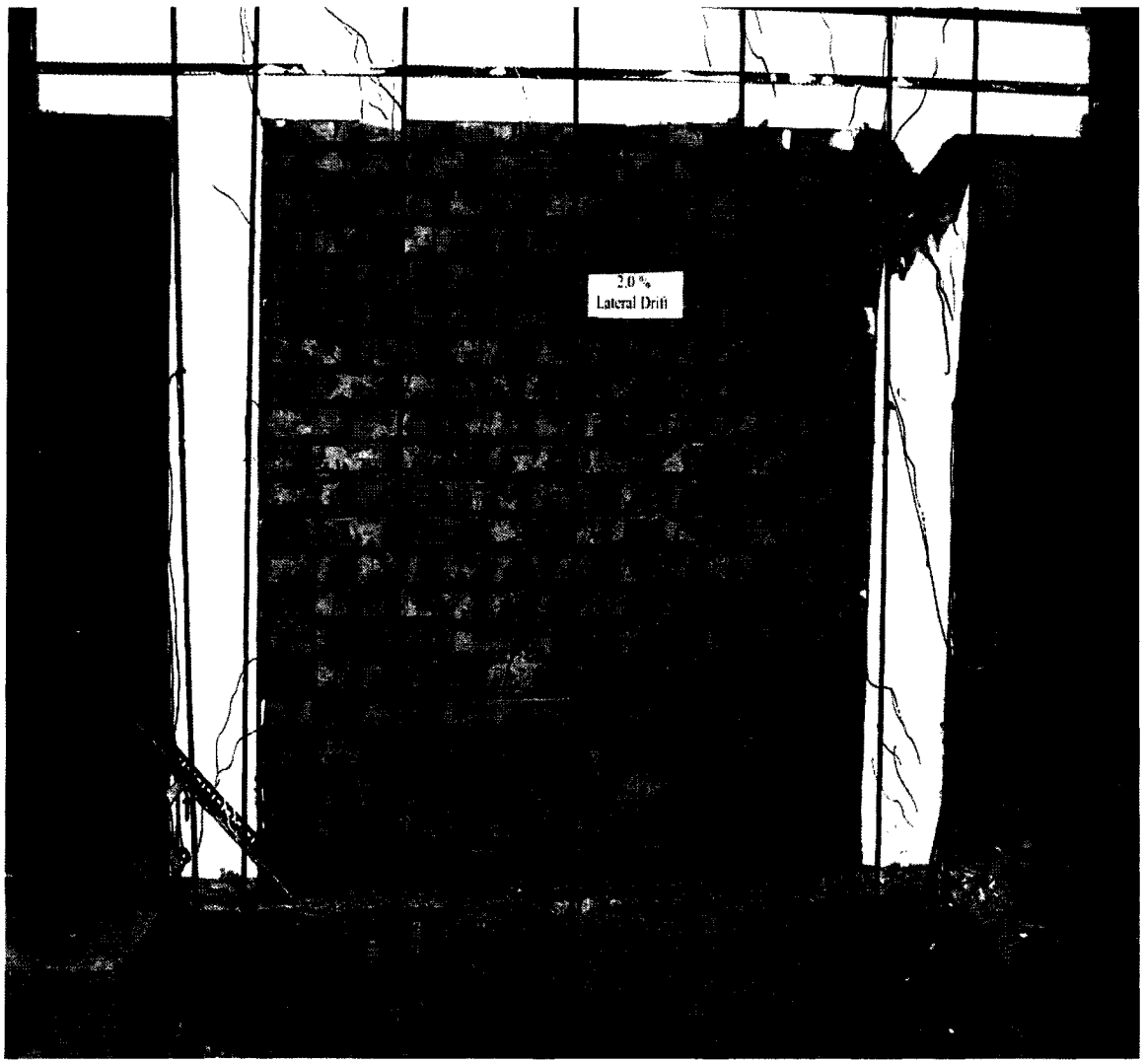

Figure 4.12: Damage to specimen BR-1 at 2.0 % lateral drift

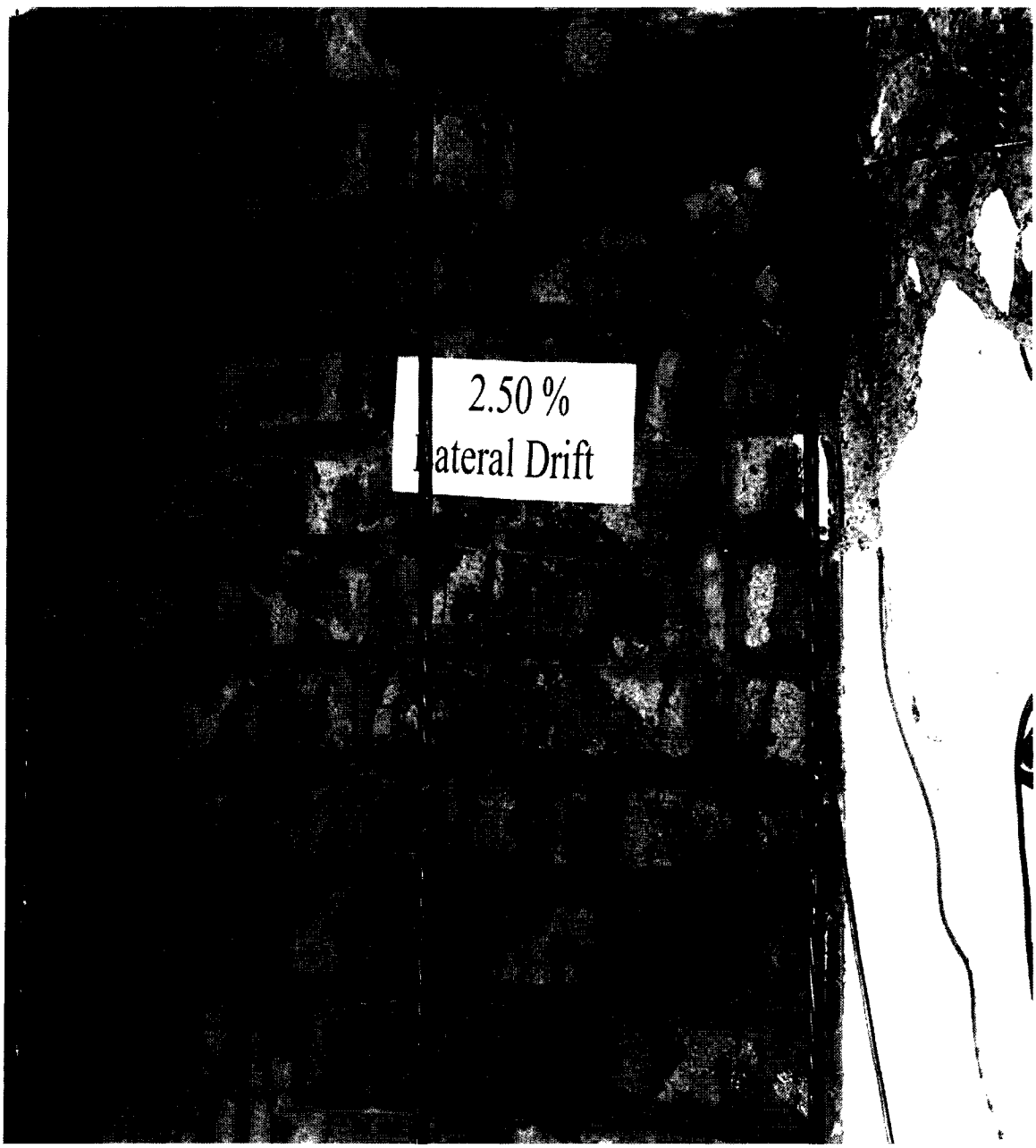

Figure 4.13: Failure of masonry and buckling of column bars at 2.5 % lateral drift (BR-1)

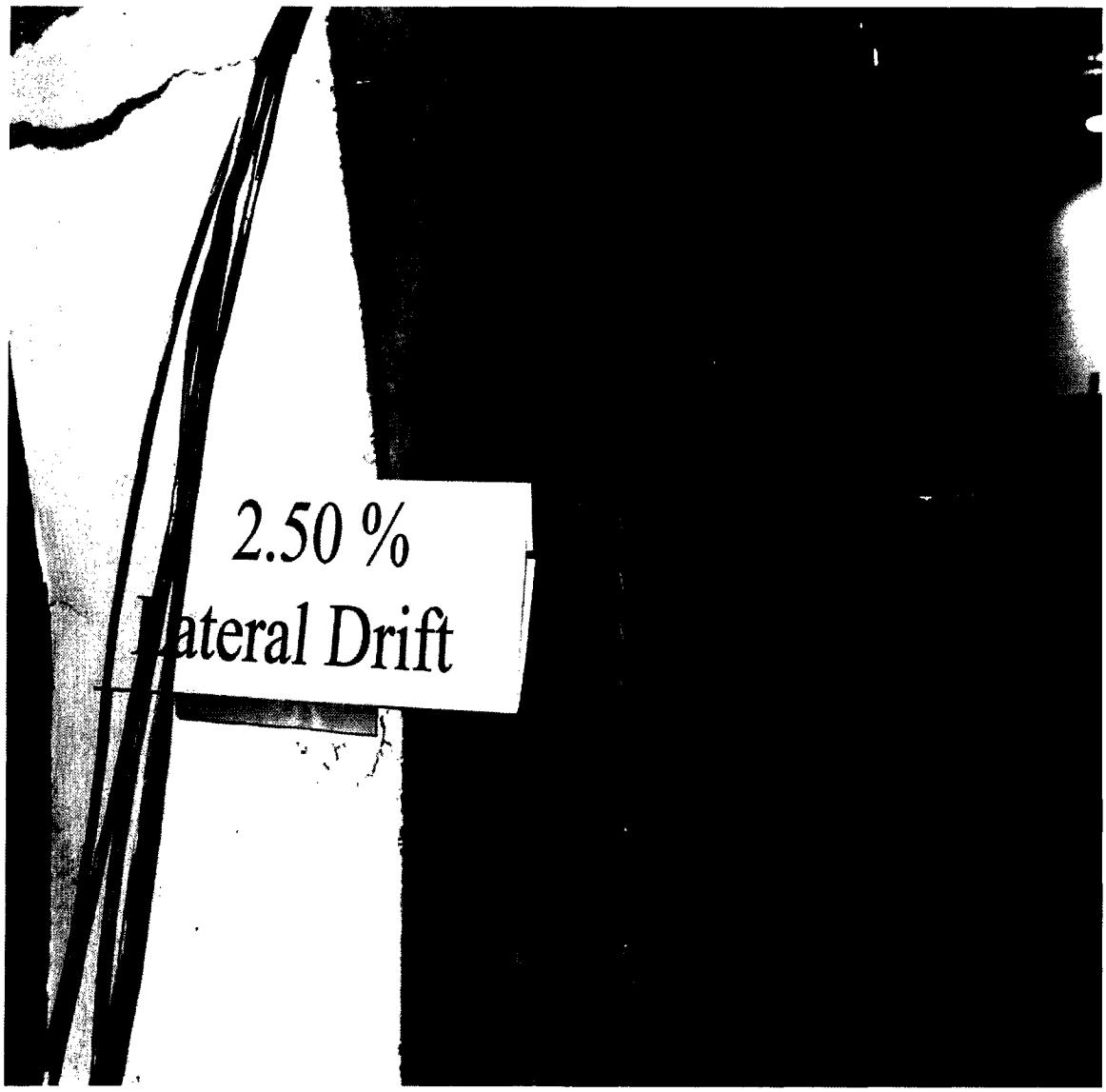

Figure 4.14: Out of plane failure of the wall at 2.5 % lateral drift (BR-1)

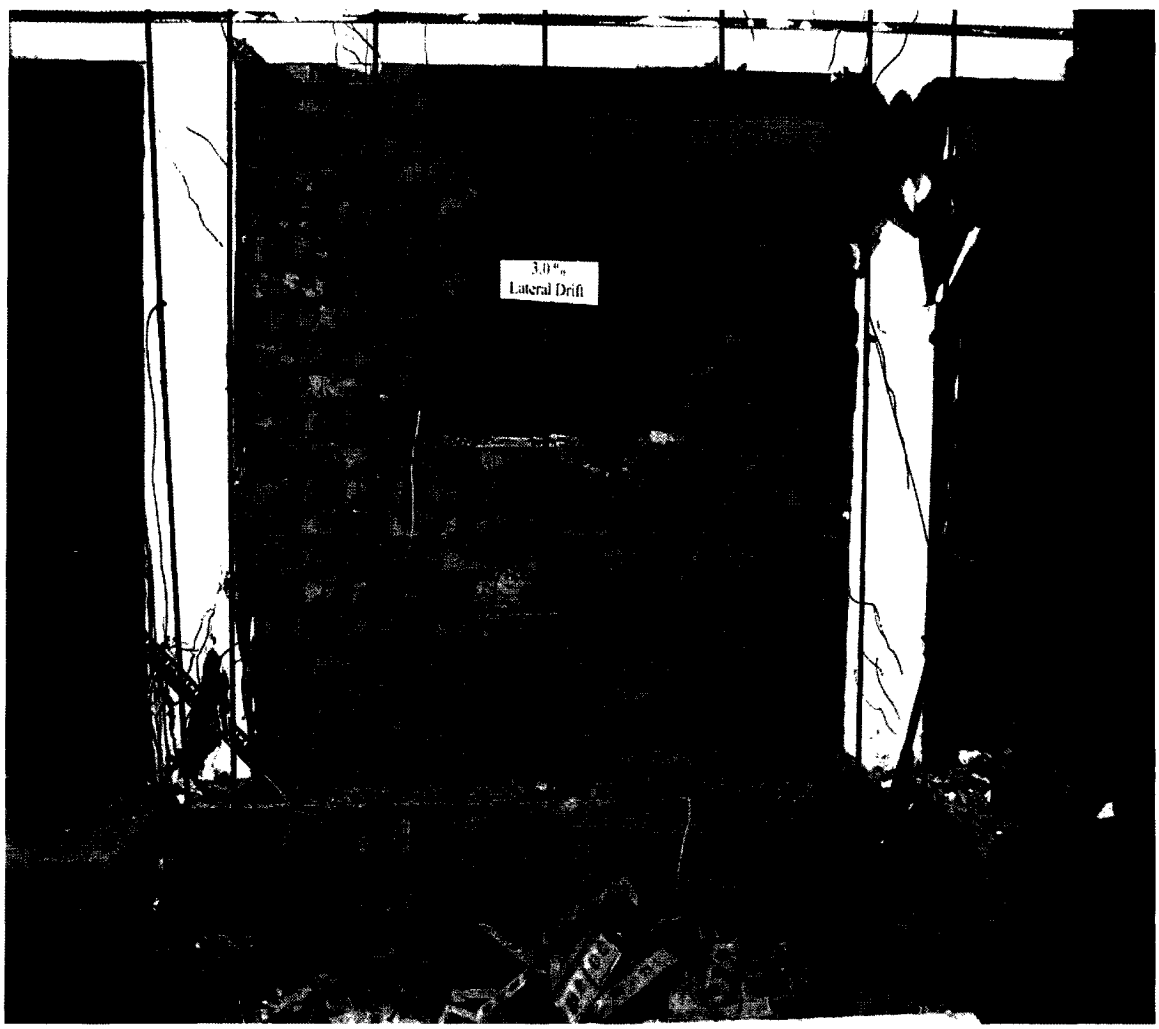

Figure 4.15: Deterioration of specimen BR-1 at 3 % lateral drift (front view)

Figure 4.16: Deterioration of specimen BR-1 at 3 % lateral drift (back view)

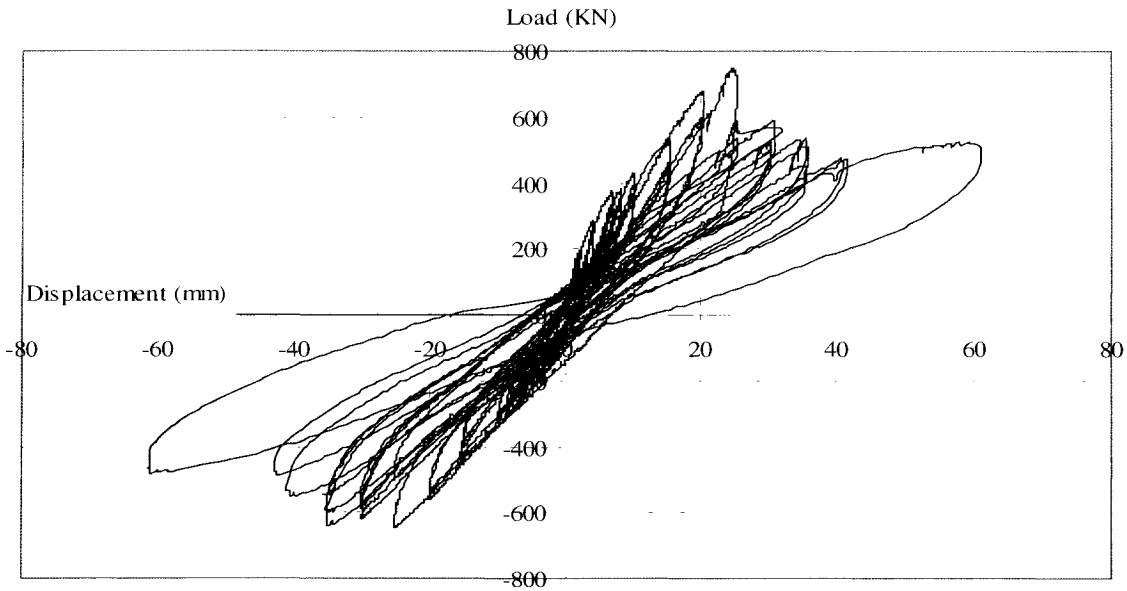

Figure 4.17: Hysteretic lateral load - lateral displacement relationship for BR-2 (Retrofitted specimen)

Figure 4.18: Flexural crack at beam critical section at 0.5 % lateral drift (BR-2)

Figure 4.19: Crack at top of the close column at 0.75 % lateral drift (BR-2)

Figure 4.20: Separation in mortar joints at 0.75 % lateral drift (BR-2)

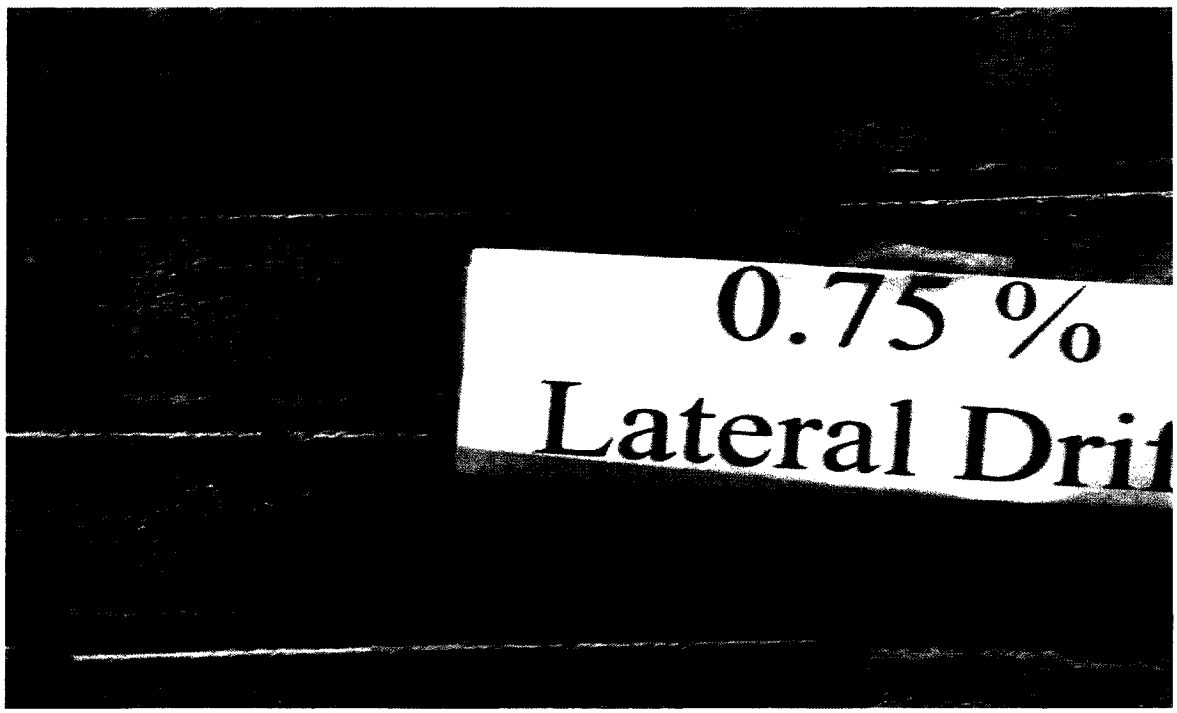

Figure 4.21: Diagonal tension cracks in masonry wall at 0.75 % lateral drift (BR-2)

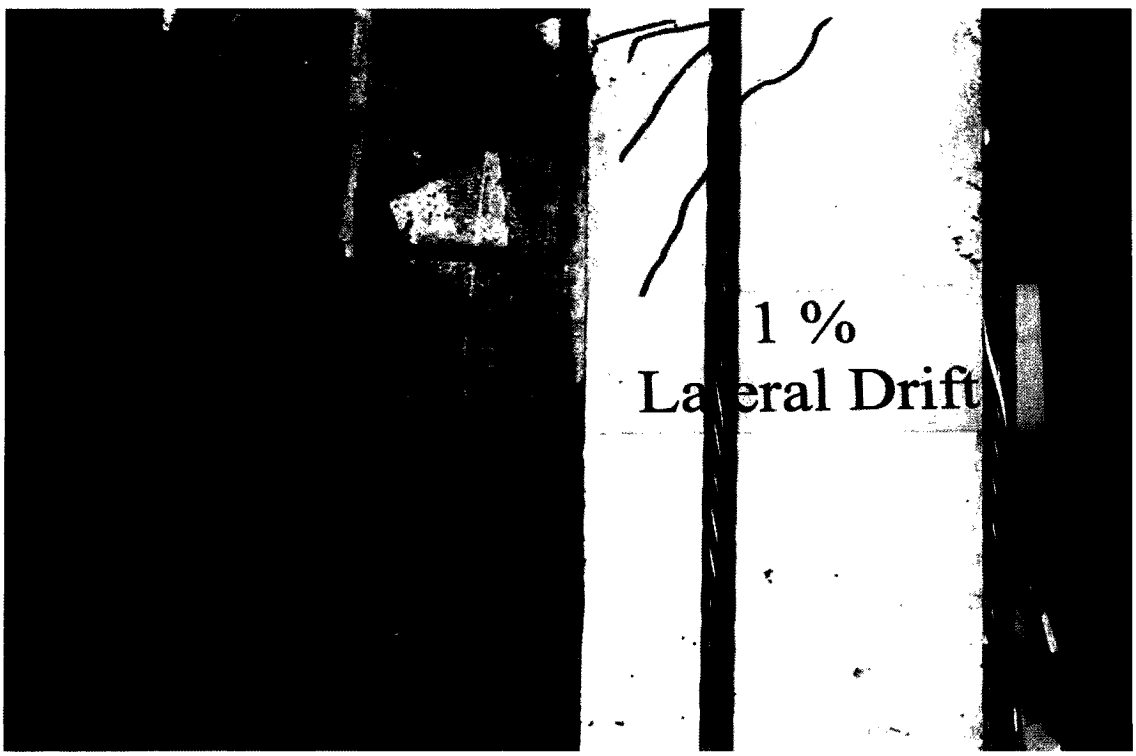

Figure 4.22: Cracks at top of close column at 1.0 % lateral drift (BR-2)

Figure 4.23: Cracks at bottom of far column at 1.0 % lateral drift (BR-2).

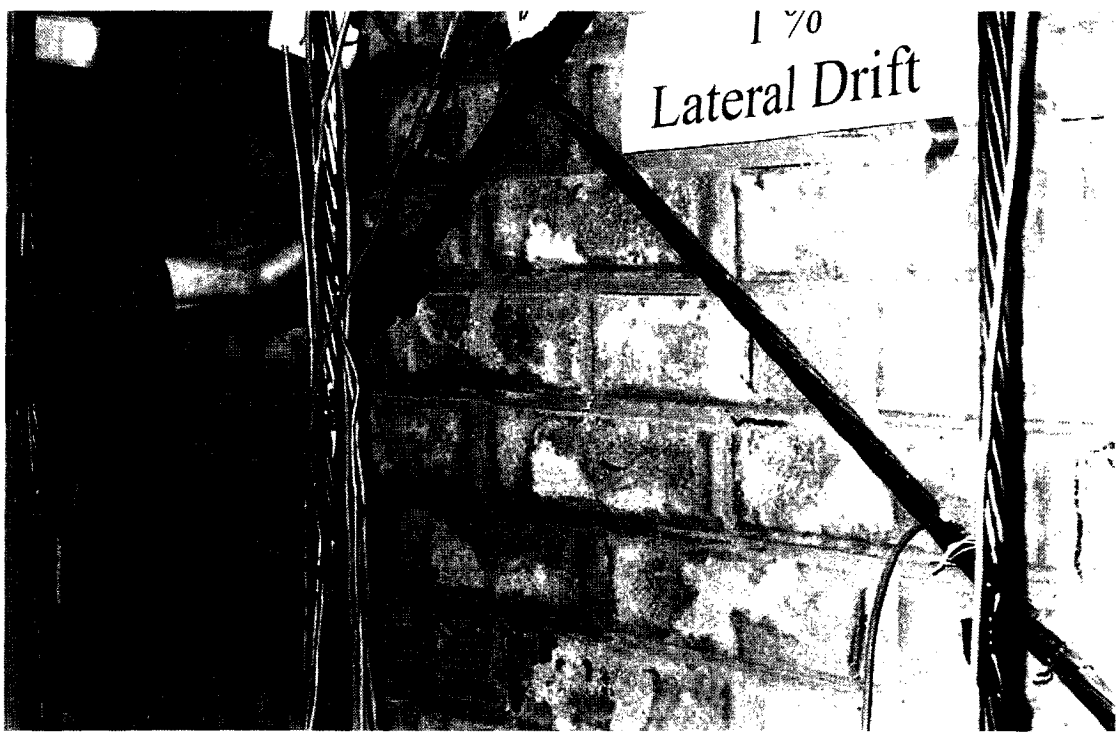

a) Front view

Figure 4.24: Relaxation of diagonal prestressed cable at 1.0% drift (BR-2)

b) Side view

Figure 4.24: (Cont'd) Relaxation of diagonal prestressed cable at 1.0% drift (BR-2)

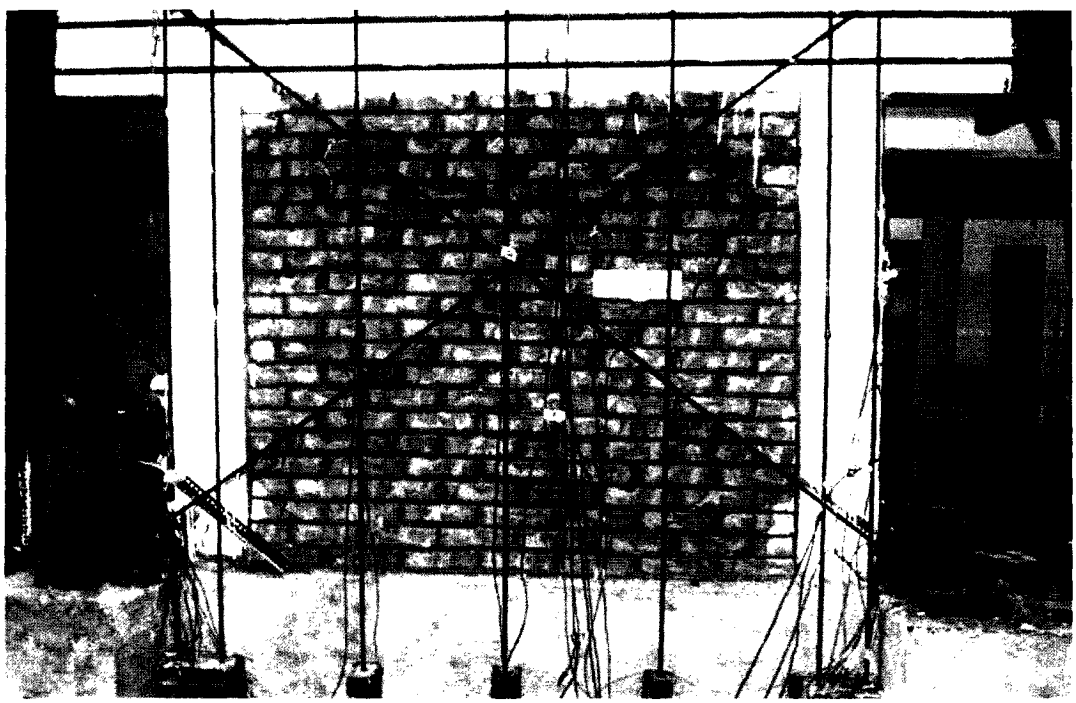

Figure 4.25: Deterioration of specimen BR-2 at 1.25 % lateral drift

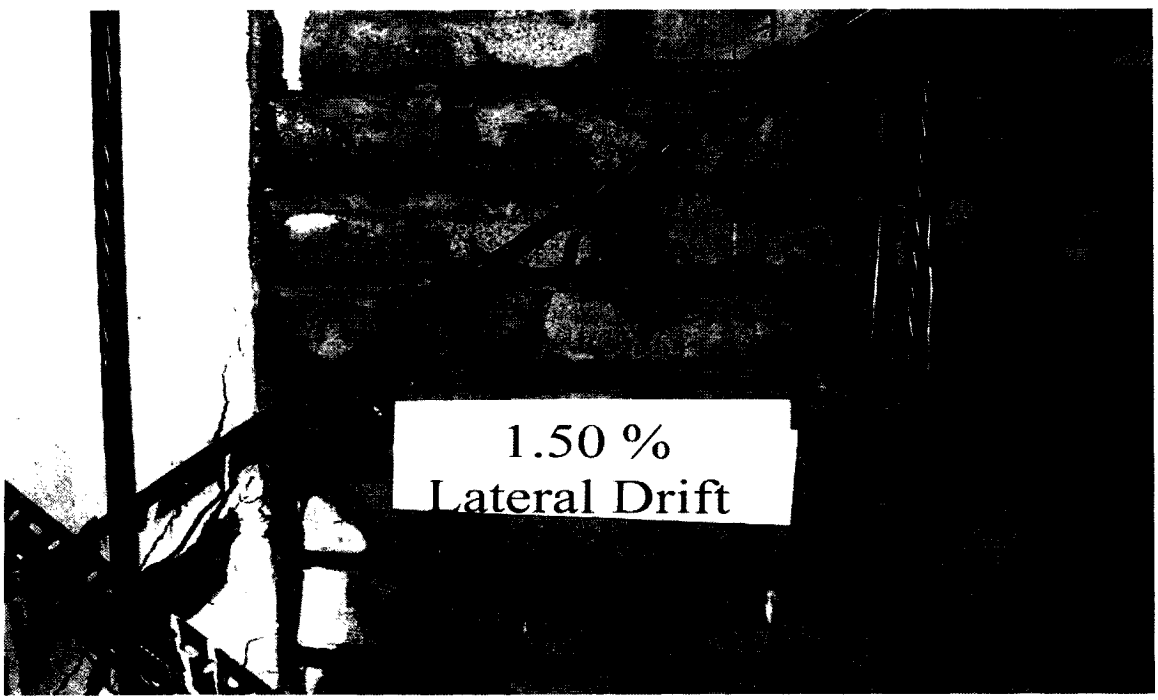

Figure 4.26: Concrete deterioration and widening of diagonal cracks in bottom of left column and wall at 1.5 % lateral drift (BR-2)

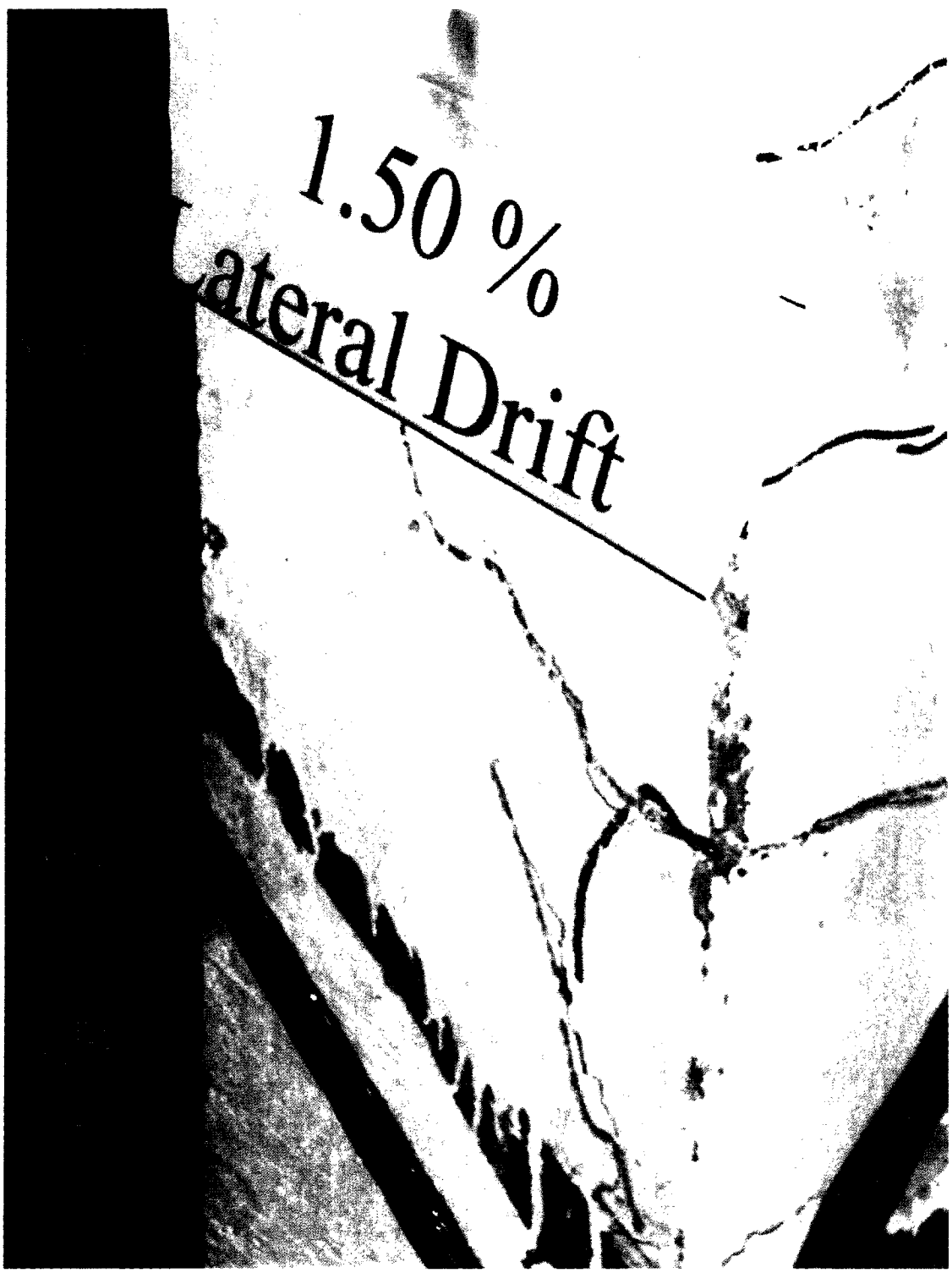

Figure 4.27: Cracks at bottom of right column, at 1.5 % lateral drift (BR-2)

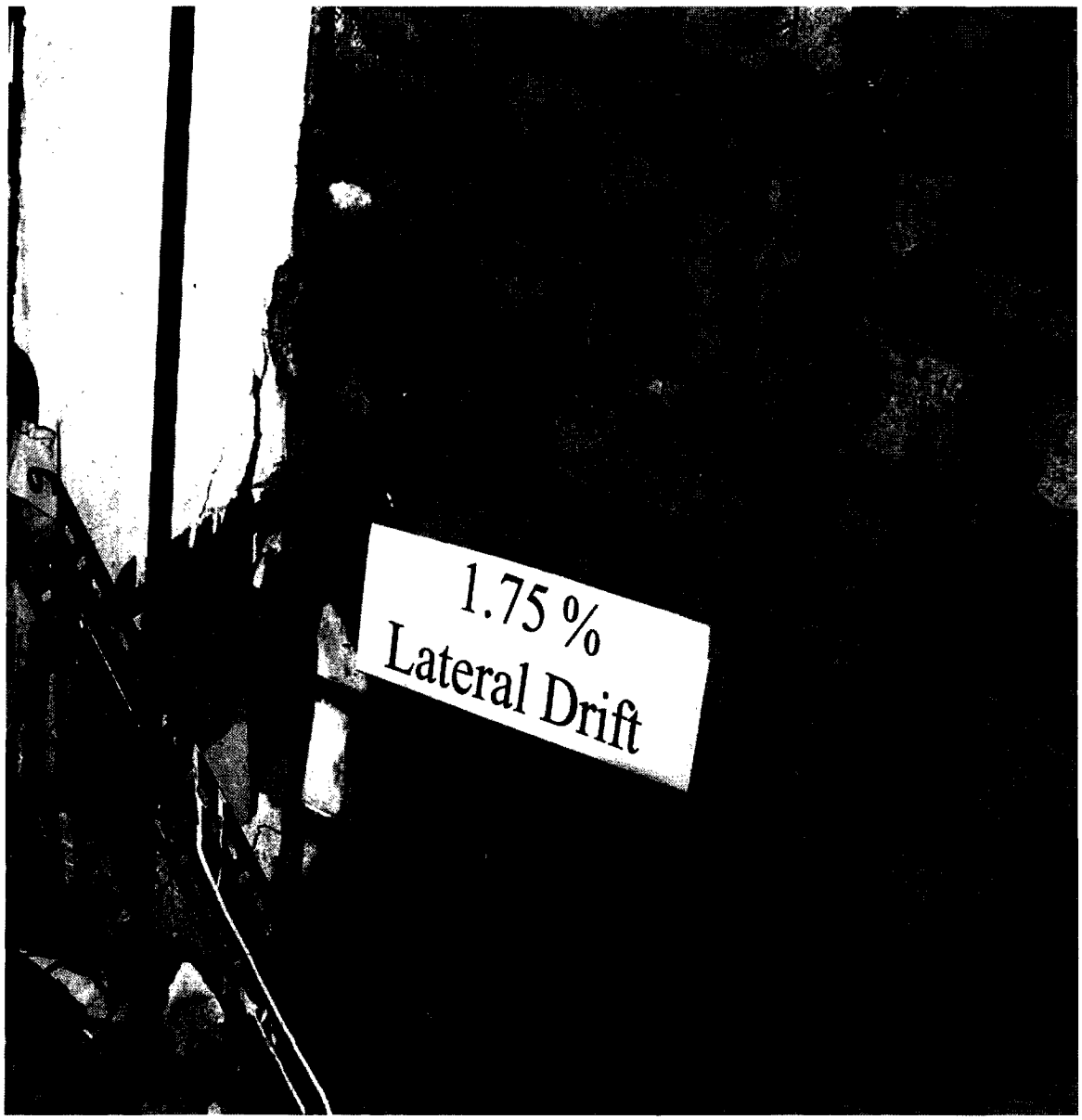

Figure 4.28: Concrete deterioration and widening of cracks at the bottom of left column and wall at 1.75 % lateral drift (BR-2)

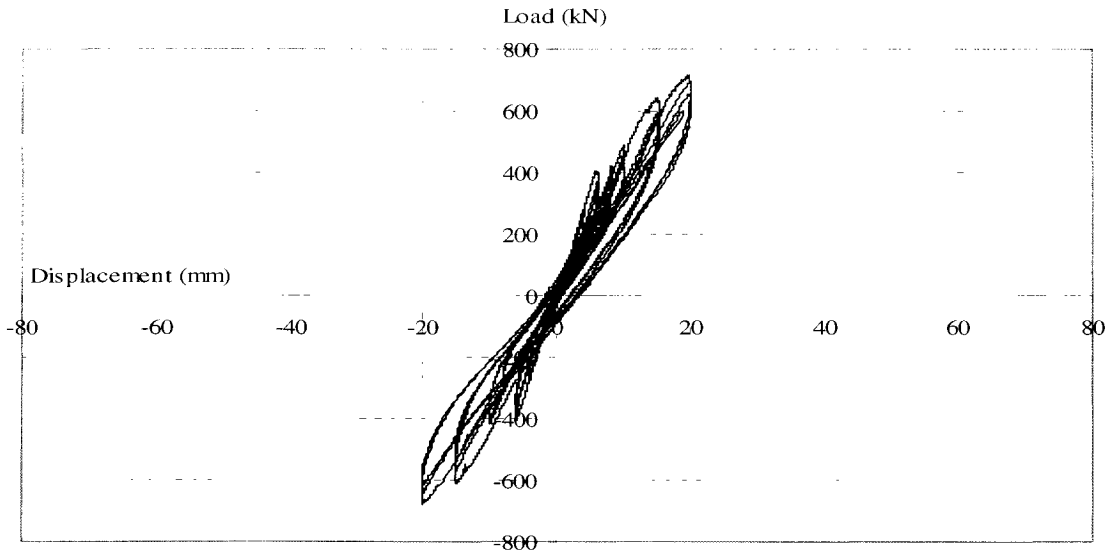

Figure 4.29: Hysteretic lateral load - lateral displacement relationship for BR-3 (Retrofitted specimen)

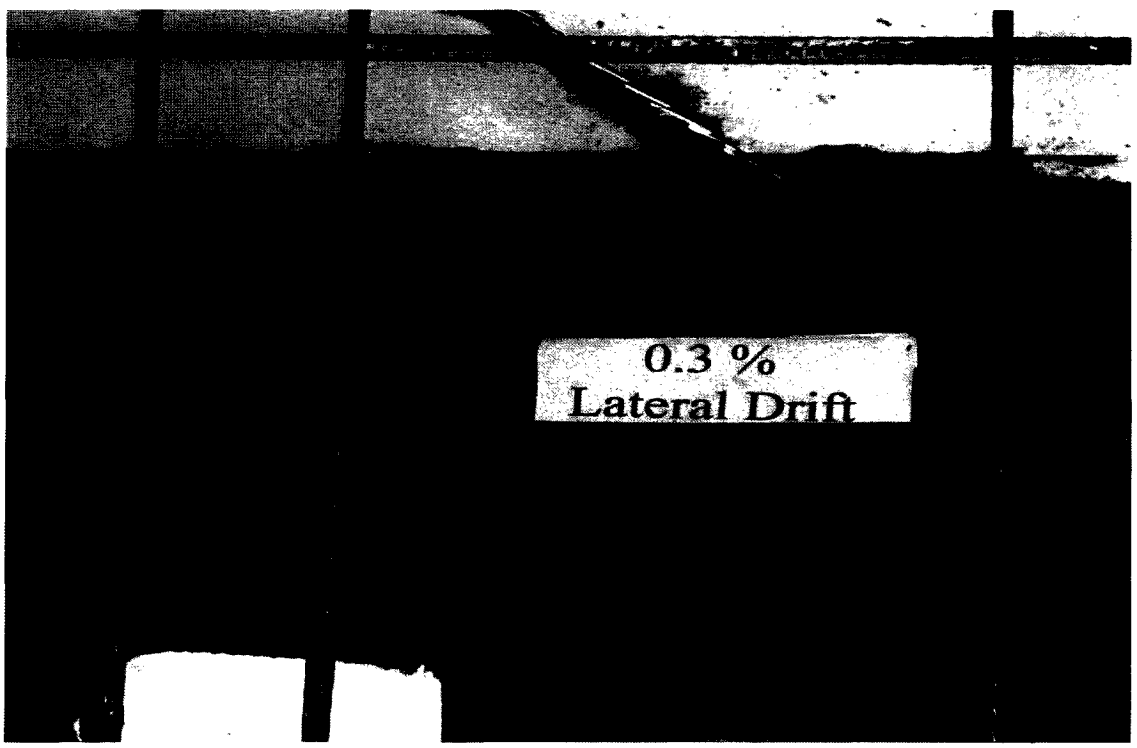

Figure 4.30: Separation in mortar between wall and column at 0.3 % lateral drift (BR-3)

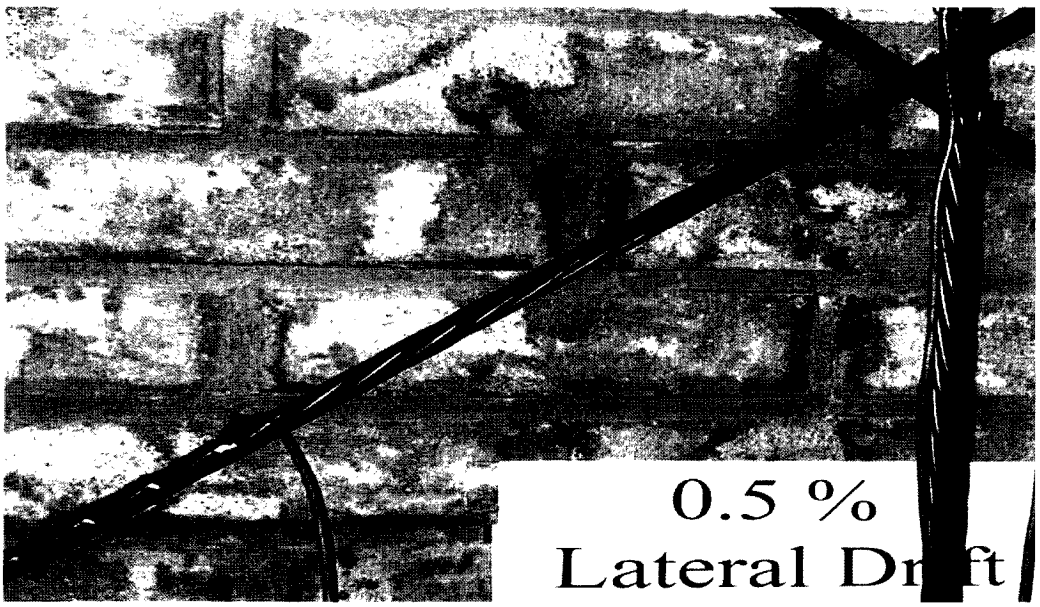

Figure 4.31: Formation of diagonal crack at 0.5 % lateral drift (BR-3)

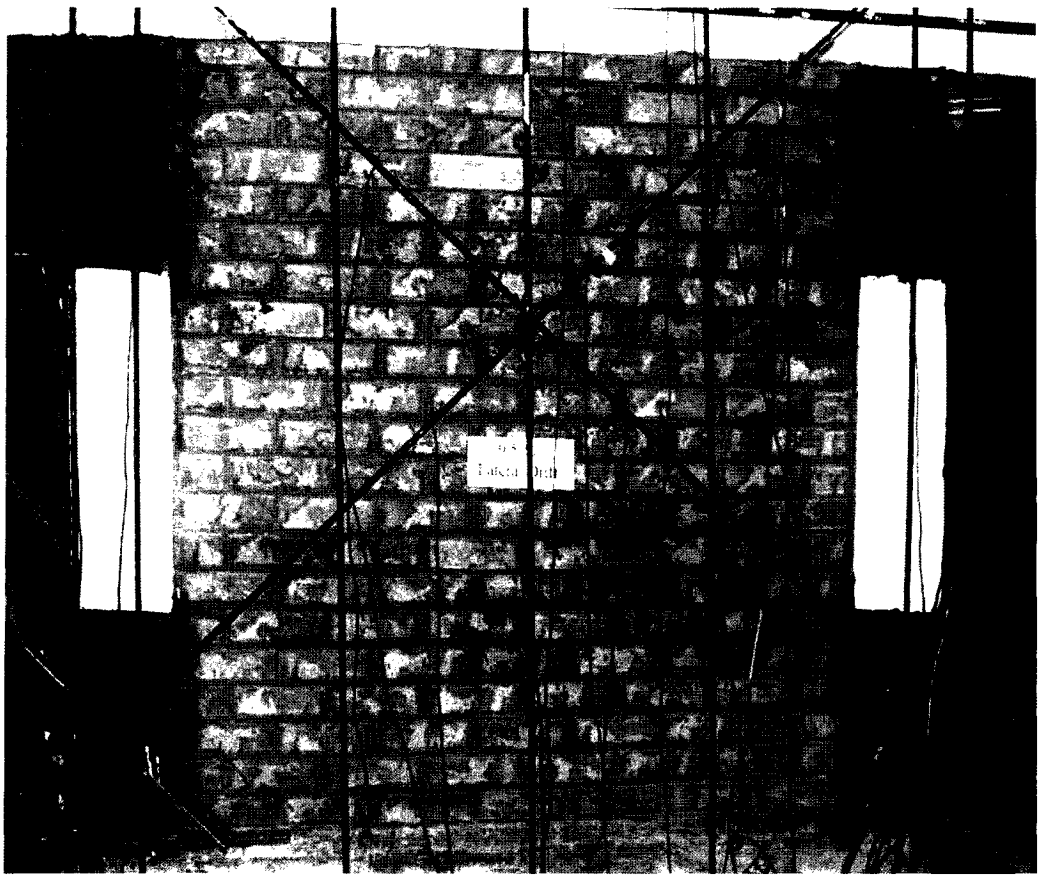

Figure 4.32: Deterioration of specimen BR-3 at 0.5 % lateral drift (BR-3)

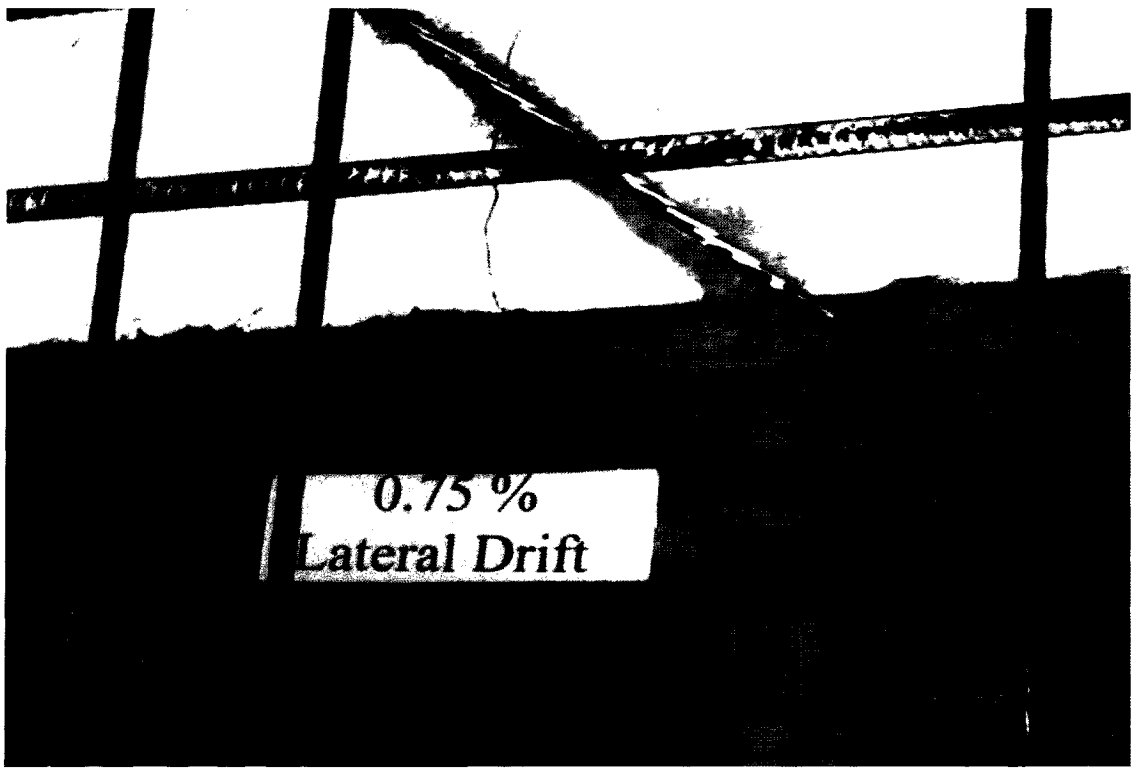

Figure 4.33: Flexural crack at beam critical section at 0.75 % lateral drift (BR-3)

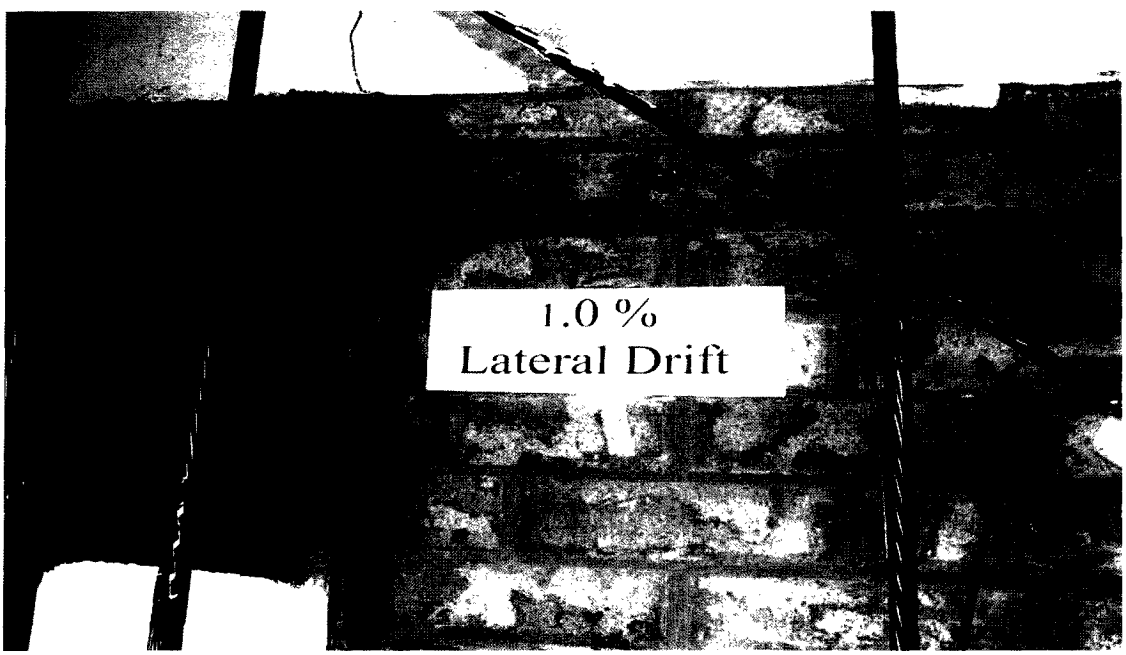

Figure 4.34: Widening of gap between wall and column at 1.0 % lateral drift (BR-3)

Figure 4.35: Increased separation in mortar joints at 1.0 % lateral drift (BR-3)

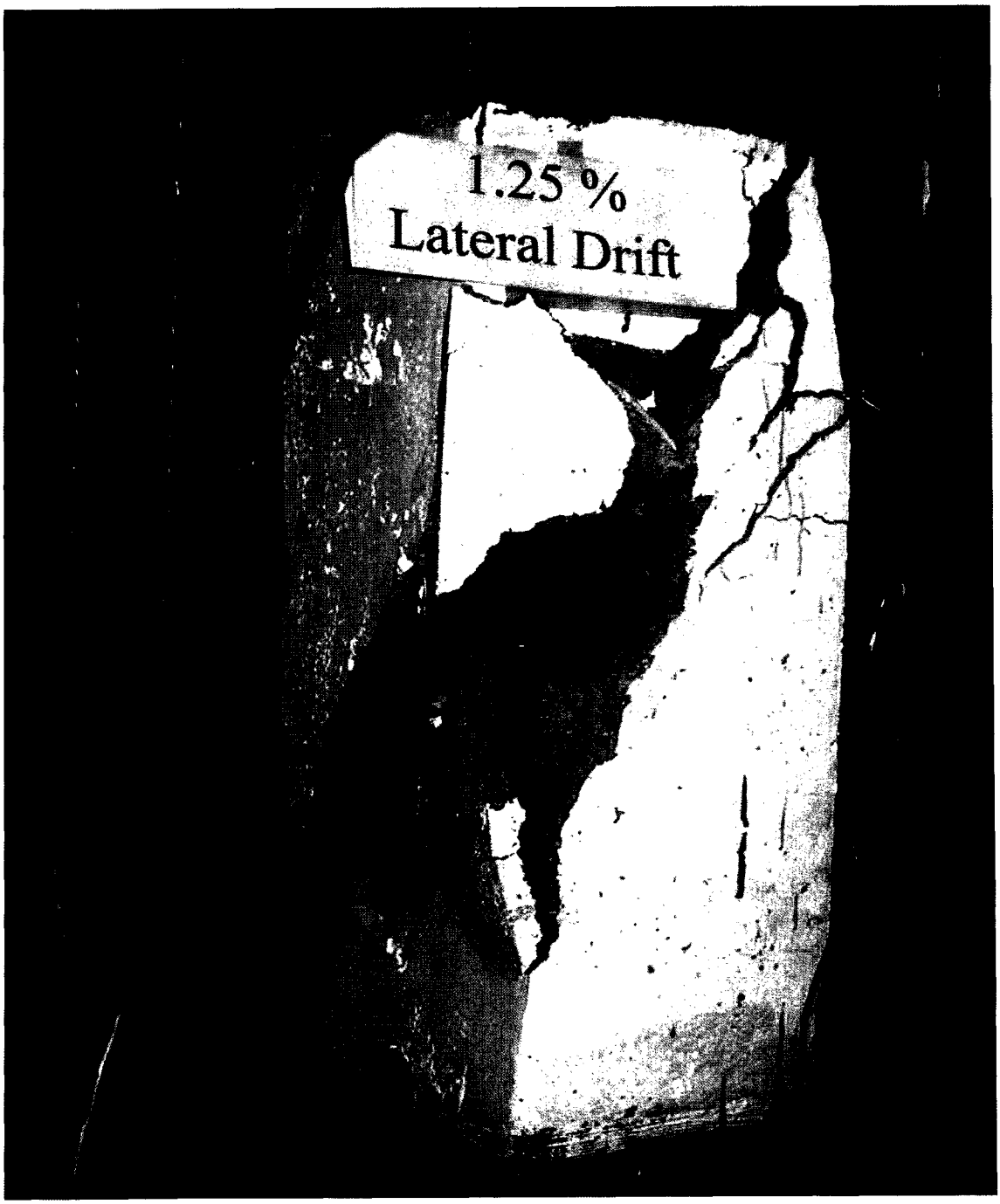

Figure 4.36: Concrete deterioration and buckling of column bars at 1.25 % lateral drift (BR-3)

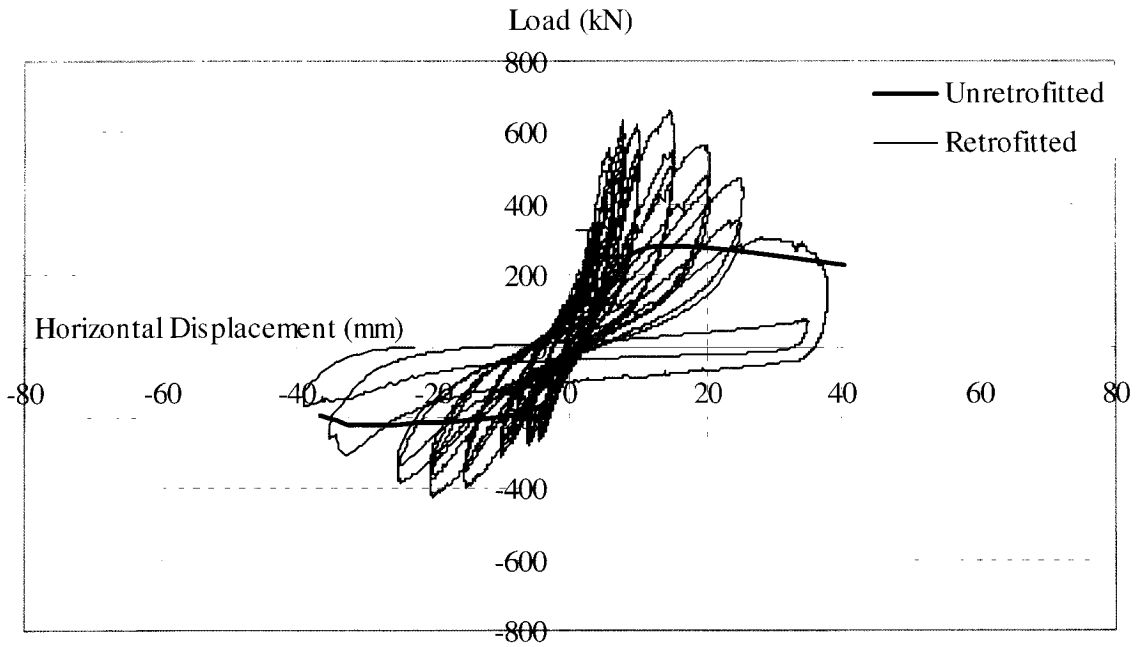

Figure 4.37: Hysteretic lateral load vs. lateral displacement relationship for retrofitted frame (BL-3)

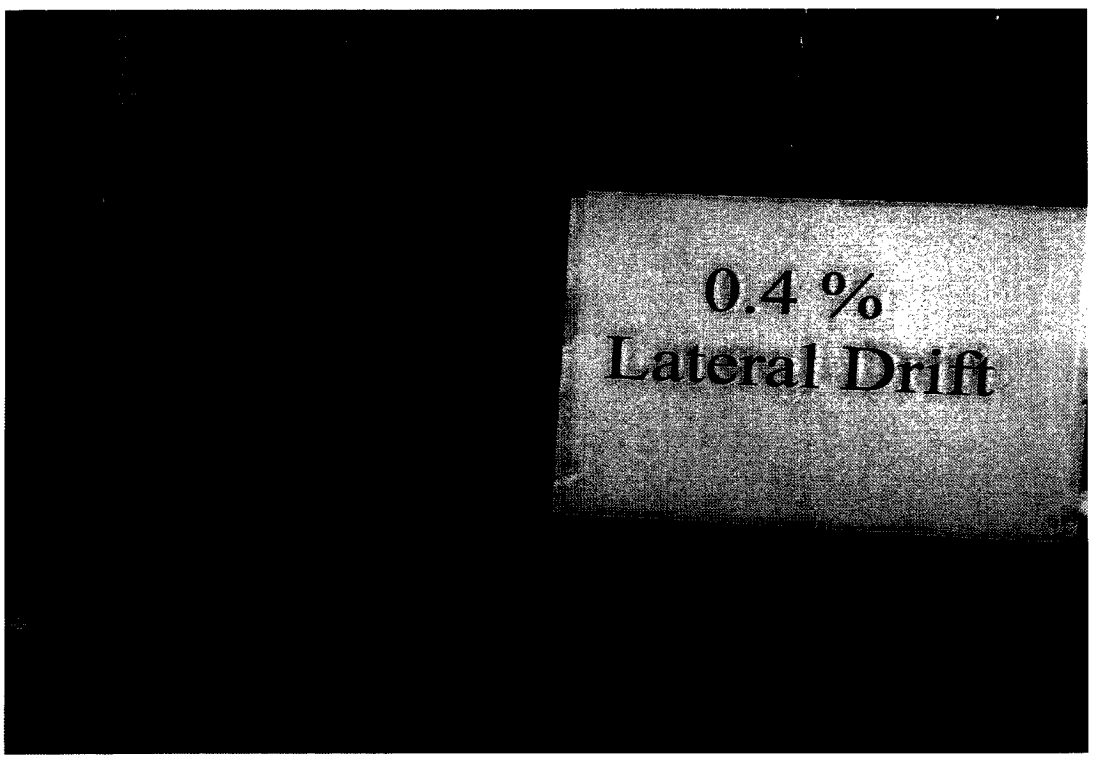

Figure 4.38: Horizontal cracks appear in column at 0.4 % Lateral drift (BL-3)

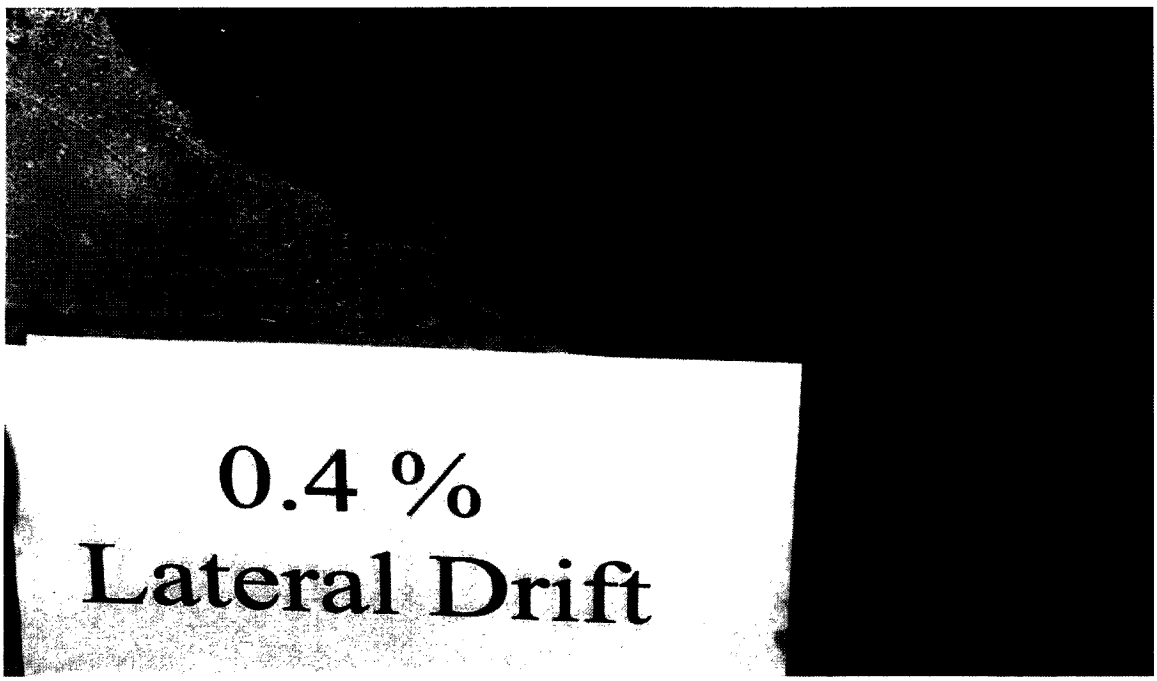

Figure 4.39: Crack at head joints start to appear at 0.4 % lateral drift (BL-3)

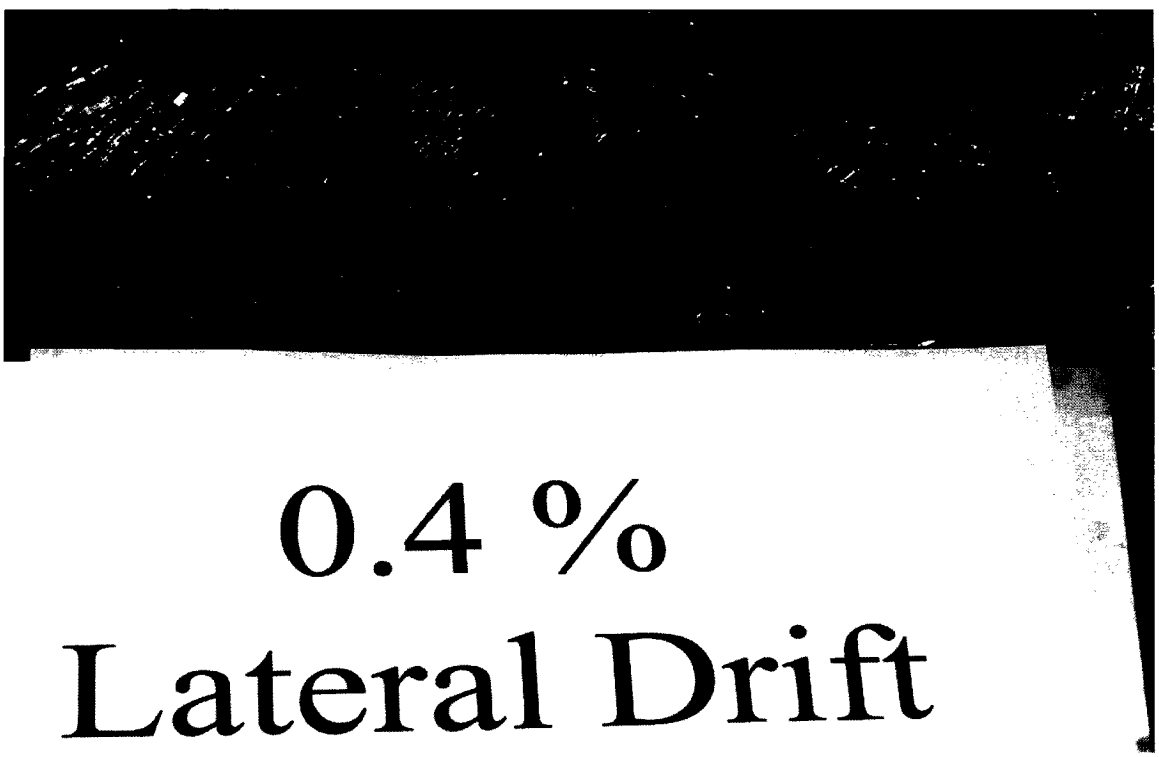

Figure 4.40: Separation of fibers along wall diagonal at 0.4 % lateral drift (BL-3)

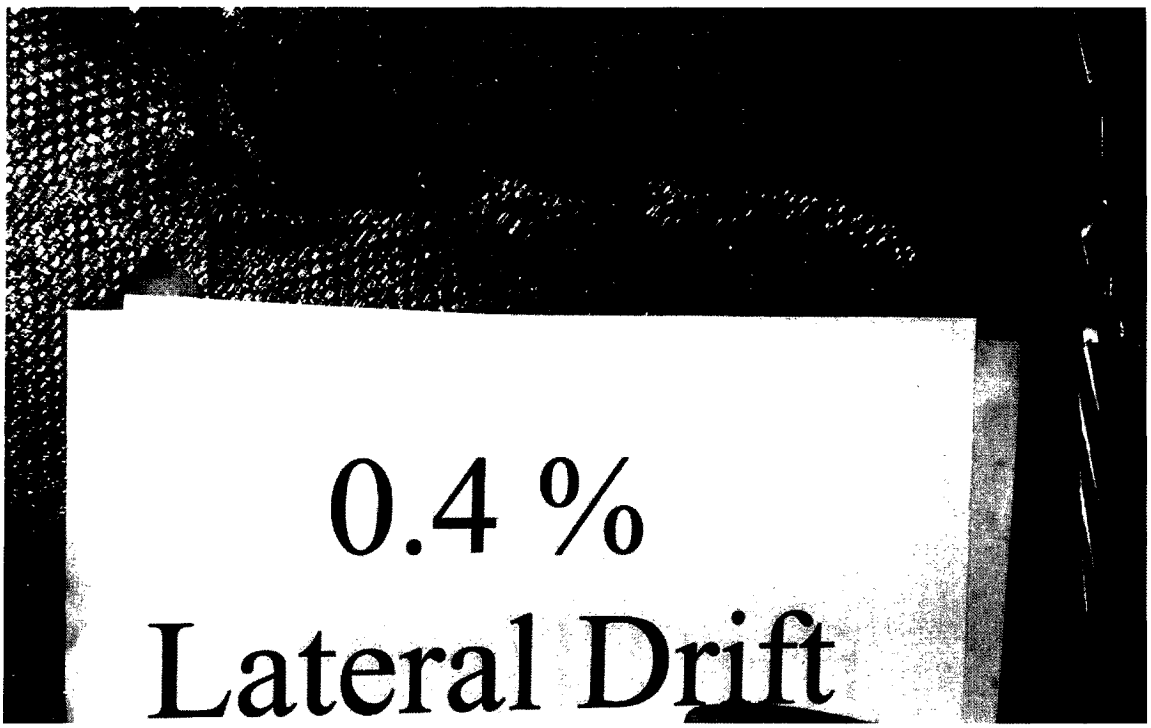

Figure 4.41: Local delamination of FRP in compression a strut at 0.4 % lateral drift (BL-3)

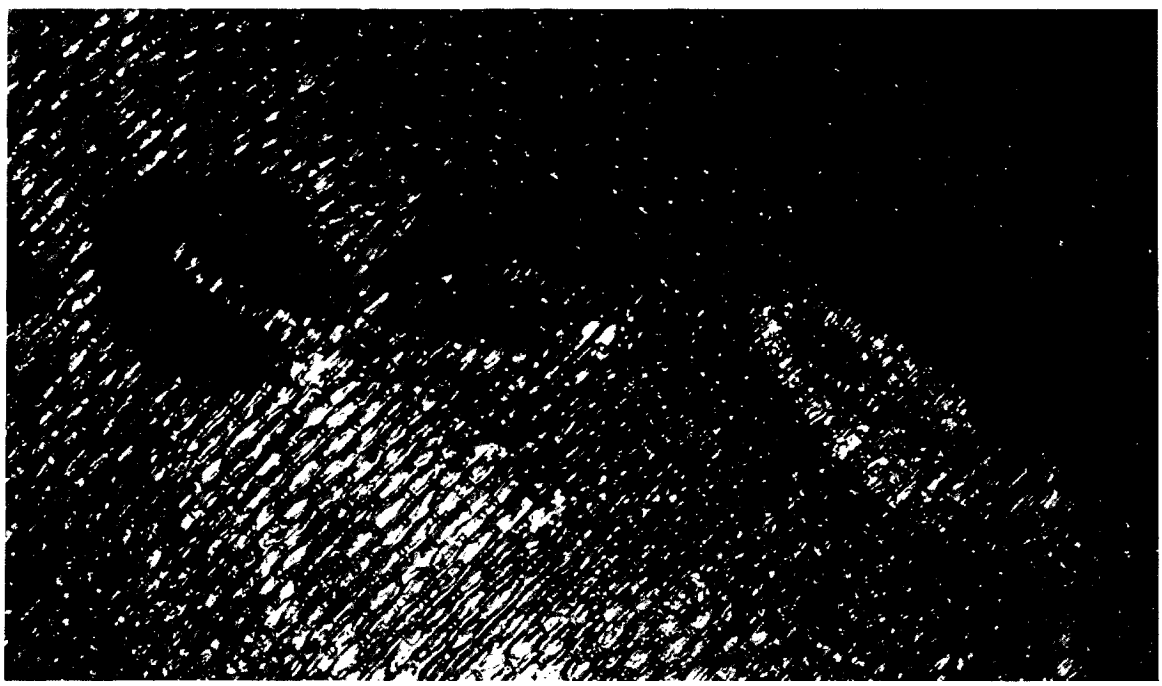

Figure 4.42: Increased local delamination of FRP in a compression strut at 0.5 % lateral drift (BL-3)

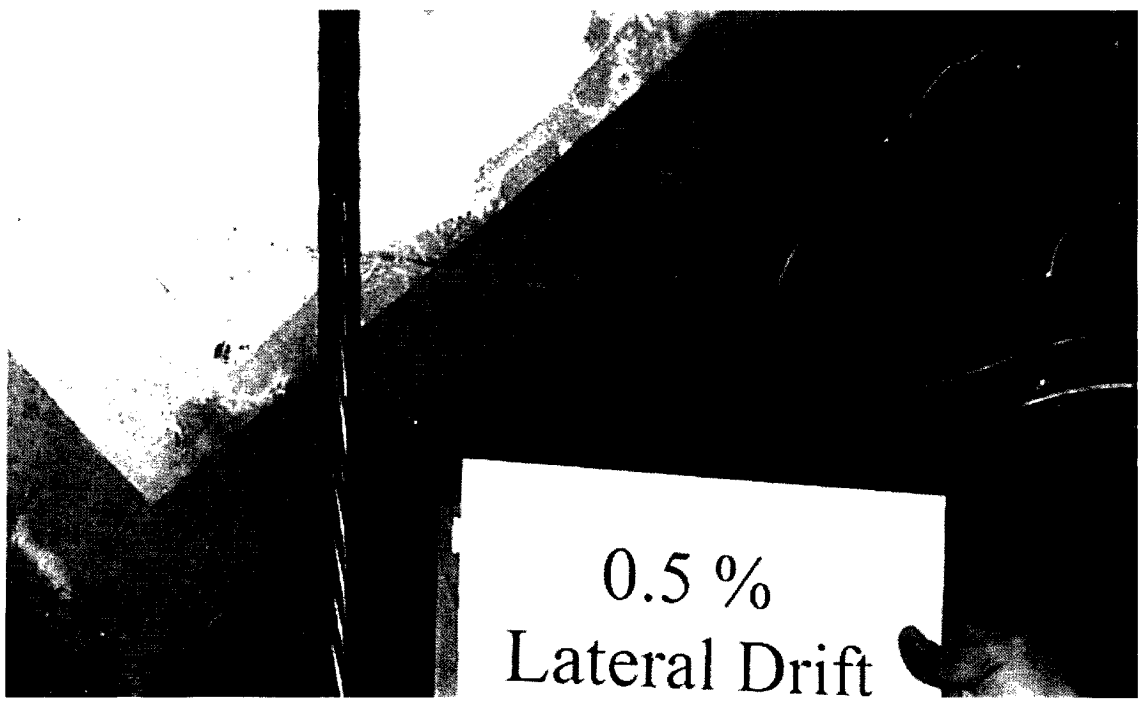

Figure4.43: Formation of horizontal cracks in the mortar joint at 0.5 % lateral drift (BL-3)

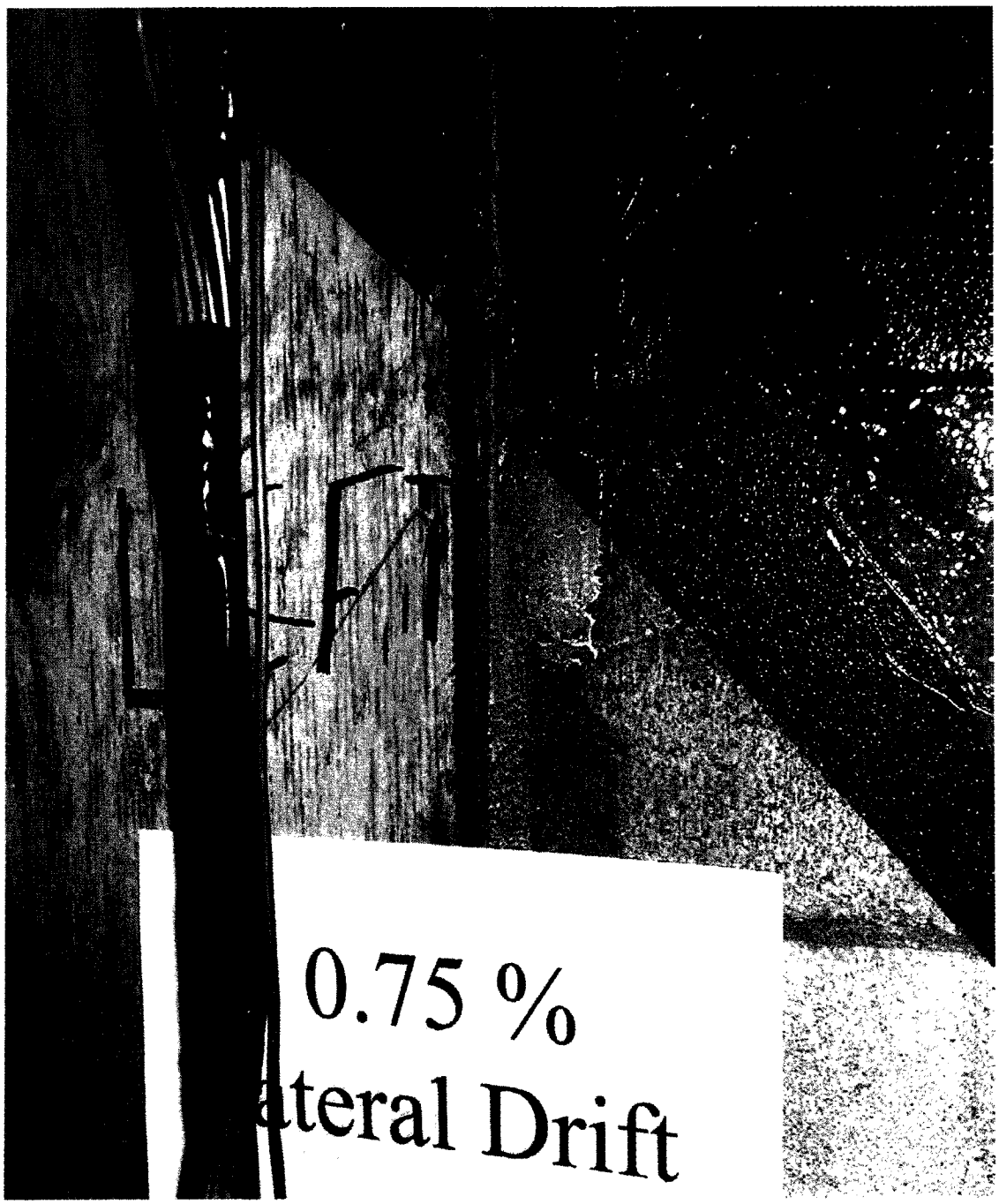

Figure 4.44: Separation between wall and column at 0.75 % lateral drift (BL-3)

Figure 4.45: Rupturing of fibers across the joint between the wall and frame, at 0.75 % lateral drift (BL-3)

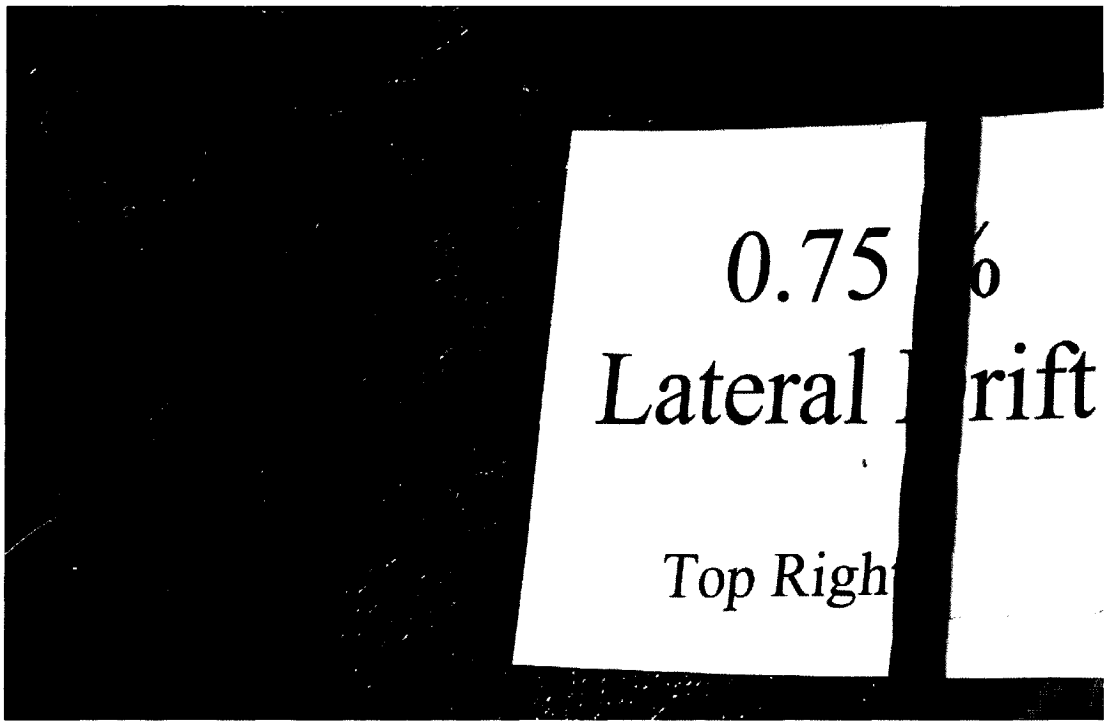

Figure 4.46: Separation of fibers along wall diagonal at 0.75 % lateral drift (BL-3)

Figure 4.47: Formation of shear cracks in a column near the top, at 1.0 % lateral drift (BL-3)

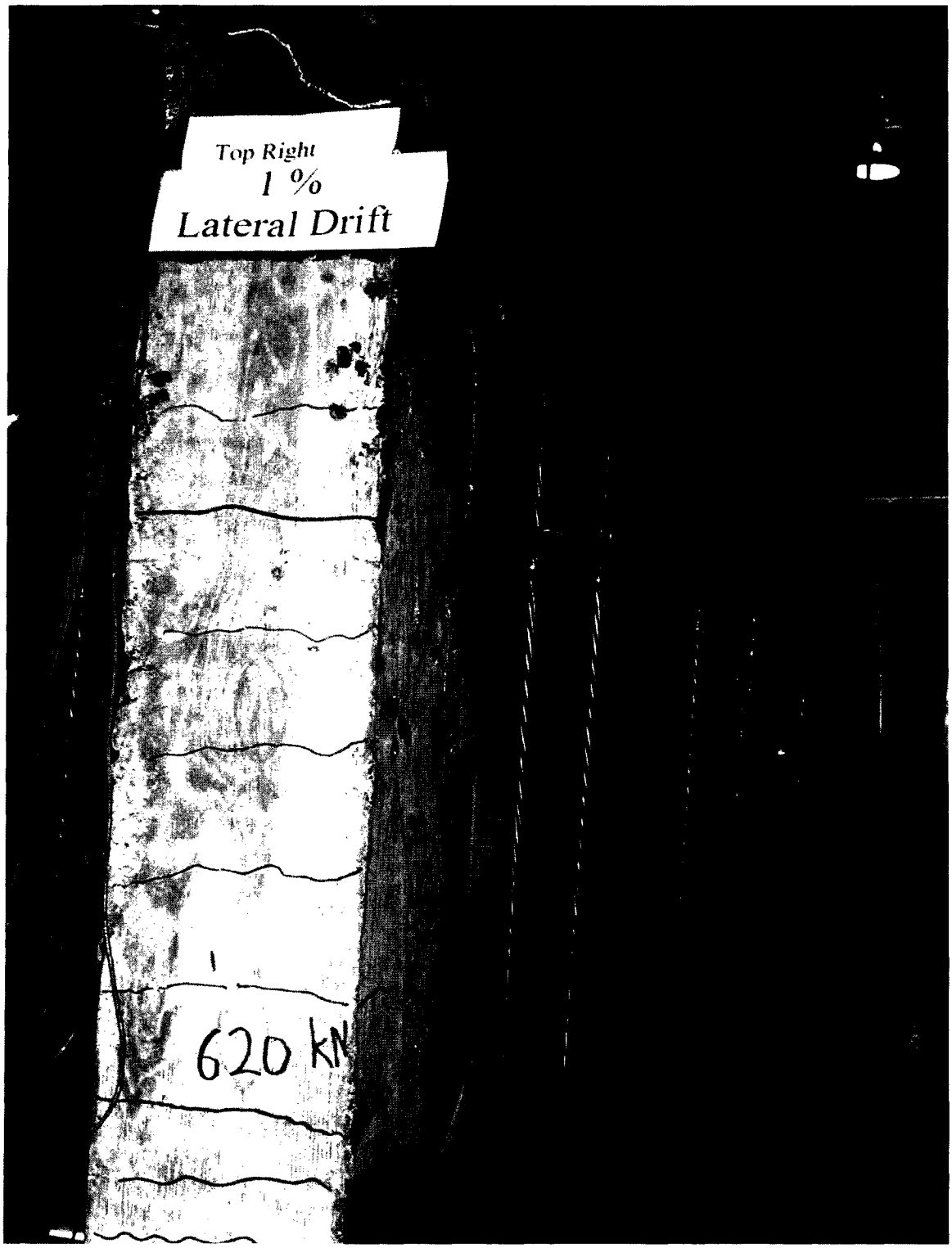

Figure 4.48: Additional horizontal cracks in column at 1.0 % lateral drift (BL-3)

Figure 4.49: More separation between the wall and column at 1.0 % lateral drift (BL-3)

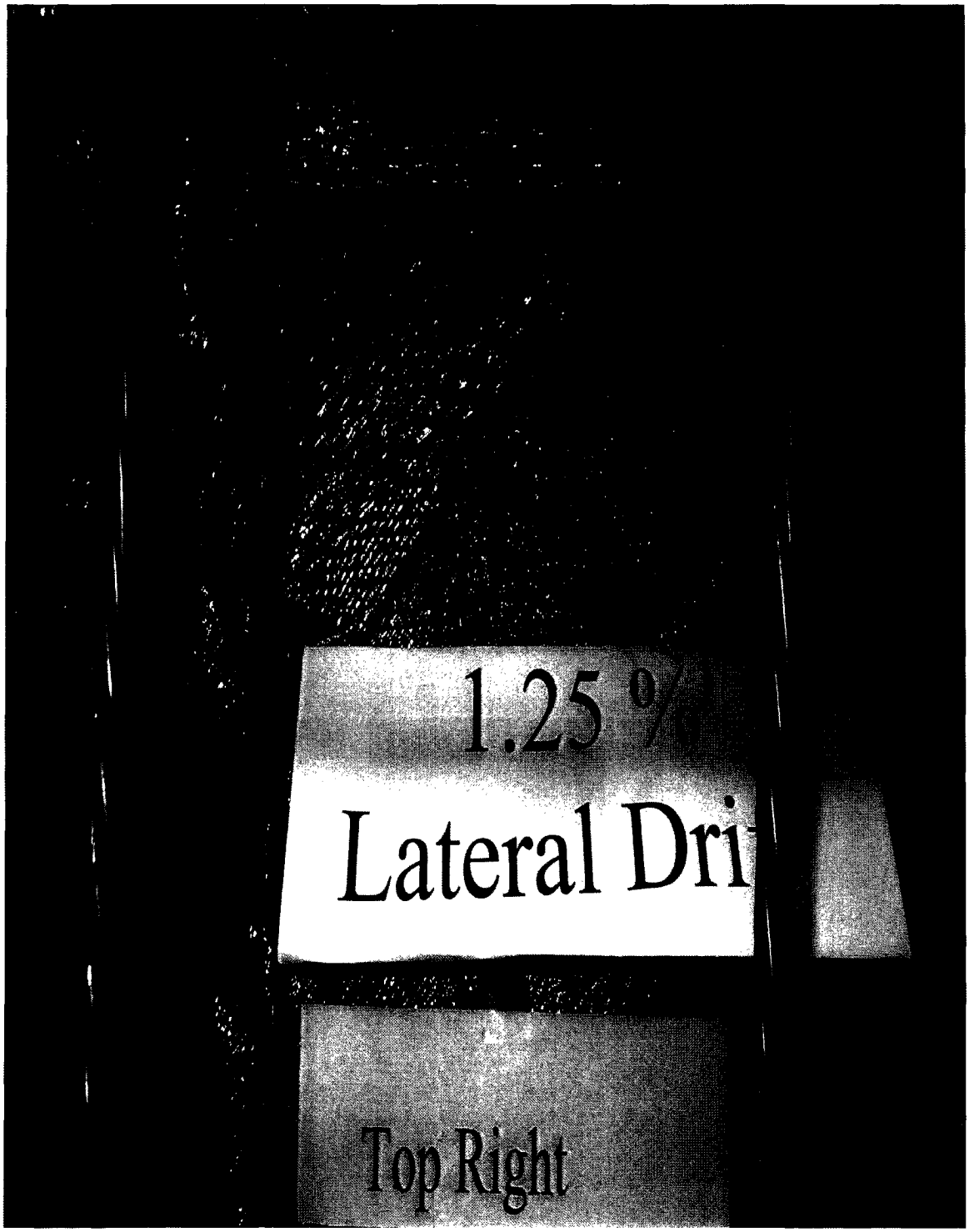

Figure 4.50: Shear cracks in a column near the top, at 1.0 % lateral drift (BL-3)

Figure 4.51: More separation between wall and column at 1.25 % lateral drift (BL-3)

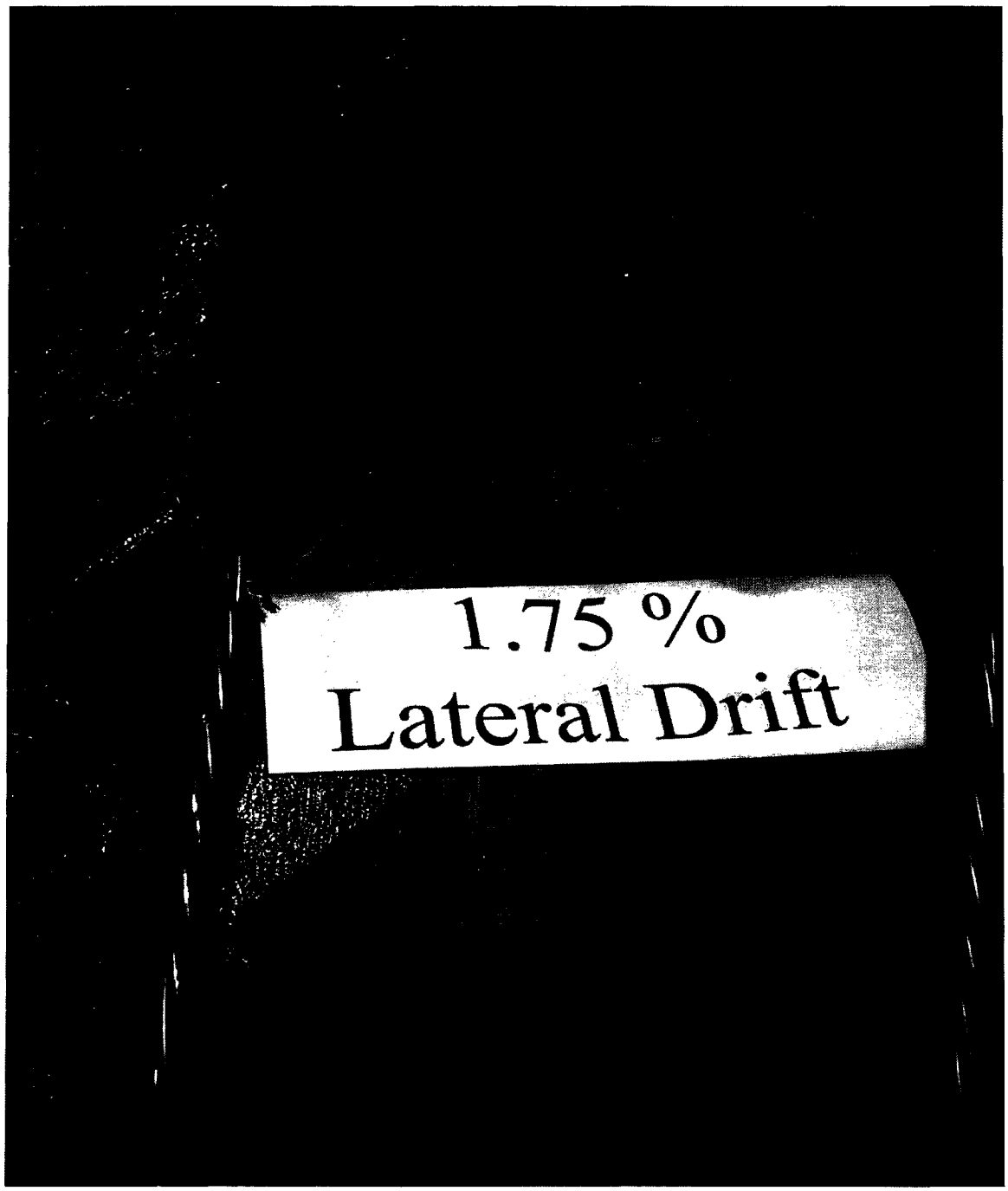

Figure 4.52: Visible bending of longitudinal reinforcement and ties in upper part of the right column at 1.75% lateral drift (BL-3)

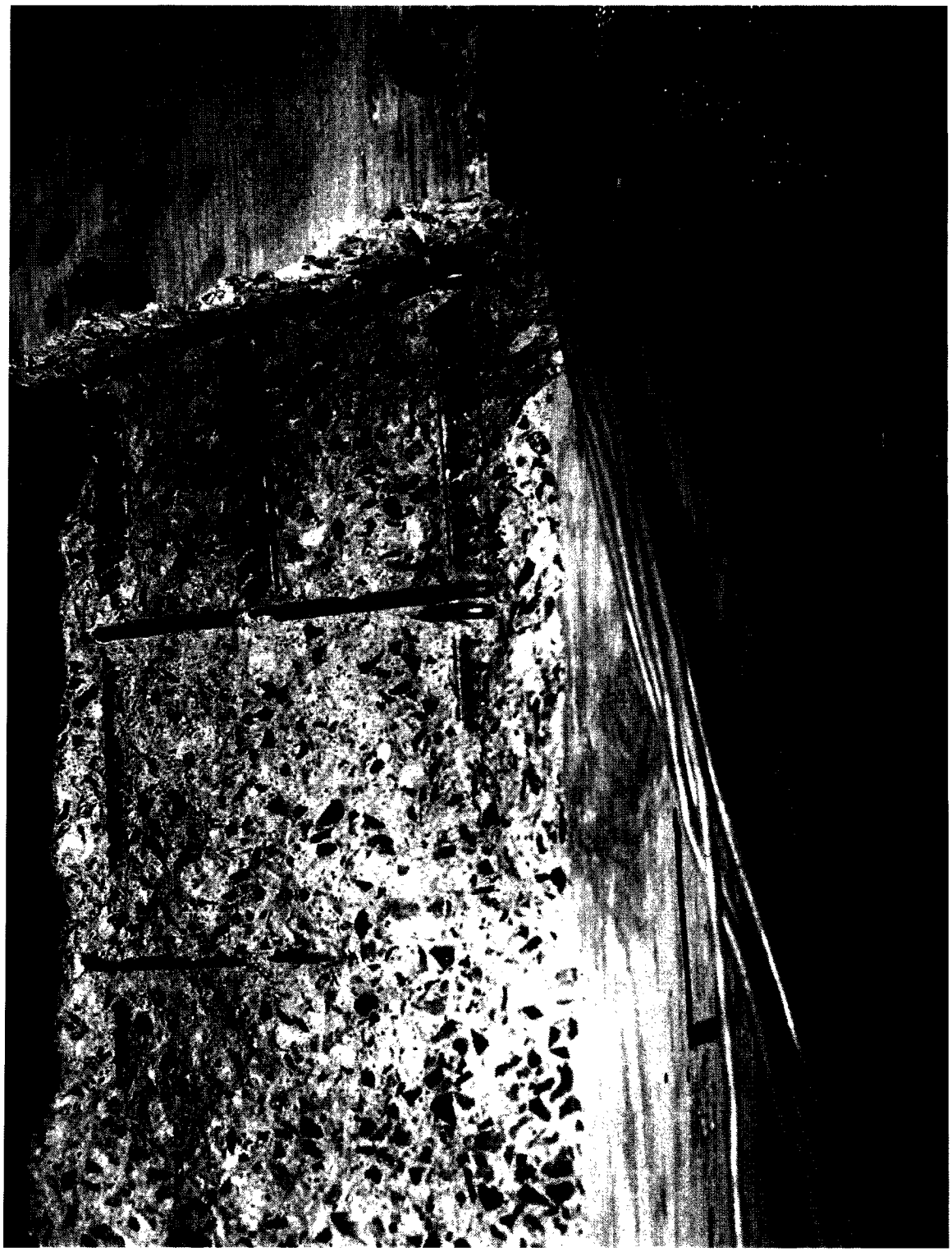

Figure 4.53: Significant concrete cover spalling in column at 1.75% lateral drift (BL-3)

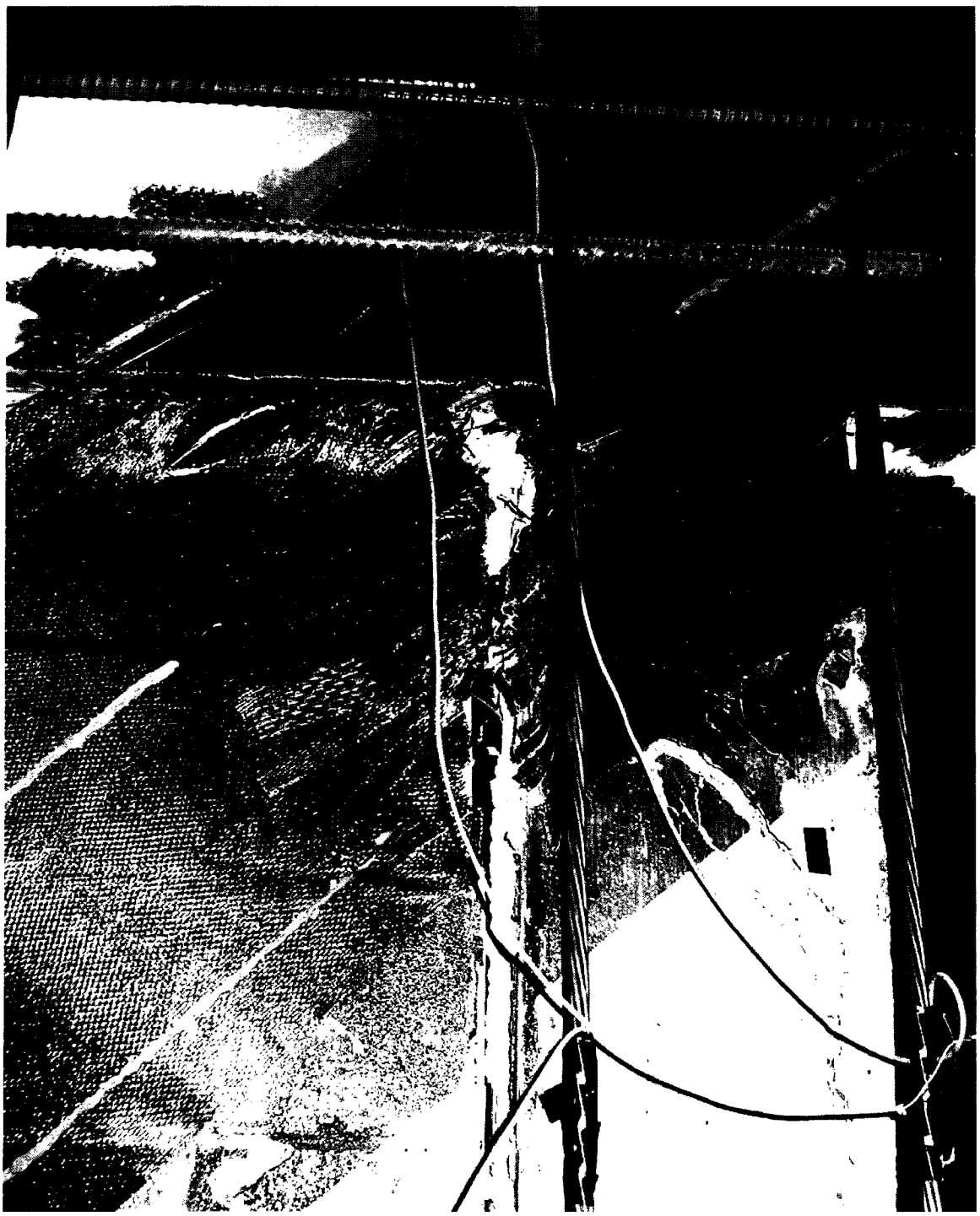

Figure 4.54: Rupturing of fiber anchors at 1.75% lateral drift (BL-3)

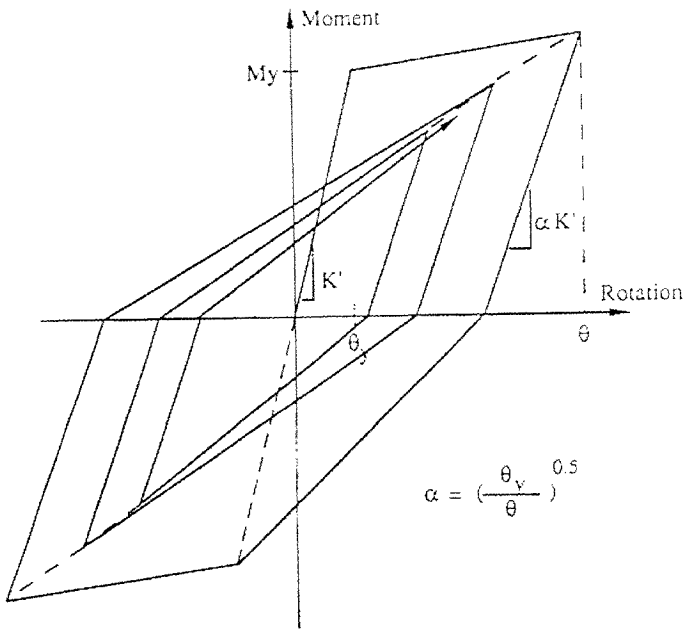

a) Modified Takeda hysteretic model (Powell1975)

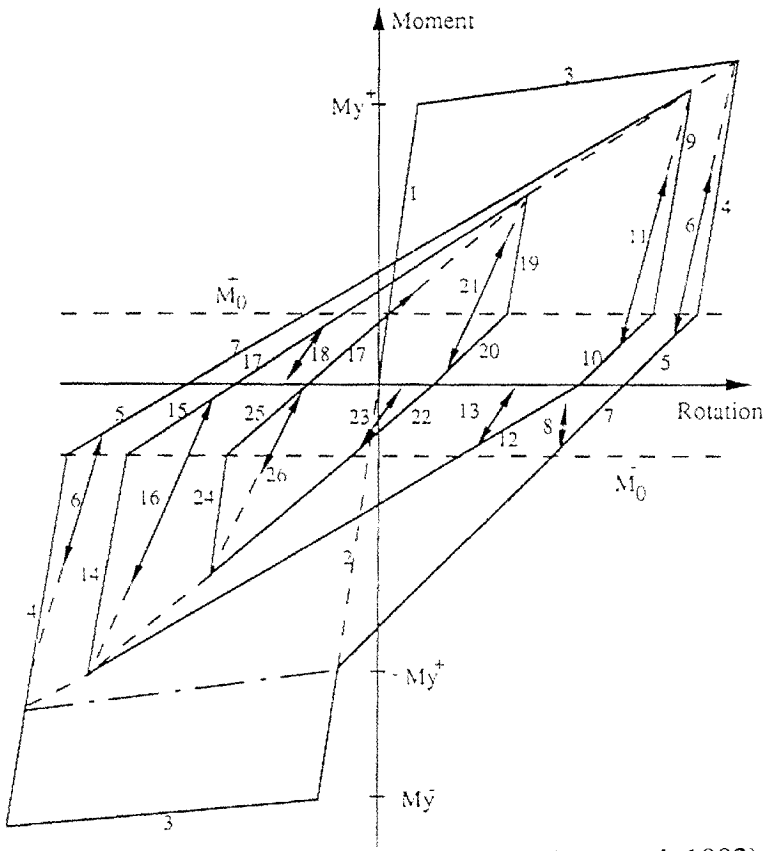

b) Hysteretic anchorage slip model (Alsiwat et al. 1992)

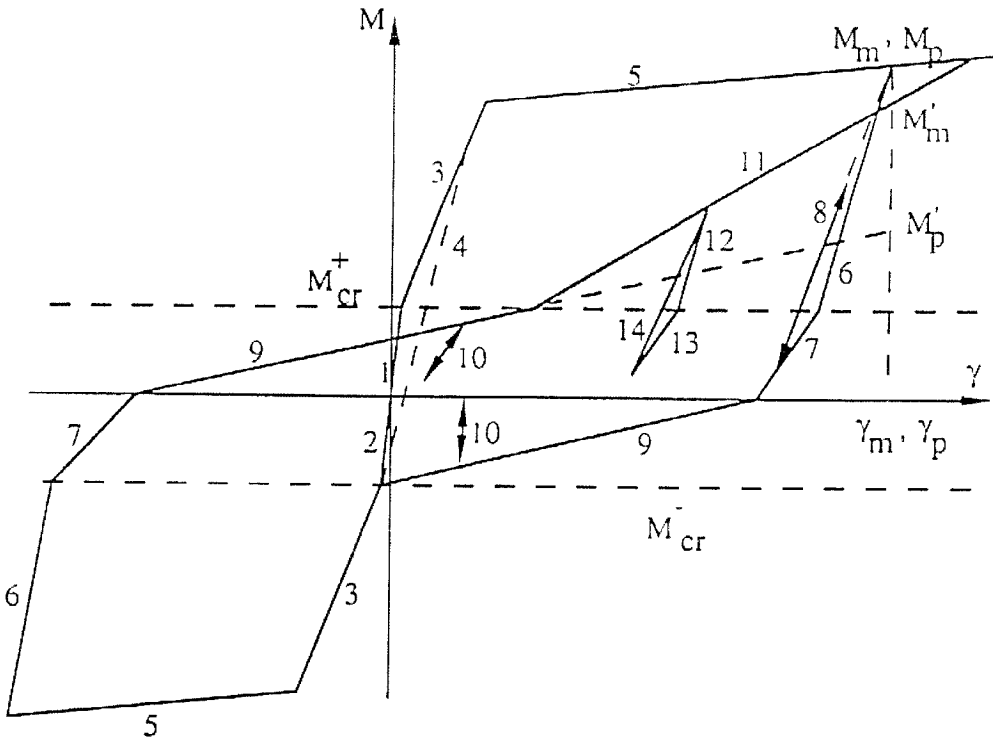

c) Hysteretic model for shear (Ozcebe and Saatcioglu 1989)

Figure 5.1: Hysteretic models used in DRAIN-RC

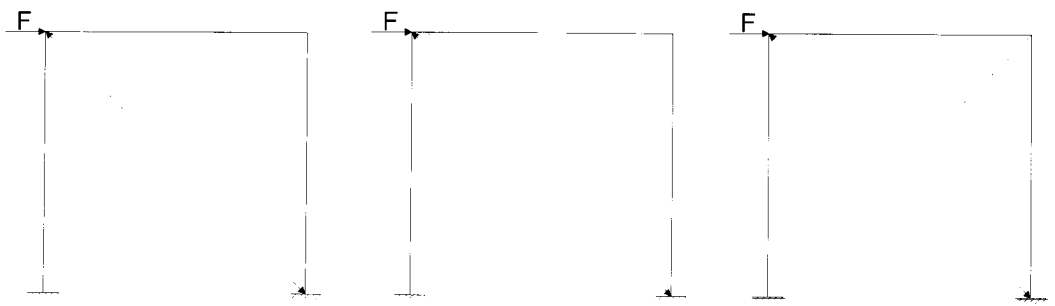

a) Unretrofitted specimen (BR-1)

b) Retrofitted specimen (BR-2 & BR-3)

c) Retrofitted specimen (BL-3)

Figure 5.2: Analytical models used for push-over analysis of test specimens

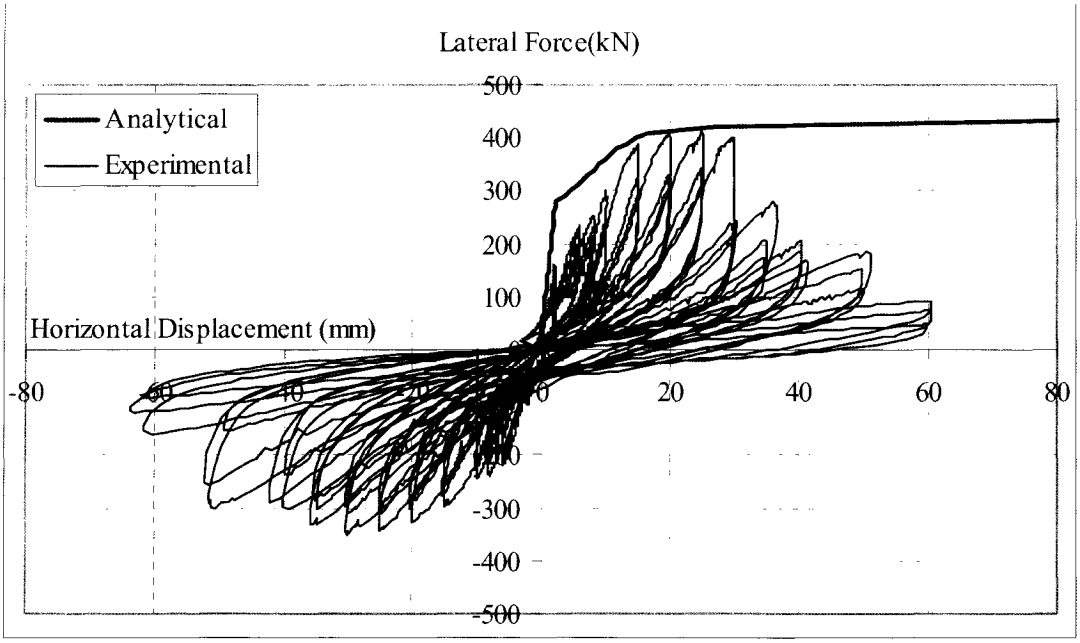

Figure 5.3: Hysteretic force-displacement relationship for BR-1
(Unretrofitted specimen)

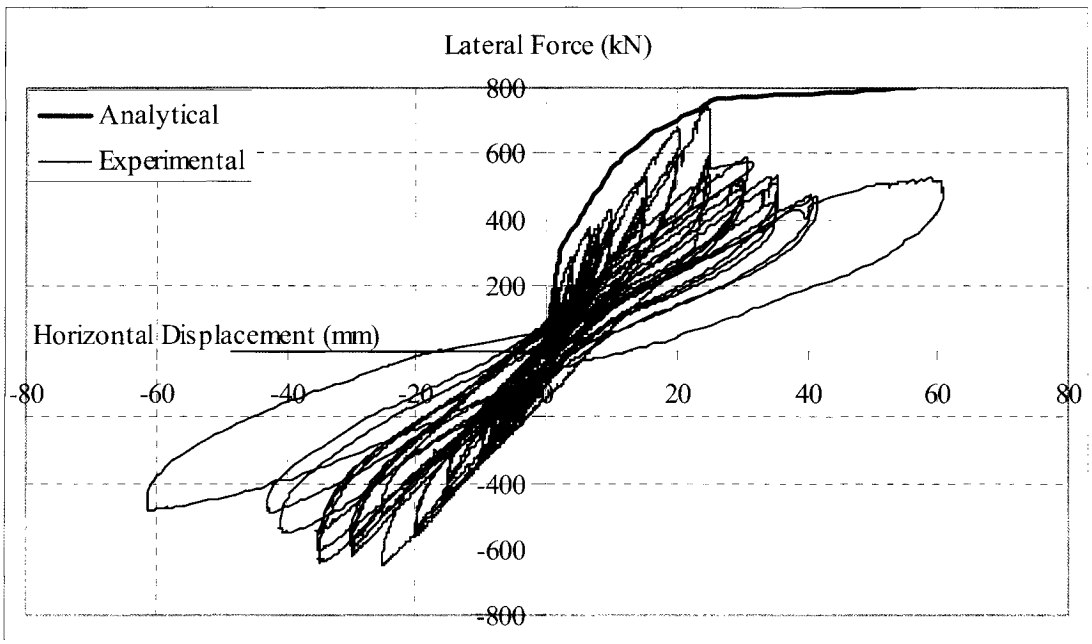

Figure 5.4: Hysteretic force-displacement relationship for BR-2
(Retrofitted with a diagonal prestressing force of 75 kN/cable)

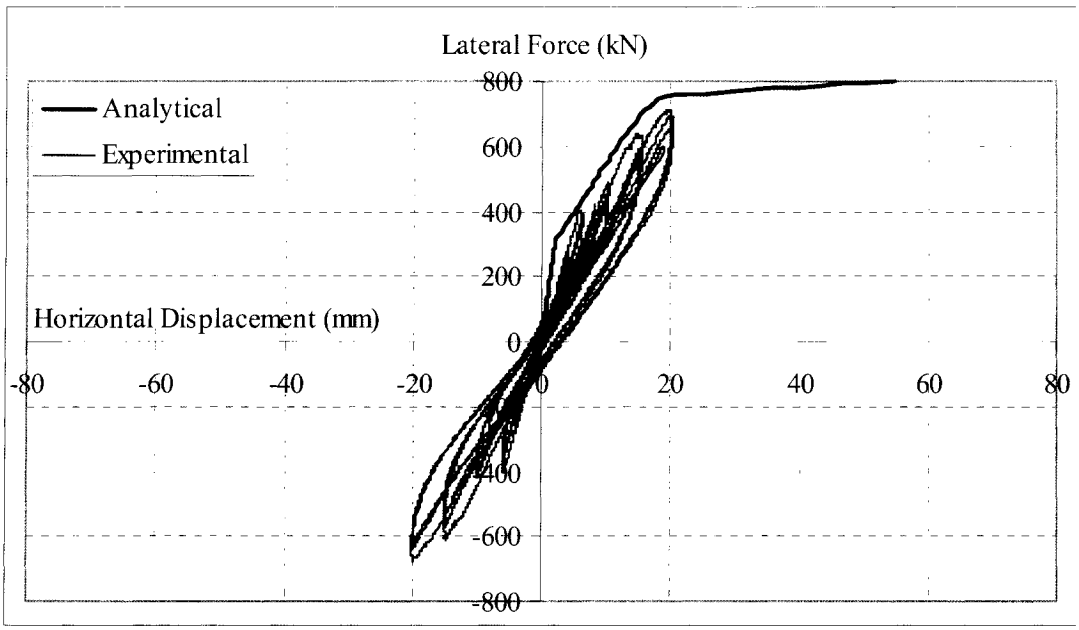

Figure 5.5: Hysteretic force-displacement relationship for BR-3
(Retrofitted with a diagonal prestressing force of 125kN/cable)

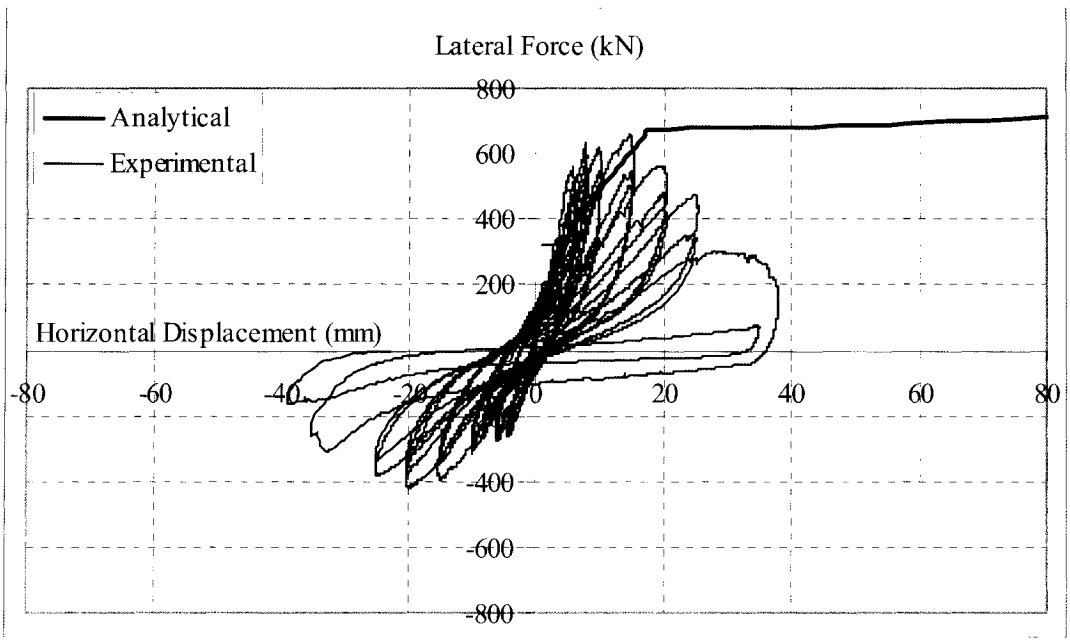

Figure 5.6: Hysteretic force-displacement relationship for BL-3
(Retrofitted with diagonal FRP strips)

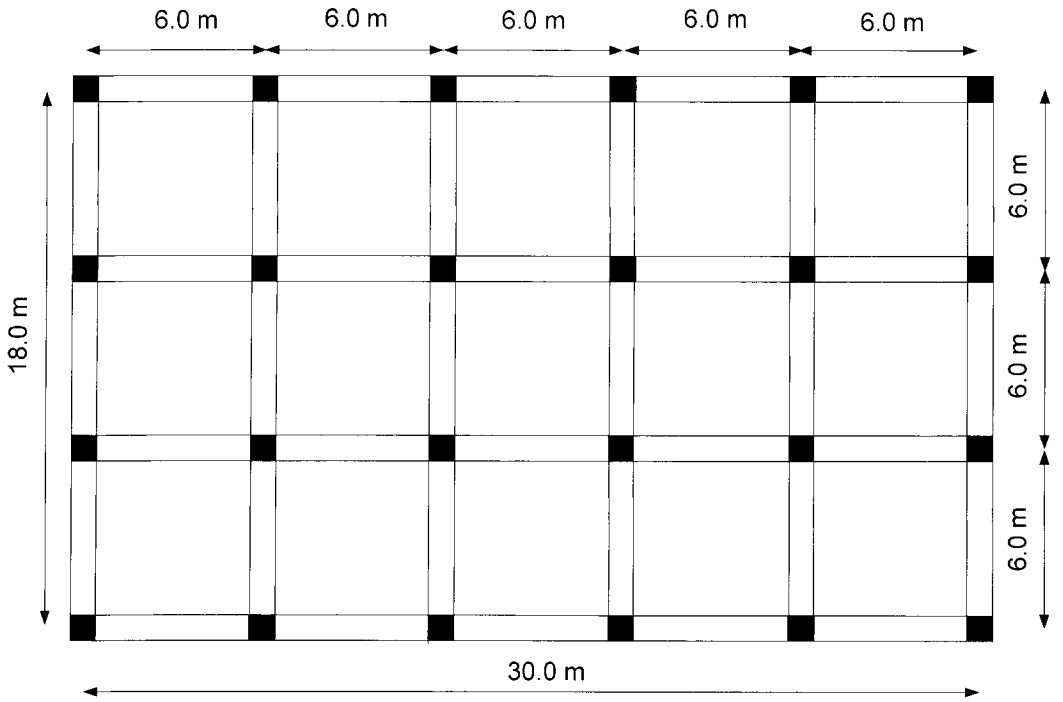

a) Plan view

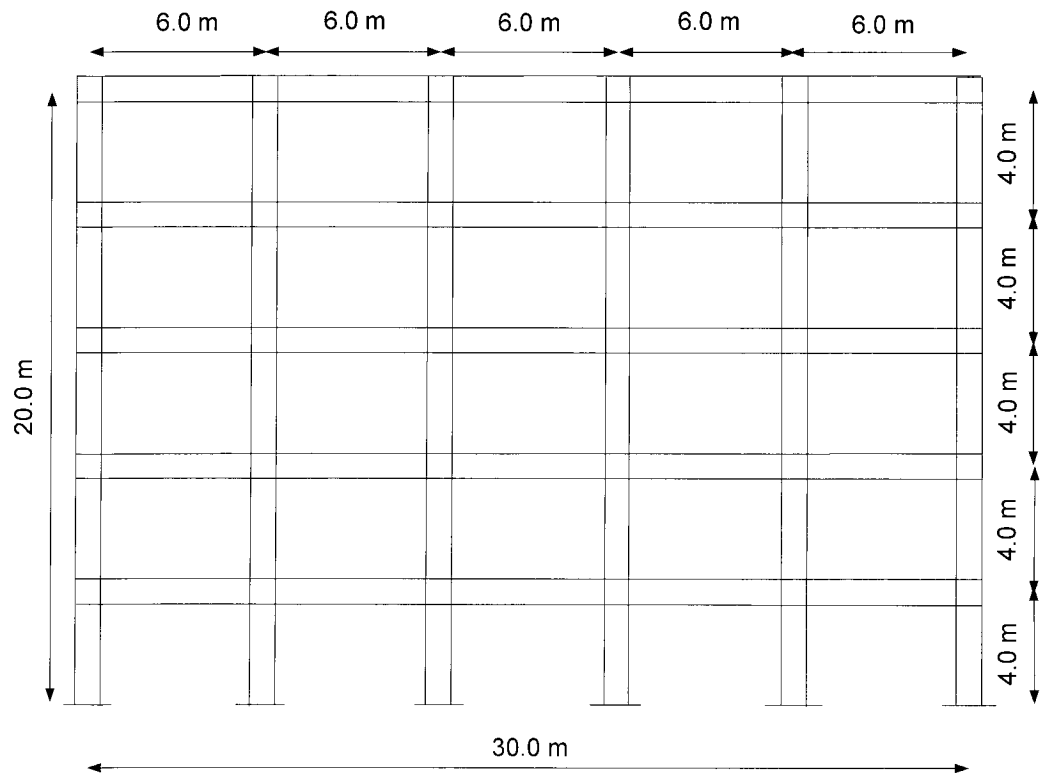

b) Elevation view

Figure 5.7: Five-storey moment resistant frame building

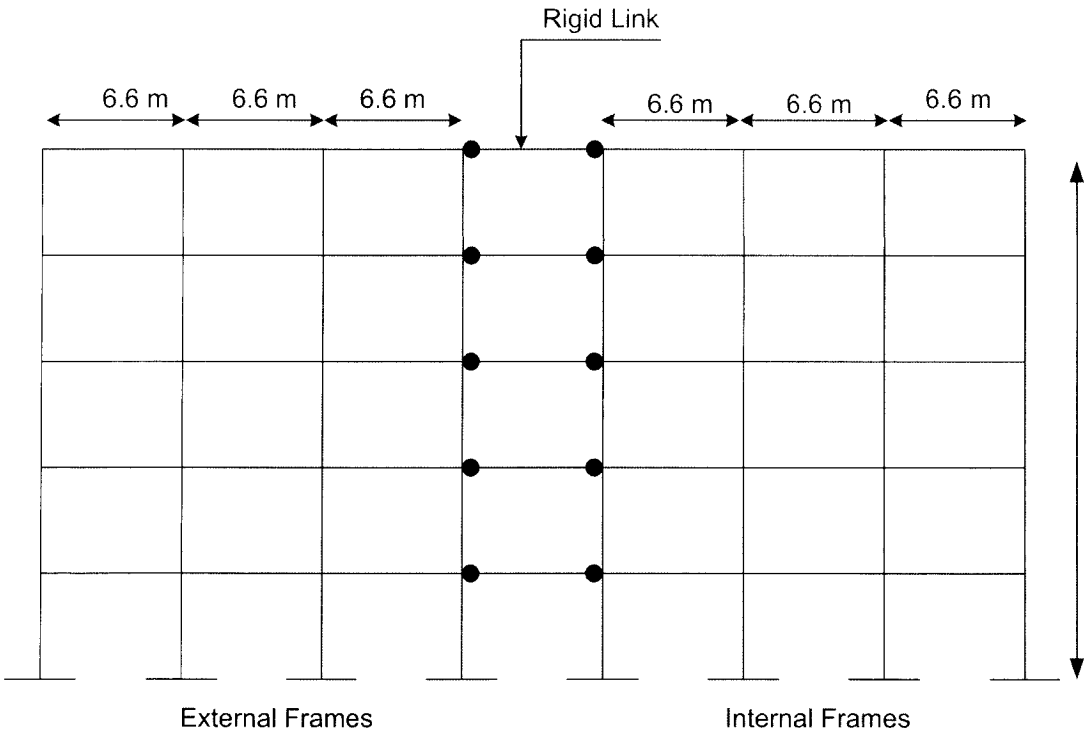

Figure 5.8: Two dimensional lumped frames used in analysis

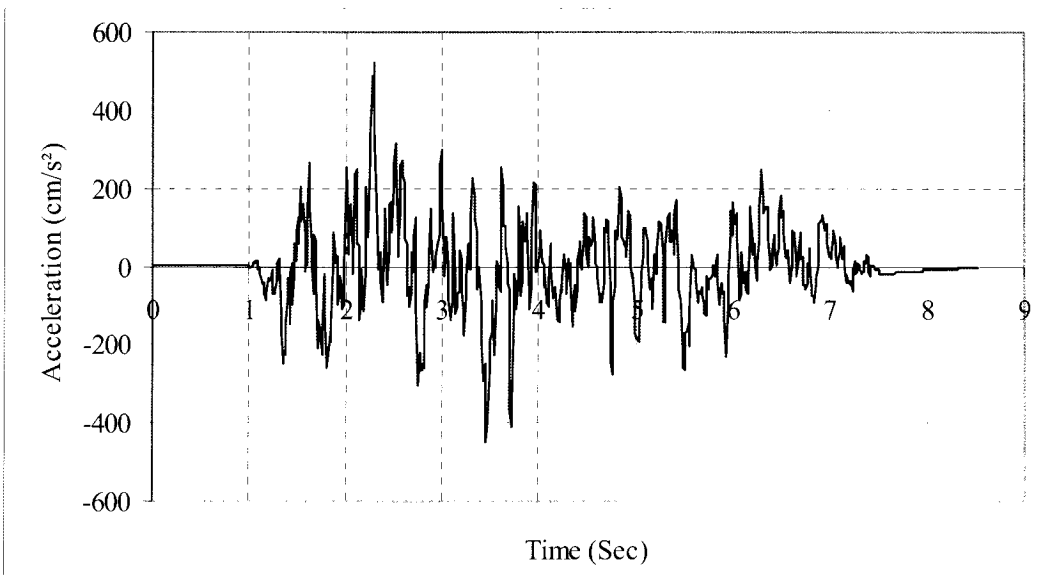

i) Short Event No.1

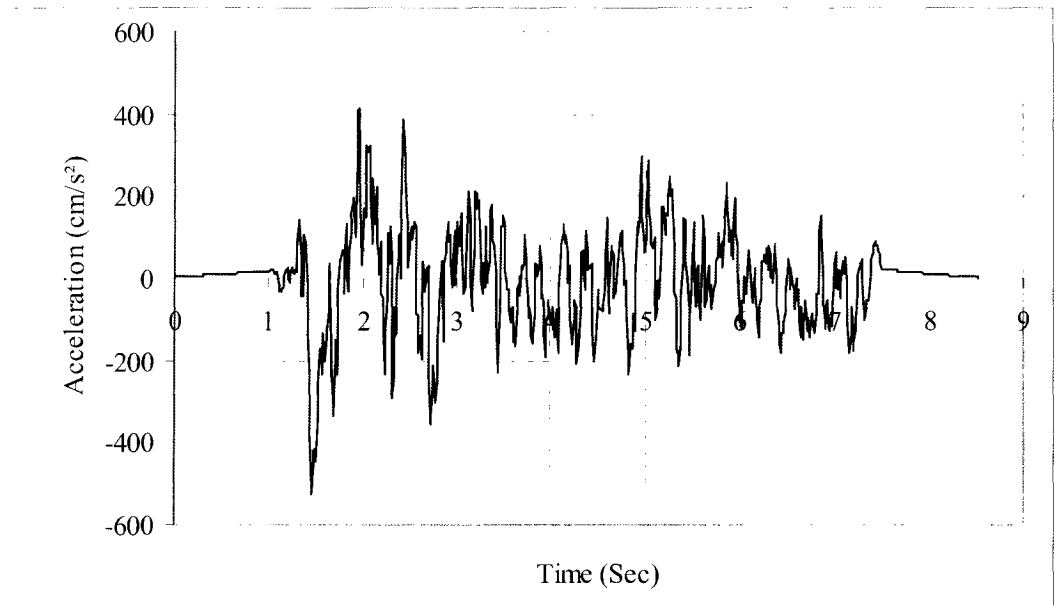

ii) Short Event No.2

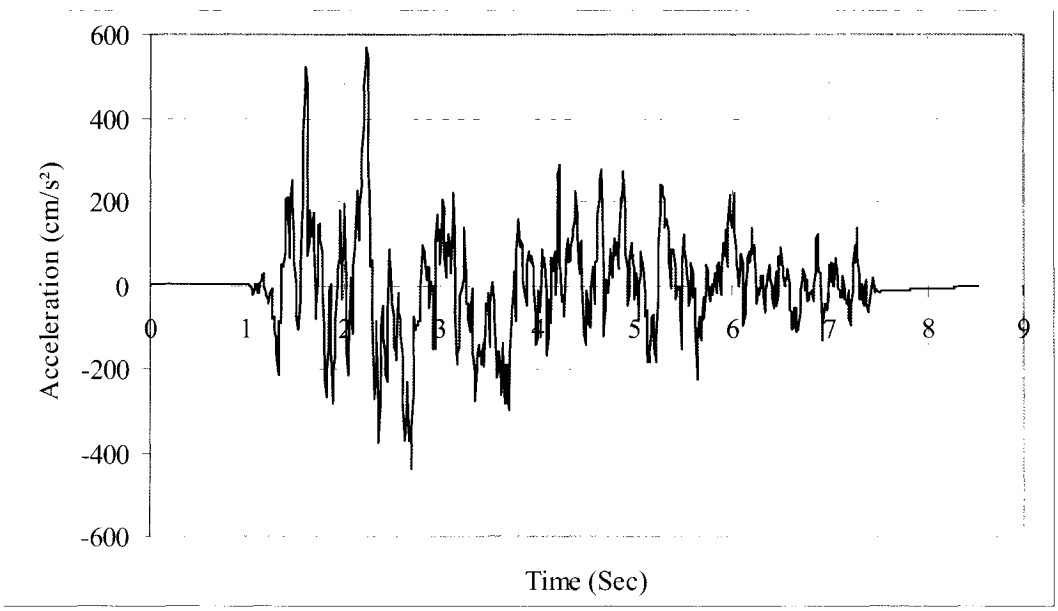

iii) Short Event No.3

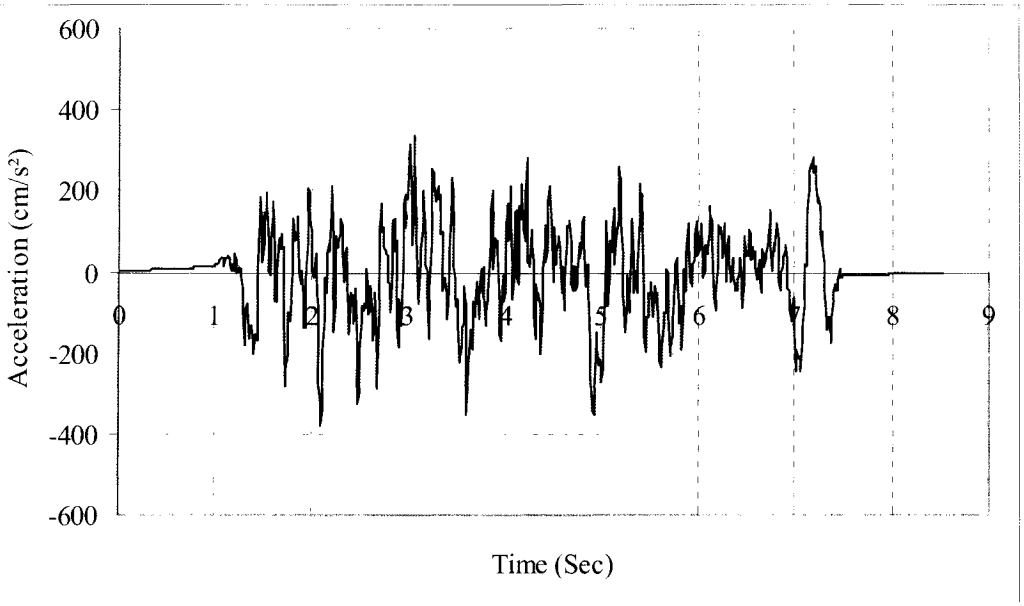

iv) Short Event No.4

a) Short event acceleration time histories

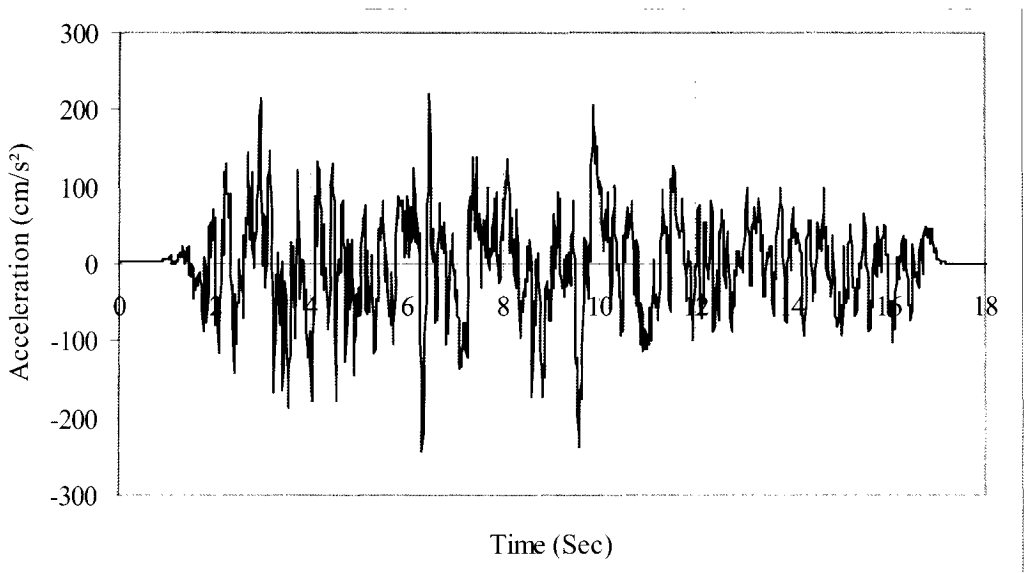

i) Long Event No.1

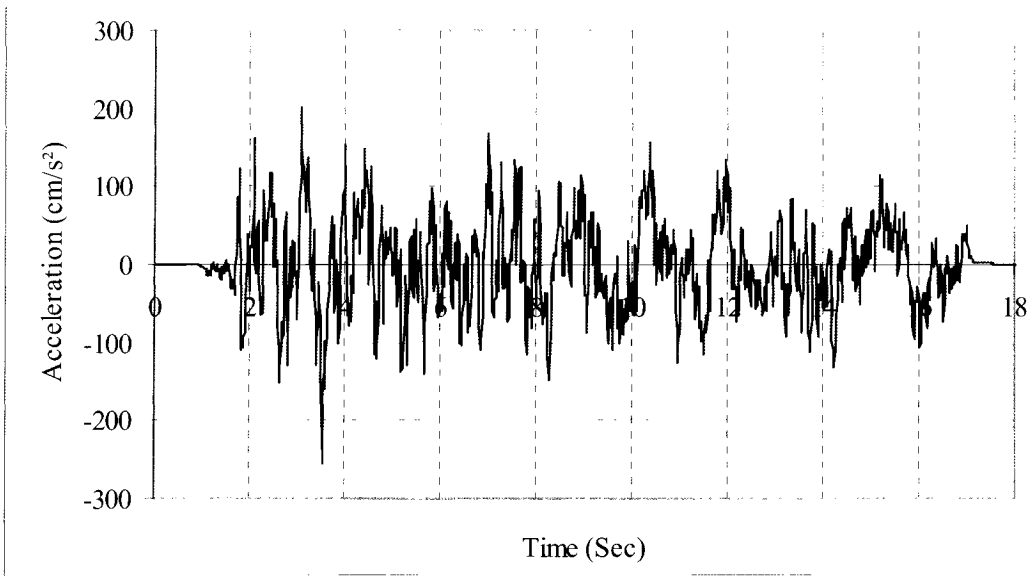

ii) Long Event No.2

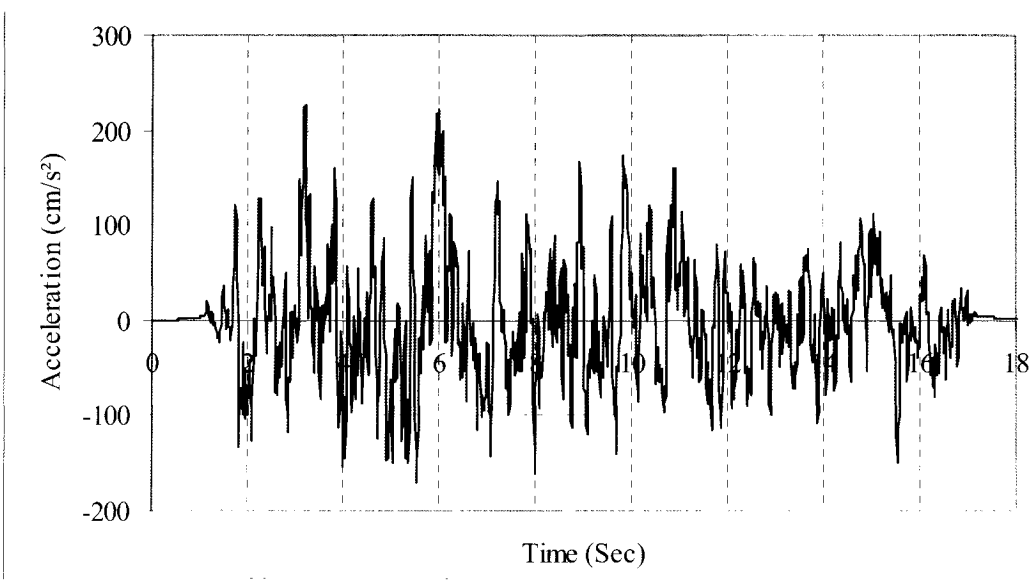

iii) Long Event No.3

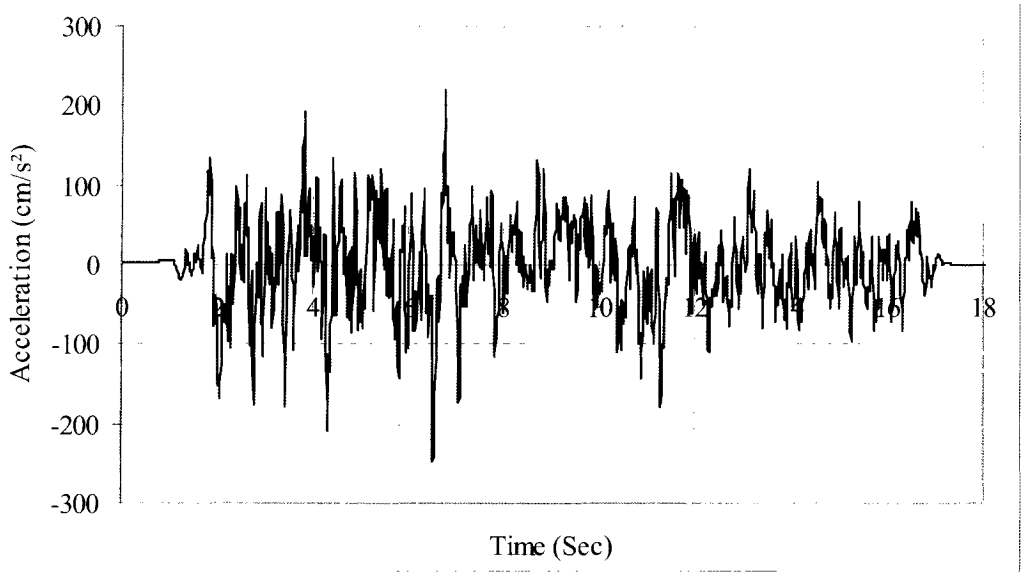

iv) Long Event No.4

b) Long event acceleration time histories

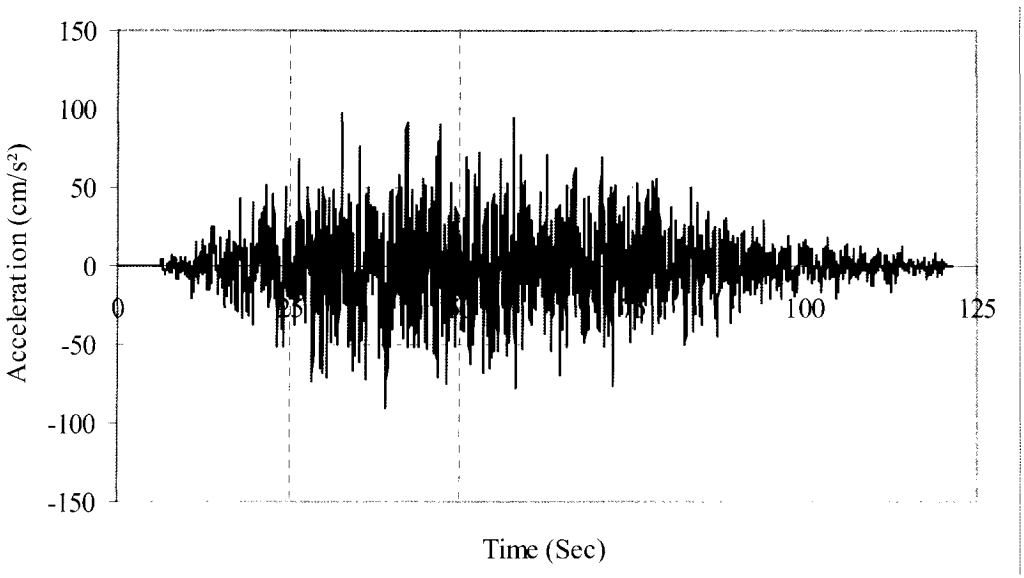

i) Cascadia No.1

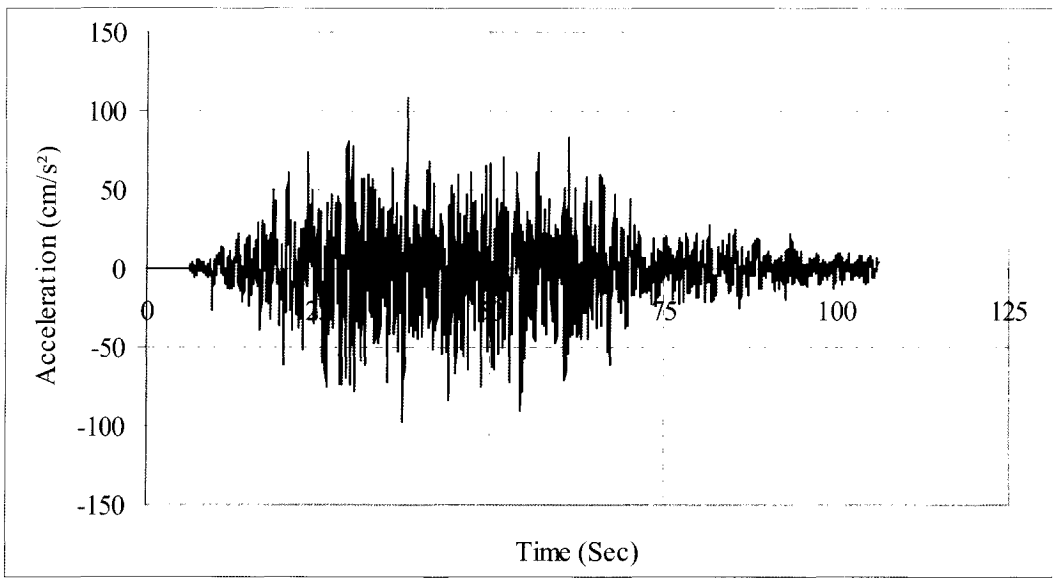

ii) Cascadia No.2

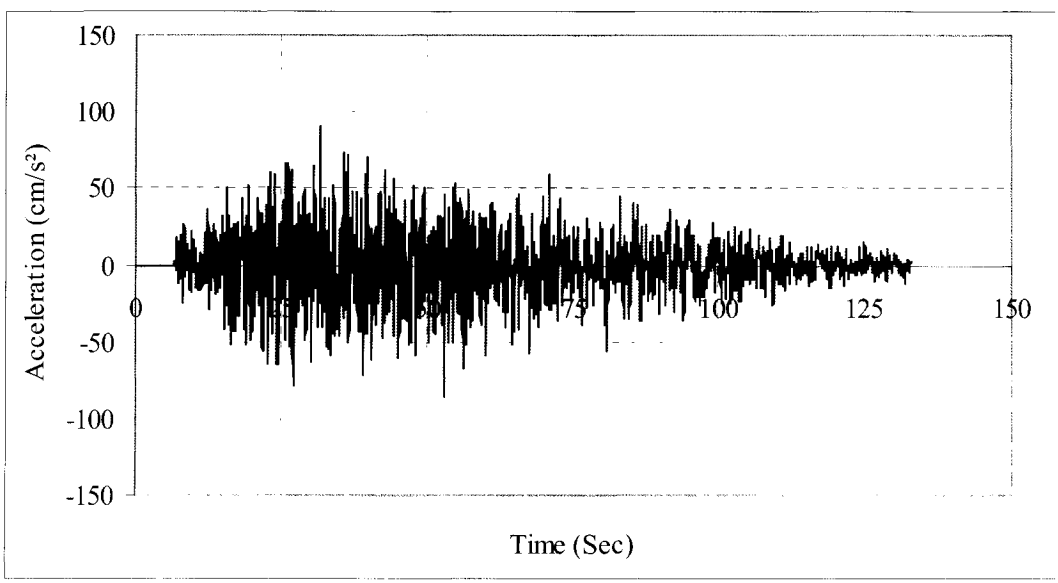

iii) Cascadia No.3

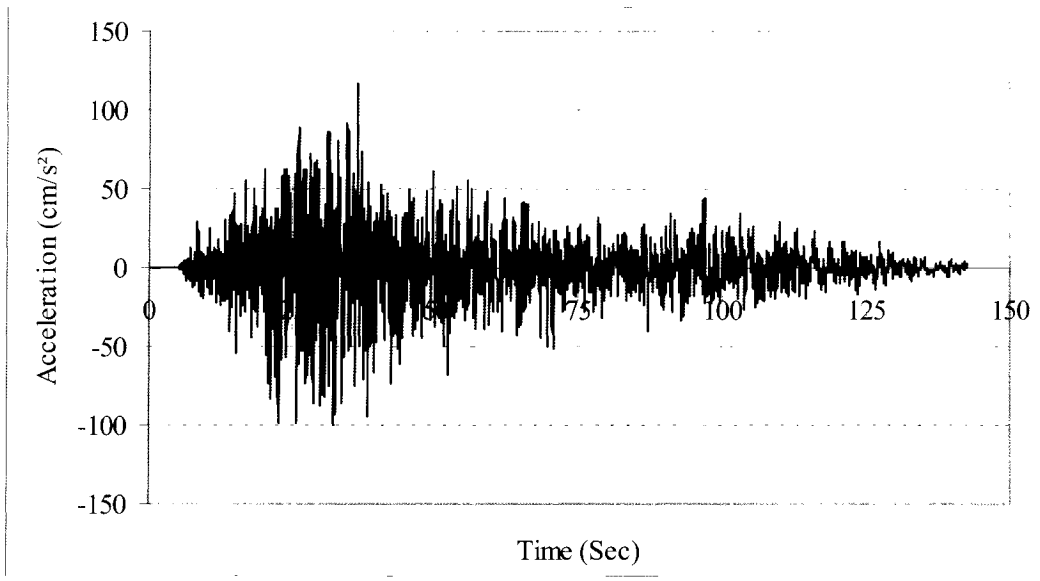

iv) Cascadia No.4

c) Cascadia acceleration time histories.

Figure 5.9: Acceleration time histories of artificial records used for Vancouver

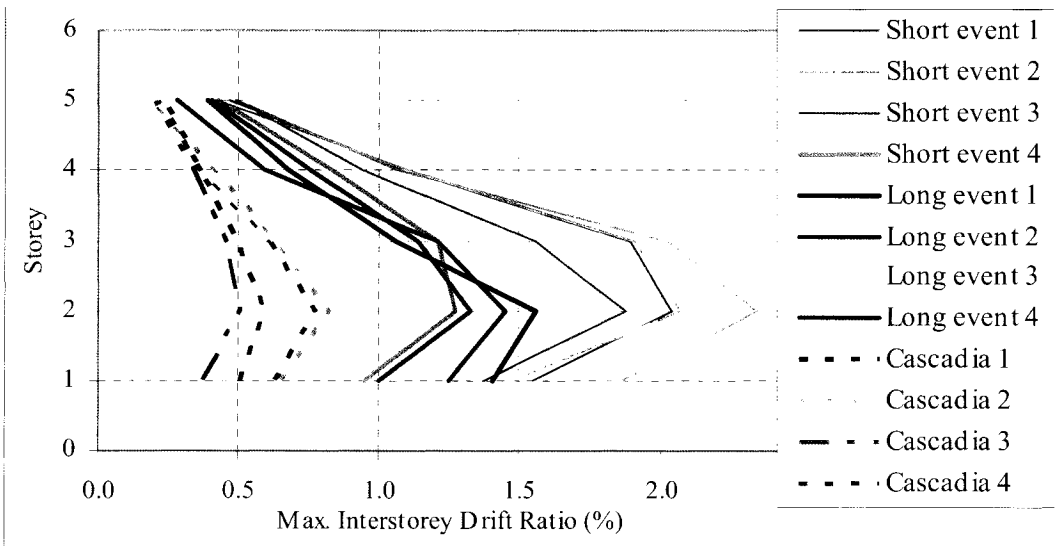

Figure 5.10: Lateral drift demand envelopes under artificial records used for Vancouver

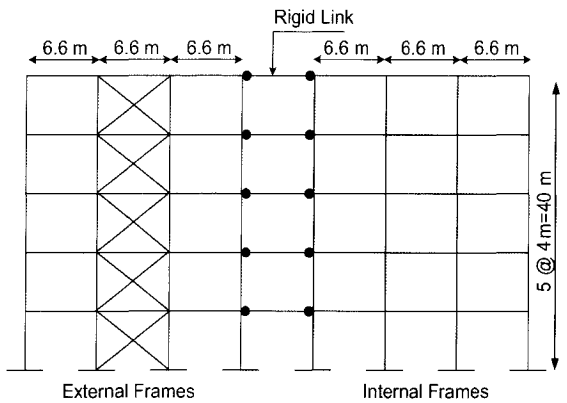

Arrangement #1

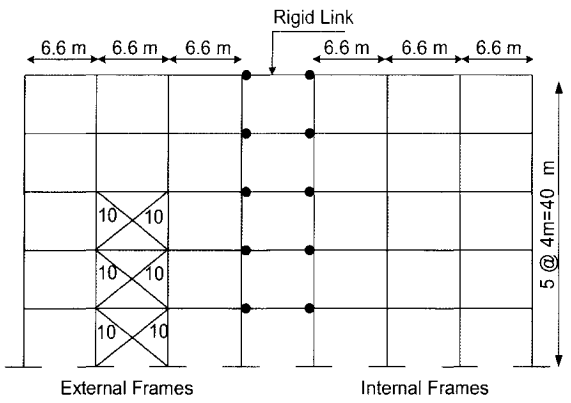

Arrangement #2

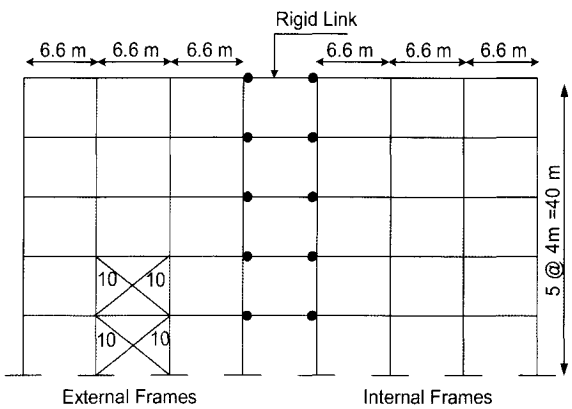

Arrangement #3

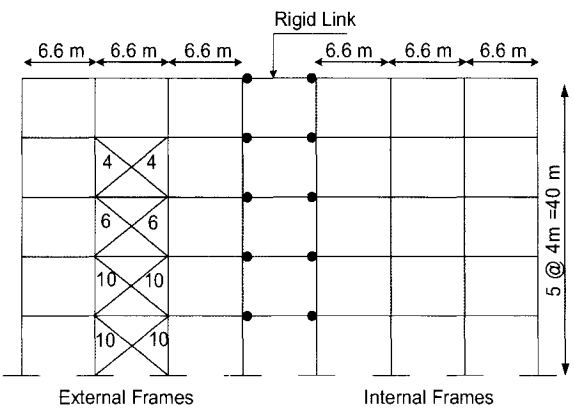

Arrangement #4

Figure 5.11: Arrangement of prestressing cables in two dimensional lumped frames

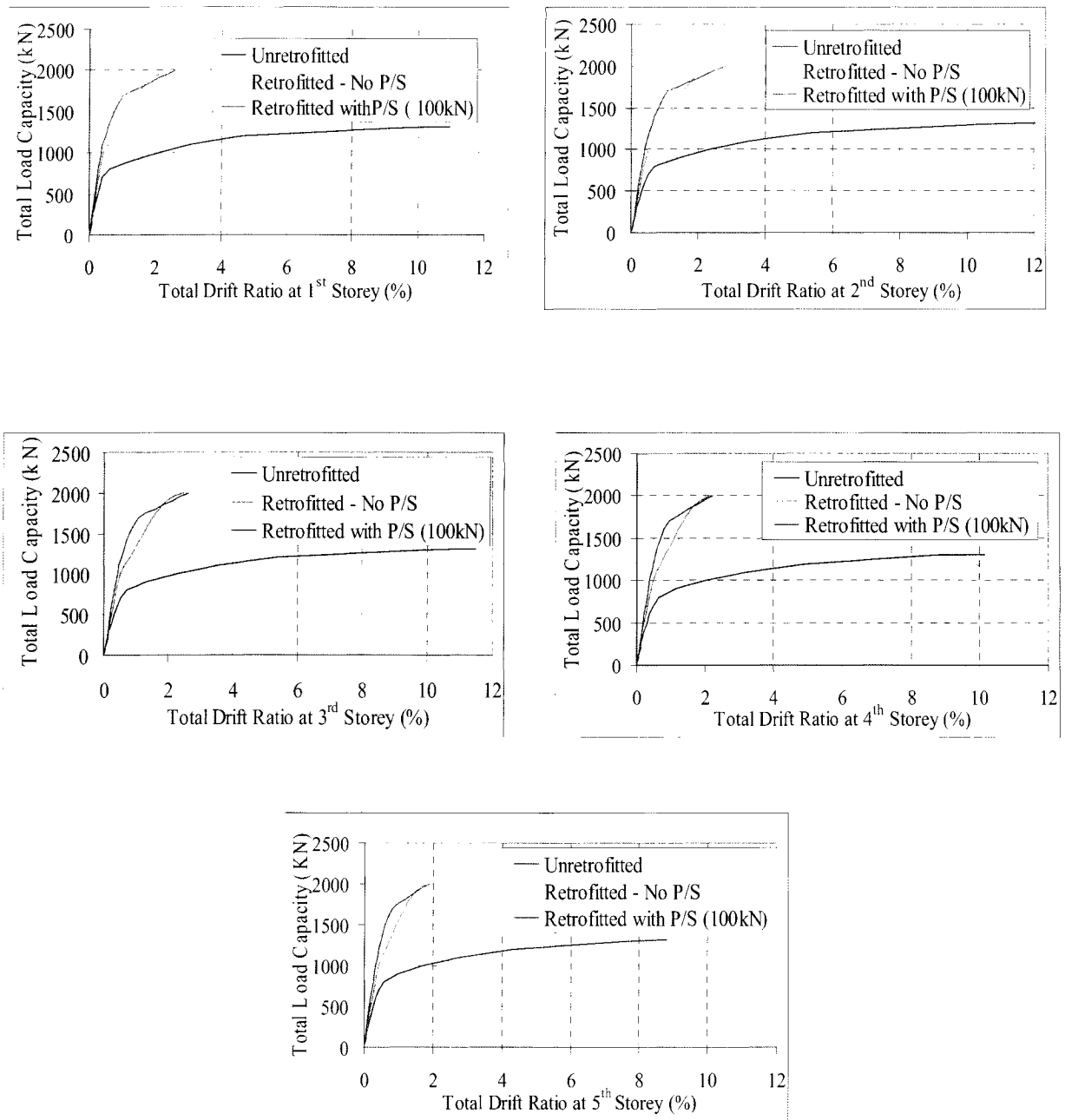

Figure 5.12: The effect of prestressing on drift demands (4 cables/diagonal in the model)

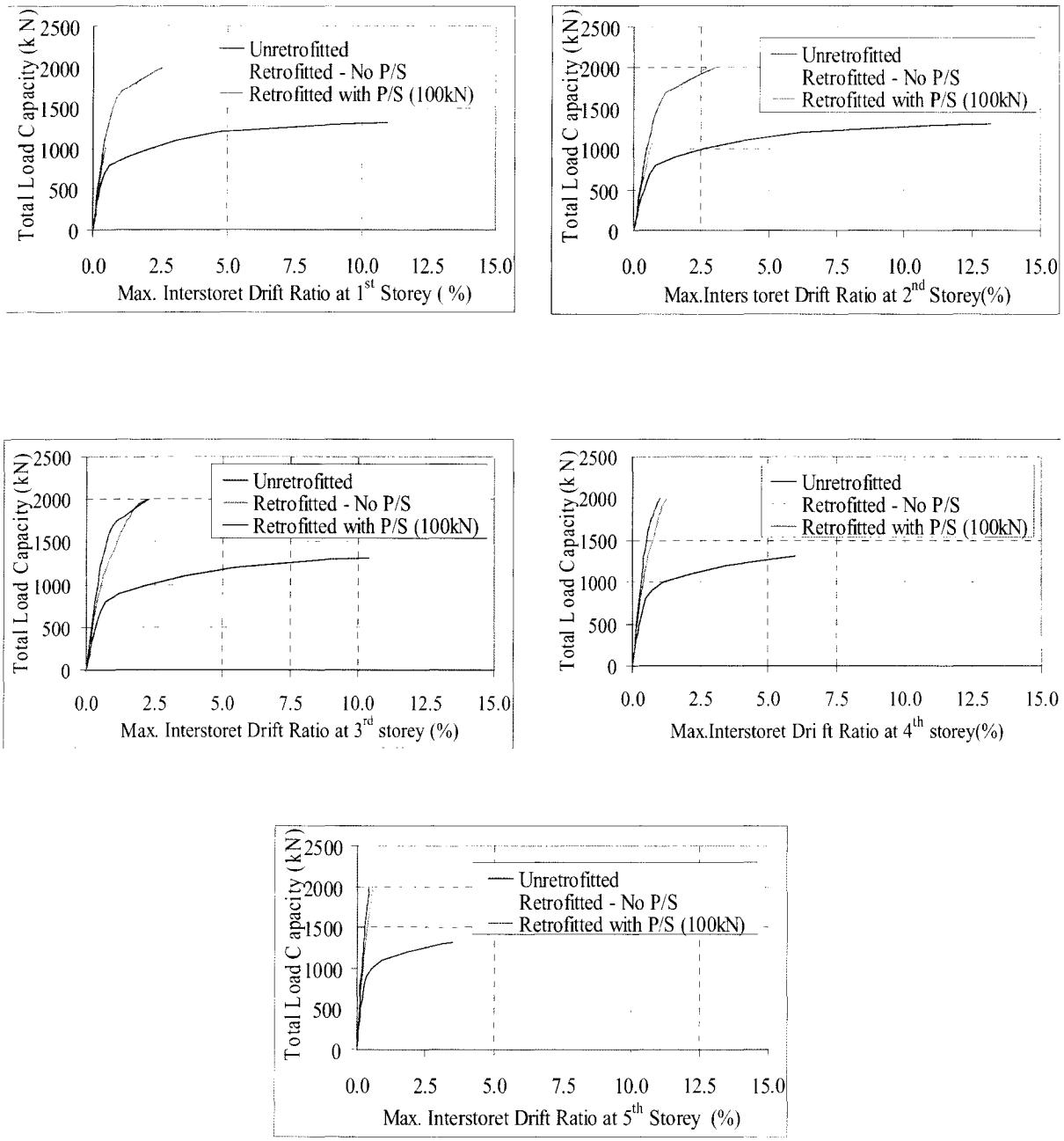

Figure 5.13: The effect of prestressing on interstorey drift demands

(4 cables/diagonal in the model)

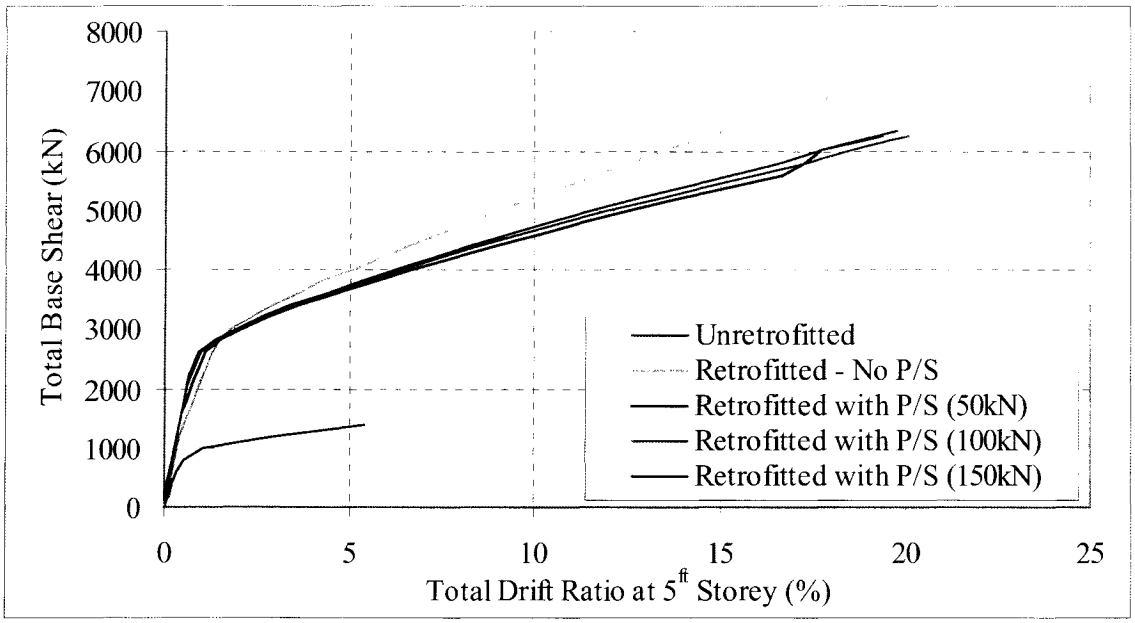

Figure 5.14: The results of pushover analysis for the 5-storey building
(Retrofitted buildings have 8 cables/diagonal in lumped frame model)

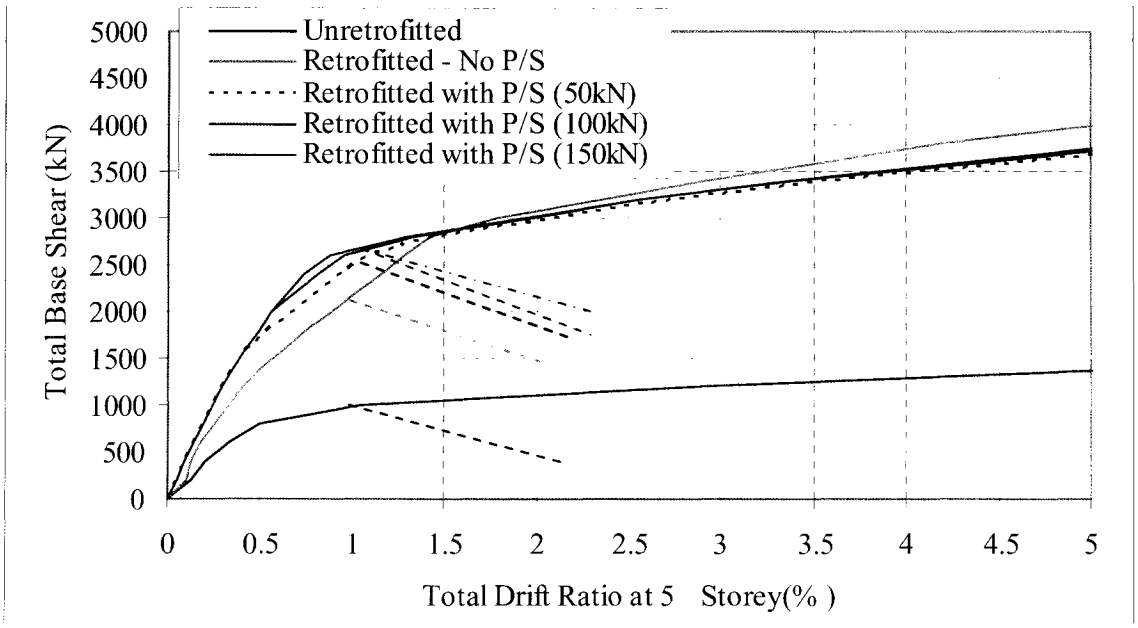

Figure 5.15: The results of pushover analysis for the 5-storey building, with potential strength decay indicated beyond 1% drift ratio
(Retrofitted buildings have 8 cables/diagonal in lumped frame model)

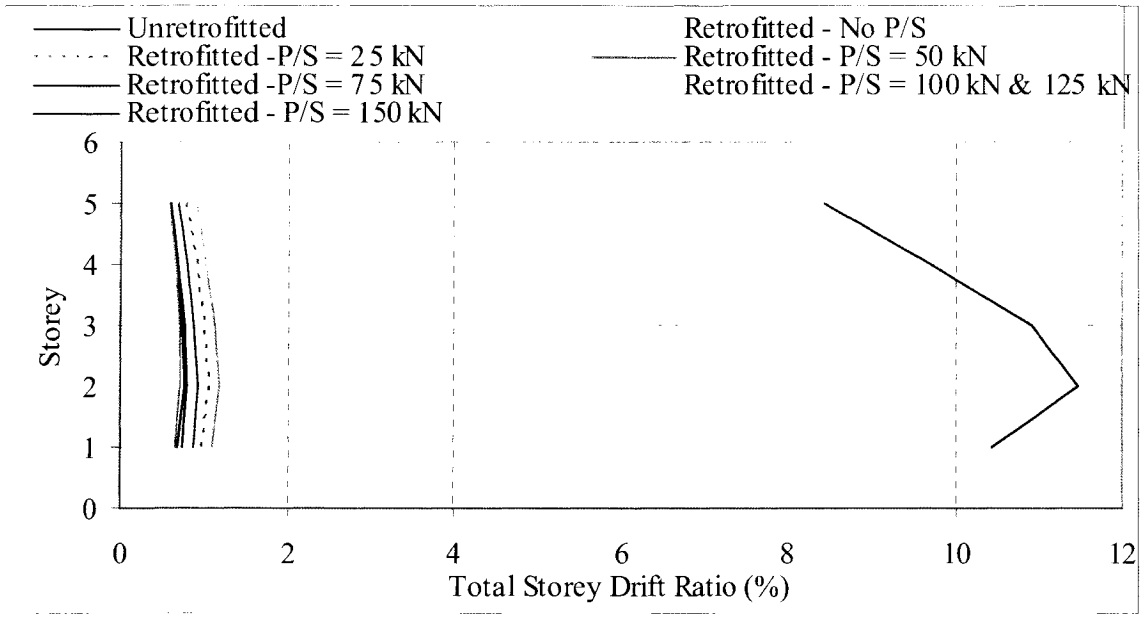

a) Drift ratio

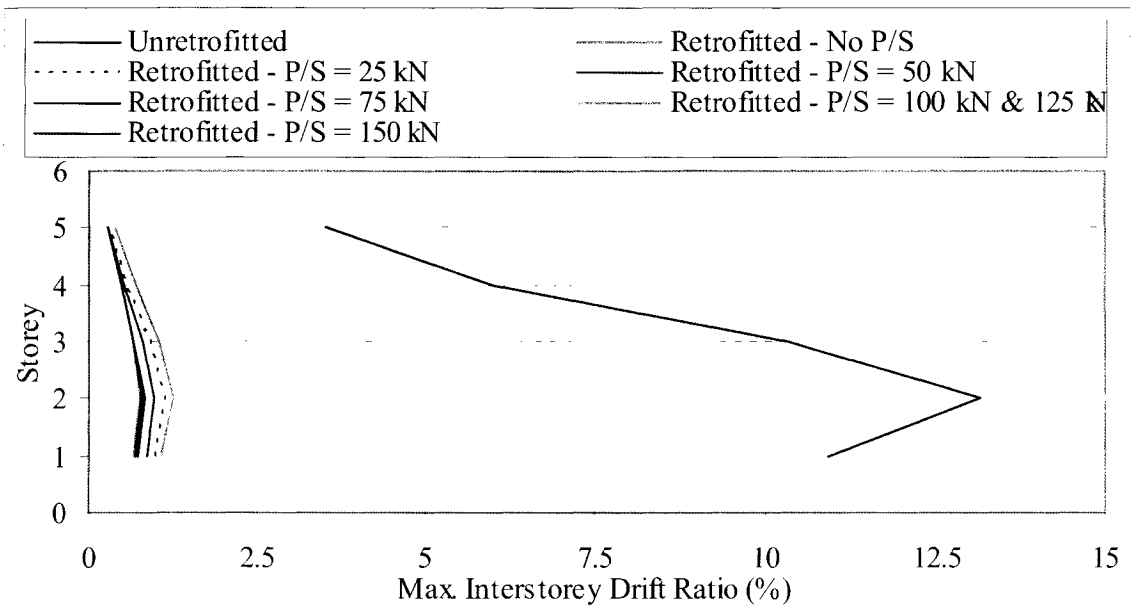

b) Interstorey drift ratio

Figure 5.16: The effect of prestressing on drift ratios and interstorey drift ratios

(Retrofitted buildings have 8 cables/diagonal in lumped frame model)

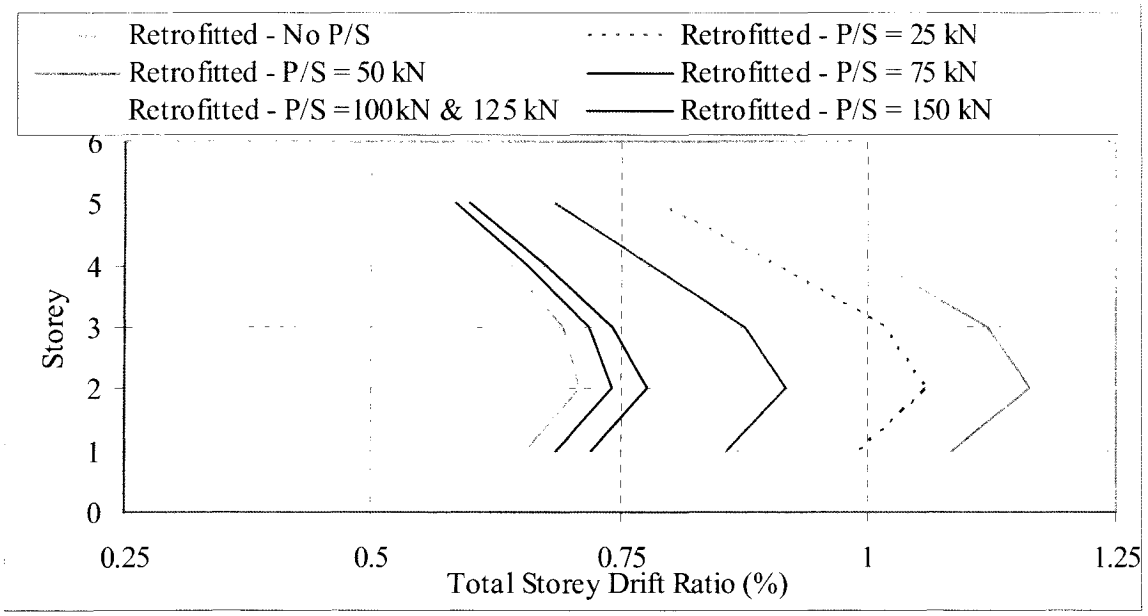

a) Total drift ratio

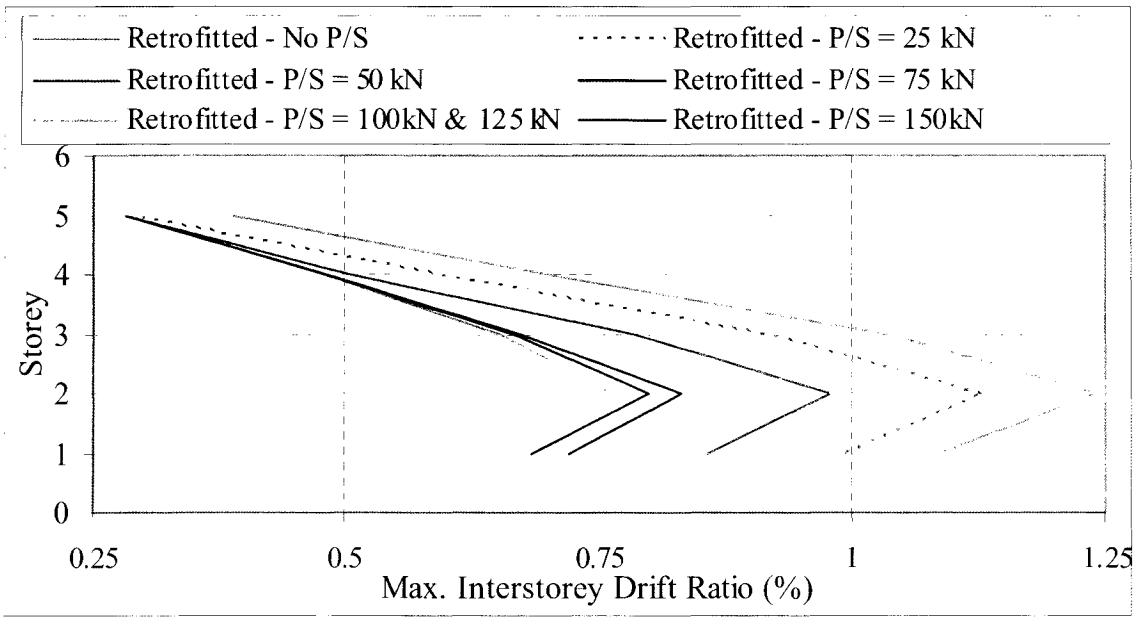

b) Interstorey drift ratio

Figure 5.17: The effect of prestressing on total and interstorey drift ratios

(8 cables/diagonal in lumped frame model)

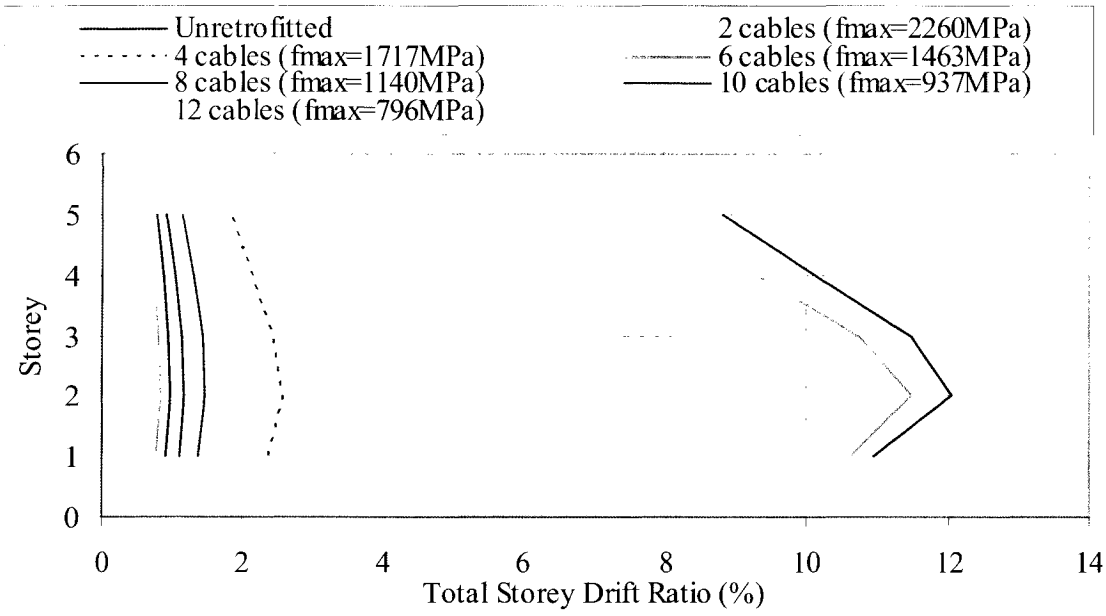

a) Total drift ratio

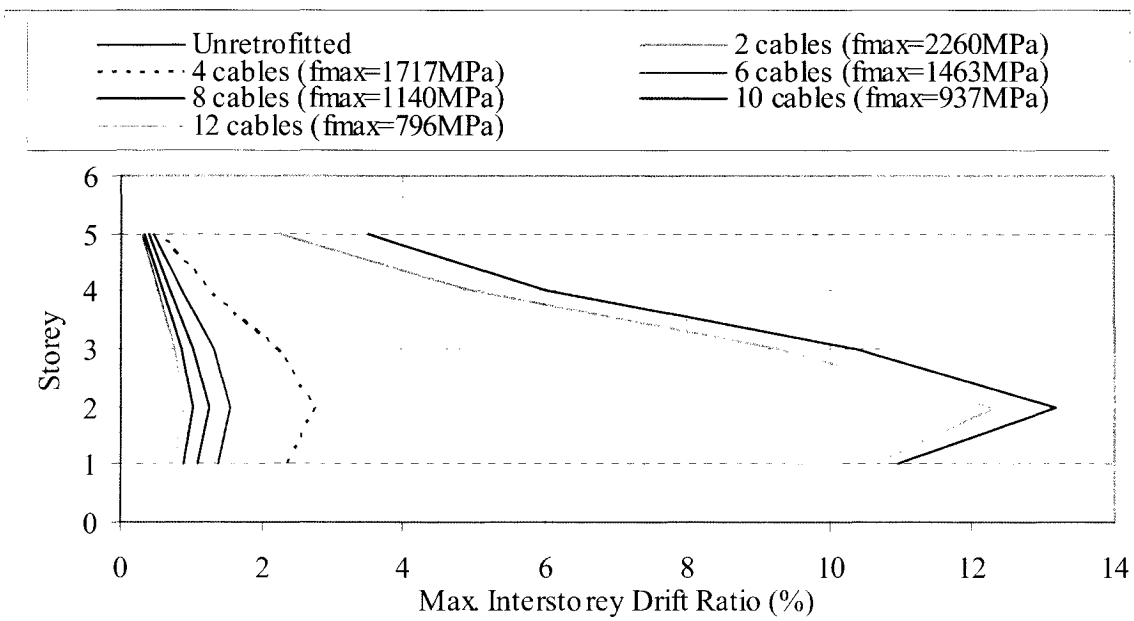

b) Interstorey drift ratio

Figure 5.18: Effect of amount of prestressing cables on total and interstorey drift ratios (Retrofitted No P/S)

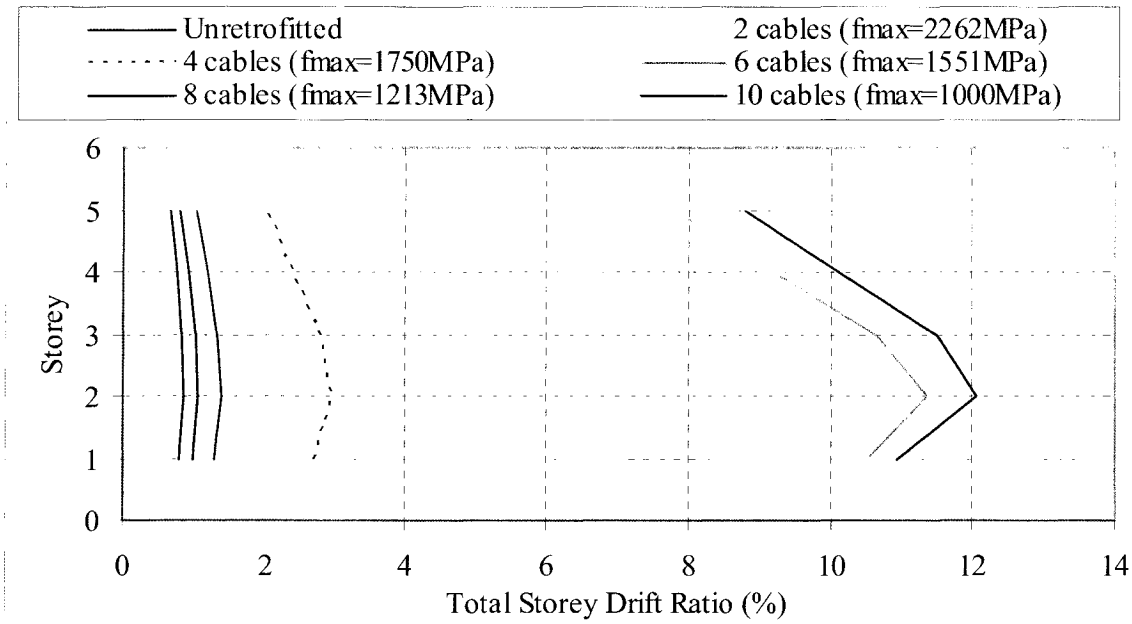

a) Drift ratio

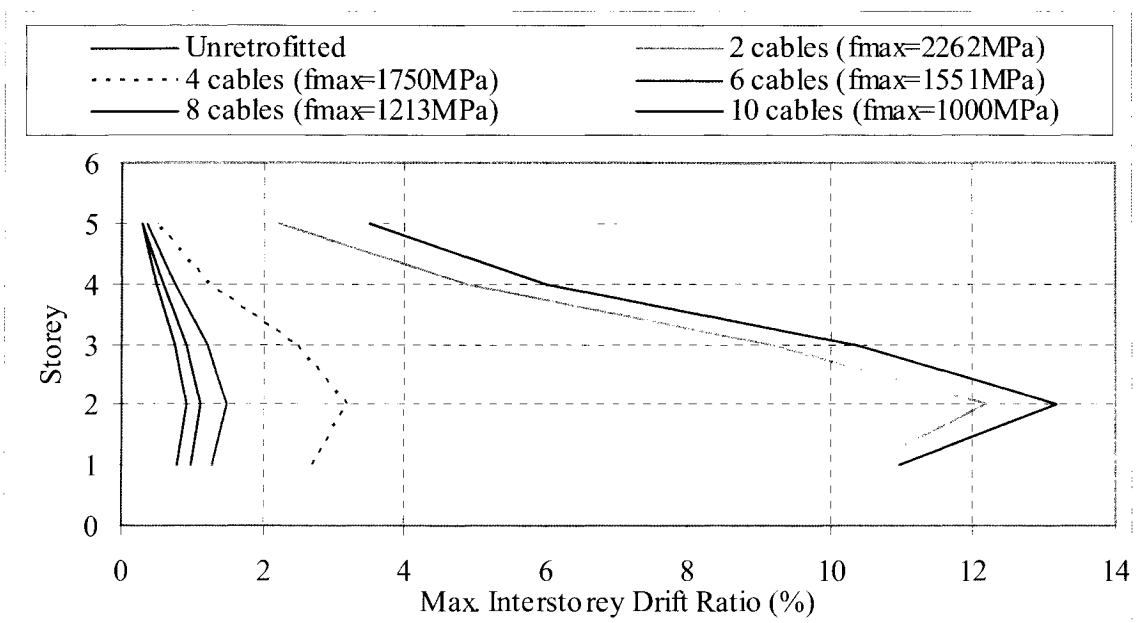

b) Interstorey drift ratio

Figure 5.19: Effect of the amount of prestressing cables on total and interstorey drift ratios (Retrofitted P/S = 25 kN)

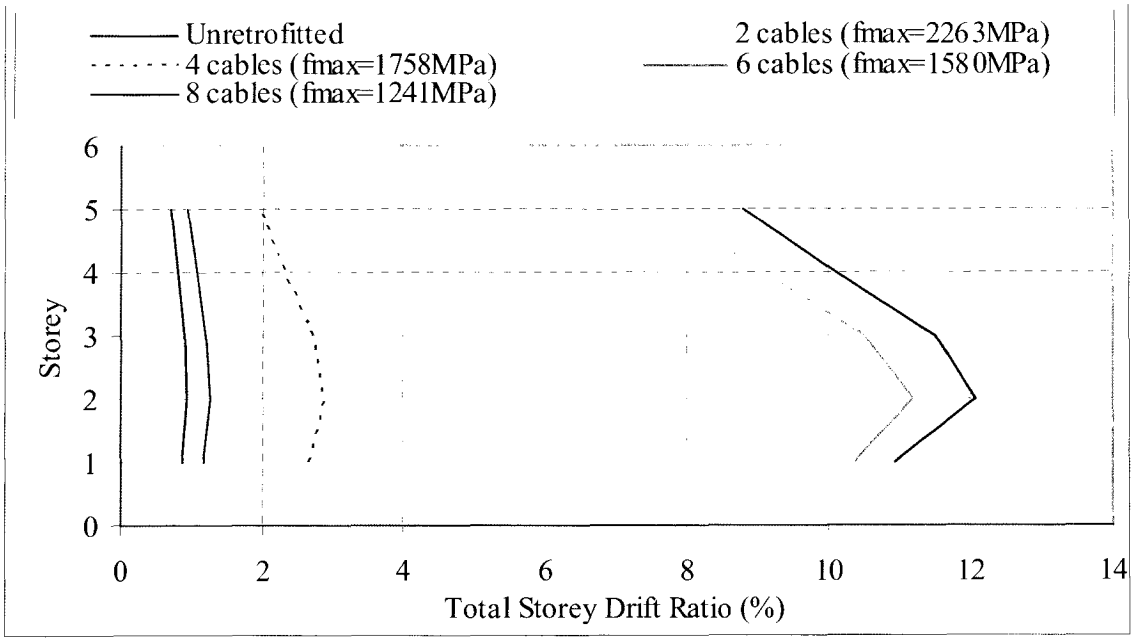

a) Total drift ratio

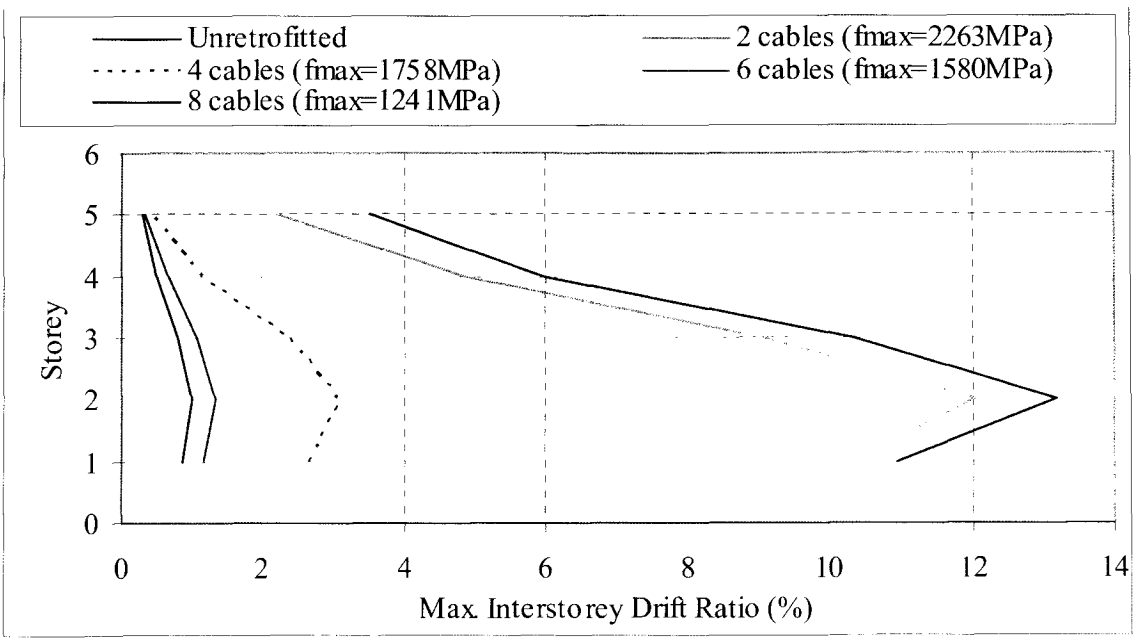

b) Interstorey drift ratio

Figure 5.20: Effect of the amount of prestressing cables on total and interstorey drift ratios (Retrofitted P/S = 50 kN)

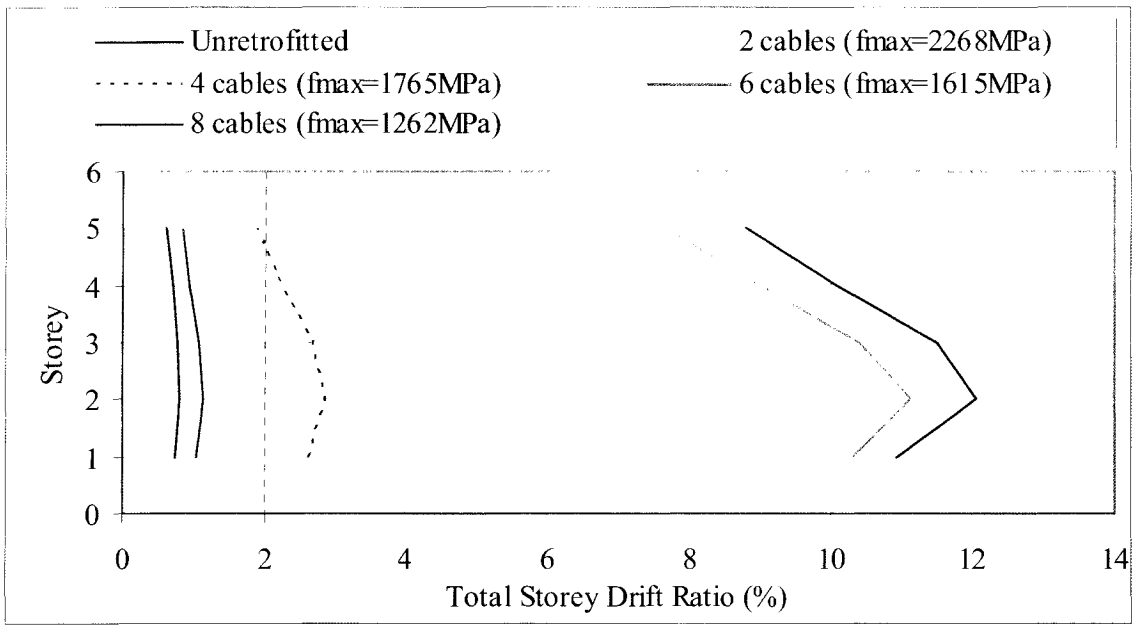

a) Total drift ratio

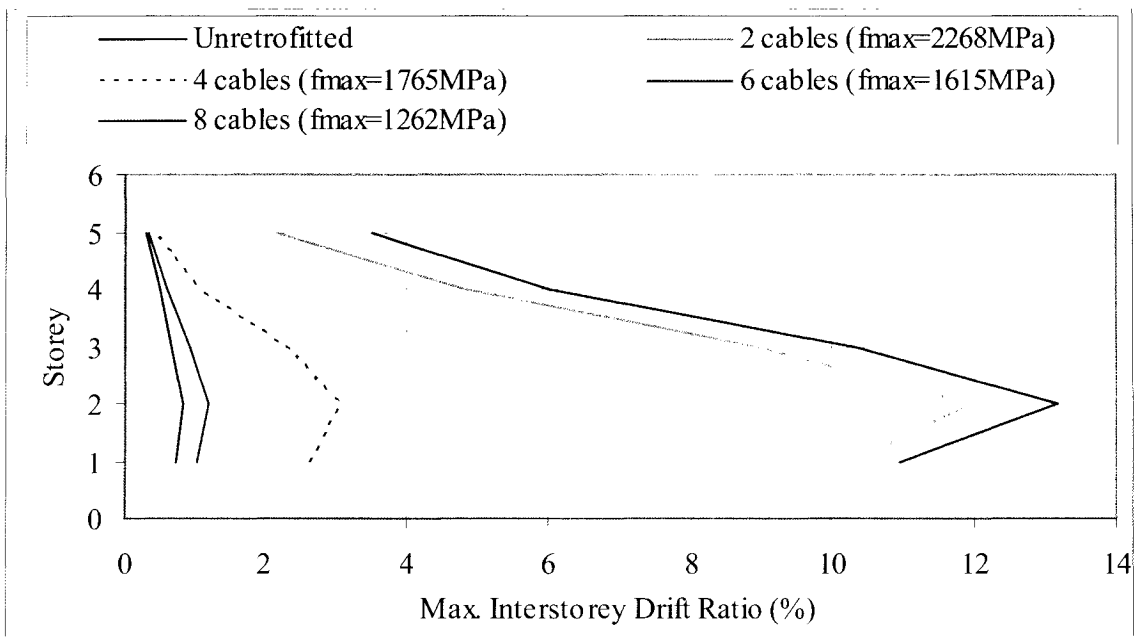

b) Interstorey drift ratio

Figure 5.21: Effect of the amount of prestressing cables on total and interstorey drift ratios (Retrofitted P/S = 75 kN)

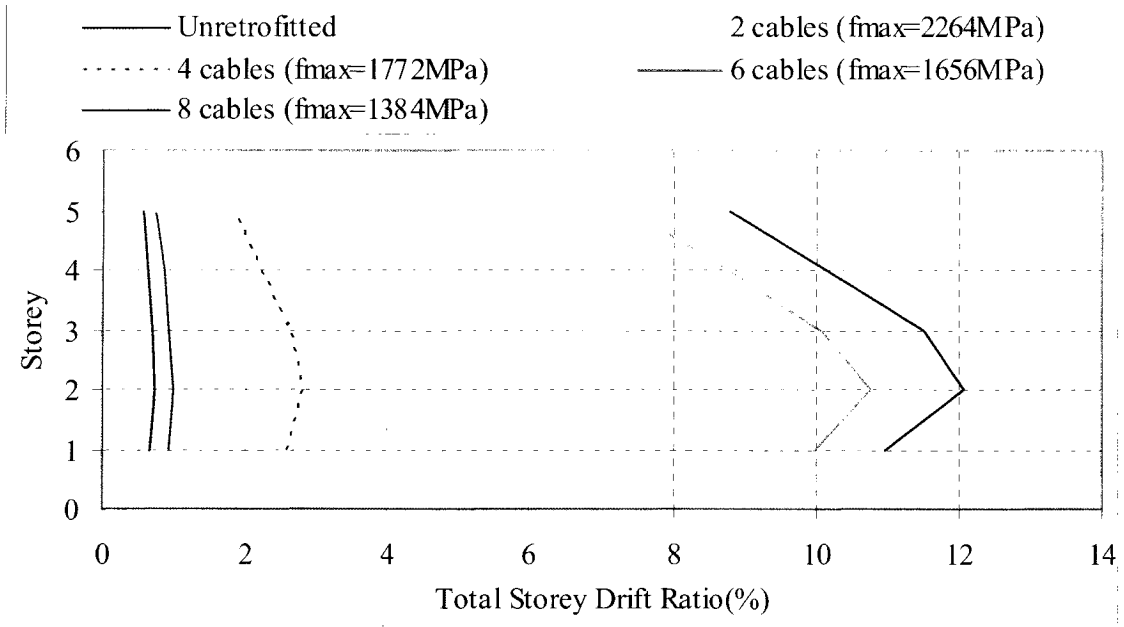

a) Total drift ratio

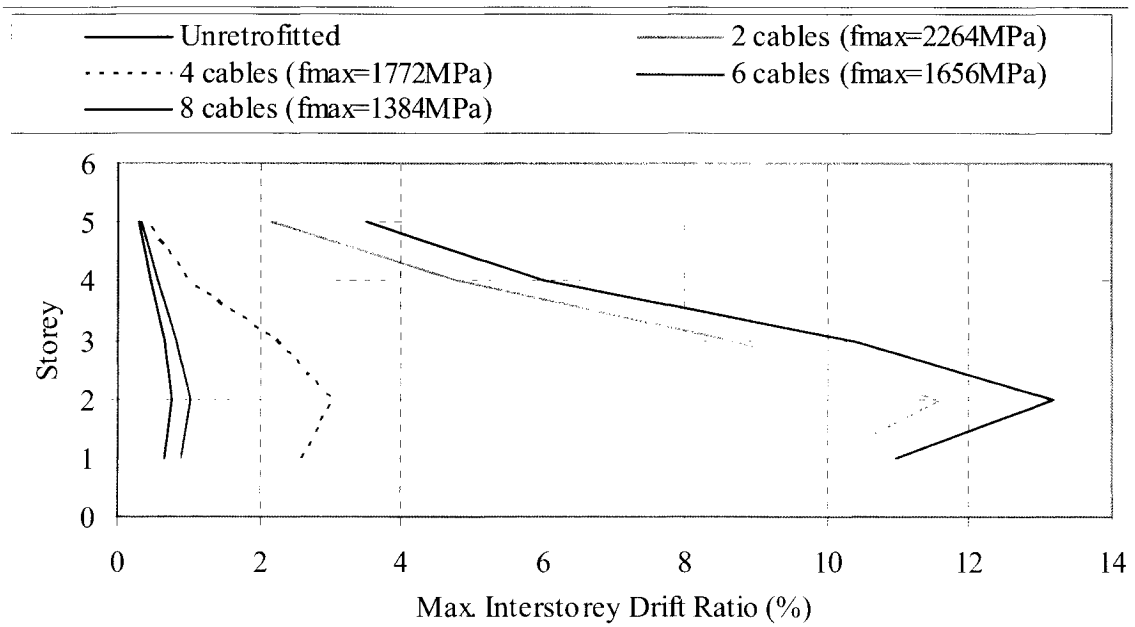

b) Interstorey drift ratio

Figure 5.22: Effect of the amount of prestressing cables on total and interstorey drift ratios (Retrofitted P/S = 100 kN)

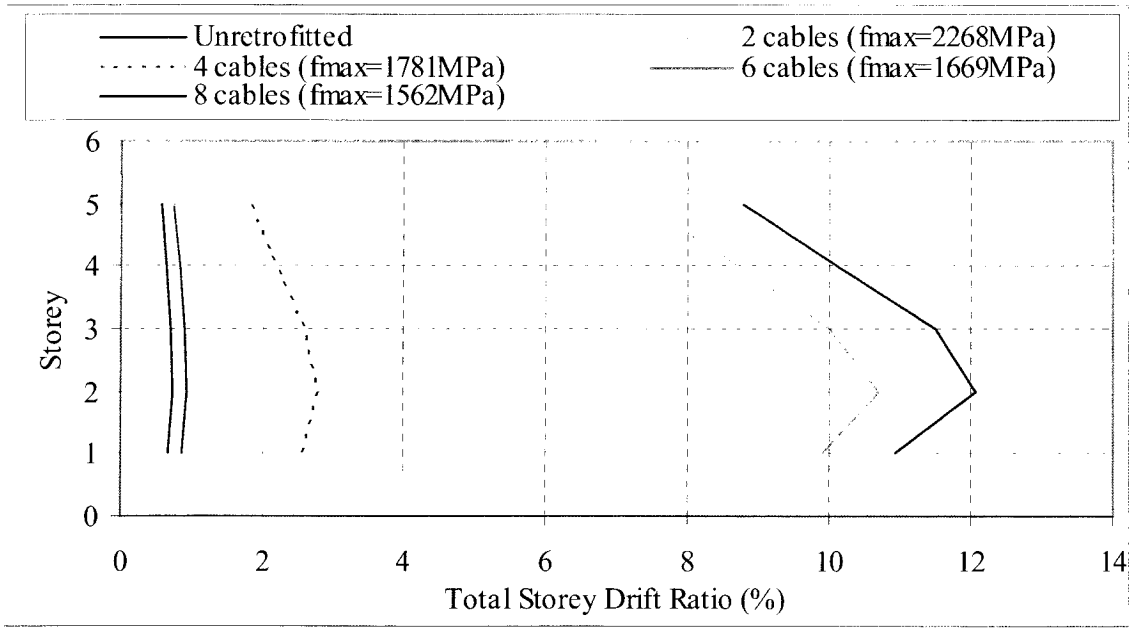

a) Total drift ratio

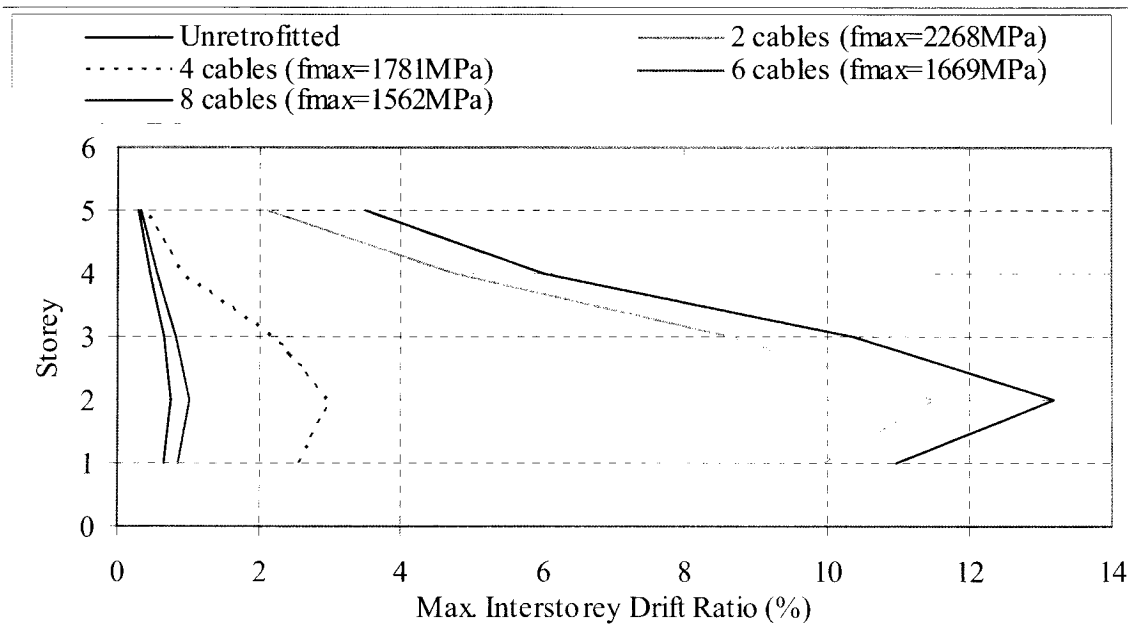

b) Interstorey drift ratio

Figure 5.23: Effect of the amount of prestressing cables on total and interstorey drift ratios (Retrofitted P/S = 125 kN)

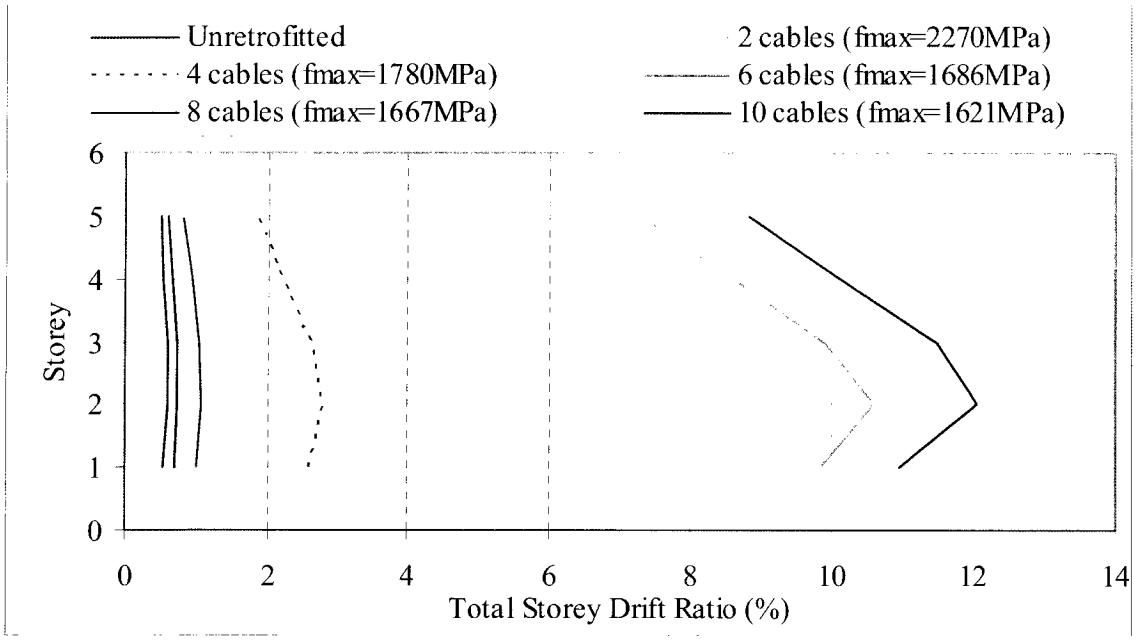

a) Total drift ratio

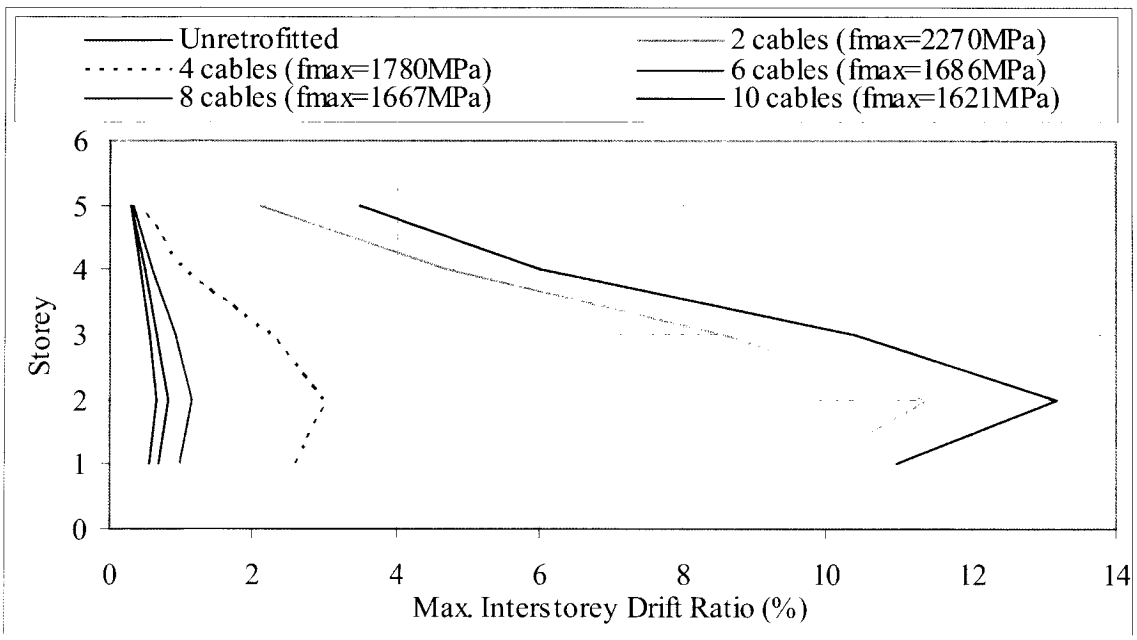

b) Interstorey drift ratio

Figure 5.24: Effect of amount of prestressing cables on total and interstorey drift ratios (Retrofitted P/S = 150 kN)

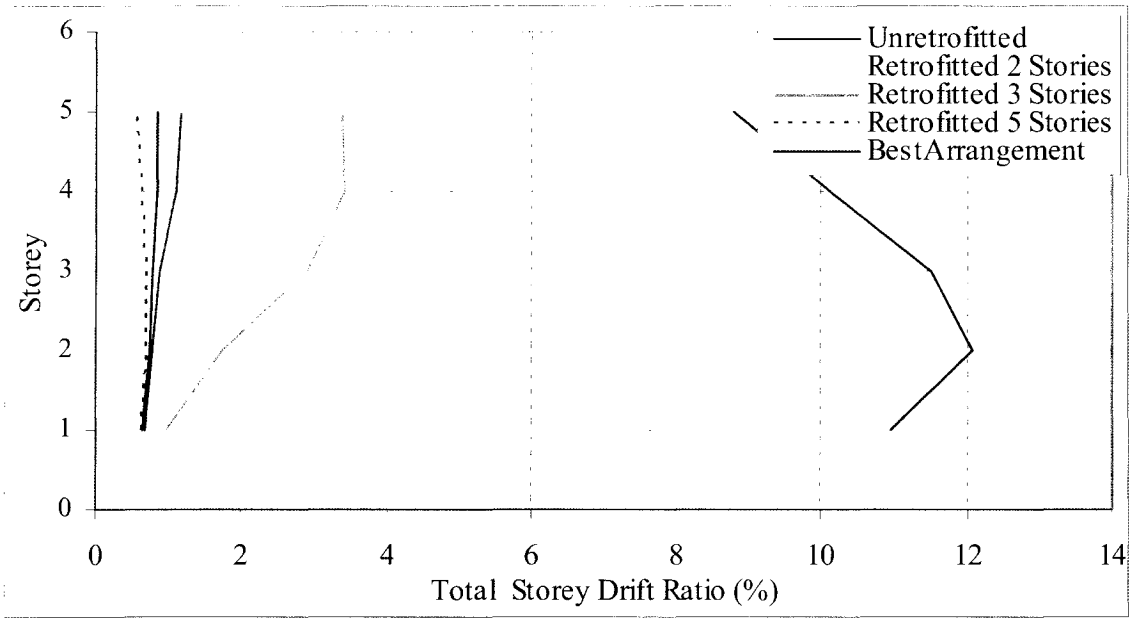

a) Total drift ratio (%)

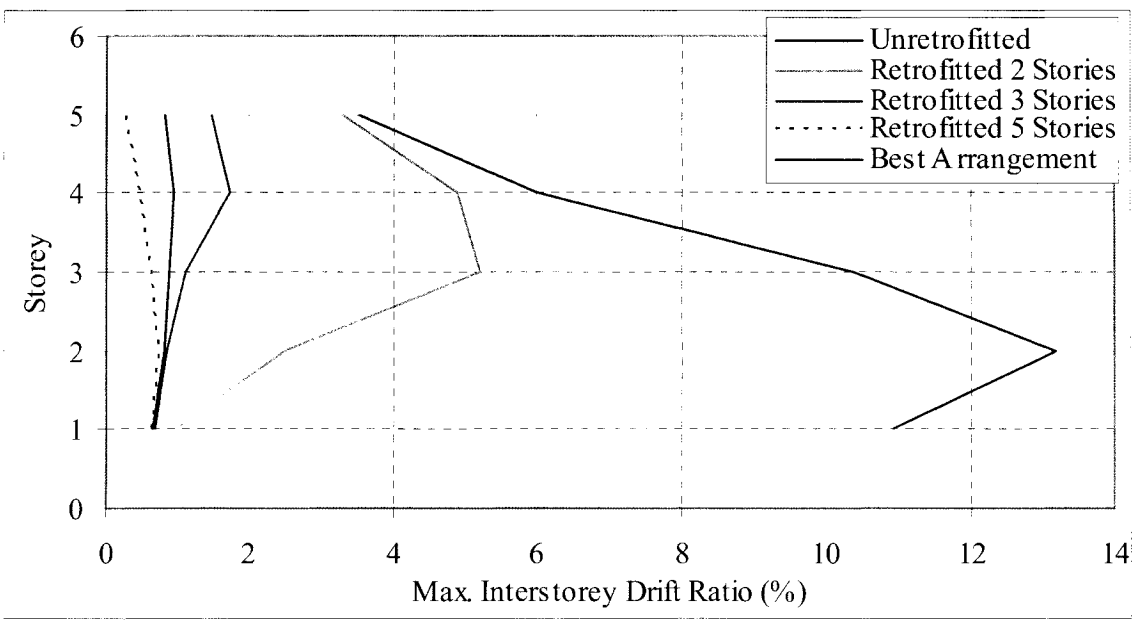

b) Interstorey drift ratio

Figure 5.25: Effect of different arrangements of prestressing cables on total and interstorey drift ratios

(Retrofitted buildings have 8 cables/diagonal in lumped frame model with P/S =100 kN))

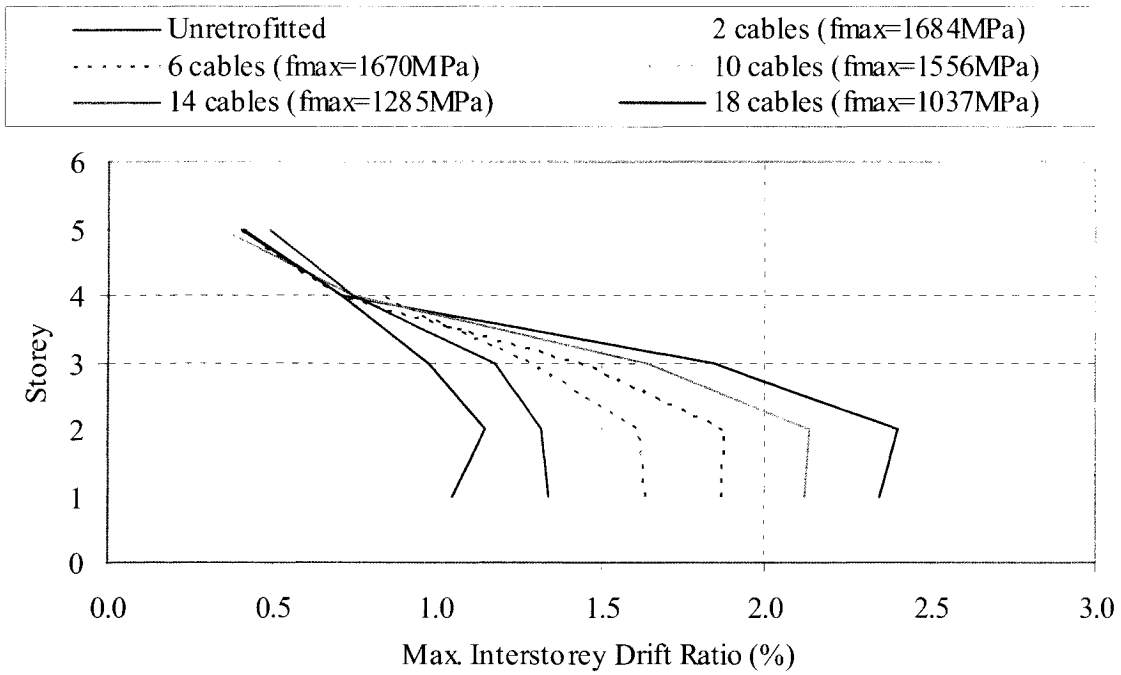

Figure 5.26: The effect of prestressing on interstorey drift ratios

(Retrofitted No P/S)

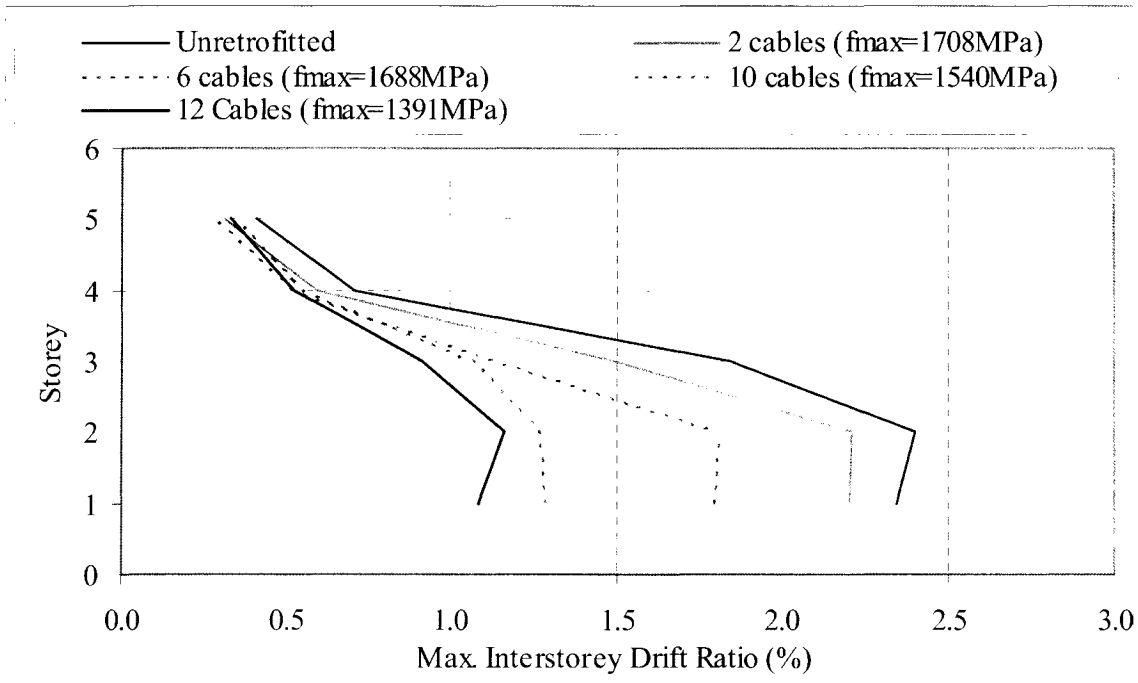

Figure 5.27: The effect of prestressing on interstorey drift ratios

(Retrofitted P/S = 50 kN)

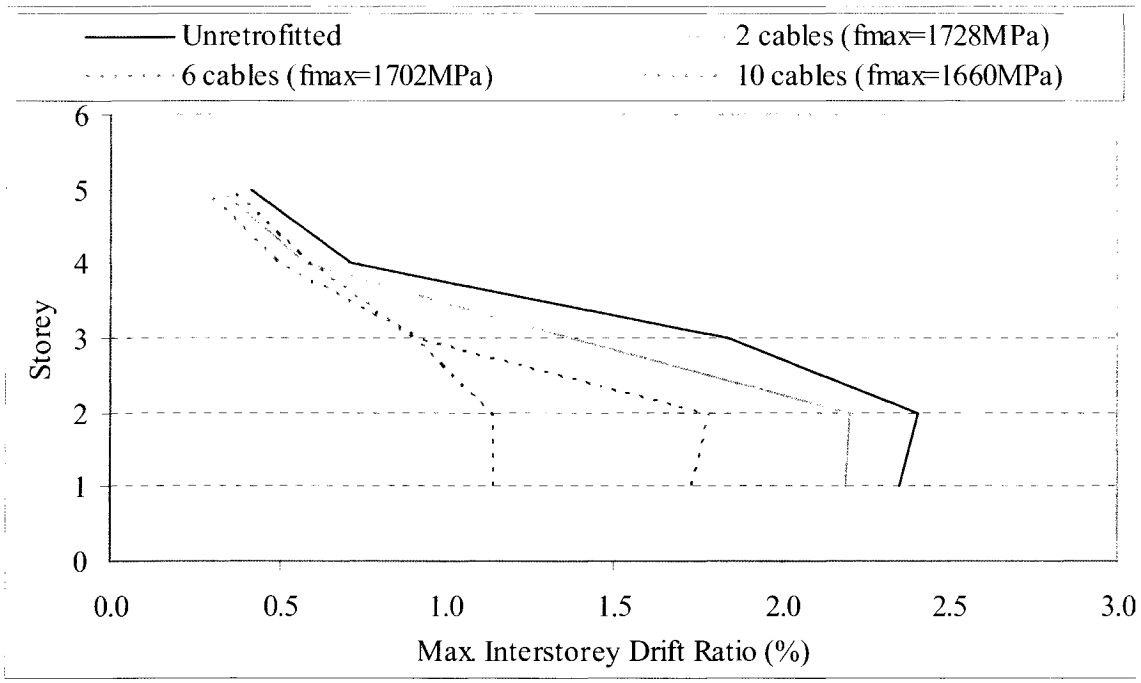

Figure 5.28: The effect of prestressing on interstorey drift ratios

(Retrofitted P/S = 100 kN)

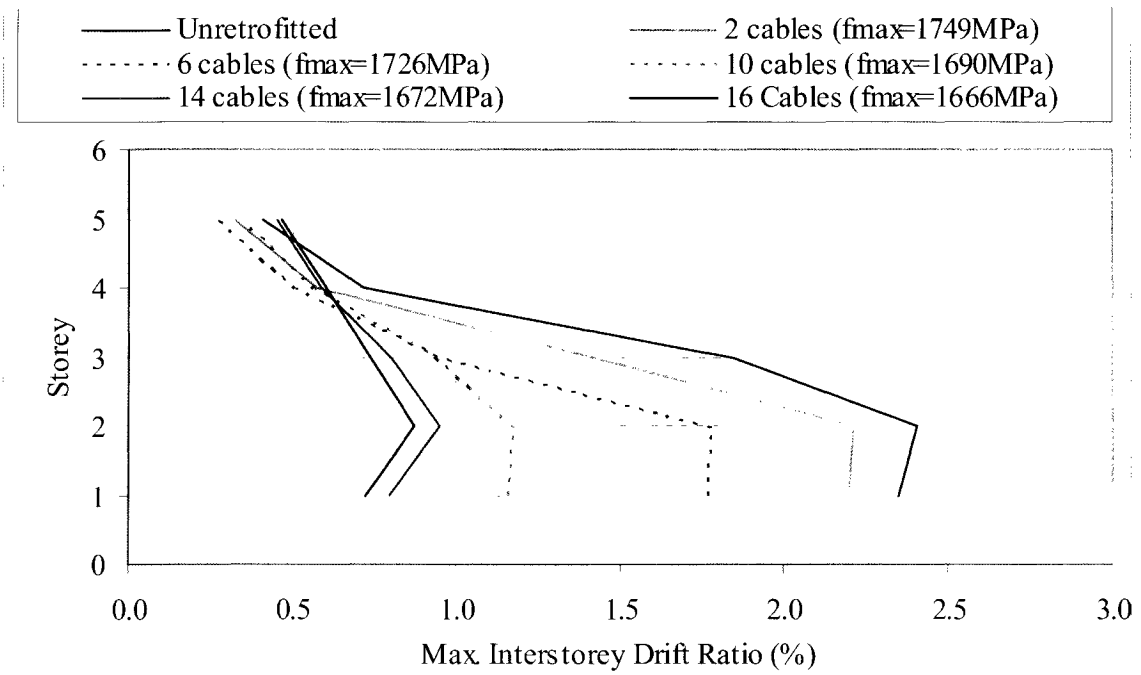

Figure 5.29: The effect of prestressing on interstorey drift ratios

(Retrofitted P/S = 150 kN)

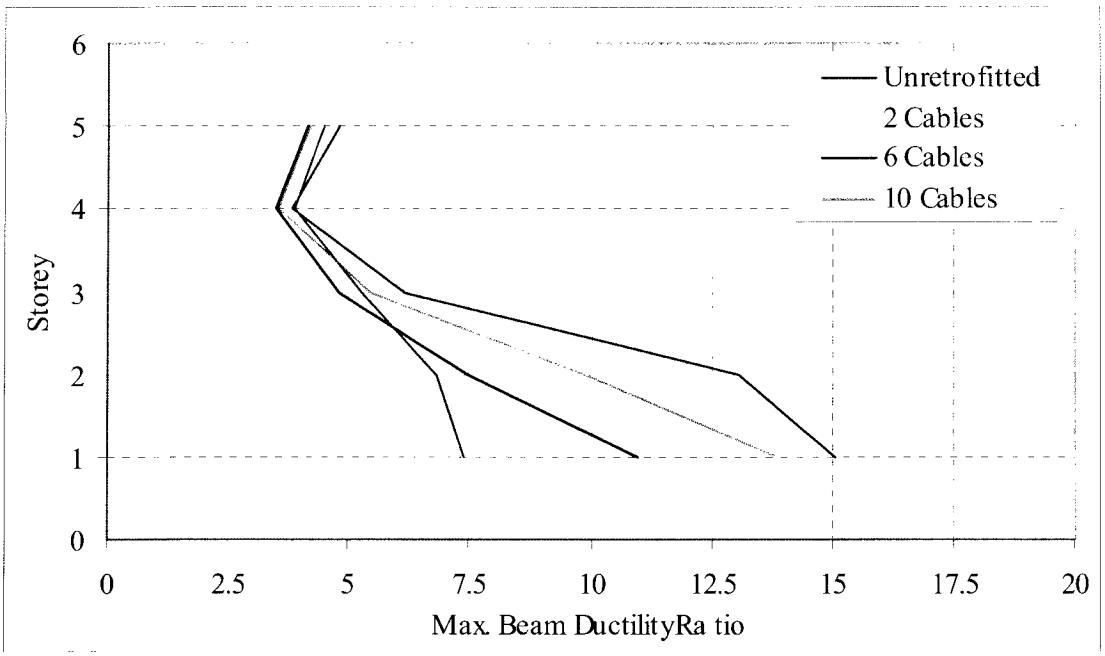

Figure 5.30: Maximum ductility response for beams at each storey

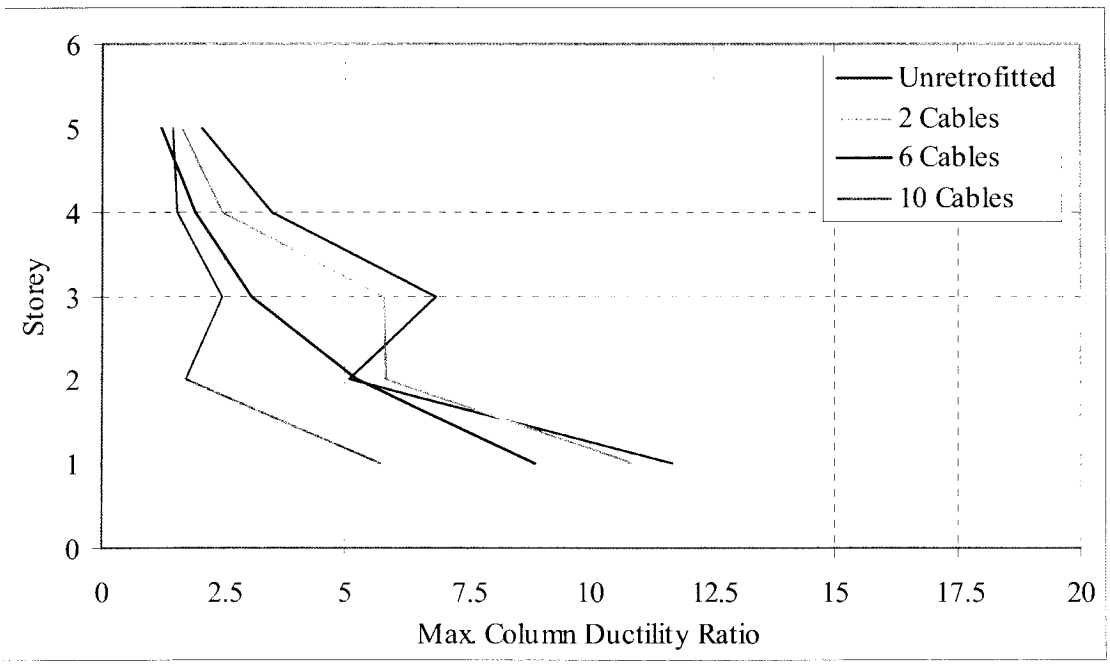

Figure 5.31: Maximum ductility response for columns at each storey

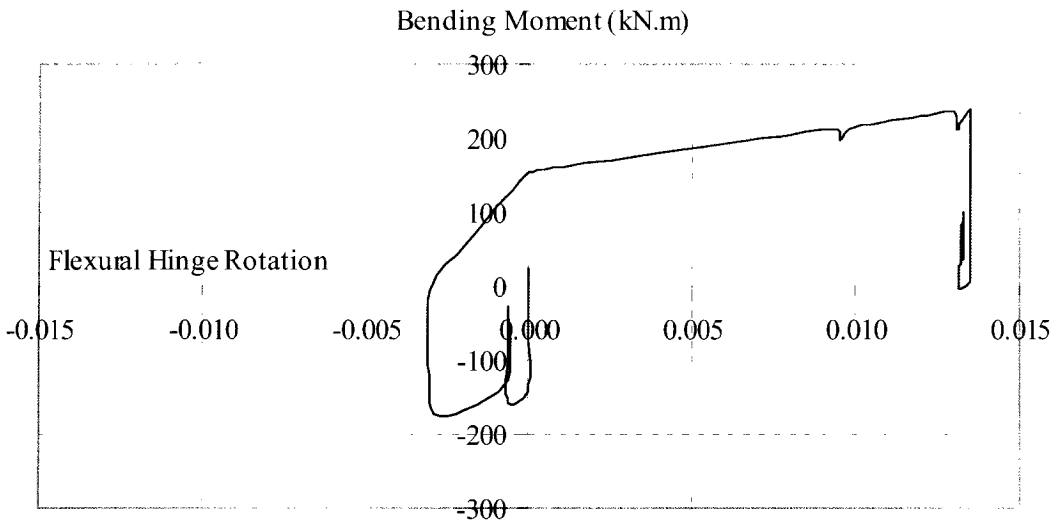

a) Unretrofitted building

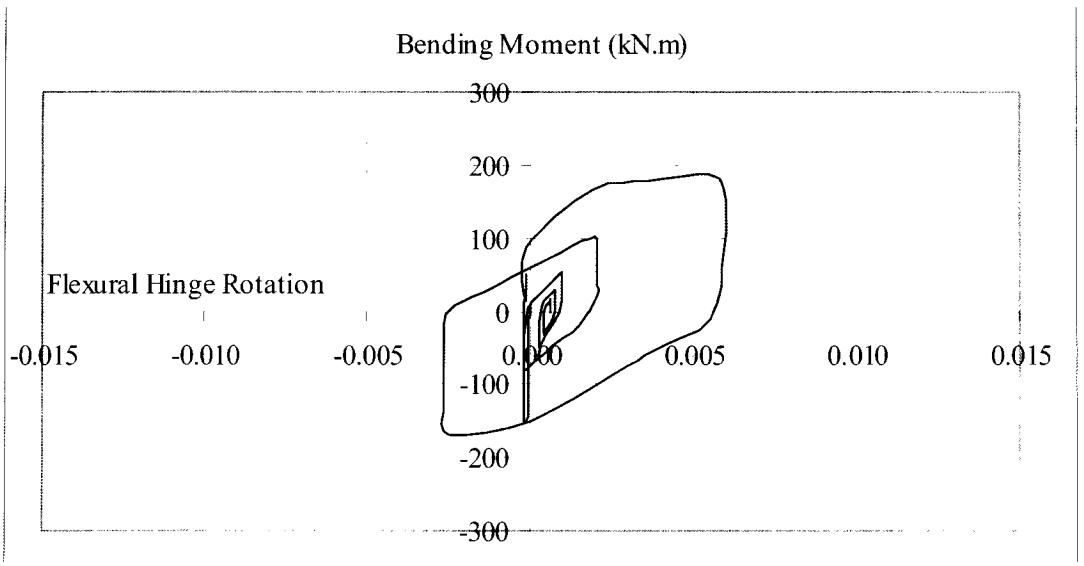

b) Retrofitted building

Figure 5.32: Moment versus flexural hinge rotation of columns for unretrofitted and retrofitted buildings

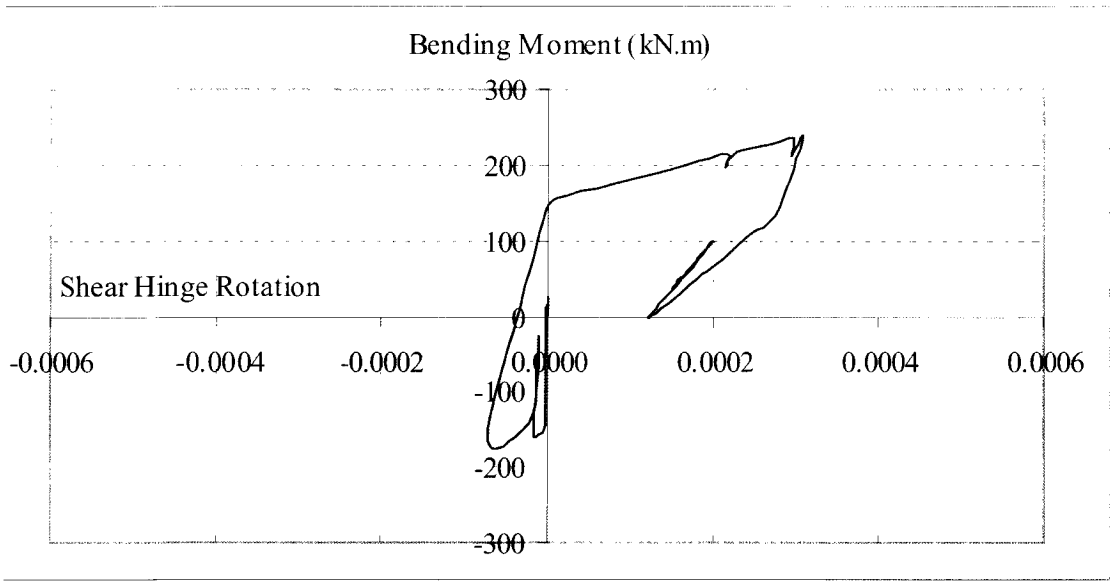

a) Unretrofitted building

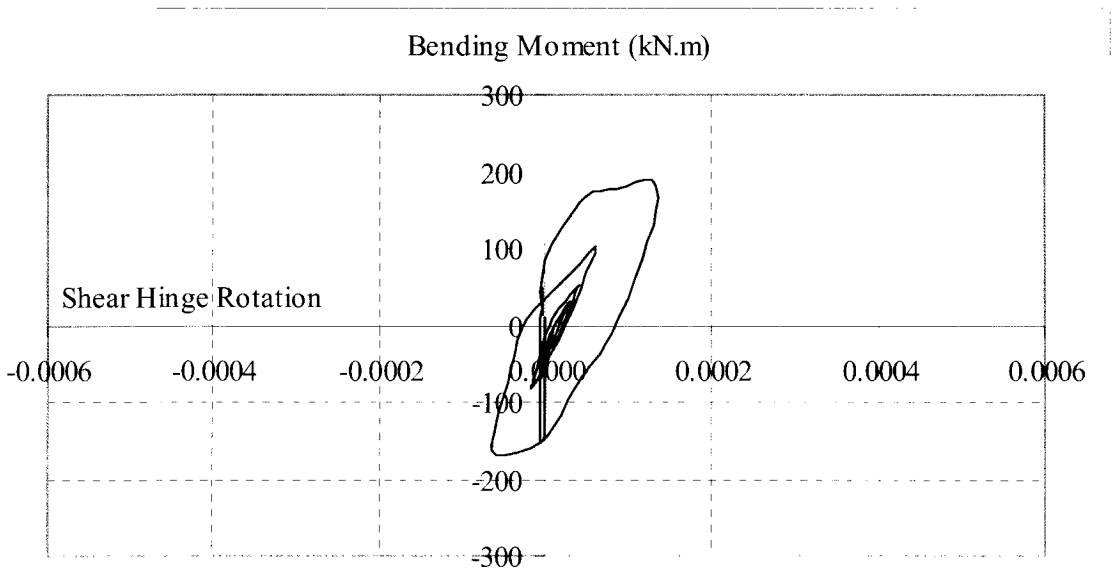

b) Retrofitted building

Figure 5.33: Moment versus shear hinge rotation of columns for unretrofitted and retrofitted buildings

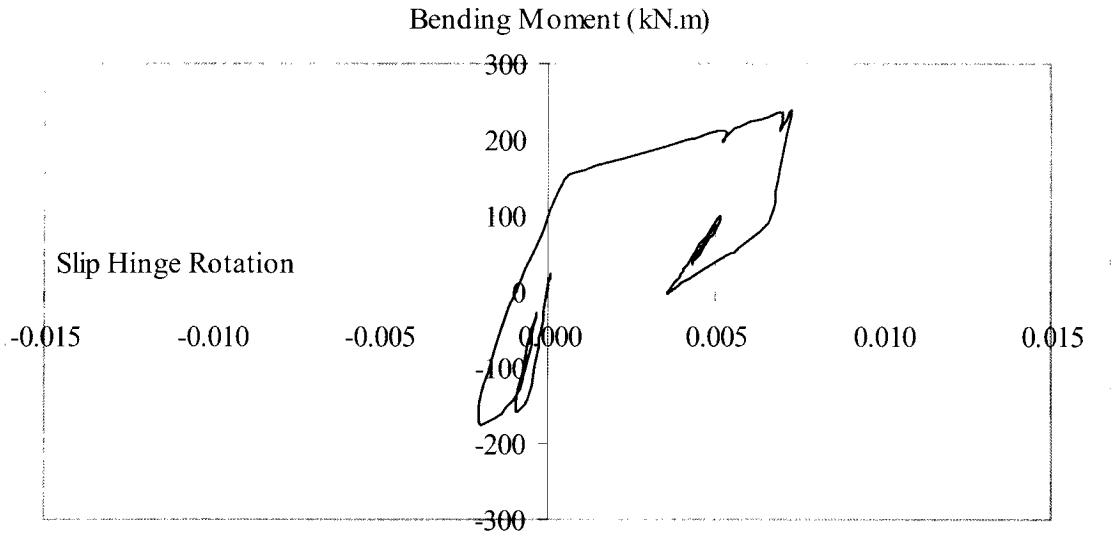

a) Unretrofitted building

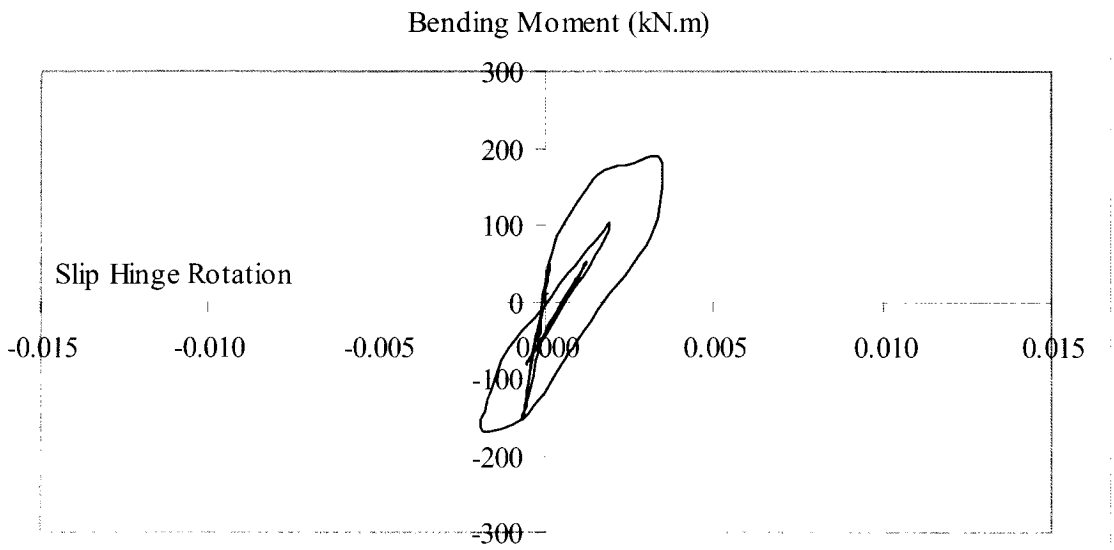

b) Retrofitted building

Figure 5.34: Moment versus flexural hinge rotation of columns for unretrofitted and retrofitted buildings

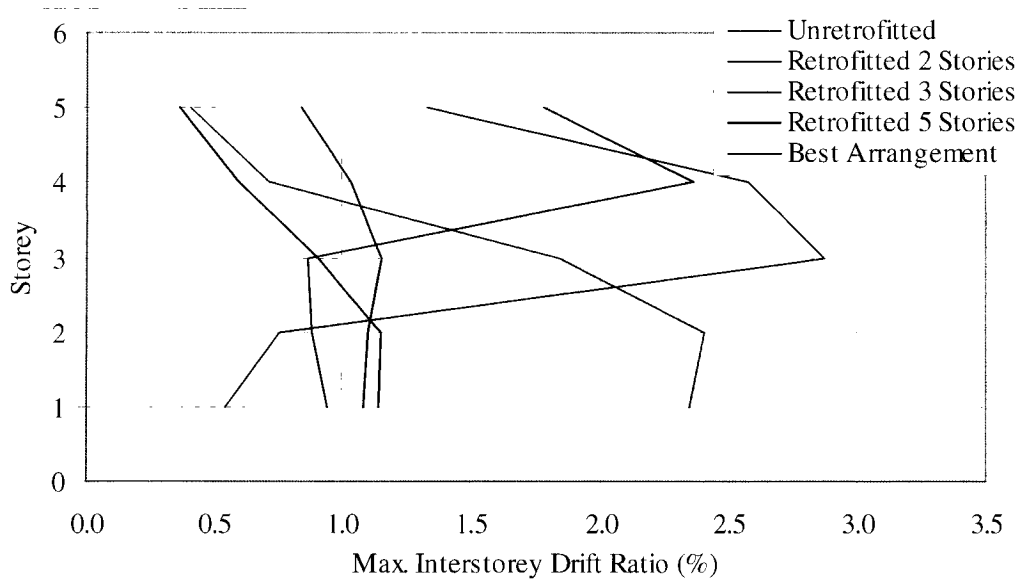

Figure 5.35: Effect of different arrangement of prestressing cables on interstorey drift (Retrofitted buildings have 8 cables/diagonal in lumped frame model with P/S =100 kN)

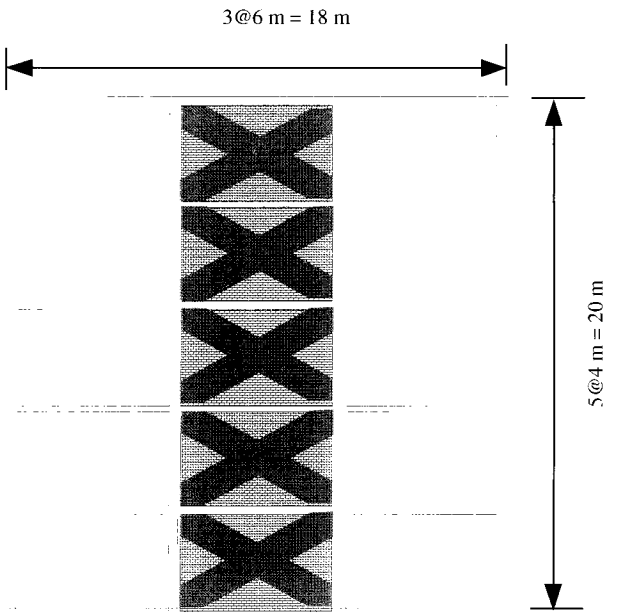

Figure 5.36: Structure retrofitted with diagonally placed CFRP strips

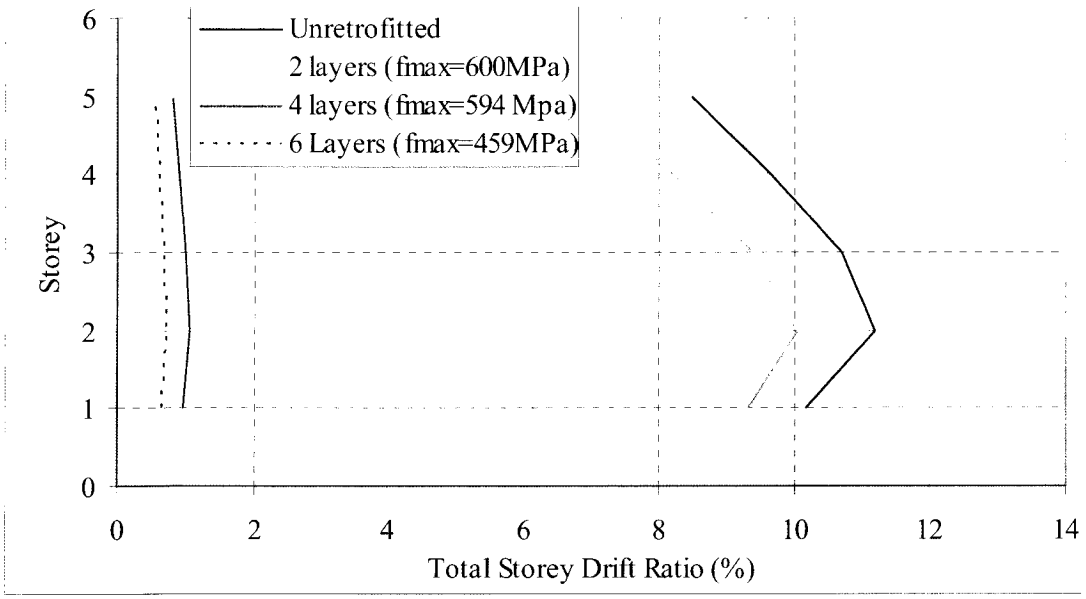

a) Total drift

b)

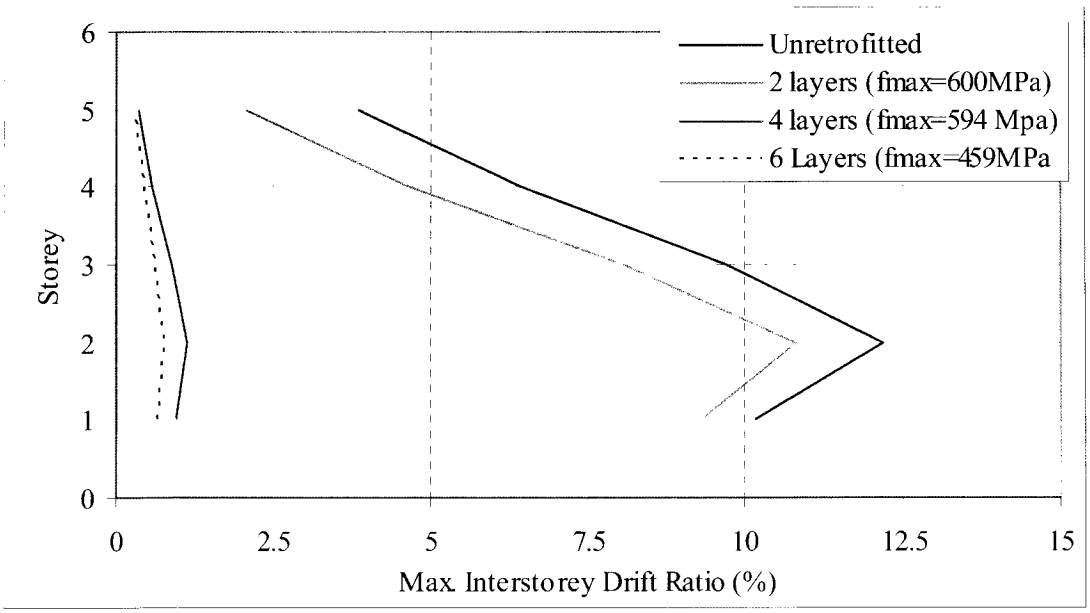

b) Interstorey drift

Figure 5.37: Effect of the amount of CFRP layers on total and interstorey drift ratios

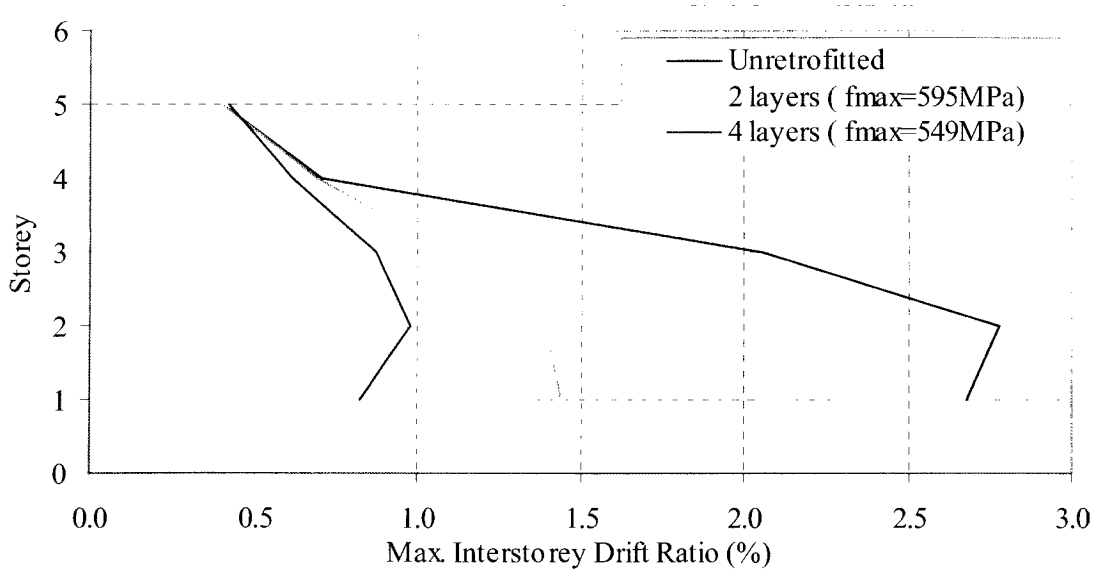

Figure5.38: Effect of the amount of CFRP layers on total drift ratio obtained from dynamic time history analysis

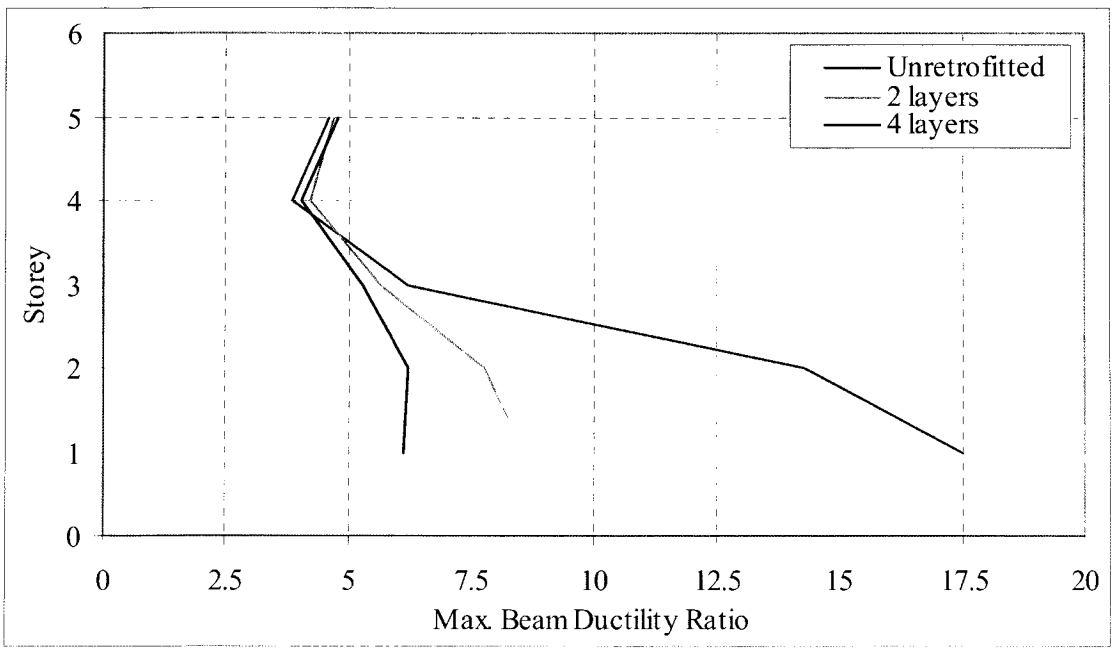

Figure 5.39: Maximum ductility response for beams at each storey, obtained from dynamic time history analysis
(Building retrofitted by FRP sheets)

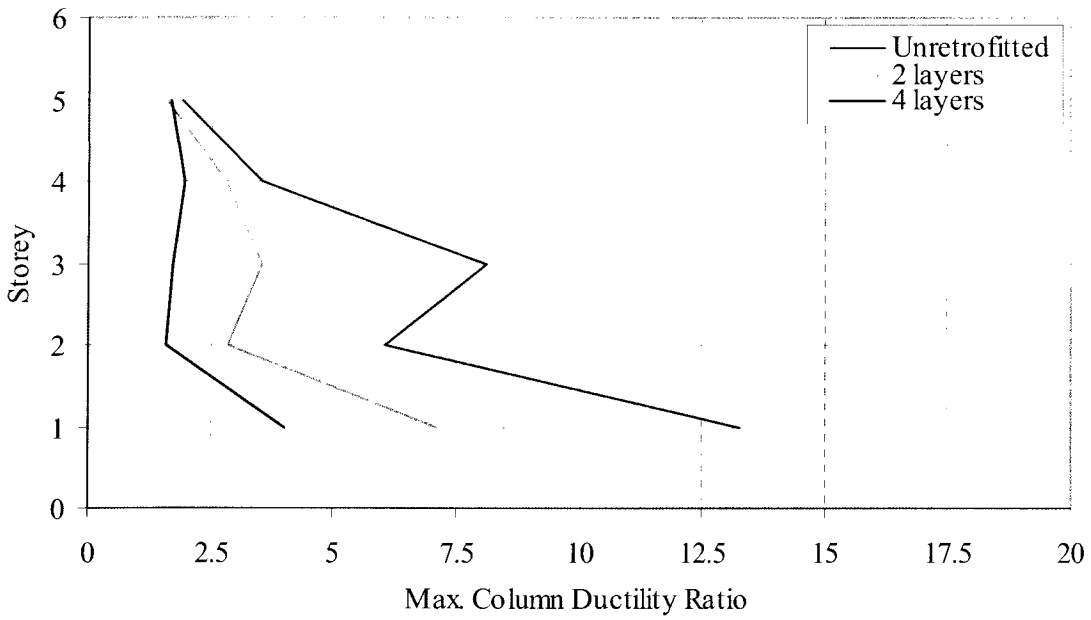

Figure 5.40: Maximum ductility response for columns at each storey obtained from dynamic time history analysis
(Building retrofitted by FRP sheets)

Appendix - A

Strain Data

The specimens tested in the experimental part of the current research project were well instrumented with strain gauges. Strain gauges placed on internal reinforcement of frame members as well as those placed on prestressing strands are presented in this Appendix. The locations of gauges are indicated on figures for easy referencing.

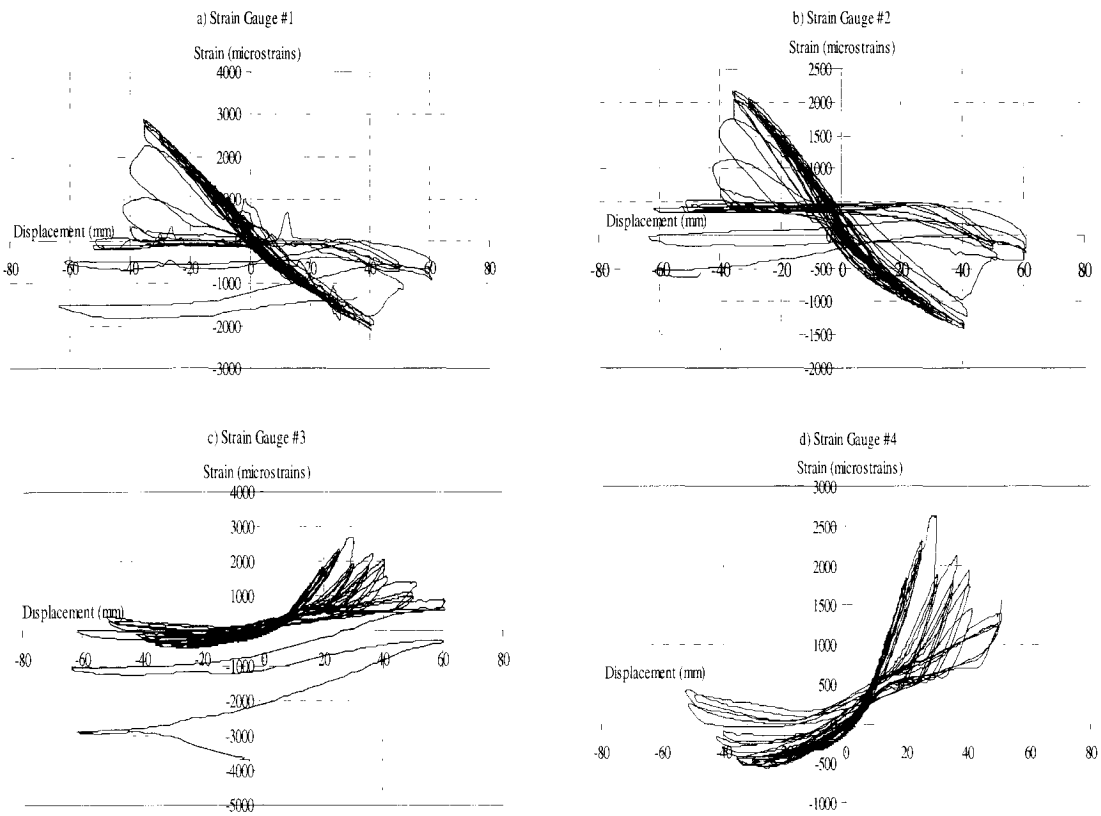

a) Lateral displacement vs. strain for strain gauges on column bars -far end column.

Figure A1: Lateral displacement versus strain for strain gauges #1 to # 28 for BR-1 (Unretrofitted specimen)

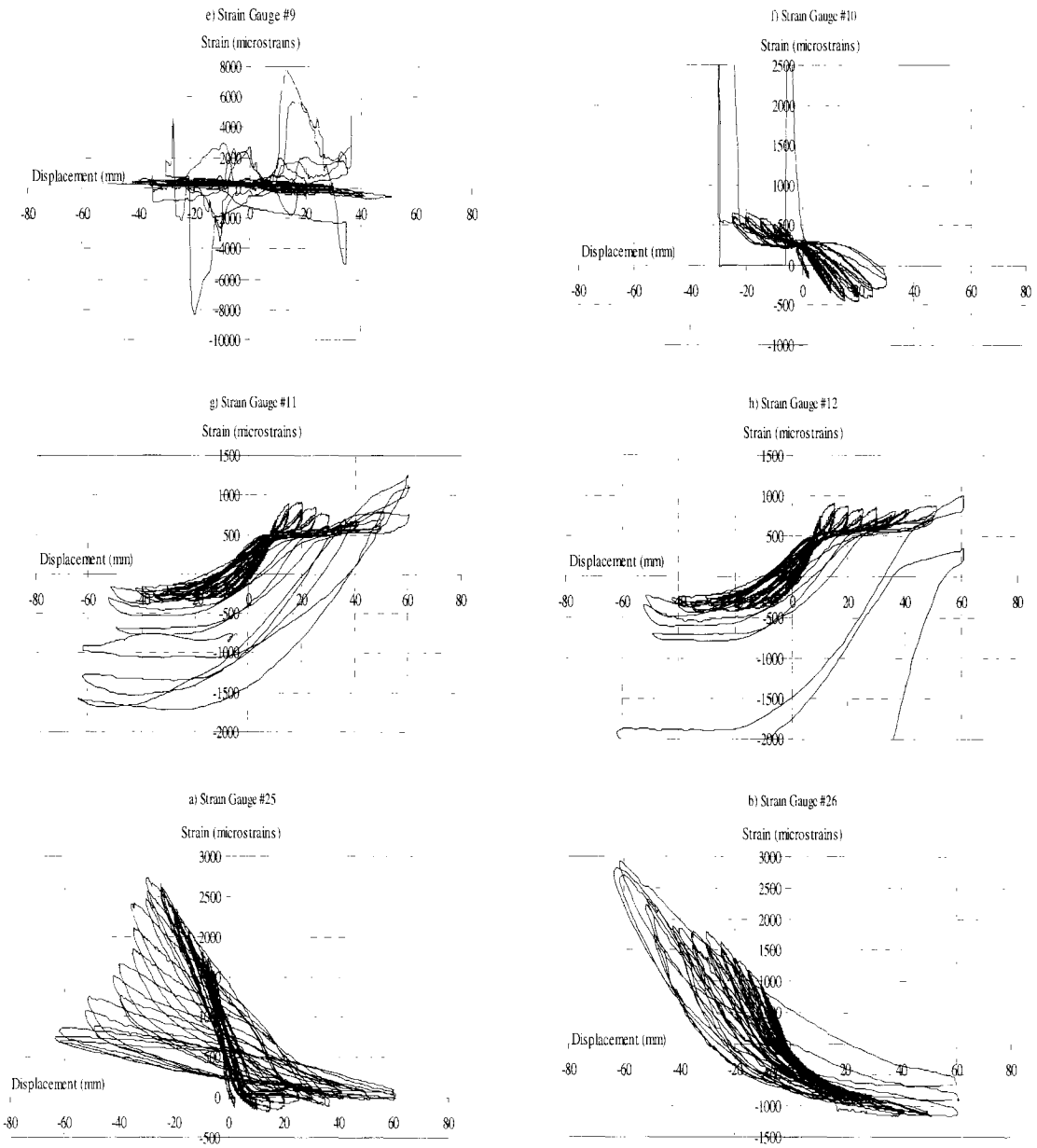

a) Lateral displacement vs. strain for strain gauges on column bars – far end column (Cont'd)

Figure A1: (Cont'd) Lateral displacement versus strain for strain gauges #1 to # 28 for BR-1 (Unretrofitted specimen)

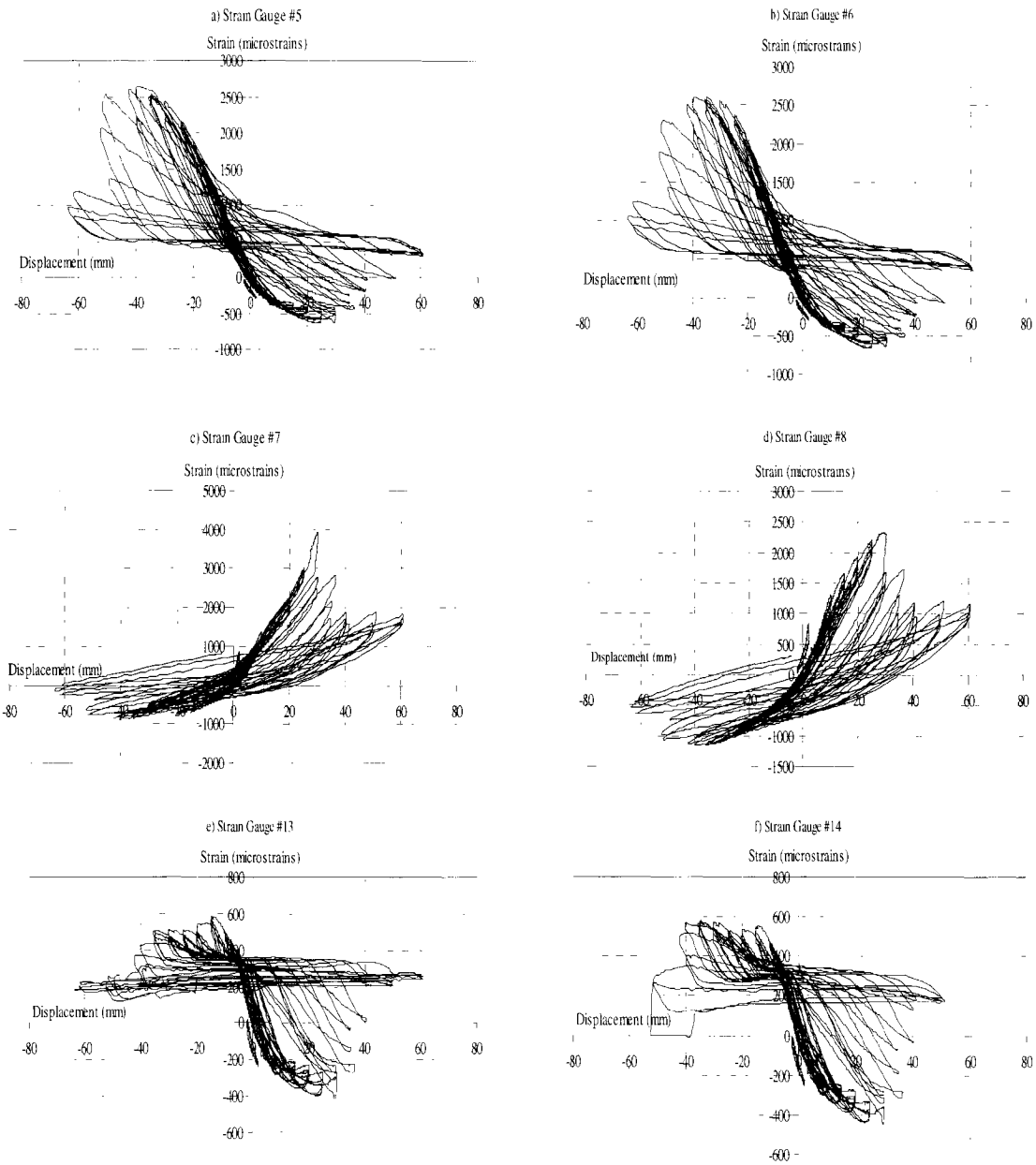

b) Lateral displacement vs. strain for strain gauges on column bars - near end column.

Figure A1: (Cont'd) Lateral displacement versus strain for strain gauges #1 to # 28 for BR-1 (Unretrofitted specimen)

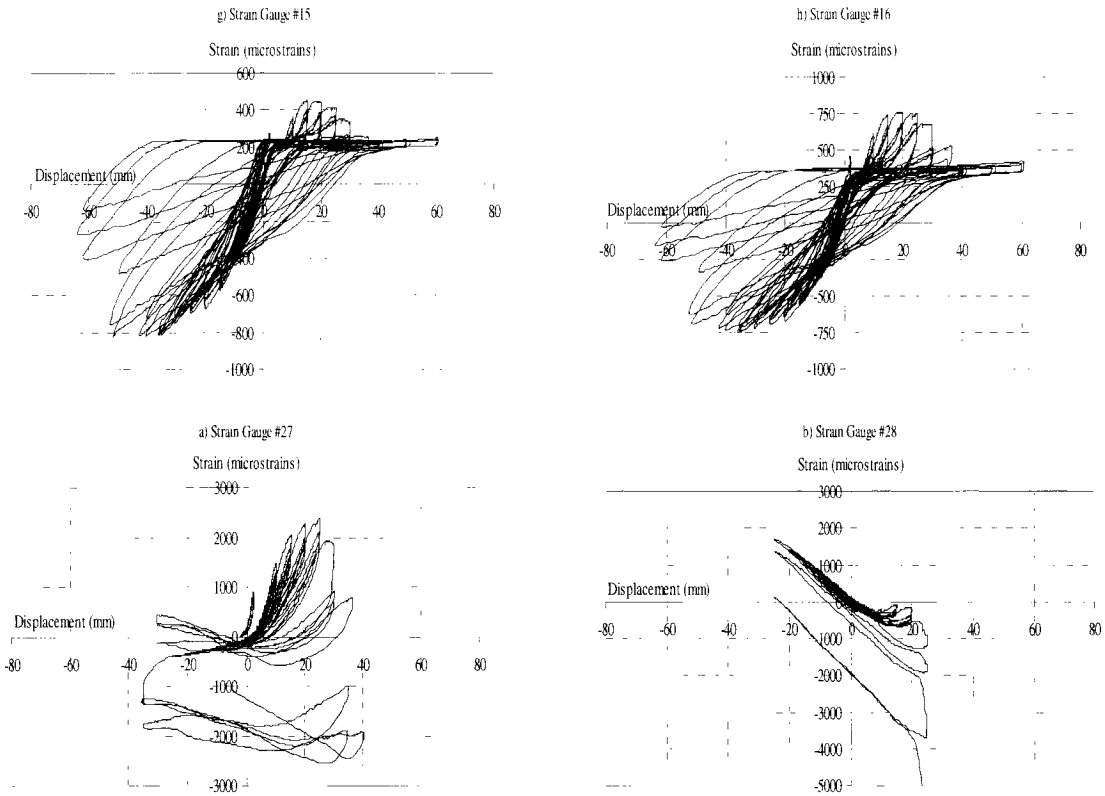

b) Lateral displacement vs. strain for strain gauges on column bars – near end column (Cont'd)

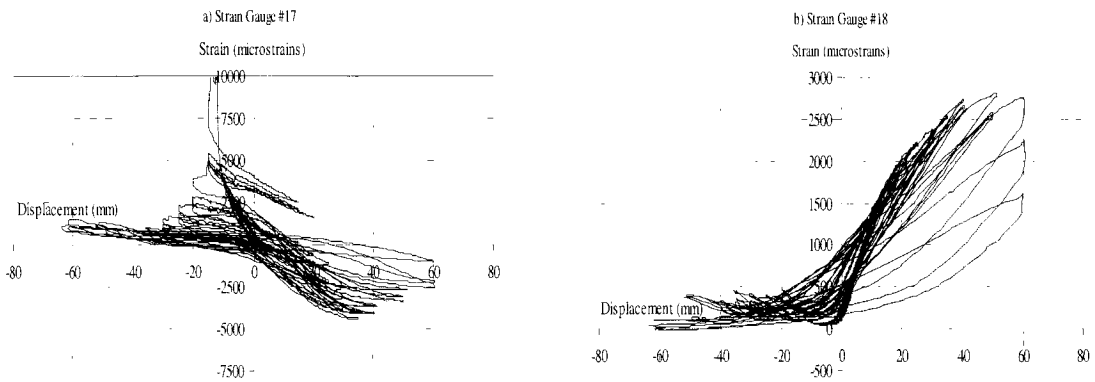

c) Lateral displacement vs. strain for strain gauges on beam bars - far end beam

Figure A1: (Cont'd) Lateral Displacement versus Strain for Strain Gauges #1 to # 28 for BR-1 (Unretrofitted specimen)

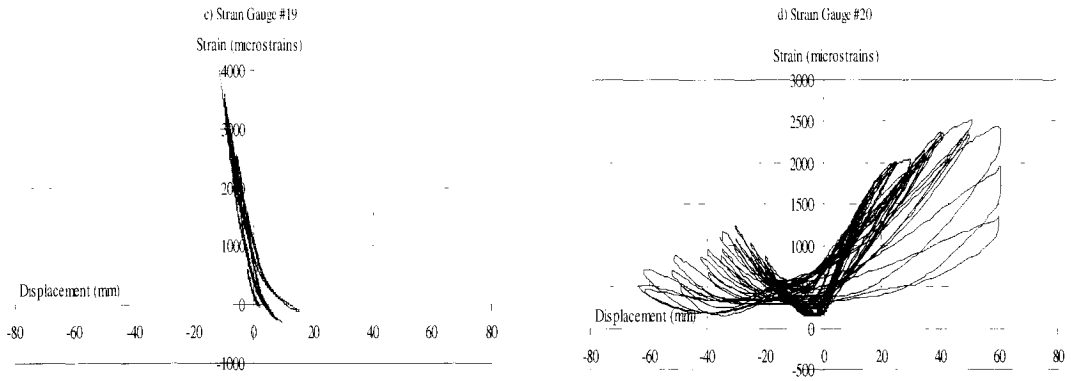

c) Lateral displacement vs. strain for strain gauges on beam bars - far end beam (Cont'd)

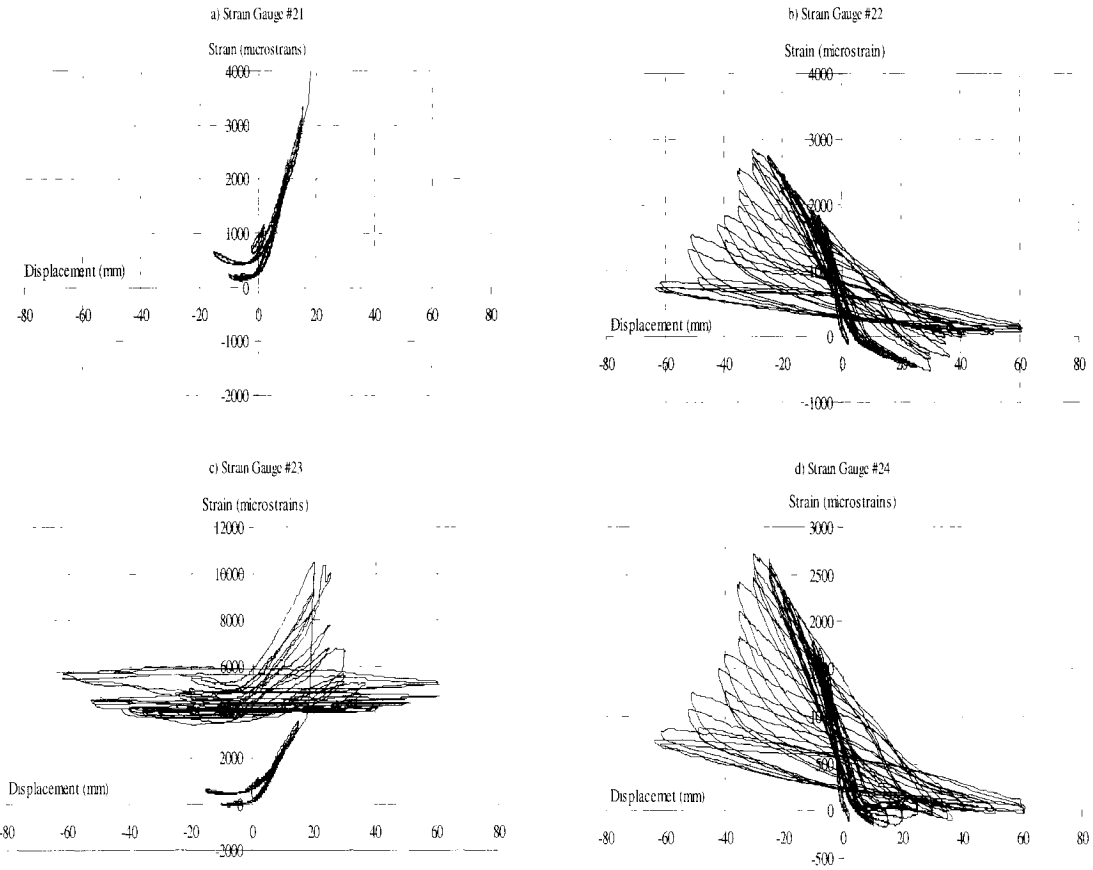

d) Lateral displacement vs. strain for strain gauges on beam bars – near end beam

Figure A1: (Cont'd) Lateral displacement versus strain for strain gauges #1 to # 28 for BR-1 (Unretrofitted frame)

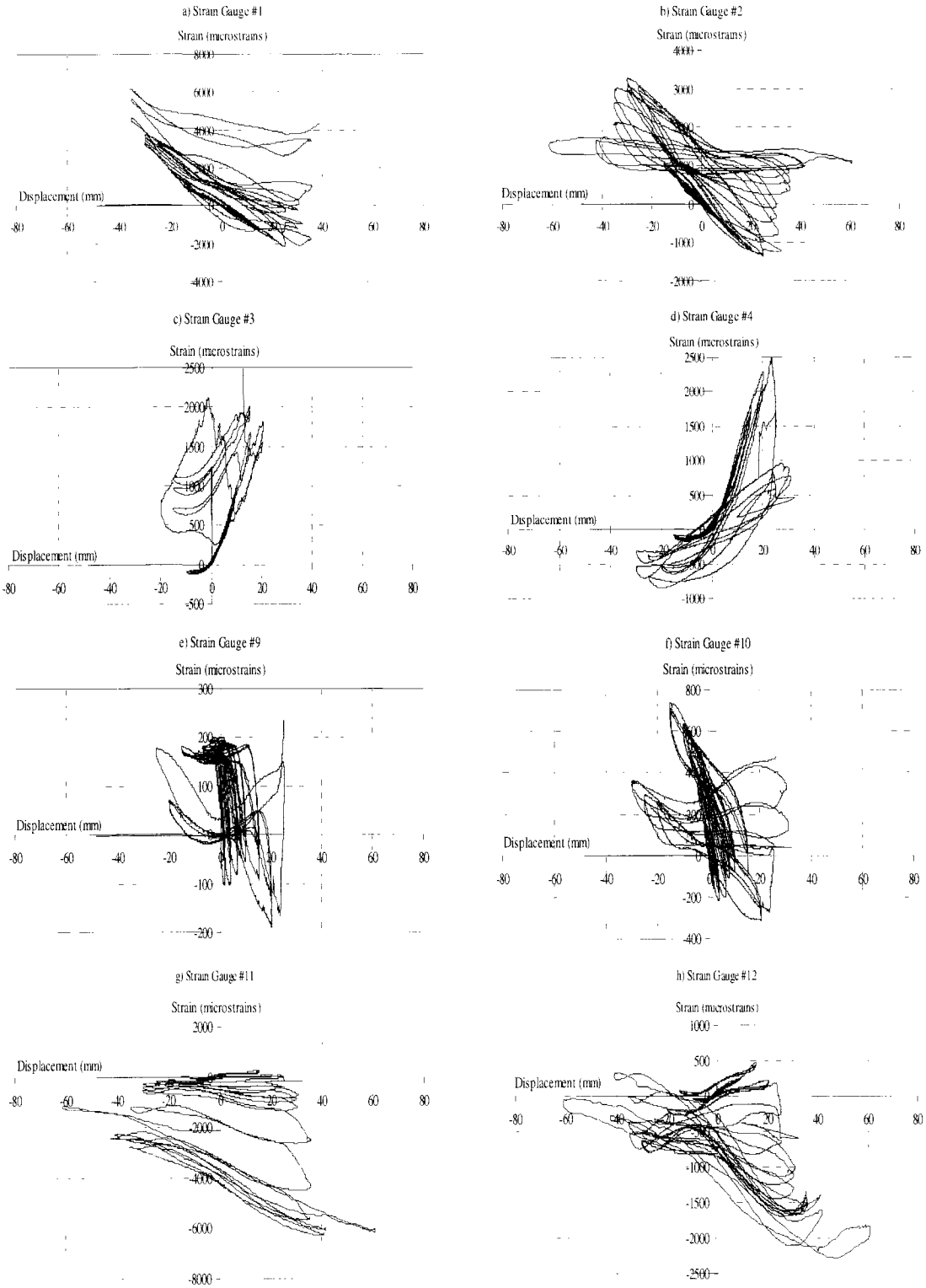

a) Lateral displacement vs. strain for strain gauges on column bars - far end column.

Figure A2: Lateral displacement versus strain for strain gauges #1 to # 28 for BR-2 (Retrofitted specimen)

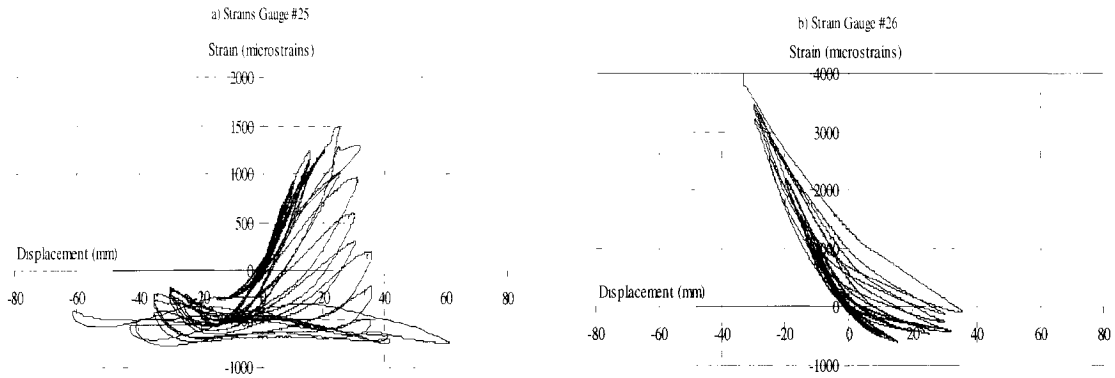

a) Lateral displacement vs. strain for strain gauges on column bars -far end column (Cont'd).

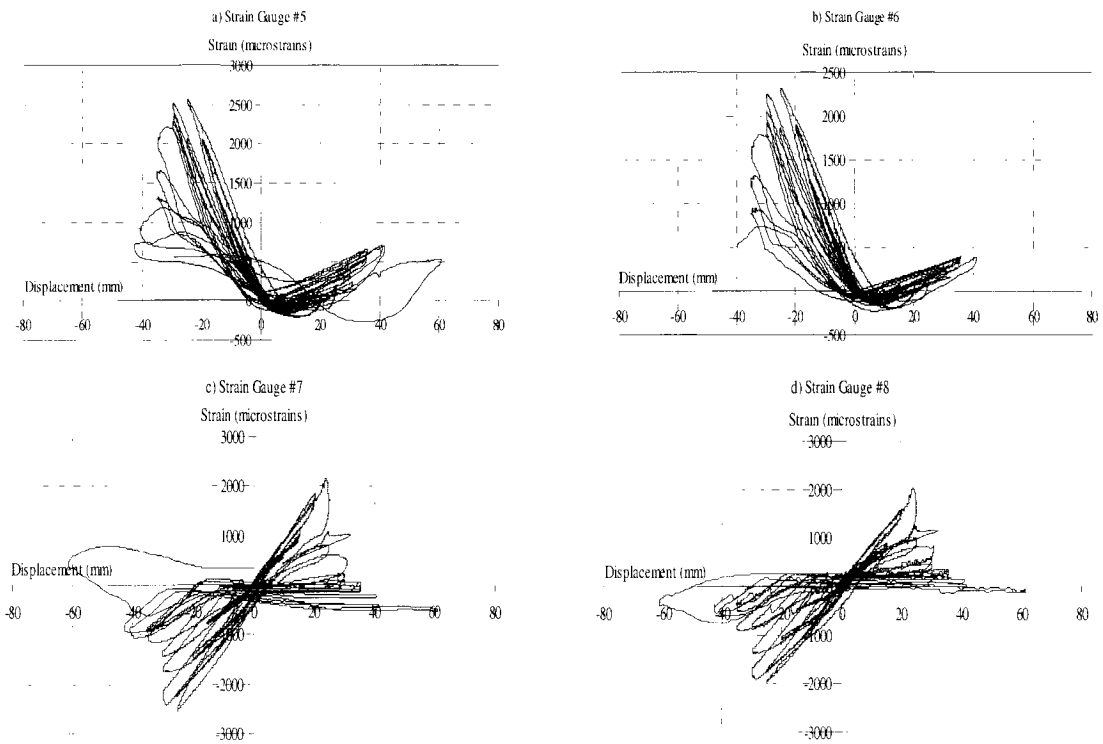

b) Lateral displacement vs. strain for strain gauges on column bars – near end column

Figure A2: (Cont'd) Lateral displacement versus strain for strain gauges #1 to # 28 for BR-2 (Retrofitted specimen)

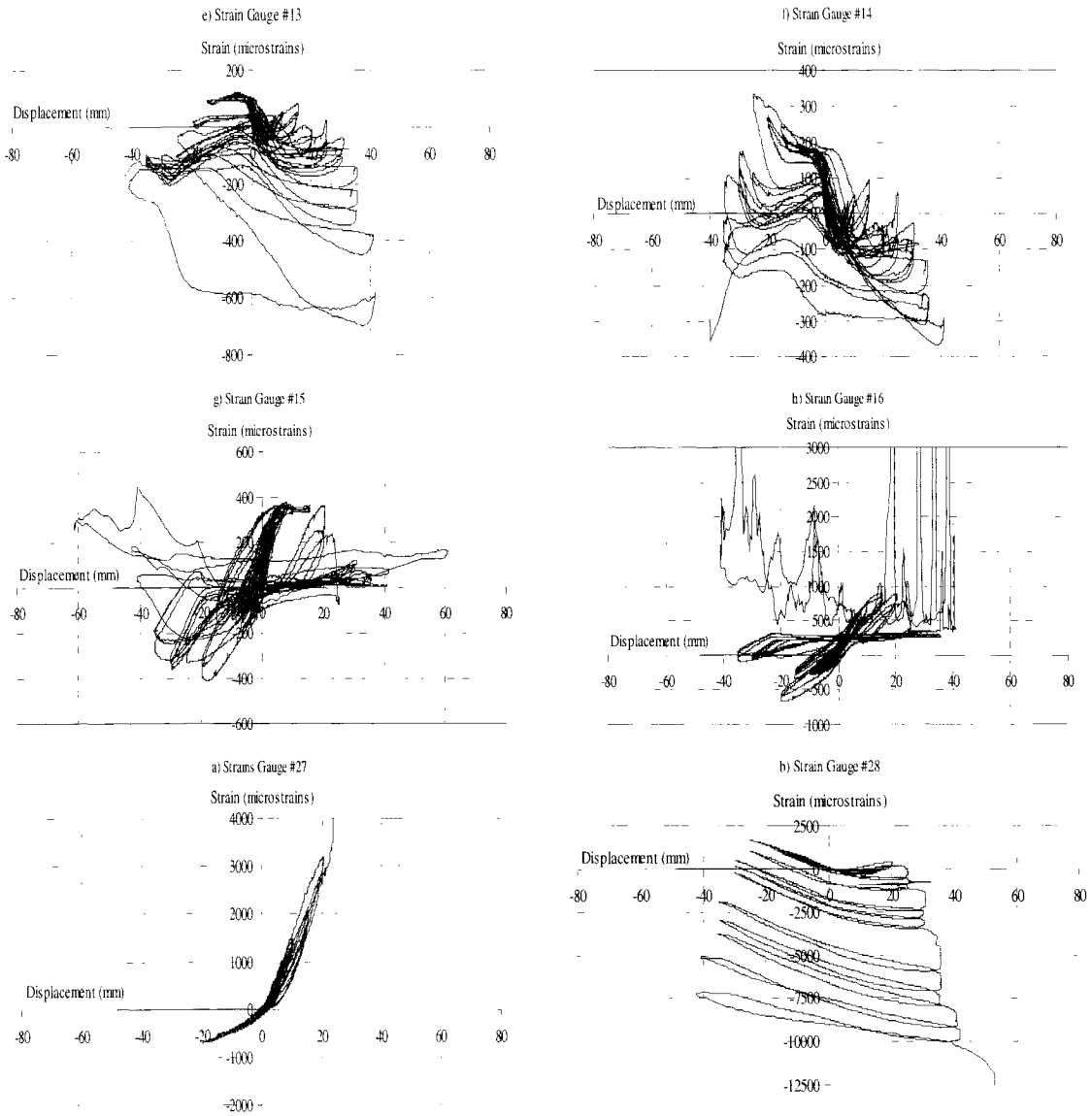

b) Lateral displacement vs. strain for strain gauges on column bars – near end column (Cont'd)

Figure A2: (Cont'd) Lateral displacement versus strain for strain gauges #1 to # 28 for BR-2 (Retrofitted specimen)

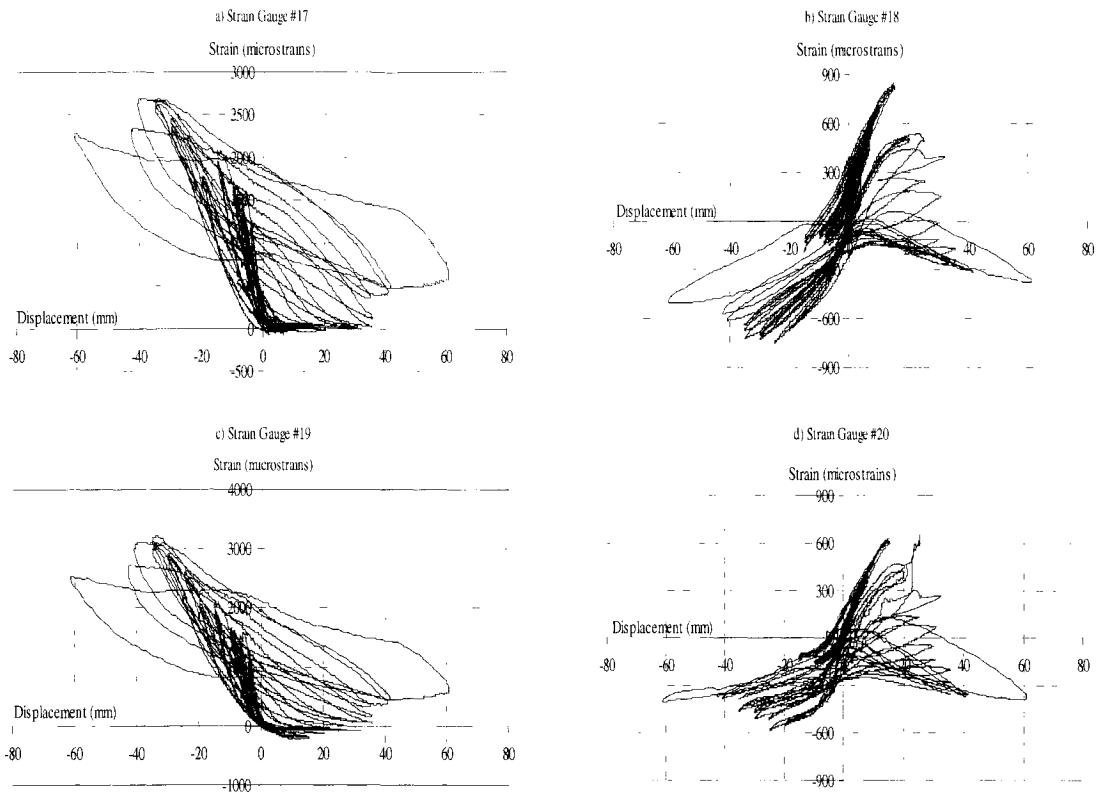

c) Lateral displacement vs. strain for strain gauges on beam bars - far end beam

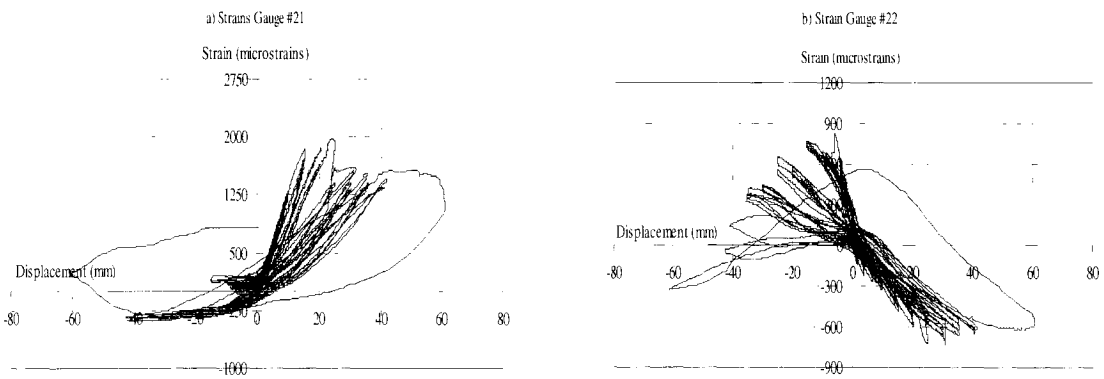

d) Lateral displacement vs. strain for strain gauges on beam bars – near end beam

Figure A2: (Cont'd) Lateral displacement versus strain for strain gauges #1 to # 28 for BR-2 (Retrofitted specimen)

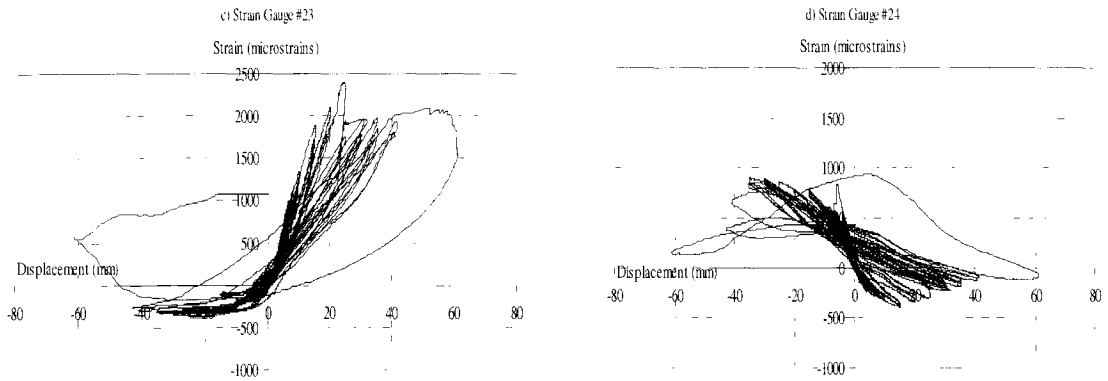

d) Lateral displacement vs. strain for strain gauges on beam bars – near end beam (Cont'd)

Figure A2: (Cont'd) Lateral displacement versus strain for strain gauges #1 to # 28 for BR-2 (Retrofitted specimen)

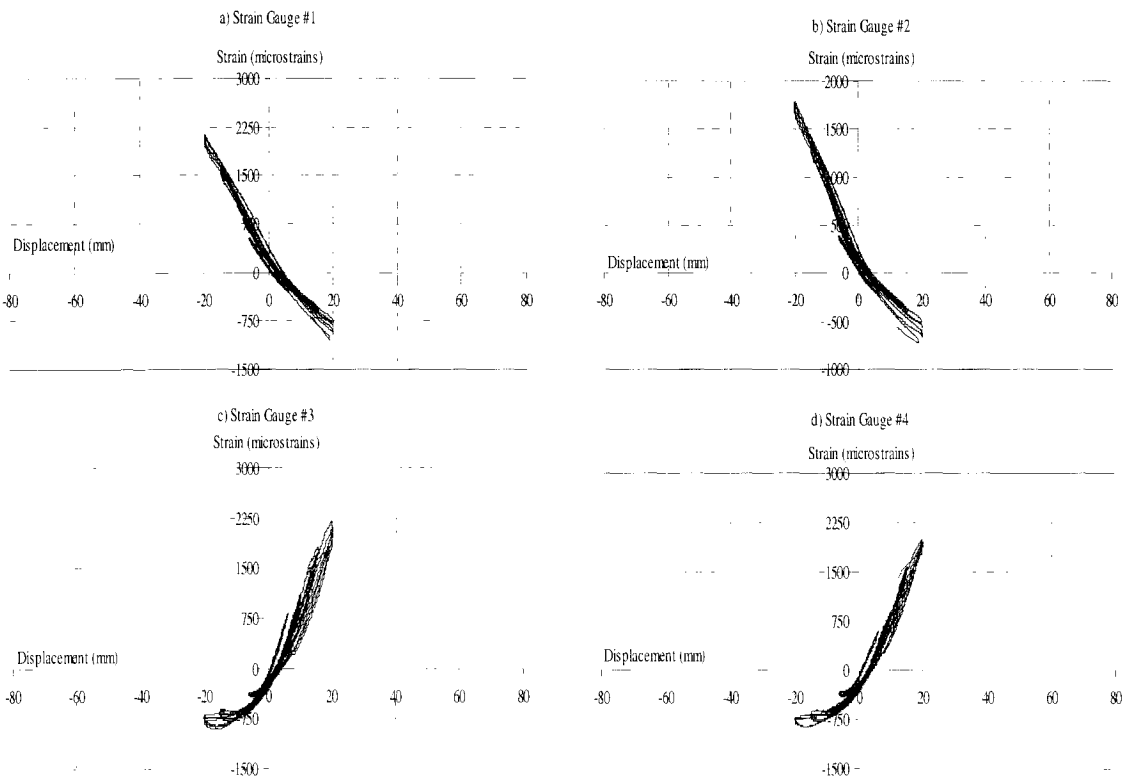

a) Lateral displacement vs. strain for strain gauges on column bars - far end column.

Figure A3: Lateral displacement versus strain for strain gauges #1 to # 28 for BR-3 (Retrofitted specimen)

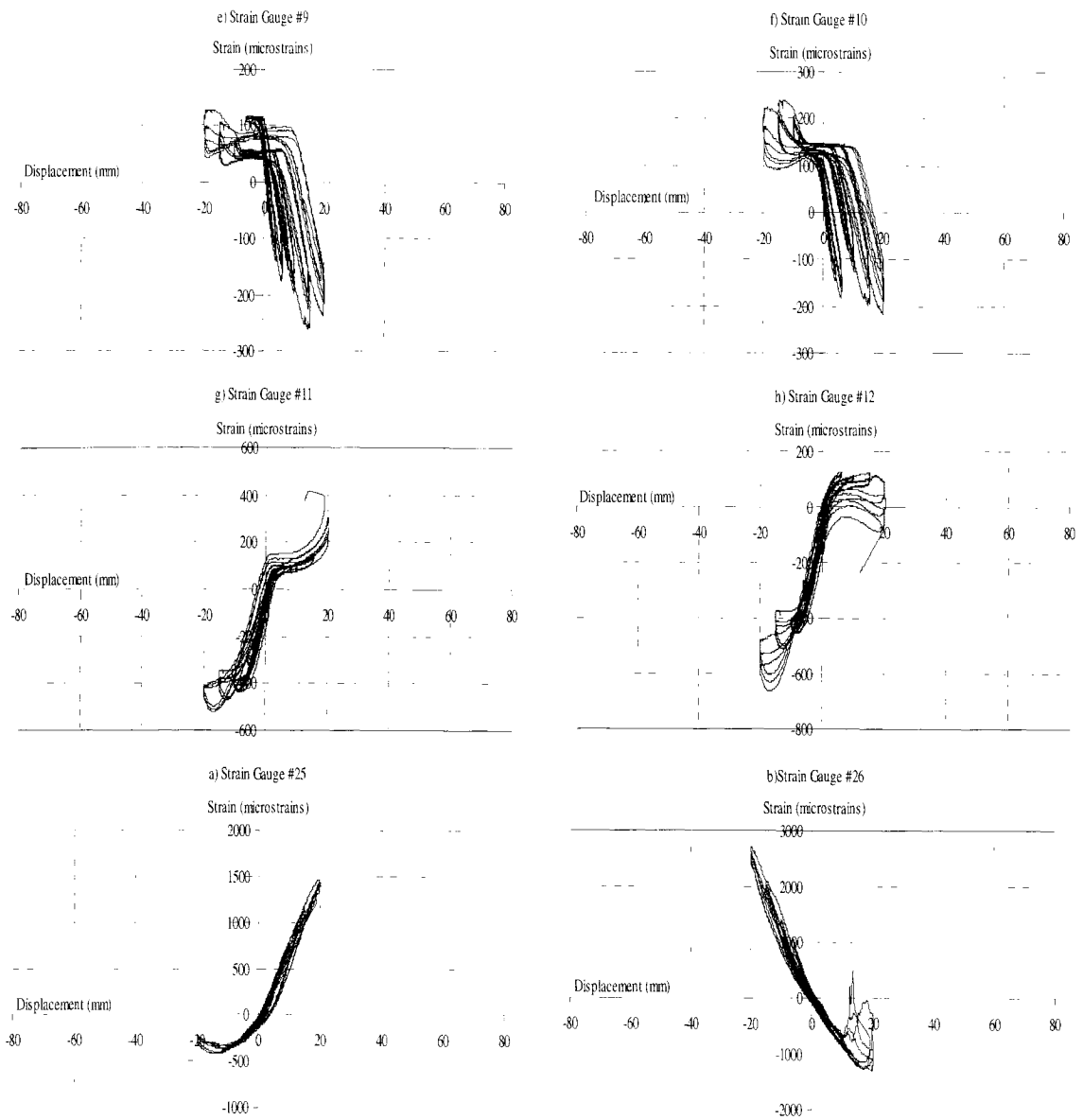

a) Lateral displacement vs. strain for strain gauges on column bars -far end column (Cont'd).

Figure A3: (Cont'd) Lateral displacement versus strain for strain gauges #1 to # 28 for BR-3 (Retrofitted specimen)

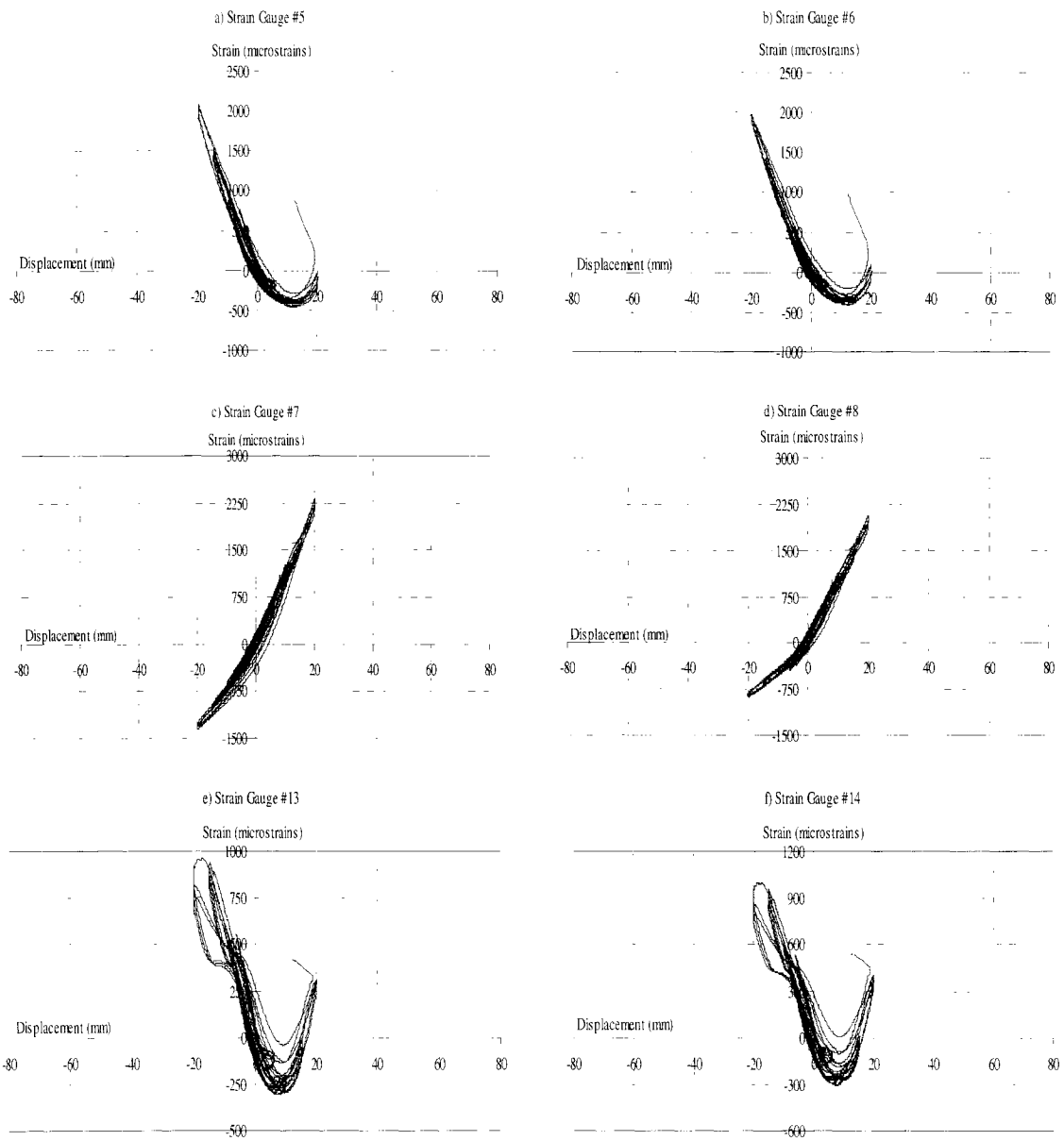

b) Lateral displacement vs. strain for strain gauges on column bars - near end column.

Figure A3: (Cont'd) Lateral displacement versus strain for strain gauges #1 to # 28 for BR-3 (Retrofitted specimen)

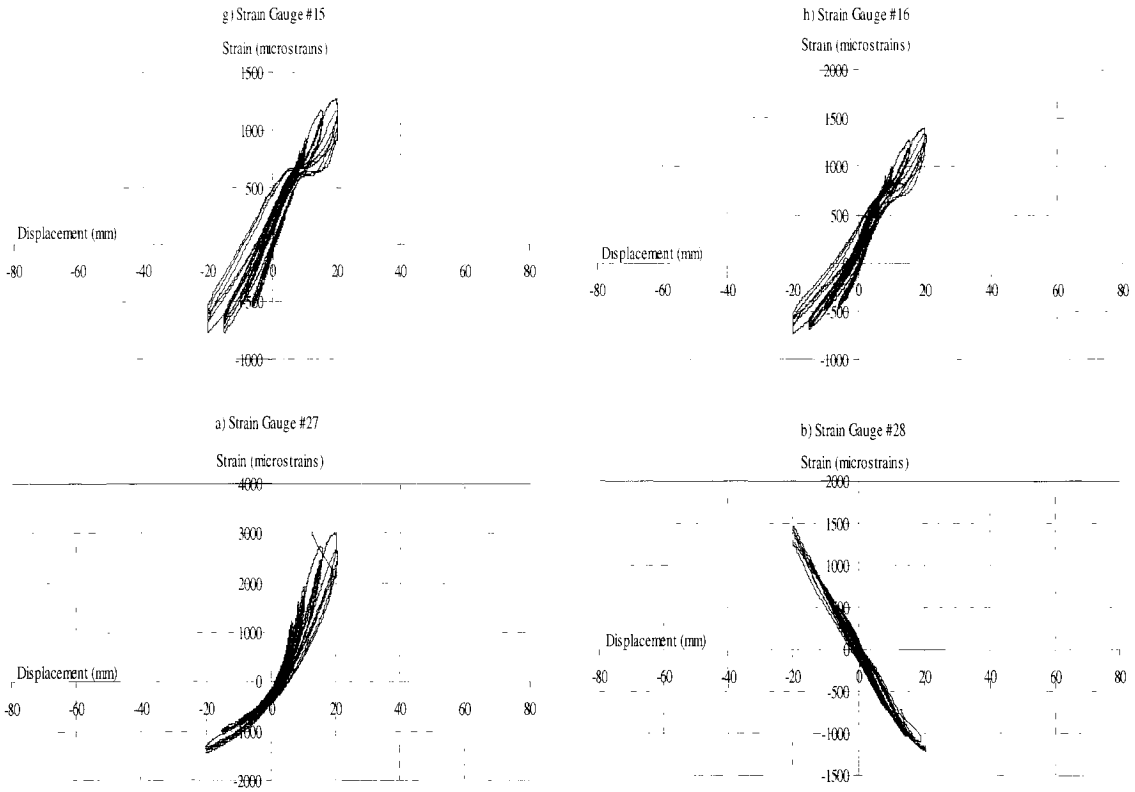

b) Lateral displacement vs. strain for strain gauges on column bars - near end column. (Cont'd).

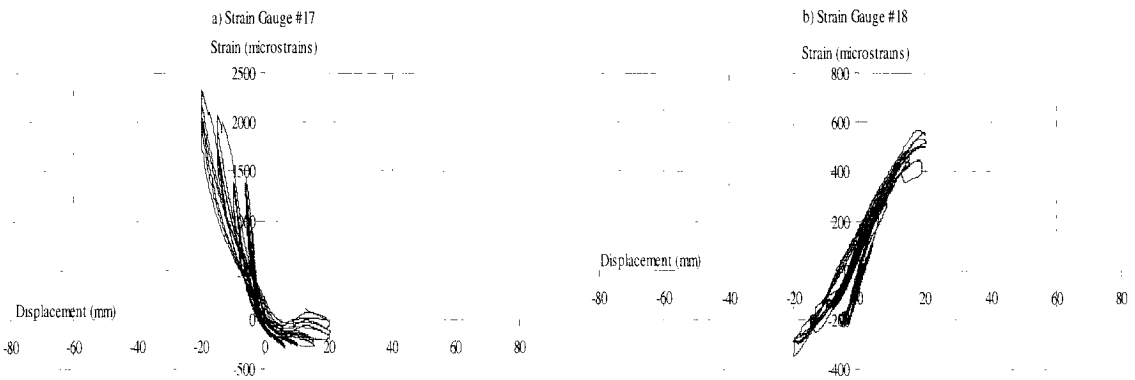

c) Lateral displacement vs. strain for strain gauges on beam bars - far end beam

Figure A3: (Cont'd) Lateral Displacement versus Strain for Strain Gauges #1 to # 28 for BR-3 (Retrofitted specimen)

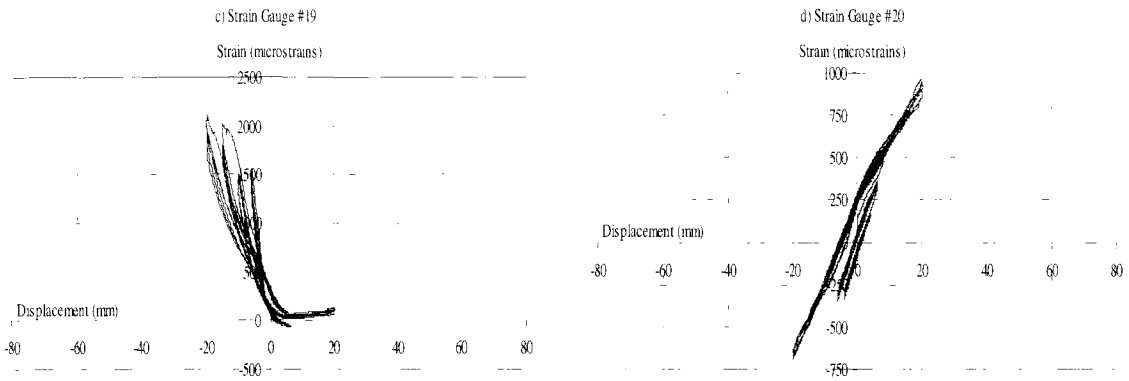

c) Lateral displacement vs. strain for strain gauges on beam bars – far end beam (Cont'd).

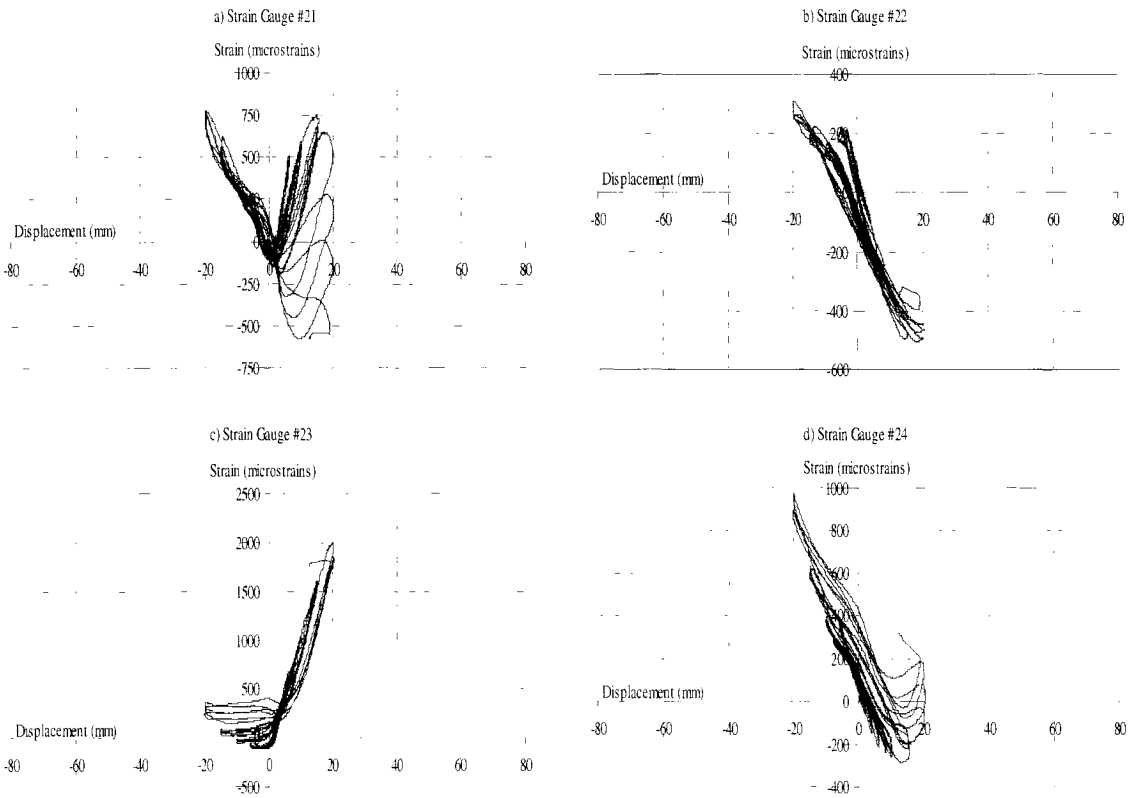

d) Lateral displacement vs. strain for strain gauges on beam bars – near end beam

Figure A3: (Cont'd) Lateral displacement versus strain for strain gauges #1 to # 28 for BR-3 (Retrofitted frame)

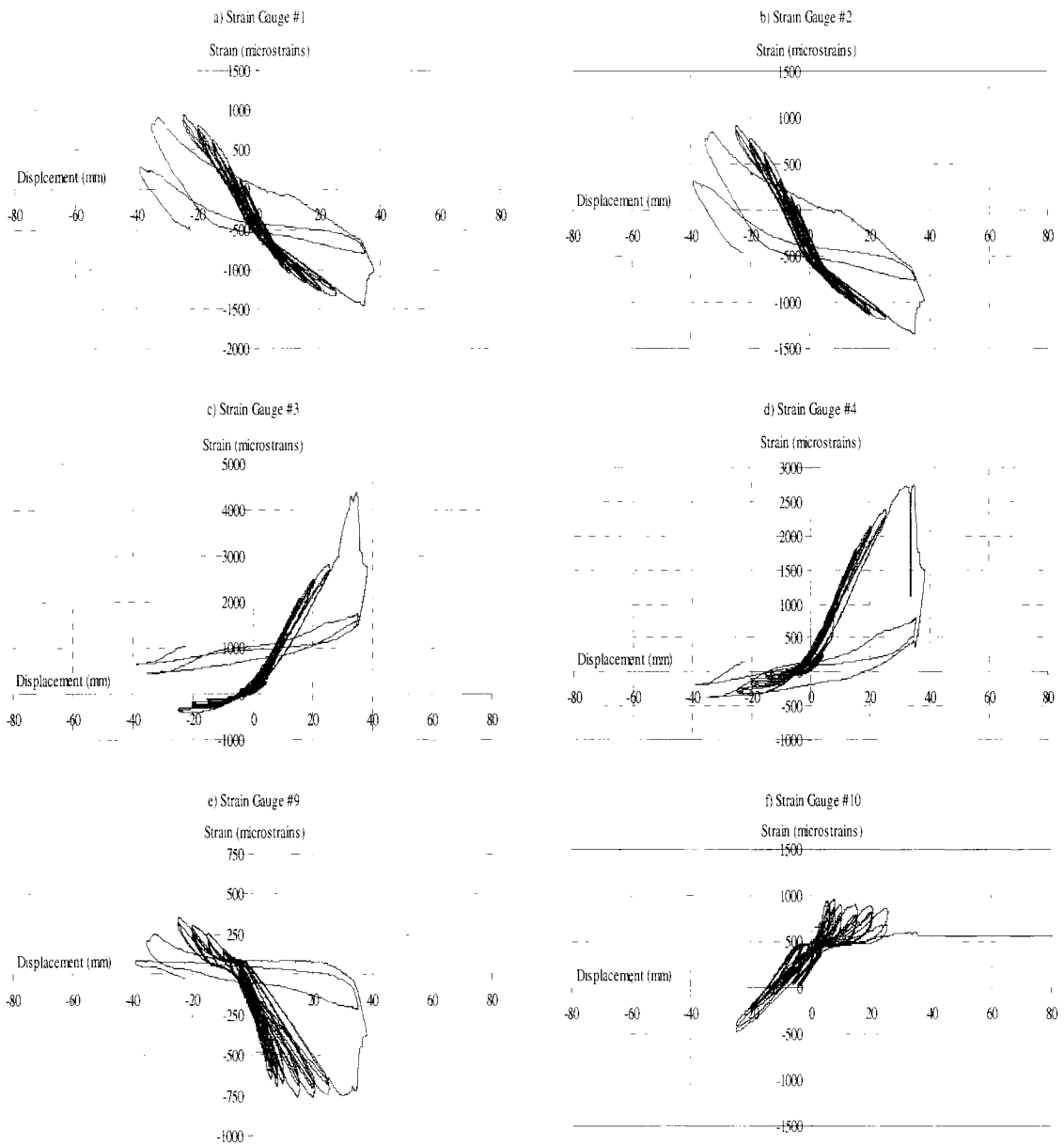

a) Lateral displacement vs. strain for strain gauges on column bars -far end column.

Figure A4: Lateral displacement versus strain for strain gauges #1 to # 28 for BL-3 (Retrofitted specimen)

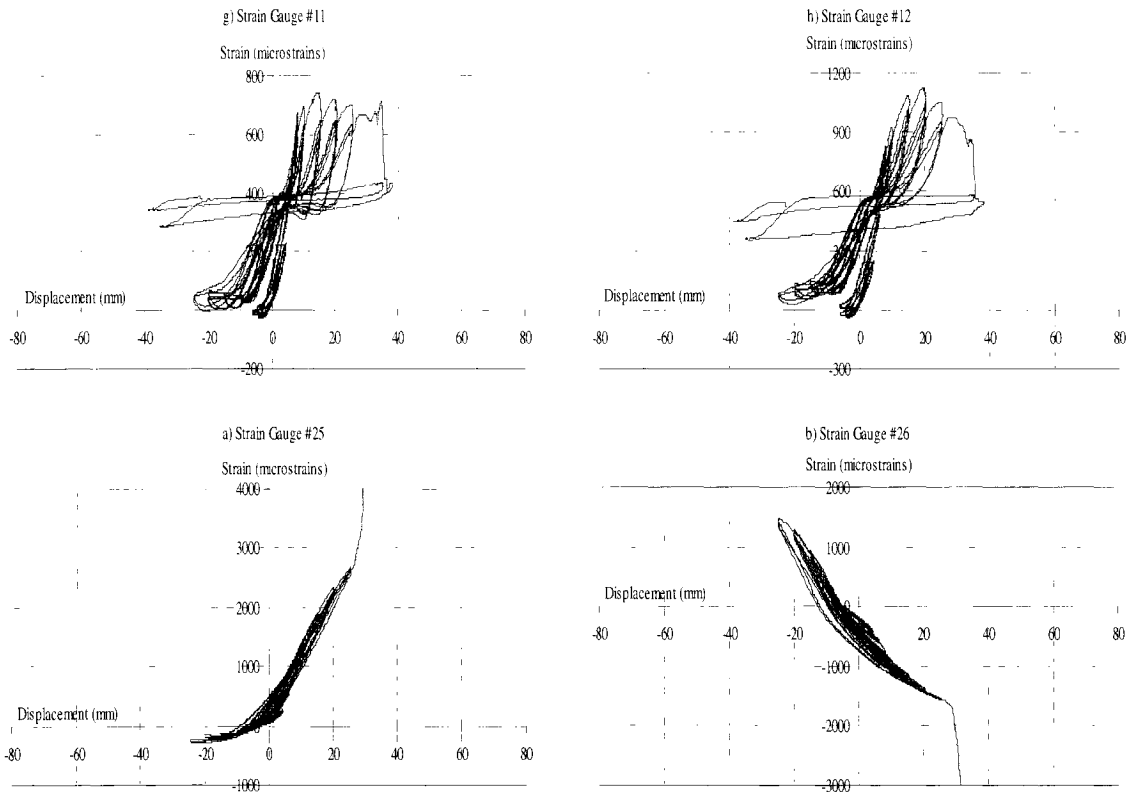

a) Lateral displacement vs. strain for strain gauges on column bars -far end column (Cont'd).

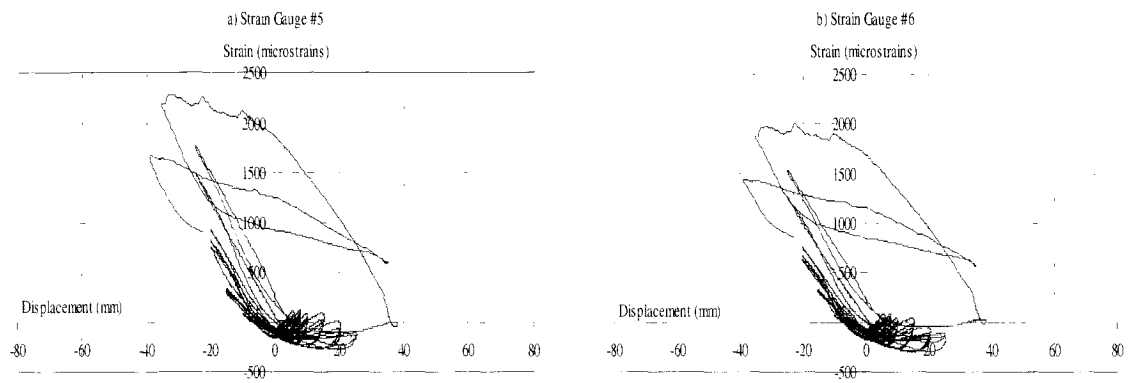

b) Lateral displacement vs. strain for strain gauges on column bars -near end column.

Figure A4: (Cont'd) Lateral displacement versus strain for strain gauges #1 to # 28 for BL-3 (Retrofitted specimen)

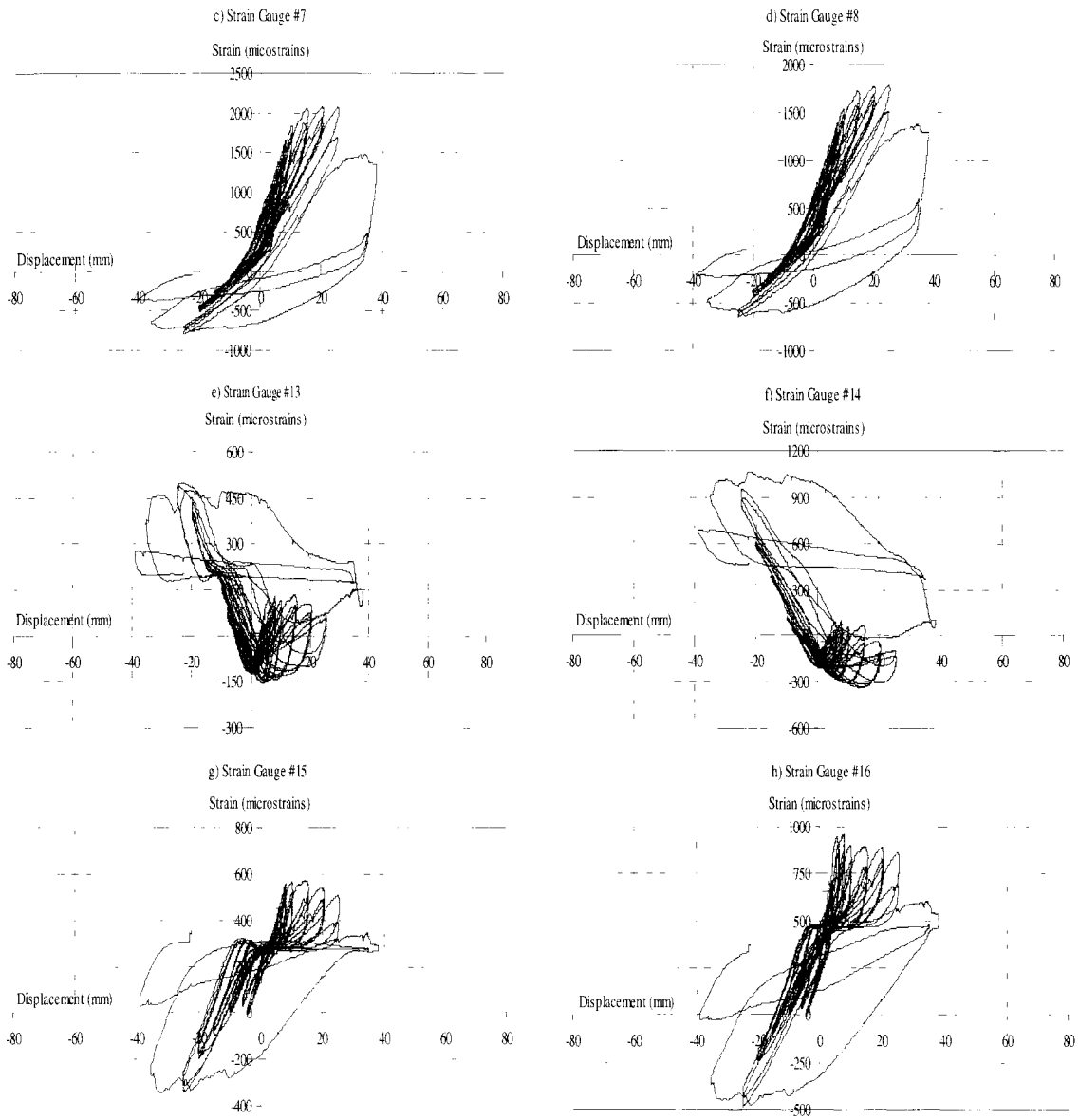

b) Lateral displacement vs. strain for strain gauges on column bars -near end column. (Cont'd)

Figure A4: (Cont'd) Lateral displacement versus strain for strain gauges #1 to # 28 for BL-3 (Retrofitted specimen)

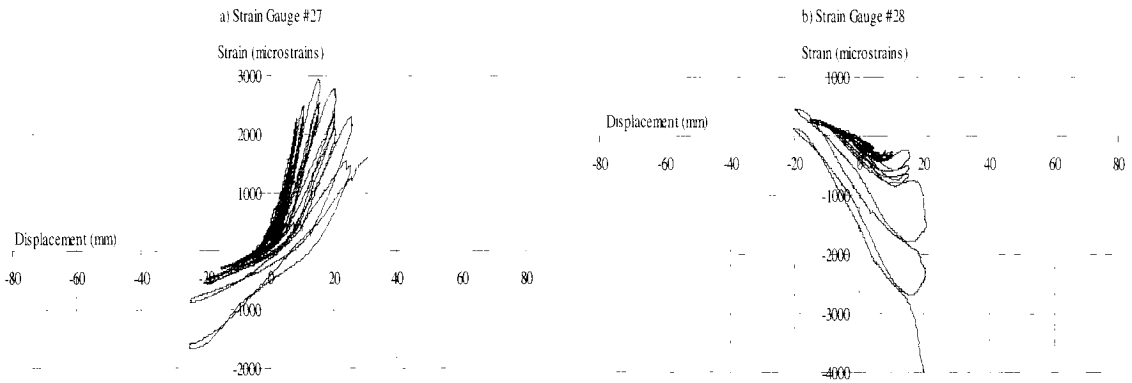

b) Lateral displacement vs. strain for strain gauges on column bars -near end column. (Cont'd)

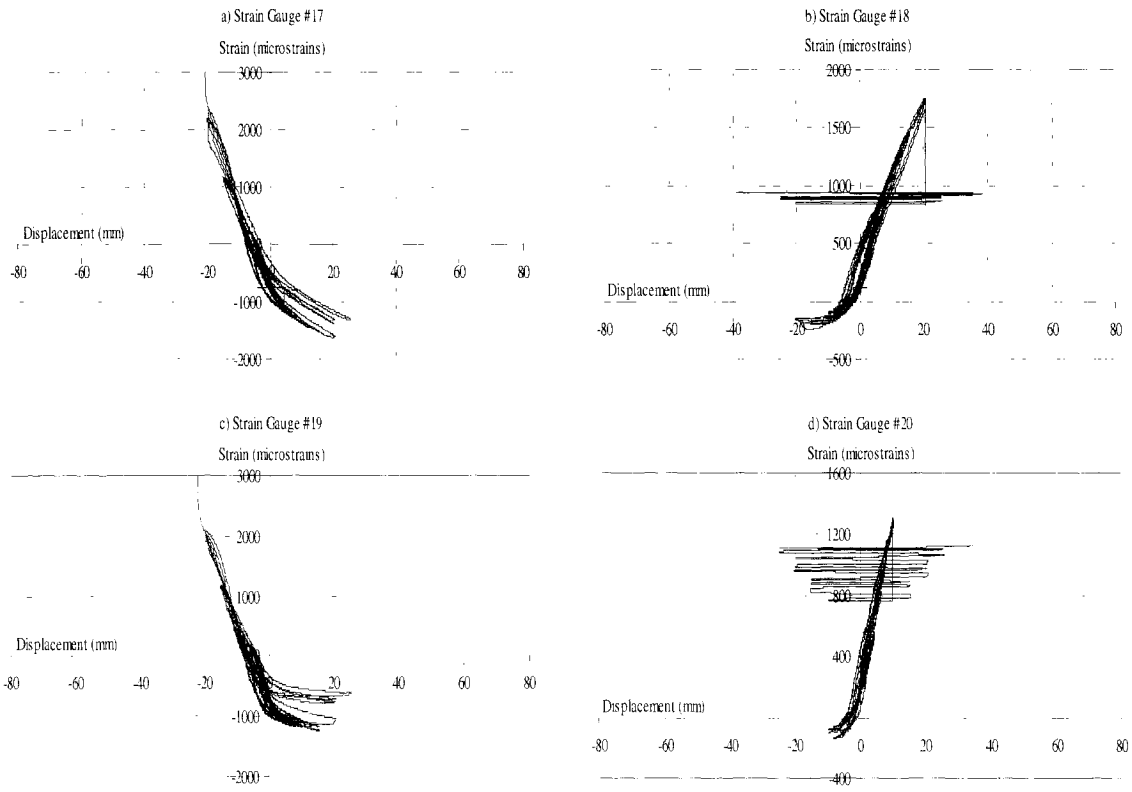

c) Lateral displacement vs. strain for strain gauges on beam bars –far end beam.

Figure A4: (Cont'd) Lateral displacement versus strain for strain gauges #1 to # 28 for BL-3 (Retrofitted specimen)

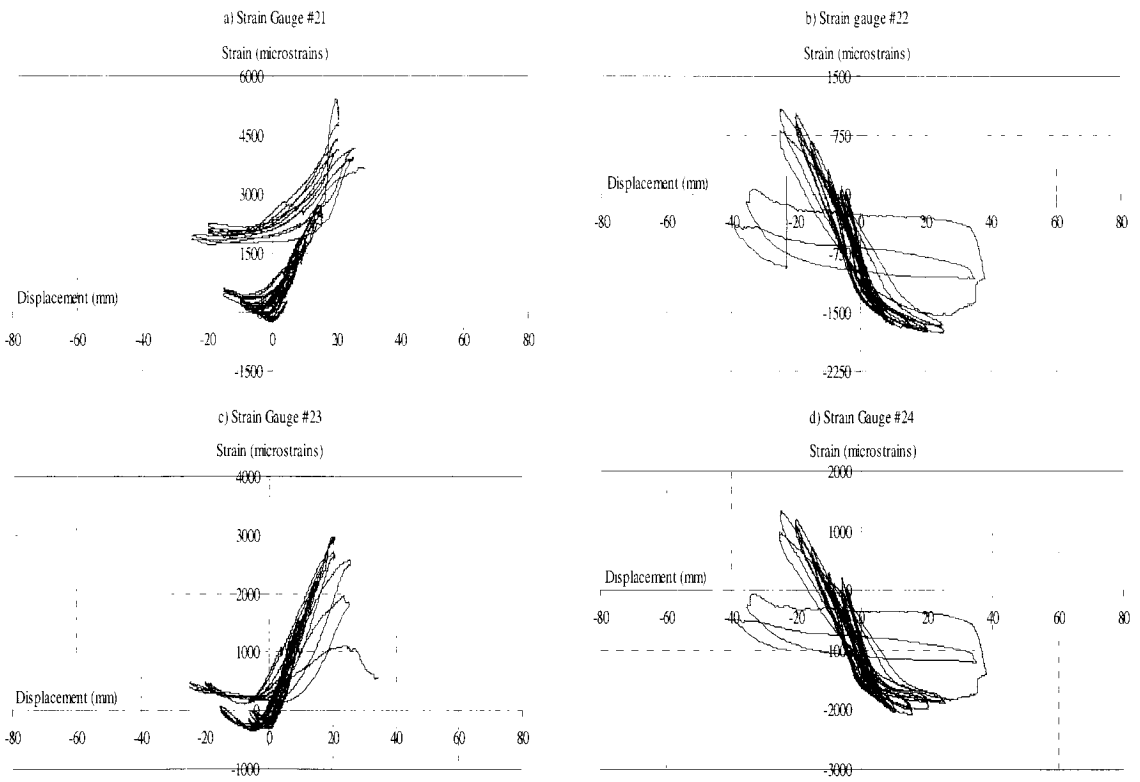

e) Lateral displacement vs. strain for strain gauges at close end of beam

Figure A4: (Cont'd) Lateral displacements vs. strain for strain Gauges #1 to # 28 for BL-3 (Retrofitted frame)

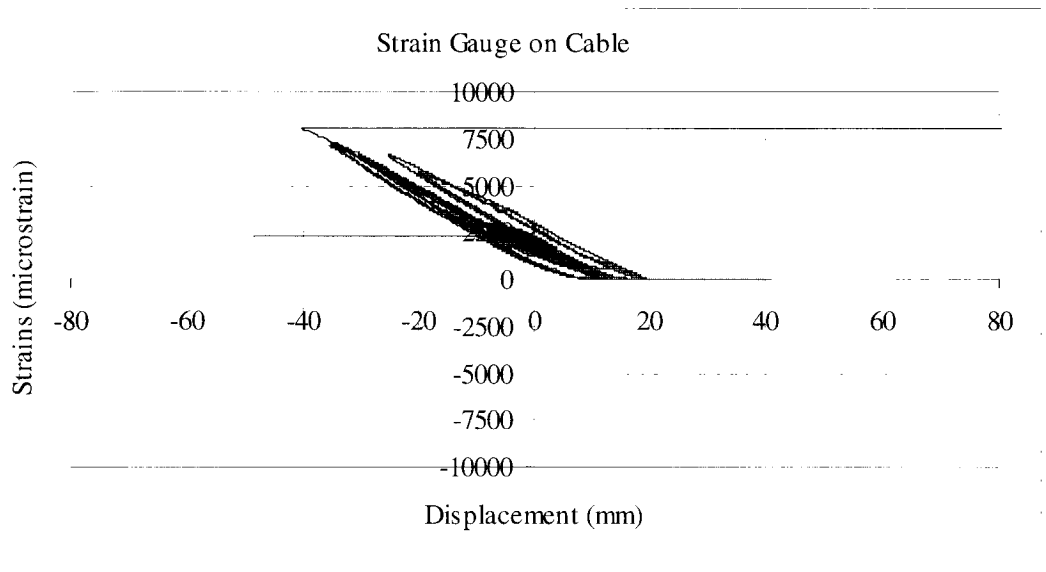

Figure A5: Lateral displacements vs. strain for strain gauge on diagonal cable for BR-2 (Retrofitted P/S = 75 kN)

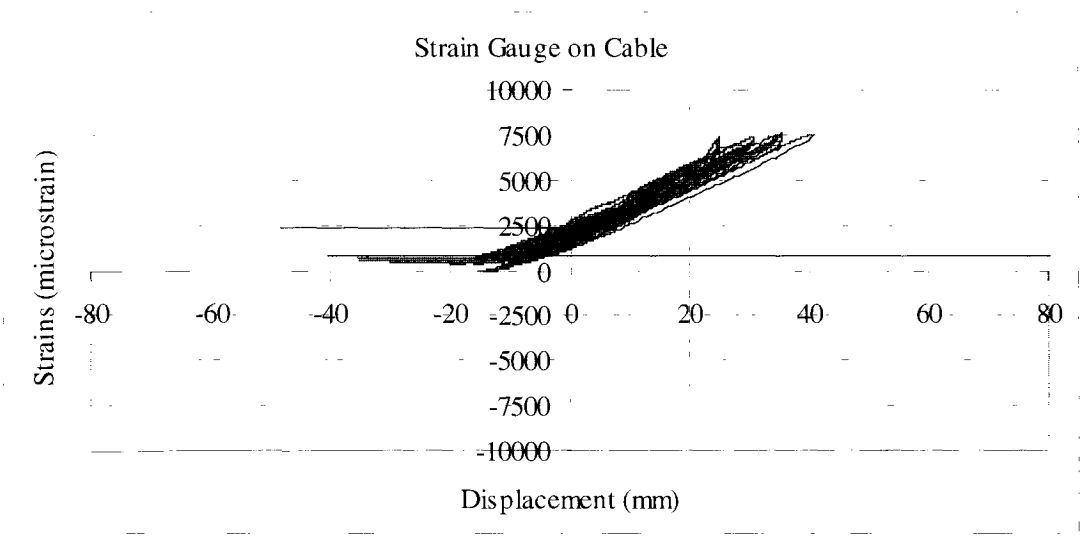

Figure A6: Lateral displacements vs. strain for strain Gauges on diagonal cable for BR-2 (Retrofitted P/S = 75 kN)

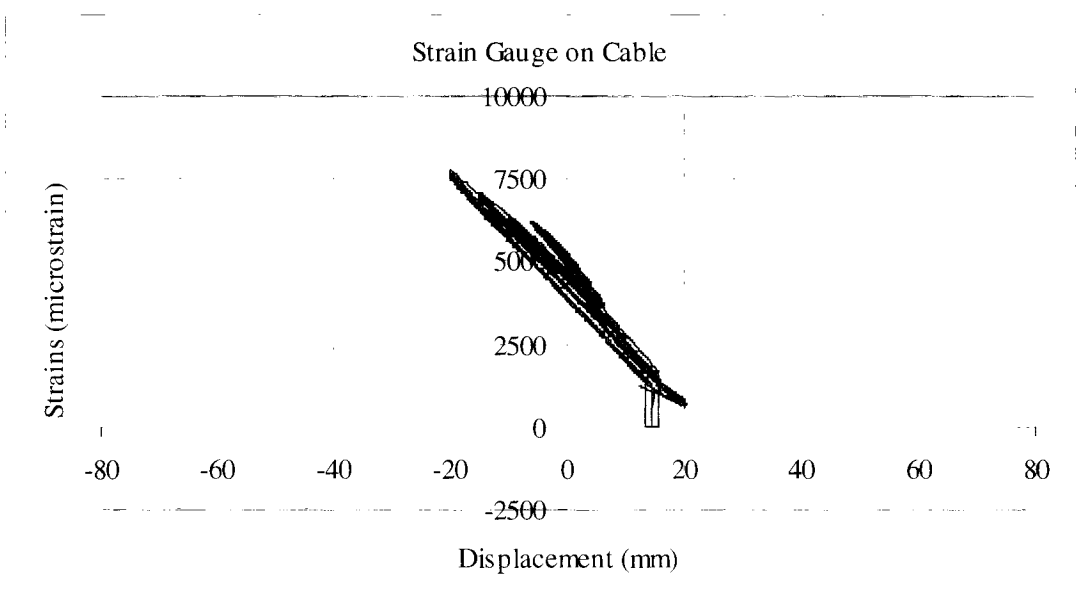

Figure A7: Lateral displacements vs. strain for strain Gauges on diagonal cable for BR-3 (Retrofitted P/S = 125 kN)

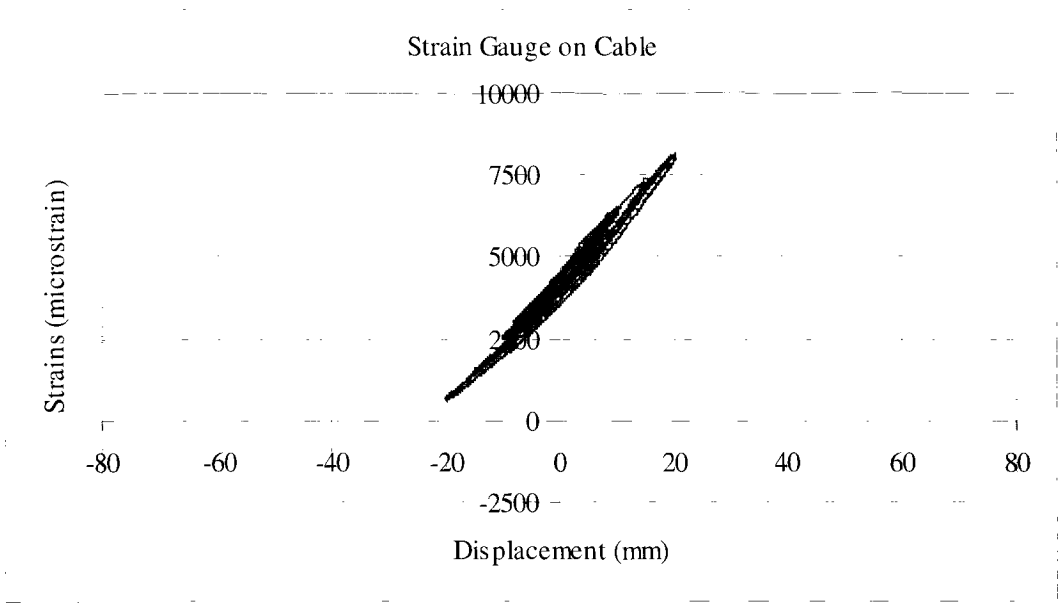

Figure A8: Lateral displacements vs. strain for strain Gauges on diagonal cable for BR-3 (Retrofitted P/S = 125 kN)